| | |
|---|---|
| **Titre:** Title: | Modeling the Phase Diagram and Density of Binary and Ternary Systems of Ionic Liquids |
| **Auteur:** Author: | Meysam Mirarabrazi |
| **Date:** | 2017 |
| **Type:** | Mémoire ou thèse / Dissertation or Thesis |
| **Référence:** Citation: | Mirarabrazi, M. (2017). Modeling the Phase Diagram and Density of Binary and Ternary Systems of Ionic Liquids [Mémoire de maîtrise, École Polytechnique de Montréal]. PolyPublie. https://publications.polymtl.ca/2674/ |

UNIVERSITÉ DE MONTRÉAL

# MODELING THE PHASE DIAGRAM AND DENSITY OF BINARY AND TERNARY SYSTEMS OF IONIC LIQUIDS

MEYSAM MIRARABRAZI

DÉPARTEMENT DE GÉNIE CHIMIQUE

ÉCOLE POLYTECHNIQUE DE MONTRÉAL

MÉMOIRE PRÉSENTÉ EN VUE DE L'OBTENTION

DU DIPLÔME DE MAÎTRISE ÈS SCIENCES APPLIQUÉES

(GÉNIE CHIMIQUE)

AOÛT 2017

UNIVERSITÉ DE MONTRÉAL

ÉCOLE POLYTECHNIQUE DE MONTRÉAL

Ce mémoire intitulé:

# MODELING THE PHASE DIAGRAM AND DENSITY OF BINARY AND TERNARY SYSTEMS OF IONIC LIQUIDS

présenté par: MIRARABRAZI Meysam

en vue de l'obtention du diplôme de: Maîtrise ès sciences appliquées

a été dûment accepté par le jury d'examen constitué de:

M. HARVEY Jean-Philippe, Ph. D., président

M. ROBELIN Christian, Ph. D., membre et directeur de recherche

M. VIRGILIO Nick, Ph. D., membre et codirecteur de recherche

M. ALPER Howard, Ph. D., membre

# DEDICATION

I would like to dedicate my dissertation work to

**My family**

A special feeling of gratitude to

**My loving parents**

Whose words of encouragement and push for tenacity ring in my ears

To

**My sister and brother**

For your continuing long-distance prayers and moral support

# ACKNOWLEDGEMENTS

This work was supported by the Natural Sciences and Engineering Research Council of Canada (NSERC).

I would like to express my sincere gratitude to my supervisor Dr. Christian Robelin for the continuous support of my Master's study and research, for his patience, motivation, enthusiasm, and knowledge. His guidance helped me for my research and for writing this thesis. I could not have imagined having a better advisor and mentor for my Master's study.

I would like also to acknowledge the valuable comments and suggestions of my co-supervisor Prof. Nick Virgilio, which have improved the quality of this work.

I would like to thank Prof. Kenneth R. Seddon, Dr. Natalia V. Plechkova and Isabel Vázquez-Fernández for measuring the phase diagrams and densities of imidazolium-based ionic liquid systems.

I would like to thank Prof. Marcin Smiglak and Olga Stolarska for conducting DSC experiments on ternary mixtures of pyrrolidinium-based ionic liquids. I also thank them for their contribution to the research paper submitted for publication in *Physical Chemistry Chemical Physics* (Chapter 4 of the present thesis).

I would like to thank Prof. João A. P. Coutinho and Mónia Martins for performing DSC experiments on ternary mixtures of $PF_6$-based ionic liquids.

I would like to thank Prof. Gildas K. Gbassi for performing part of the literature search on the thermodynamic properties of the imidazolium-based compounds.

I would like also to acknowledge Emeritus Professor Arthur D. Pelton for many useful comments and discussions.

I am grateful to my lab mate Evgenii Nekhoroshev for helping me to use his PC software for the optimization of the heat capacities of pure ionic liquids.

I would like to thank Evguenia Sokolenko for managing the ionic liquid database using Endnote.

Last but not least, I would like to thank my family (my parents, my brother and my sister) for supporting me spiritually throughout the process of writing this thesis and throughout my life in general.

# RÉSUMÉ

Les liquides ioniques sont généralement constitués d'un gros cation organique asymétrique et d'un anion organique ou inorganique, avec une température de fusion inférieure à 100°C. Les mélanges ternaires de liquides ioniques ont reçu très peu d'attention jusqu'à présent. Ce travail décrit des modèles thermodynamiques pour les diagrammes de phases de systèmes ternaires variés de liquides ioniques (à cation commun, à anion commun, et ternaire réciproque avec deux cations et deux anions), et des modèles de densité pour quelques systèmes ternaires de liquides ioniques (à cation commun et à anion commun). Les données expérimentales nécessaires à la calibration et à la validation des modèles sont à la fois issues de la littérature et obtenues à travers des collaborations scientifiques avec des groupes de recherche. Les nouvelles données obtenues par ces groupes étaient les transitions thermiques mesurées pour des mélanges binaires et ternaires de liquides ioniques à l'aide de la calorimétrie différentielle à balayage (DSC), et les densités de quelques systèmes binaires de liquides ioniques (incluant les liquides purs).

Le Modèle Quasichimique Modifié dans l'Approximation des Paires (MQMPA) a été utilisé pour modéliser la solution liquide des systèmes de liquides ioniques à ion commun suivants : les systèmes ternaires à cation commun [$C_4$mpyrr]{Cl, Br, $BF_4$} et [$C_4$mim]{Cl, $NO_3$, $CH_3SO_3$} (où [$C_4$mpyrr] et [$C_4$mim] désignent le 1-butyl-1-methyl-pyrrolidinium et le 1-butyl-3-methyl-imidazolium, respectivement); et le système quaternaire à anion commun {[$C_3$mim], [$C_3$mpy], [$C_3$mpyrr], [$C_3$mpip]}$PF_6$ (où [$C_3$mim], [$C_3$mpy], [$C_3$mpyrr] et [$C_3$mpip] désignent le 1-propyl-3-methyl-imidazolium, le 1-propyl-3-methyl-pyridinium, le 1-propyl-1-methyl-pyrrolidinium et le 1-propyl-1-methyl-piperidinium, respectivement). Le Modèle Quasichimique Modifié dans l'Approximation des Quadruplets (MQMQA) a été utilisé pour modéliser la solution liquide du système ternaire réciproque [$C_2$py]Cl - [$C_2$py]Br - [$C_4$py]Cl - [$C_4$py]Br (où [$C_n$py] désigne le 1-alkyl-pyridinium). Finalement, le "Compound Energy Formalism" a été utilisé pour modéliser les solutions solides pertinentes.

Pour le système ternaire à cation commun [$C_4$mpyrr]{Cl, Br, $BF_4$}, un petit paramètre ternaire en excès a été inclus pour la phase liquide de façon à reproduire au mieux les sections isoplèthes mesurées à une teneur constante en [$C_4$mpyrr]$BF_4$ de 50% molaire et à un ratio molaire constant [$C_4$mpyrr]Cl / ([$C_4$mpyrr]Cl + [$C_4$mpyrr]Br) de 0.85. Pour le système ternaire à cation commun [$C_4$mim]{Cl, $NO_3$, $CH_3SO_3$}, aucune mesure ternaire de diagramme de phases n'a été tentée à

cause des données très dispersées obtenues pour le sous-système binaire $[C_4mim]Cl$ - $[C_4mim]NO_3$, étudié à l'aide de la DSC et de l'observation visuelle. Ces données très dispersées ont été attribuées au caractère très hygroscopique de ce système particulier. Une projection provisoire du liquidus du système ternaire a été calculée à partir des paramètres binaires optimisés du modèle.

Le système quaternaire à anion commun $\{[C_3mim], [C_3mpy], [C_3mpyrr], [C_3mpip]\}PF_6$ inclut les quatre sous-systèmes ternaires suivants: (1) $[C_3mim]PF_6$ - $[C_3mpip]PF_6$ - $[C_3mpyrr]PF_6$, (2) $[C_3mpy]PF_6$ - $[C_3mpip]PF_6$ - $[C_3mpyrr]PF_6$, (3) $[C_3mpip]PF_6$ - $[C_3mpy]PF_6$ - $[C_3mim]PF_6$, et (4) $[C_3mpyrr]PF_6$ - $[C_3mpy]PF_6$ - $[C_3mim]PF_6$. Les systèmes (1) et (2) incluent tous deux la solution solide continue binaire ($s_3$-$s_3$), qui a été rapportée dans la littérature entre les allotropes de haute température de $[C_3mpip]PF_6$ et $[C_3mpyrr]PF_6$ (chacun de ces deux composés présente trois allotropes distincts.) Deux scénarios différents ont été considérés dans ce travail: le premier scénario a supposé une solubilité à l'état solide négligeable entre les allotropes de basse température ($s_1$-$s_1$) et aussi entre les allotropes de température intermédiaire ($s_2$-$s_2$); le second scénario a supposé une solution solide continue entre les allotropes de basse température ($s_1$-$s_1$) et aussi entre les allotropes de température intermédiaire ($s_2$-$s_2$). Le second scénario a finalement été favorisé de façon à reproduire au mieux les sections isoplèthes mesurées dans le système (1) à une teneur constante en $[C_3mim]PF_6$ de 40% molaire et à un ratio molaire constant $[C_3mpyrr]PF_6$ / ($[C_3mpyrr]PF_6$ + $[C_3mpip]PF_6$) de 0.60. Aucun paramètre ternaire en excès n'a été requis pour la phase liquide, et les énergies de Gibbs en excès des solutions solides de basse température ($s_1$-$s_1$) et de température intermédiaire ($s_2$-$s_2$) ont été ajustées. L'accord entre les calculs et les données ternaires était satisfaisant, mais le modèle n'a pas pu reproduire les arrêts thermiques expérimentaux dans la gamme de températures intermédiaires, dans la première section isoplèthe. Ces arrêts thermiques pourraient être associés à un polymorphisme de $[C_3mpyrr]PF_6$, avec l'existence de deux conformations préférées des cations pyrrolidinium. De manière similaire, la projection du liquidus du système (2) très semblable a été prédite. Aucun paramètre ternaire en excès n'a été requis pour reproduire de manière satisfaisante les sections isoplèthes mesurées dans le système (3) à une teneur constante en $[C_3mpy]PF_6$ de 40% molaire et à un ratio molaire constant $[C_3mpy]PF_6$ / ($[C_3mpy]PF_6$ + $[C_3mim]PF_6$) de 0.60. La projection du liquidus du système (4) très semblable a également été prédite. Finalement, les propriétés thermodynamiques du liquide quaternaire à anion commun $\{[C_3mim], [C_3mpy], [C_3mpyrr], [C_3mpip]\}PF_6$ ont été calculées uniquement à partir des paramètres binaires optimisés, avec une précision raisonnable attendue.

Pour le système ternaire réciproque [$C_2$py], [$C_4$py] || Cl, Br, les propriétés thermodynamiques du liquide ont été calculées seulement à partir des paramètres optimisés pour les quatre sous-systèmes binaires à ion commun. Les sections diagonales expérimentales [$C_4$py]Br-[$C_2$py]Cl et [$C_4$py]Cl-[$C_2$py]Br ont été reproduites de manière très satisfaisante par le modèle. La "thermodynamique basée sur le volume" (VBT) de Glasser et Jenkins a été utilisée en conjonction avec les données disponibles dans la littérature pour estimer les propriétés thermodynamiques ($\Delta H^o_{298.15K}$, $S^o_{298.15K}$, et $C_p(T)$) des liquides ioniques purs de type pyridinium, permettant ainsi d'évaluer la variation d'énergie de Gibbs pour la réaction d'échange [$C_2$py]Br (liquide) + [$C_4$py]Cl (liquide) = [$C_2$py]Cl (liquide) + [$C_4$py]Br (liquide). Il a été conclu que la VBT n'est pas suffisamment précise pour modéliser les diagrammes de phases de systèmes réciproques. La VBT a également été appliquée aux composés de type imidazolium [$C_4$mim]Cl, [$C_4$mim]$NO_3$ et [$C_4$mim]$CH_3SO_3$.

Dans ce travail, un modèle de densité, basé sur le MQMPA et précédemment appliqué avec succès à plusieurs systèmes de sels fondus multicomposants inorganiques, a été appliqué aux systèmes de liquides ioniques suivants: les liquides ternaires à cation commun [$C_4$mim]{Cl, $NO_3$, $CH_3SO_3$} (encore en cours) et [$C_4$mim]{$BF_4$, $PF_6$, $NTf_2$} (où $NTf_2$ désigne le bis(trifluoromethylsulfonyl)imide), et les liquides ternaires à anion commun {[$C_2$mim], [$C_8$mim], [$C_{10}$mim]}$NTf_2$ et {[$C_4$mim], [$C_8$mim], [$C_{10}$mim]}$NTf_2$. Pour les trois derniers systèmes, les lignes iso-valeurs du volume molaire en excès ont été calculées: le volume molaire de chaque liquide ternaire a été prédit à partir des valeurs optimisées des expansivités dépendant de la température et des volumes molaires à 298.15K des liquides purs, et à partir des paramètres binaires optimisés dépendant de la pression en utilisant une méthode d'interpolation symétrique standard.

# ABSTRACT

Ionic liquids are generally composed of a large asymmetric organic cation and an organic or inorganic anion, with a melting temperature below 100°C. Ternary ionic liquid mixtures have received very little attention until now. The present work describes thermodynamic models for the phase diagrams of various ternary ionic liquid systems (common-cation, common-anion, and ternary reciprocal with two cations and two anions), and density models for a few ternary ionic liquid systems (common-cation and common-anion). The experimental data necessary to calibrate and validate the models were both taken from the literature and obtained through scientific collaborations with research groups. The new data obtained by these groups were the thermal transitions measured for some binary and ternary ionic liquid mixtures using Differential Scanning Calorimetry (DSC), and the densities of a few binary ionic liquid systems (including the pure liquids).

The Modified Quasichemical Model in the Pair Approximation (MQMPA) was used to model the liquid solution of the following common-ion ionic liquid systems : the [$C_4$mpyrr]{Cl, Br, $BF_4$} and [$C_4$mim]{Cl, $NO_3$, $CH_3SO_3$} common-cation ternary systems (where [$C_4$mpyrr] and [$C_4$mim] are 1-butyl-1-methyl-pyrrolidinium and 1-butyl-3-methyl-imidazolium, respectively); and the {[$C_3$mim], [$C_3$mpy], [$C_3$mpyrr], [$C_3$mpip]}$PF_6$ common-anion quaternary system (where [$C_3$mim], [$C_3$mpy], [$C_3$mpyrr] and [$C_3$mpip] are 1-propyl-3-methyl-imidazolium, 1-propyl-3-methyl-pyridinium, 1-propyl-1-methyl-pyrrolidinium and 1-propyl-1-methyl-piperidinium, respectively). The Modified Quasichemical Model in the Quadruplet Approximation (MQMQA) was used to model the liquid solution of the ternary reciprocal system [$C_2$py]Cl - [$C_2$py]Br - [$C_4$py]Cl - [$C_4$py]Br (where [$C_n$py] is 1-alkyl-pyridinium). Finally, the Compound Energy Formalism was used to model the relevant solid solutions.

For the [$C_4$mpyrr]{Cl, Br, $BF_4$} common-cation ternary system, a small ternary excess parameter was included for the liquid phase in order to best reproduce the experimental isoplethal sections at constant 50 mol% [$C_4$mpyrr]$BF_4$ and at constant molar ratio [$C_4$mpyrr]Cl / ([$C_4$mpyrr]Cl + [$C_4$mpyrr]Br) of 0.85. For the [$C_4$mim]{Cl, $NO_3$, $CH_3SO_3$} common-cation ternary system, no ternary phase diagram measurements were attempted owing to the very scattered phase diagram data for the [$C_4$mim]Cl - [$C_4$mim]$NO_3$ binary subsystem, investigated using both DSC and visual observation. These rather scattered data were attributed to the very hygroscopic character of this

particular system. A tentative liquidus projection of the ternary system was calculated from the optimized binary model parameters.

The {[$C_3$mim], [$C_3$mpy], [$C_3$mpyrr], [$C_3$mpip]}$PF_6$ common-anion quaternary system includes the following four ternary subsystems: (1) [$C_3$mim]$PF_6$ - [$C_3$mpip]$PF_6$ - [$C_3$mpyrr]$PF_6$, (2) [$C_3$mpy]$PF_6$ - [$C_3$mpip]$PF_6$ - [$C_3$mpyrr]$PF_6$, (3) [$C_3$mpip]$PF_6$ - [$C_3$mpy]$PF_6$ - [$C_3$mim]$PF_6$, and (4) [$C_3$mpyrr]$PF_6$ - [$C_3$mpy]$PF_6$ - [$C_3$mim]$PF_6$. Systems (1) and (2) both include the continuous binary solid solution ($s_3$-$s_3$), which was reported in the literature between the high-temperature allotropes of [$C_3$mpip]$PF_6$ and [$C_3$mpyrr]$PF_6$ (each of these two compounds displays three different allotropes.) Two different scenarios were considered in the present work: the first scenario assumed a negligible solid solubility between the low-temperature allotropes ($s_1$-$s_1$) and also between the intermediate-temperature allotropes ($s_2$-$s_2$); the second scenario assumed a continuous solid solution between the low-temperature allotropes ($s_1$-$s_1$) and also between the intermediate-temperature allotropes ($s_2$-$s_2$). The second scenario was finally favoured in order to best reproduce the isoplethal sections measured in system (1) at constant 40 mol% [$C_3$mim]$PF_6$ and at constant molar ratio [$C_3$mpyrr]$PF_6$ / ([$C_3$mpyrr]$PF_6$ + [$C_3$mpip]$PF_6$) of 0.60. No ternary excess parameter was required for the liquid phase, and the excess Gibbs free energies of the low-temperature ($s_1$-$s_1$) and intermediate-temperature ($s_2$-$s_2$) solid solutions were adjusted. Agreement between the calculations and the ternary data was satisfactory, but the model was not able to reproduce the experimental thermal arrests in the intermediate temperature range, in the former isoplethal section. These thermal arrests might be associated with [$C_3$mpyrr]$PF_6$ polymorphism, with the existence of two preferred conformations of the pyrrolidinium cations. Similarly, the liquidus projection of the closely related system (2) was predicted. No ternary excess parameter was required to reproduce satisfactorily the isoplethal sections measured in system (3) at constant 40 mol% [$C_3$mpy]$PF_6$ and at constant molar ratio [$C_3$mpy]$PF_6$ / ([$C_3$mpy]$PF_6$ + [$C_3$mim]$PF_6$) of 0.60. The liquidus projection of the closely related system (4) was also predicted. Finally, the thermodynamic properties of the {[$C_3$mim], [$C_3$mpy], [$C_3$mpyrr], [$C_3$mpip]}$PF_6$ common-anion quaternary liquid were calculated solely from the optimized binary parameters, with an expected reasonable accuracy.

For the [$C_2$py], [$C_4$py] || Cl, Br ternary reciprocal system, the thermodynamic properties of the liquid were calculated solely from the optimized parameters for the four common-ion binary subsystems. The experimental diagonal sections [$C_4$py]Br - [$C_2$py]Cl and [$C_4$py]Cl-[$C_2$py]Br were very satisfactorily reproduced by the model. The Volume-based Thermodynamics (VBT) from

Glasser and Jenkins was used in conjunction with the available data from the literature in order to assess the thermodynamic properties ($\Delta H^{o}_{298.15K}$, $S^{o}_{298.15K}$, and $C_p(T)$) of the pyridinium-based pure ionic liquids, making it possible to estimate the exchange Gibbs free energy for the exchange reaction $[C_2py]Br$ (liquid) + $[C_4py]Cl$ (liquid) = $[C_2py]Cl$ (liquid) + $[C_4py]Br$ (liquid). It was concluded that the VBT is not accurate enough to model the phase diagrams of reciprocal systems. The VBT was also applied to the imidazolium-based compounds $[C_4mim]Cl$, $[C_4mim]NO_3$ and $[C_4mim]CH_3SO_3$.

In the present work, a density model, based on the MQMPA and previously applied successfully to various multicomponent inorganic molten salts, was applied to the following ionic liquid systems: the $[C_4mim]\{Cl, NO_3, CH_3SO_3\}$ (still in progress) and $[C_4mim]\{BF_4, PF_6, NTf_2\}$ common-cation ternary liquids (where $NTf_2$ is bis(trifluoromethylsulfonyl)imide), and the $\{[C_2mim], [C_8mim], [C_{10}mim]\}NTf_2$ and $\{[C_4mim], [C_8mim], [C_{10}mim]\}NTf_2$ common-anion ternary liquids. For the three latter systems, iso-excess molar volume lines were calculated: the molar volume of each ternary liquid was predicted from the optimized temperature-dependent expansivities and molar volumes at 298.15K of the pure liquids, and from the optimized binary pressure-dependent parameters using a standard symmetric interpolation method.

# TABLE OF CONTENTS

# LIST OF TABLES

# LIST OF FIGURES

# LIST OF SYMBOLS AND ABBREVIATIONS

| | |
|---|---|
| 1,3-diMeIm | 1,3-dimethylimidazolium |
| 4,5-di$NO_2$-Im | 4,5-dinitroimidazolate |
| 4empy | 1-ethyl-4-methylpyridinium |
| 4-$NO_2$-Tri | 4-nitro-1,2,3-triazolate |
| AC | Adiabatic Calorimetry |
| $a_i$ | Activity of component $i$ |
| $b_3$mpy | 1-butyl-3-methyl-pyridinium |
| $b_4$mpy | 1-butyl-4-methylpyridinium |
| BC | Bomb Calorimetry |
| $BCN_3$py | 1-butyl-3-cyanopyridinium |
| bmpy | 1-butyl-3-methylpyridinium |
| bupy | 1-butylpyridinium |
| $C(CN)_3$ | tricyanomethanide |
| $C_2$pz | 1-ethyl-2-methylpyrazolium |
| $C_3$mpip | 1-propyl-1-methyl-piperidinium |
| $C_3$mpy | 1-propyl-3-methyl-pyridinium |
| $C_n$mpyrr | 1-alkyl-1-methyl-pyrrolidinium |
| $C_4F_9SO_3$ | Nonafluorobutanesulfonate |
| CEF | Compound Energy Formalism |
| $CF_3SO_3$ | Trifluoromethanesulfonate |
| $CH_3COO$ | Acetate |
| $C_nC_m$im | 1-alkyl-3-alkyl-imidazolium |
| $C_nC_m$pyrr | N,N-dialkylpyrrolidinium |

| | |
|---|---|
| $C_n$mim | 1-alkyl-3-methyl-imidazolium |
| $C_n$py | 1-alkyl-pyridinium |
| $C_p$ | Heat capacity (J/mol.K) |
| DCA | Dichloroacetic acid |
| DEA | Dielectric thermal analysis |
| DES | Deep Eutectic Solvents |
| DMA | Dynamic mechanical analysis |
| DSC | Differential Scanning Calorimetry |
| DTA | Differential thermal analysis |
| eepy | 1,2-diethylpyridinium |
| EGA | Evolved gas analysis |
| eOHmim | 1-(2-hydroxyethyl)-3-methylimidazolium |
| epy | 1-ethylpyridinium |
| $eSO_4$ | ethylsulfate |
| $EtNH_3$ | Ethylammonium |
| FNN | First-nearest-neighbor |
| FSA | Bis(fluorosulfonyl)amide |
| FSI | Bis(fluorosulfonyl)imide |
| $G^E$ | Molar excess Gibbs free energy (J/mol) |
| $g^o_i$ | Molar Gibbs free energy of component i (J/mol) |
| $HCN_3$py | 1-hexyl-3-cyanopyridinium |
| $HCN_4$py | 1-hexyl-4-cyanopyridinium |
| HCOO | formate |
| HEA | 2-hydroxyethylammonium |

| | |
|---|---|
| hmpy | 1-hexyl-3-methylpyridinium |
| *I* | Ionic strength factor |
| L | Redlich-Kister term (J/mol) |
| m | Mass (g) |
| MADS | Mesh Adaptive Direct Search |
| mpy | 1-methylpyridinium |
| MQM | Modified Quasichemical Model |
| MQMPA | Modified Quasichemical Model in the Pair Approximation |
| MQMQA | Modified Quasichemical Model in the Quadruplet Approximation |
| $mSO_4$ | methylsulfate |
| $N(C_4F_9SO_2)_2$ | Bis(nonafluorobutylsulfonyl)imide |
| $N_{0002}$ | Ethylammonium |
| $N_{0003}$ | Propylammonium |
| $N_{0004}$ | Butylammonium |
| $N_{0022}$ | Diethylammonium |
| $N_{0222}$ | Triethylammonium |
| $N_{1112(OH)}$ | (2-hydroxyethyl)trimethylammonium |
| $N_{2222}$ | tetraethylammonium |
| $N_{4444}$ | Tetrabutylammonium |
| $n_i$ | Number of moles of component i |
| $NTf_2$ | bis(trifluoromethylsulfonyl)imide |
| $O_3mpy$ | 1-octyl-3-methylpyridinium |
| $OCN_3py$ | 1-octyl-3-cyanopyridinium |
| OTf | Trifluoromethanesulfonate |

| | |
|---|---|
| P | Pressure (bar) |
| $P_{4444}$ | Tetrabutylphosphonium |
| $P_{6,6,6,14}$ | trihexyl(tetradecyl)phosphonium |
| $PPh_4$ | tetraphenylphosphonium |
| ppy | 1-propylpyridinium |
| QUILL | Queen's University Ionic Liquid Laboratories |
| R | Gas constant (J/mol.K) |
| R-DBU | Diazabicycloundecenium |
| SNN | Second-nearest-neighbor |
| $S^o_{298.15K}$ | Standard absolute molar entropy at 298.15K (J/mol.K) |
| SRO | Short-range ordering |
| ss | Solid solution |
| T | Temperature (K) |
| $T_c$ | Crystallization temperature (K) |
| $T_{cc}$ | Cold crystallization temperature (K) |
| $T_{eu}$ | Eutectic temperature (K) |
| TFSI | bis(trifluoromethanesulfonyl)imide |
| $T_{fus}$ | Temperature of fusion (K) |
| $T_g$ | Glass transition temperature (K) |
| TGA | Thermogravimetric analysis |
| $T_m$ | Melting temperature (K) |
| TOA | Thermo optical analysis |
| $T_{ref}$ | Reference temperature (K) |
| $T_{ss}$ | Solid-solid transition temperature (K) |

| | |
|---|---|
| $T_{tr}$ | Temperature of solid-solid transition (K) |
| $U_{POT}$ | Lattice potential energy (J/mol) |
| VBT | Volume-based Thermodynamics |
| $V^E$ | Excess molar volume ($cm^3$/mol) |
| $V_m$ | Molar volume ($cm^3$/mol) |
| $X_{eu}$ | Eutectic composition |
| $x_i$ | Mole fraction of component $i$ |
| $x_{ii}$ | Second-nearest-neighbor pair fraction |
| Y | Coordination-equivalent fraction |
| $y_i^A$ | Site fraction of ion $i$ on the anionic sublattice |
| $Z$ | Second-nearest-neighbor coordination number |
| $z_i$ | Valence of ion $i$ |
| $\alpha(T)$ | Thermal expansion (1/K) |
| $\beta^o_i$ | Parameter of density model (J/mol-bar) |
| $\gamma_i$ | Activity coefficient of component $i$ |
| $\Delta_{fus}C_P$ | Heat capacity change at temperature of fusion (J/mol.K) |
| $\Delta_{fus}H$ | Enthalpy of fusion (J/mol) |
| $\Delta g$ | Gibbs free energy change (J/mol) |
| $\Delta H_L$ | Lattice enthalpy (J/mol) |
| $\Delta H^o_{298.15K}$ | Standard molar enthalpy at 298.15K (J/mol) |
| $\Delta S^{config}$ | Configurational entropy of mixing (J/mol.K) |
| $\Delta S^o_{fusion}$ | Entropy change at temperature of fusion (J/mol.K) |
| $\Delta_{tr}H$ | Enthalpy of solid-solid transition (J/mol) |
| $\Delta\rho_{MAX}$ | Largest density shift ($g/cm^3$) |

| | |
|---|---|
| $\zeta_{A/X}$ | Number of quadruplets emanating from, or containing, a first-nearest-neighbor A-X pair |
| $\theta$ | Scattering angle |
| $\nu_m$ | Molecular volume ($nm^3$) |
| $\rho$ | Density ($g/cm^3$) |
| $\chi$ | Composition variable |

# CHAPTER 1 INTRODUCTION

By definition, ionic liquids (ILs) are salts with a melting point below an arbitrary temperature of 100°C (boiling point of water) [1]. Whereas inorganic salts are symmetric in shape, ionic liquids possess a remarkably lower symmetry so that cation and anion charges are distributed over a large volume of the molecule by resonance. Consequently, the melting point of ionic liquids occurs at much lower temperatures. These ionic compounds have also been designated as "designer solvents" due to the possibility of changing a wide range of potential cation and anion combinations in order to fine-tune their physicochemical properties [2]. The structures of some commonly used cations (organic) and anions (either organic or inorganic) are presented in figure 1.1. Owing to distinctive characteristics including a very low vapor pressure (i.e. a low volatility), and a high chemical and thermal stability over a broad temperature range (-40 to 200°C) [3], ionic liquids have found many potential applications in various fields such as analytics [4], chemical processing [5], solvents and catalysts [6], electrochemistry [7], biomass processing [8], etc. As reported by Stark and Seddon [9], at a zeroth order approximation, the physical properties of ionic liquids (such as density, viscosity, and temperature of fusion) are controlled by the cations, whereas the anions govern the chemistry and reactivity. It may thus be required to fine-tune the properties of ionic liquids to achieve a specific application.

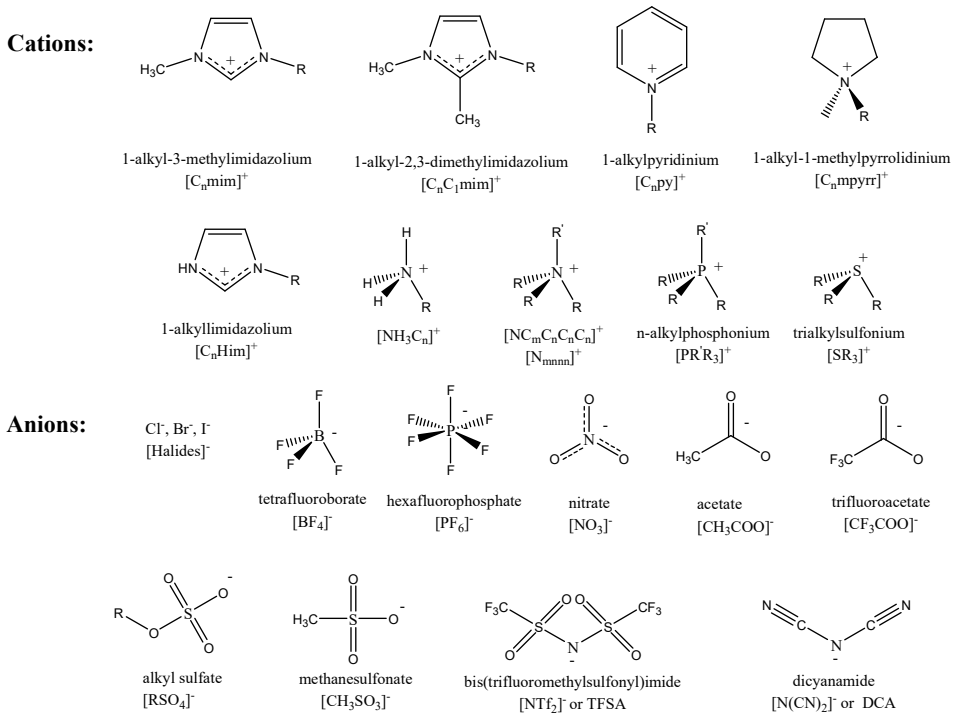


Figure 1.1: Some cations and anions commonly used for ionic liquids

Since 2000 a wide variety of studies have been conducted on the design of single ionic liquids with "tailor-made" properties [10]. A possible technique to modify the properties of ionic liquids is to add other substances such as molecular solvents, that are broadly accessible and whose properties have been widely investigated. Even though molecular solvents may decrease the viscosity of ionic liquids, they can lead to an increased volatility and consequently to a reduced thermal stability. The combination of single ionic liquids (IL-IL mixtures) may be an interesting alternative for further fine-tuning of the properties [11]. Throughout this work, the term "ionic liquid mixtures/systems" will refer to the combination of one single ionic liquid with one or more other ionic liquids.

So far, relatively few studies dealing with ionic liquid mixtures are available in the literature. Niedermeyer et al. [2] performed a critical review of mixtures of ionic liquids. These authors studied thermodynamics, physical and chemical properties, as well as applications of ionic liquid mixtures. To the best of our knowledge, ternary ionic liquid mixtures have received very little attention until now, thus motivating the present study. As pointed out by Plechkova and Seddon [10], ternary systems of ionic liquids may be worth considering, where the chemistry of the system would be controlled by the first component, the physical properties (such as density and viscosity) of the system would be adjusted by the second component, and the overall cost of the system would be lowered (through a dilution of the other two components) by adding a third component, cheap and chemically inert.

The present work describes models for the phase diagrams of various ternary ionic liquid systems (common-cation, common-anion, and ternary reciprocal with two cations and two anions) along with a density model for ternary ionic liquids (common-cation and common-anion).

In the Centre for Research in Computational Thermochemistry (CRCT), we have developed thermodynamic databases for various multicomponent high temperature inorganic molten salt systems, using the Modified Quasichemical Model (MQM) for short-range ordering [12-14]. Theoretical models based on the MQM have been developed for the density and viscosity of multicomponent inorganic liquids. (The viscosity model also depends on the density model.) These various models have been applied successfully to the $NaCl – KCl – MgCl_2 – CaCl_2$ electrolyte used for magnesium production [15-17] as well as the $NaF – AlF_3 – CaF_2 – Al_2O_3$ electrolyte used for aluminium production [18-20].

It is proposed to apply the same methodology to ionic liquid systems. In particular, the minimum liquidus temperature in a given ternary ionic liquid system can be identified from the calculated phase diagram.

Experimental measurements of phase diagrams for ionic liquid systems have been reviewed and are presented in detail in Chapter 2 (Literature Review). These studies were mostly conducted on binary common-ion (common-cation or common-anion) systems, and Differential Scanning Calorimetry (DSC) was usually used. Most of the binary ionic liquid systems investigated in the literature exhibited a simple eutectic phase behavior. Very little attention has been paid to the ternary phase diagrams of ionic liquids in the literature. In 2009, Kubota et al. [21] made an early attempt to measure the phase diagram of a ternary system of alkali bis(fluorosulfonyl)amides MFSA (with M=$Li^+$, $K^+$, $Cs^+$). These authors [22] also studied the ternary phase diagrams of alkali bis(trifluoromethylsulfonyl)imides $MNTf_2$ (with M=$Li^+$, $Na^+$, $K^+$, $Cs^+$). Finally, Kubota et al. [23] measured the ternary phase diagrams of alkali bis(fluorosulfonyl)amides MFSA (with M=$Li^+$, $Na^+$, $K^+$, $Cs^+$). It should be noted that these studies investigated ternary systems of ionic liquids with inorganic cations, while the present work deals with compounds having organic cations with relatively small alkyl chains (ethyl, propyl or butyl).

The present work mainly aims at modeling the phase diagrams of three categories of ternary systems of ionic liquids: common-cation ([A][X][Y][Z] with A as the cation, and X, Y and Z as the anions), common-anion ([A][B][C][X] with A, B and C as the cations, and X as the anion), and ternary reciprocal ([A][B][X][Y] with A and B as the cations, and X and Y as the anions). The Modified Quasichemical Model (MQM) is used to model the liquid phase of these various systems. It assumes the distribution of cations and anions on the sites of two different sublattices, and each ion occupies exactly one site. This model does not consider short-range interactions such as hydrogen bonding, van der Waals and π-π stacking interactions. The MQM may have to be modified since the cations (and sometimes also the anions) in ionic liquid systems are large. In particular, Robelin [24] reported that this model would fail to reproduce the experimental phase diagram $[C_2mim]AlCl_4$ - $NaAlCl_4$ owing to the large size difference between the inorganic $Al^{3+}$ and organic $[C_2mim]^+$ cations.

The Modified Quasichemical Model in the Pair approximation (MQMPA) [12, 13] is used for the liquid phase of the common-ion ternary systems. The model parameters are the Gibbs free energy

changes for pair exchange reactions such as $(X-A-X)+(Y-A-Y)=2(X-A-Y)$ (where $A$ is the common cation, and $X$ and $Y$ are two anions). They can be expressed as a function of the composition by empirical polynomial expressions in order to reproduce the experimental data (phase diagram in the present case) available for the binary common-ion subsystems. The Gibbs free energy change represents the degree of short-range ordering. For instance, in a common-cation binary system, when the Gibbs free energy change is small, the degree of short-range ordering is small, and the solution approximates a random mixture (Bragg-Williams) of anions on the anionic sublattice. The liquid phase of all common-ion ionic liquid systems studied in the present work displays relatively small deviations from ideality. The MQM was used in this work because it is suitable for liquids which exhibit either small or extensive short-range ordering, and also for liquids which display positive deviations from ideality [24]. The thermodynamic properties of the common-ion ternary liquid are estimated from the optimized binary parameters using a Kohler-like (i.e. symmetric model) or a Kohler-Toop-like (i.e. asymmetric model) interpolation method [25]. Small empirical ternary parameters may have to be included in the liquid model in order to obtain a quantitative fit.

The Modified Quasichemical Model in the Quadruplet Approximation (MQMQA) [14] is used for the liquid phase of a ternary reciprocal system (i.e. A, B || X, Y ). This model considers coupled 1$^{st}$- and 2$^{nd}$-nearest-neighbor short-range order. A quadruplet consists of two second-nearest-neighbor cations and two second-nearest-neighbor anions, which are mutual first-nearest-neighbors. The extent of first-nearest-neighbor (cation-anion) short-range ordering is related to the exchange Gibbs free energy for the reaction $AX\ (liquid)+BY\ (liquid)=AY\ (liquid)+BX(liquid)$. Small empirical "ternary reciprocal parameters" may have to be included in order to obtain a quantitative fit for the A, B || X, Y system. Finally, the Compound Energy Formalism (CEF) [26, 27] is used to model the relevant solid solutions. A more detailed description of the thermodynamic models used in this work for the liquid and solid solutions is given in Chapter 3.

The thermodynamic properties ($C_p$ (T), $S^o_{298.15K}$, $\Delta H^o_{298.15K}$) of pure compounds are required to model the phase diagram of a ternary reciprocal system in order to estimate the exchange Gibbs free energy. No compilation tables exist for the thermodynamic properties of pure ionic liquids. In the present work, the missing thermodynamic properties are thus assessed by estimation techniques such as the Volume-Based Thermodynamics (VBT) from Glasser and Jenkins [28-33]. The VBT method relies on the molecular volume ($v_m$) of the pure ionic liquids, which can be derived from

density measurements for the pure liquid phase and from crystallographic data for the pure solid phase. This approach considers only long-range Coulombic interactions, and short-range interactions such as van der Waals and hydrogen bonding are not yet taken into account [33]. More details about the VBT are given in Chapter 3.

As mentioned previously, the present work mainly consists in modeling the phase diagrams of three categories of ternary systems of ionic liquids: common-cation, common-anion and ternary reciprocal. The experimental data were mainly obtained by DSC. They were both collected from the literature and obtained through a scientific collaboration with three different research groups: QUILL (Queen's University Ionic Liquid Laboratories) in Belfast: Isabel Vázquez-Fernández, Dr. Natalia V. Plechkova and Prof. Kenneth R. Seddon; Poznań Science and Technology Park, Adam Mickiewicz University Foundation in Poznań (Poland): Olga Stolarska and Prof. Marcin Smiglak; and University of Aveiro in Portugal: Mónia Martins and Prof. João A. P. Coutinho. First of all, two different common-cation ternary ionic liquid systems were investigated: (i) a pyrrolidinium-based system with 1-butyl-1-methylpyrrolidinium ($[C_4mpyrr]^+$) as the common cation, and $Cl^-$, $Br^-$ and $BF_4^-$ as the anions (in collaboration with Smiglak's group); (ii) an imidazolium-based system with 1-butyl-3-methylimidazolium ($[C_4mim]^+$) as the common cation, and $Cl^-$, $NO_3^-$ and $CH_3SO_3^-$ as the anions (in collaboration with Seddon's group). For system (i), experimental phase diagrams for the three binary subsystems ($[C_4mpyrr]Cl$ – $[C_4mpyrr]BF_4$, $[C_4mpyrr]Br$ – $[C_4mpyrr]BF_4$ and $[C_4mpyrr]Cl$ – $[C_4mpyrr]Br$) were available in the literature [34]. In order to test the capability of prediction of the MQMPA applied to ionic liquid systems, two isoplethal sections were measured by DSC: the isoplethal section at constant 50 mol% $[C_4mpyrr]BF_4$ and the isoplethal section at constant molar ratio $[C_4mpyrr]Cl$ / ($[C_4mpyrr]Cl$ + $[C_4mpyrr]Br$) of 0.85. As will be shown in Chapter 4, one small ternary excess parameter was introduced for the liquid in order to best reproduce these new measurements. For system (ii), the phase diagrams of the three binary subsystems ($[C_4mim]Cl$ – $[C_4mim]NO_3$, $[C_4mim]Cl$ – $[C_4mim]CH_3SO_3$ and $[C_4mim]NO_3$ – $[C_4mim]CH_3SO_3$) were measured by DSC, and also by visual observation for the first subsystem. As will be presented in Chapter 5, the $[C_4mim]Cl$ – $[C_4mim]NO_3$ experimental phase diagram is rather scattered owing to the highly hygroscopic nature of this particular system. As a result, the corresponding calculated phase diagram has a limited accuracy. Therefore, no ternary DSC measurements were conducted, and only a tentative liquidus projection of the $[C_4mim]Cl$ – $[C_4mim]NO_3$ – $[C_4mim]CH_3SO_3$ system was calculated. The VBT from Glasser and Jenkins [28-

33] was used in conjunction with the available data from the literature to assess the thermodynamic data ($\Delta H^{o}_{298.15K}$, $S^{o}_{298.15K}$, $C_p$ (T)) of the three pure compounds.

As a second step, a common-anion quaternary system was studied in collaboration with Coutinho's group: the common anion was hexafluorophosphate ($PF_6^-$), and the various cations were 1-methyl-3-propylimidazolium ($[C_3mim]^+$), 1-methyl-1-propylpyrrolidinium ($[C_3mpyrr]^+$), 1-methyl-3-propylpyridinium ($[C_3mpy]^+$), and 1-methyl-1-propylpiperidinium ($[C_3mpip]^+$). Experimental phase diagrams for the six binary subsystems ($[C_3mim]PF_6$ - $[C_3mpy]PF_6$, $[C_3mim]PF_6$ - $[C_3mpyrr]PF_6$, $[C_3mim]PF_6$ - $[C_3mpip]PF_6$, $[C_3mpy]PF_6$ - $[C_3mpyrr]PF_6$, $[C_3mpy]PF_6$ - $[C_3mpip]PF_6$ and $[C_3mpyrr]PF_6$ - $[C_3mpip]PF_6$) were available in the literature [35]. Whereas the $[C_3mpip]PF_6$ - $[C_3mpy]PF_6$ - $[C_3mim]PF_6$ and $[C_3mpyrr]PF_6$ - $[C_3mpy]PF_6$ - $[C_3mim]PF_6$ ternary subsystems do not exhibit any solid solubility, the $[C_3mim]PF_6$ - $[C_3mpip]PF_6$ - $[C_3mpyrr]PF_6$ and $[C_3mpy]PF_6$ - $[C_3mpip]PF_6$ - $[C_3mpyrr]PF_6$ ternary subsystems display some extensive binary solid solubility. Indeed, the $[C_3mpip]PF_6$ and $[C_3mpyrr]PF_6$ pure compounds both have three allotropes ($s_1$, $s_2$, $s_3$), and a high-temperature ($s_3$-$s_3$) solid solution was observed over the entire composition range [35]. Some binary solid solutions may also exist in the intermediate-temperature ($s_2$-$s_2$) and low-temperature ($s_1$-$s_1$) ranges. In order to elucidate this, two isoplethal sections in the $[C_3mim]PF_6$ - $[C_3mpip]PF_6$ - $[C_3mpyrr]PF_6$ system were measured by DSC: the isoplethal section at constant 40 mol% $[C_3mim]PF_6$ and the isoplethal section at constant molar ratio $[C_3mpyrr]PF_6$ / ($[C_3mpyrr]PF_6$ + $[C_3mpip]PF_6$) of 0.60. Similarly, two isoplethal sections in the $[C_3mpip]PF_6$ - $[C_3mpy]PF_6$ - $[C_3mim]PF_6$ system were measured by DSC: the isoplethal section at constant 40 mol% $[C_3mpy]PF_6$ and the isoplethal section at constant molar ratio $[C_3mpy]PF_6$ / ($[C_3mpy]PF_6$ + $[C_3mim]PF_6$) of 0.60. The corresponding thermodynamic models were adjusted in order to best reproduce the new data. Using the programme FactOptimal [36], which is a coupling of the FactSage thermochemical software with the powerful Mesh Adaptive Direct Search (MADS) algorithm, we identified the composition in the quaternary system $[C_3mim]PF_6$ - $[C_3mpyrr]PF_6$ - $[C_3mpy]PF_6$ - $[C_3mpip]PF_6$ corresponding to the global minimum of the liquidus temperature.

As a third step, a ternary reciprocal system was investigated in collaboration with Smiglak's group: 1-ethylpyridinium ($[C_2py]^+$) and 1-butylpyridinium ($[C_4py]^+$) were the two cations, while $Cl^-$ and $Br^-$ were the two anions. Experimental phase diagrams obtained by DSC were published recently [37] for the four common-ion binary subsystems ($[C_2py]Br$ - $[C_4py]Br$, $[C_2py]Cl$ - $[C_4py]Cl$, $[C_2py]Cl$ - $[C_2py]Br$ and $[C_4py]Cl$ - $[C_4py]Br$) along with two diagonal sections inside the ternary

reciprocal system ([$C_4$py]Br - [$C_2$py]Cl and [$C_4$py]Cl - [$C_2$py]Br). The VBT from Glasser and Jenkins [28-33] was used in conjunction with the available data from the literature to assess the exchange Gibbs free energy for the reaction [$C_2$py]Br (liquid) + [$C_4$py]Cl (liquid) = [$C_2$py]Cl (liquid) + [$C_4$py]Br (liquid). As will be shown in Chapter 4, the experimental diagonal sections were satisfactorily reproduced using solely the optimized model parameters for the four common-ion binary subsystems.

The present work also aims at modeling the density of binary and ternary common-ion (common-cation and common-anion) ionic liquid systems. As mentioned previously, the density model is based on the MQM and has been applied successfully to inorganic molten salt systems [16, 19]. First of all, two different common-cation ternary ionic liquid systems were studied:

(i) an imidazolium-based system with 1-butyl-3-methylimidazolium ($[C_4mim]^+$) as the common cation, and $Cl^-$, $NO_3^-$, and $CH_3SO_3^-$ as the anions (in collaboration with Seddon's group).

(ii) another imidazolium-based system with $[C_4mim]^+$ as the common cation, and $BF_4^-$, $PF_6^-$ and bis(trifluoromethylsulfonyl)imide ($NTf_2^-$) as the anions (based on the published density data from Canongia Lopes et al. [38]).

As a second step, two different common-anion ternary ionic liquid systems were investigated: the common anion was $NTf_2^-$, and a series of 1-alkyl-3-methylimidazolium cations ($[C_2mim]^+$ - $[C_8mim]^+$ - $[C_{10}mim]^+$ and $[C_4mim]^+$ - $[C_8mim]^+$ - $[C_{10}mim]^+$) was considered. For both systems, the published density measurements of Canongia Lopes et al. [38] were used.

The molar volume (and thus the density) of each common-ion ternary ionic liquid system was modeled by introducing in the Gibbs free energy of the liquid phase temperature-dependent molar volume expressions for the pure components and pressure-dependent excess parameters for the binary interactions.

For system (i), the density of the three pure liquids and of the [$C_4$mim]Cl – [$C_4$mim]$NO_3$ and [$C_4$mim]Cl – [$C_4$mim]$CH_3SO_3$ binary liquids was measured in Seddon's group (QUILL). All samples were then sent by QUILL to a Portuguese research group (University of Lisboa: Prof. Luis P. Rebelo) who has a more accurate equipment than that of QUILL. This latter group measured the density of the three pure liquids and of the three binary liquids. For the [$C_4$mim]Cl – [$C_4$mim]$NO_3$ and [$C_4$mim]Cl – [$C_4$mim]$CH_3SO_3$ binary liquids, the excess molar volumes ($V^E$) measured by the two research groups showed opposite trends (i.e. positive or negative values). Therefore, the

density of these two systems was finally not modeled and a prediction of the density of the $[C_4mim]Cl – [C_4mim]NO_3 – [C_4mim]CH_3SO_3$ ternary liquid was not possible.

For all other ternary ionic liquid systems considered, their density was predicted, based on the optimized density model parameters for the binary subsystems. Details are given in Chapter 7.

The present thesis is organized as follows: Chapter 2 presents the relevant literature review; it describes the thermal behavior of pure ionic liquids and the main published studies dealing with phase diagram and density measurements for binary and ternary ionic liquid systems. Chapter 3 is devoted to the thermodynamic models used in this work for the liquid phase and the relevant solid solutions, as well as the density model used for the liquid phase of ionic liquid systems. The principles of the Volume-based Thermodynamics (VBT) for the estimation of the missing thermodynamic properties of pure ionic liquids is also discussed. Chapter 4 presents the scientific paper submitted for publication in "Physical Chemistry Chemical Physics" and dealing with models for the phase diagrams of a pyrrolidinium-based common-cation ternary ionic liquid system, and of a pyridinium-based ternary reciprocal ionic liquid system. The phase diagram of an imidazolium-based common-cation ternary ionic liquid system is discussed in Chapter 5. Chapter 6 is devoted to a thermodynamic model for a $PF_6$-based common-anion quaternary system. Chapter 7 presents a density model for two common-cation and two common-anion (all imidazolium-based) ternary ionic liquid systems. Finally, Chapter 8 presents a general discussion on the main results of the present work.

# CHAPTER 2 LITERATURE REVIEW

This chapter first describes the thermal behavior of pure ionic liquids. Then, it presents an overview of the published studies dealing with phase diagram measurements for binary and ternary ionic liquid systems. Finally, it summarizes the key literature on density measurements for common-ion (common-cation or common-anion) ionic liquid systems.

## 2.1 Phase behavior

### 2.1.1 Pure ionic liquids

The first ionic liquid, ethylammonium nitrate ($[EtNH_3]NO_3$) with a melting point of 12°C, was reported by Walden in 1914 [39]. As mentioned previously, ionic liquids (ILs) are usually composed of a large organic cation (with alkyl chains of variable length) and an organic or inorganic anion, with an estimated number of $10^{18}$ possible ionic liquids [40].

It is well known that the physicochemical properties and phase behavior of ionic liquids can be tailored by use of an appropriate combination of cations and anions [4]. Strong Coulombic interactions between cations and anions play a major role in the properties of ionic liquids. However, short-range interactions such as van der Waals and hydrogen bonding may also affect the ionic liquid characteristics [41, 42]. Knowledge of the thermophysical properties of pure ionic liquids (including freezing, melting, solid-solid transition, cold crystallization, and glass transition) allows us to better understand the structure and stability of these compounds. It is also important for evaluating and choosing ionic liquids for a specific application in addition to process design. The thermal behavior of pure ionic liquids has been investigated by many researchers using various methodologies and equipments [43-53]. A general overview is given below.

By definition, thermal analysis is a procedure in which physical or chemical properties (enthalpy, heat capacity, mass changes, etc.) of a sample are monitored as a function of temperature or time while the sample is subject to a controlled temperature program. There are a wide variety of techniques available; the major differences are the properties of the substance being studied [54]. The most common thermoanalytical techniques are presented in table 2.1.

Table 2.1: Thermoanalytical techniques applied to the analysis of materials [54]

| Technique | abbreviation | Property measured |
|---|---|---|
| Differential thermal analysis | DTA | Temperature difference |
| Differential scanning calorimetry | DSC | Enthalpy |
| Thermogravimetric analysis | TGA | Mass |
| Dynamic mechanical analysis | DMA | Deformation |
| Dielectric thermal analysis | DEA | Deformation |
| Evolved gas analysis | EGA | Gaseous decomposition |
| Thermo optical analysis | TOA | Optical properties |

In the case of ionic liquids, properties such as heat capacity, glass transition temperature, melting temperature, thermal decomposition temperature, and enthalpy of phase transitions can be determined using Differential Scanning Calorimetry (DSC) and Thermogravimetric Analysis (TGA) [55-57]. DSC is a technique in which the difference in the amount of heat needed to raise the temperature of a sample and a reference material is measured as a function of temperature while the sample and the reference material are subject to a controlled temperature program [58]. On the other hand, TGA, which is applied to determine the thermal stability of a substance and its volatile content, monitors the weight changes of a substance as a function of temperature or time under a controlled atmosphere as the sample is subject to a controlled temperature program [54].

The most common procedure for analyzing the thermal history of ionic liquids is to run a heating/cooling/heating cycle using the DSC technique. It helps to know how they behave and to perform comparative studies. The first heating cycle gives information regarding the thermal transitions occurring in the sample. This step enables to "erase" the thermal history of the substance. It should be noted that the final temperature must be not too high, because it may lead to decomposition of the sample, but it must be high enough for melting to occur. The cooling step provides data for a standard heating history of the sample at a controlled cooling rate. The second heating step enables us to compare substances directly to each other [56].

Various thermal transitions of ionic liquids such as melting, solid-solid transition, crystallization, and glass transition can be observed and measured using DSC. The melting point is the temperature at which a phase transition occurs from the solid state to the liquid state upon heating under atmospheric pressure. A solid-solid transition occurs at a temperature where the compound exhibits two different polymorphic forms. Crystallization is the formation of a crystalline solid from a primary liquid phase upon cooling. Another type of crystallization called cold crystallization occurs above the glass transition temperature upon heating, forming a crystalline structure from an

amorphous solid. Glass transition occurs at a temperature where an amorphous region forms between the glassy and rubbery states.

Regarding the interpretation of a DSC thermogram, the melting temperature ($T_m$) is taken as the onset of an endothermic peak (downward deflection of the curve peak) upon heating, the crystallization temperature ($T_c$) as the onset of an exothermic peak (upward deflection of the curve peak) upon cooling, the cold crystallization temperature ($T_{cc}$) as the onset of an exothermic peak upon heating from a supercooled liquid state to a crystalline solid state, the solid-solid transition temperature ($T_{ss}$) as the onset of an endothermic peak upon heating from a crystalline solid state, and the glass transition temperature ($T_g$) as the midpoint of a small heat capacity change upon heating from an amorphous glass state to a liquid state [55, 56, 59]. An overview of the various thermal transitions possible for pure ionic liquids is shown schematically in figure 2.1.

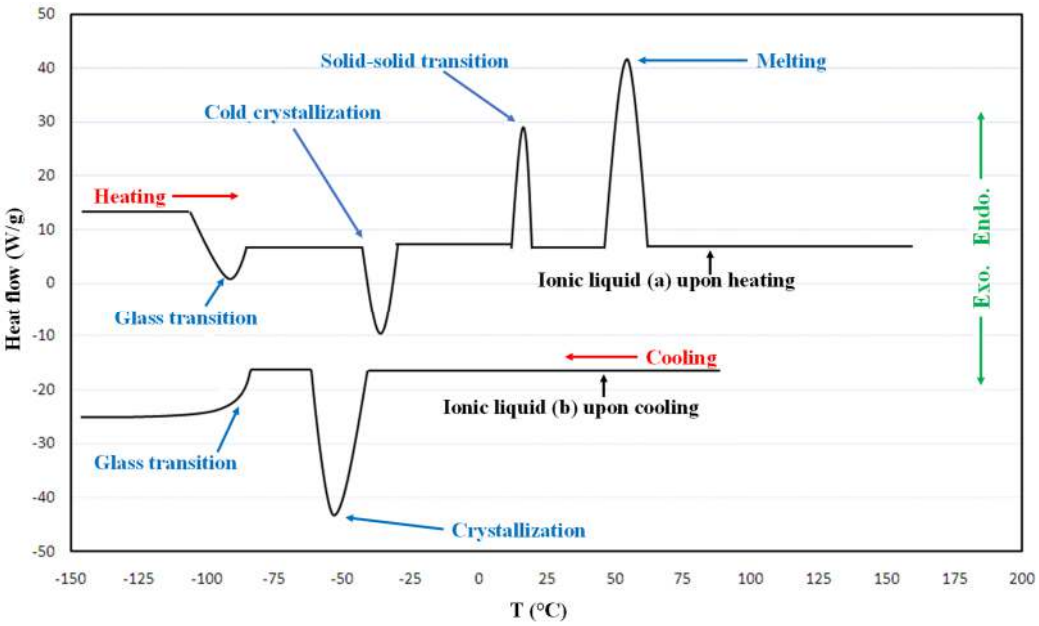


Figure 2.1: Various types of thermal transitions possible for pure ionic liquids: hypothetical ionic liquids (a) {upon heating} and (b) {upon cooling}.

In general, pure ionic liquids can exhibit three types of thermal behavior [55, 56]:

1) Some ionic liquids display no true phase transitions (i.e. melting and freezing), and only the formation of an amorphous glass upon cooling and the reformation of the liquid upon heating are observed. For example, [$C_4$mim][$BF_4$] and [$C_3$mim][$NTf_2$] present this type of behavior [44, 60].

2) Some ionic liquids easily crystallize and do not form glasses, showing a crystallization transition. A crystalline solid is formed upon cooling and melting occurs upon heating. For instance, [$C_4$mim][OTf], [$C_2$mim][$NTf_2$], and [$C_6$mim][TFO] belong to this group [44, 60].
3) For some ionic liquids, upon cooling there is the formation of a glass with no tendency to crystallize; however, upon heating, the compound shows a phase transition from a glassy state to a supercooled liquid phase, and then a cold crystallization occurs. An increase in the heating/cooling rate may lead to the disappearance of the cold crystallization. Then, as the temperature increases, melting occurs. [$C_4$mim][$NTf_2$] and [$C_6$mim][$NTf_2$] belong to this group [44, 60].

One of the most influential factors in DSC is the heating/cooling rates, inasmuch as the crystallization transition is strongly dependent on the heating/cooling rates because there would be enough time for a compound to form a crystalline phase at low rates. The influence of the variation of heating/cooling rates on the thermal behavior of some imidazolium-based ionic liquids showed that, as the scan rate increased, the glass transition (e.g. [$C_3$mim][$NTf_2$], [$C_4$mim][$NTf_2$], [$C_6$mim][$NTf_2$], and [$C_6$mim][DCA]) and cold crystallization temperatures increased, while the freezing temperature decreased. Moreover, the heating/cooling rates had no impact on the melting temperature, as was observed for [$C_2$mim][$NTf_2$], [$C_4$mim][$NTf_2$], [$C_6$mim][$NTf_2$], and [$C_6$mim][TFO] [60].

Changes in heating/cooling rates provide useful information regarding the thermal transitions of ionic liquids. At fast rates, the thermal analysis gives an overlapped phase transition peak, while at slow rates these peaks can move apart from each other. To obtain valid information regarding the thermal behavior of pure ionic liquids, including whether it is a crystal or a glass former, the presence of polymorphs, etc., it is suggested to begin the analysis of the sample by a scan performed at a relatively low heating rate of 2°C/min [55].

There are various factors which may affect the melting temperature of ionic liquids such as the alkyl chain length, the symmetry of cations, the type of anion, the pressure, dissolved gases, etc. The effect of the alkyl chain length on the melting temperature of one of the widely known ionic liquids, [$C_n$mim][$BF_4$], has been studied. The melting point decreases as the alkyl chain lengthens as a result of the lower overall symmetry of the cation (symmetry-breaking region) until, beyond a certain length ($n \approx 10$), it increases owing to attractive van der Waals interactions between the alkyl

side chains which start outweighing the symmetry effect (hydrophobic region) [61, 62]. Dissolved gases have a significant impact on the melting temperature; for instance, adding $CO_2$ to ionic liquids with fluorinated anions can provoke decreases up to 70 K into the melting temperature [63, 64]. Furthermore, the type of anion has a profound impact on the melting temperature of ionic liquids. Typically, substitution with an asymmetric anion and an increase in the anion size both cause a decrease in the melting temperature [65]. The melting point of ionic liquids with $[C_4mim]^+$ as the common cation and various anions such as $Cl^-$, $OTf^-$, $NTf_2^-$, $PF_6^-$, or $BF_4^-$ showed a decrease in this order [61].

### 2.1.2 Binary systems

Over the last few years, the phase behavior of single ionic liquids has been widely investigated, but there have been relatively few studies conducted on the phase diagrams of ionic liquid systems. An overview of the experimental phase diagram measurements for ionic liquid systems with organic cations is given in table 4.1 (Chapter 4). These are almost exclusively binary common-ion (common-cation or common-anion) systems, and the main experimental technique used was DSC.

From the thermodynamic modeling viewpoint, Maximo et al. [35] modeled the phase diagrams of nine $[PF_6]$-based binary ionic liquid systems with imidazolium ($[C_3mim]^+$ or $[C_{12}mim]^+$), pyrrolidinium ($[C_3mpyrr]^+$), pyridinium ($[C_3mpy]^+$), piperidinium ($[C_3mpip]^+$), tetrabutylammonium ($[N_{4444}]^+$) and tetrabutylphosphonium ($[P_{4444}]^+$) as the different cations. These authors considered the following thermodynamic model:

$$\ln\left(\frac{a_i^L}{a_i^S}\right) = \ln\left(\frac{x_i^L\gamma_i^L}{x_i^S\gamma_i^S}\right) = \frac{\Delta_{fus}H}{R}\left(\frac{1}{T_{fus}} - \frac{1}{T}\right) + \sum_{tr=1}^{n}\left[\frac{\Delta_{tr}H}{R}\left(\frac{1}{T_{tr}} - \frac{1}{T}\right)\right] + \frac{\Delta_{fus}C_p}{R}\left(\frac{T_{fus}}{T} - \ln\left(\frac{T_{fus}}{T}\right) - 1\right) \quad (1)$$

where $a_i^L$ and $a_i^S$ are the activities of component i in the liquid and solid phases, respectively; $x_i^L$ and $x_i^S$ are the mole fractions of component i in the liquid and solid phases, respectively; $\gamma_i^L$ and $\gamma_i^S$ are the activity coefficients of component i in the liquid and solid phases, respectively; T is the liquidus temperature (K) of the binary mixture; R is the gas constant; $T_{fus}$ and $\Delta_{fus}H$ are the melting temperature (K) and enthalpy ($J.mol^{-1}$) of component i; $T_{tr}$ and $\Delta_{tr}H$ are the thermal transition

temperatures (K) and enthalpies (J.mol$^{-1}$) of the n solid-solid transitions of component i; and $\Delta_{fus}C_p$ is the heat capacity (J.mol$^{-1}$.K$^{-1}$) of component i at the melting temperature $T_{fus}$. For the phase diagram calculations, Maximo et al. [35] simplified Eq. (1) taking into account that the binary system has a simple eutectic behavior with no solid solubility ($a_i^S = x_i^S\gamma_i^S = 1$) and neglecting the differences in heat capacity ($\Delta_{fus}C_p = 0$). In the case of an ideal liquid phase, they considered that $\gamma_i^L = 1$. As explained in Chapter 4, these authors reported that most of the binary systems investigated are simple eutectic systems with a liquid close to ideal, while one particular binary system ([$C_3$mpyrr][$PF_6$] – [$C_3$mpip][$PF_6$]) displays an extensive solid solution confirmed by powder X-ray diffractometry of the solid phase.

Kick et al. [66] modeled the phase diagram of the [$C_2$mim]Cl – [$C_4$mim]Cl common-anion binary system. These authors used Eq. (1) in its simplest form, assuming an ideal liquid ($\gamma_i^L = 1$) and crystallization of the pure components ($a_i^S = x_i^S\gamma_i^S = 1$), and neglecting the differences in heat capacity ($\Delta_{fus}C_p = 0$). Since no solid-solid transitions were observed for the pure components, $\Delta_{tr}H = 0$.

Recently, Teles et al. [67] measured the phase diagrams of four binary systems of fluorinated ionic liquids, and modeled three of them ([$C_4$mpyrr]N($C_4F_9SO_2$)$_2$ - [$C_4$mpyrr]$C_4F_9SO_3$, [$C_2$mpyrr]N($C_4F_9SO_2$)$_2$ - [$C_2$mpyrr]$CF_3SO_3$, and [$C_2$mpyrr]N($C_4F_9SO_2$)$_2$ - [$C_4$mpyrr]N($C_4F_9SO_2$)$_2$). They used Eq. (1) to calculate the phase diagrams, assuming negligible differences in the heat capacity ($\Delta_{fus}C_p = 0$) and no polymorphic forms ($\Delta_{tr}H = 0$).

The phase diagrams of binary systems of salts with ions commonly used for the preparation of ionic liquids have also been investigated (see table 4.2 in Chapter 4). These are exclusively common-anion systems with alkali metals as the cations.

### 2.1.3 Ternary systems

An overview of the phase diagram measurements available in the literature for ternary systems of salts with ions commonly used for the preparation of ionic liquids is given in table 4.3 (Chapter 4). Again, these are common-anion ternary systems with alkali metals as the cations. Studies of ionic liquid ternary systems involving organic cations are still lacking, which motivated the present study.

### 2.1.4 General remarks

Water is the most important source of impurities in ionic liquids due to the hygroscopic nature of these compounds. Water can be present in ionic liquids either because of insufficient drying or due to absorption from the atmospheric air. The presence of residual water in ionic liquids has a significant impact on their properties such as melting point, density, viscosity, electrical conductivity, reactivity, etc. [68-72]. For instance, the thermal transitions measured by DSC for the common-cation binary system $[C_2mim]NO_3$ - $[C_2mim]Cl$ were found to be unreliable with very poor reproducibility owing to the highly hygroscopic character of this system [73].

Some ionic liquids may exhibit a large degree of supercooling during DSC measurements. Upon cooling, these compounds remain liquid until forming glasses at very low temperatures instead of showing a crystallization. This may lead to experimental problems while measuring the solid-liquid equilibria for ionic liquid systems. For example, Stolarska et al. [73] only reported the DSC thermograms of the first heating run for the $[C_4mim]Cl$-$[C_2mim]Cl$ common-anion binary system, since no thermal transition (either melting or crystallization) was observed during the second and third heating/cooling cycles in the $[C_4mim]Cl$-rich region owing to the tendency of this compound to form a supercooled liquid phase.

Some thermal transitions might be missing due to the dynamic nature of the DSC technique. For instance, no melting transition was observed in the DSC thermograms for the $[C_2mim]PF_6$-$[C_2mim]Cl$ common-cation binary system at compositions between 25 mol% and 75 mol% $[C_2mim]Cl$ due to the highly hygroscopic nature of $[C_2mim]Cl$ [73]. Some missing thermal transitions (either melting or eutectic) were also reported for the $[C_4mim]Cl$-$[C_2mim]Cl$ common-anion binary system because of the following reasons: 1) supercooling behavior of the system; 2) wide melting peak in the heating curve of the $[C_2mim]Cl$ compound; 3) coincidence of the eutectic transition temperature and of the temperature range in which was observed an exothermic peak corresponding to the cold crystallization of the $[C_2mim]Cl$ compound [73].

## 2.2 Density

A considerable number of papers has been published up to now on the density of pure ionic liquids. In recent years, the density and excess molar volume of ionic liquid mixtures have attracted much attention. Niedermeyer et al. [2] gave a comprehensive review of the density of ionic liquid

mixtures. Early work on the density and excess molar volume of ionic liquid binary mixtures was undertaken by Canongia Lopes et al. [38]. These authors measured at 298K and 333K the density of six common-anion systems with $NTf_2^-$ as the common anion and various $[C_nmim]^+$ cations (n=2, 4, 6, 8, 10), and of three common-cation binary systems with $[C_4mim]^+$ as the common cation and $NTf_2^-$, $BF_4^-$ and $PF_6^-$ as the anions. They reported a small symmetric positive deviation from ideality of the order of a few tenths of $cm^3.mol^{-1}$ (less than 0.1% of the mixture's molar volume) for the excess molar volume ($V^E$) of all systems. It was also found that the $V^E$ values are essentially temperature- and pressure-independent. It was well demonstrated for the common-anion binary systems investigated that the $V^E$ values increased with the difference between the alkyl chain lengths of the two cations (about 0.25 $cm^3.mol^{-1}$ as the maximum value reported for the $[C_2mim]NTf_2$ – $[C_{10}mim]NTf_2$ binary liquid). A similar dependence of $V^E$ on the size difference between the anions was observed for the common-cation binary systems studied.

Navia et al. [74] studied the volumetric behavior of two common-cation ($[C_4mim]BF_4$ – $[C_4mim]MeSO_4$ and $[C_4mim]PF_6$ – $[C_4mim]BF_4$) and two common-anion ($[C_2mim]BF_4$ – $[C_6mim]BF_4$ and $[C_4mim]BF_4$ – $[C_6mim]BF_4$) binary mixtures in the temperature range 298.15-308.15K. A very small positive deviation from ideality was observed for the $[C_4mim]PF_6$ – $[C_4mim]BF_4$ binary system, while the other systems exhibited a negative deviation.

Song and Chen [75] measured the density of three binary mixtures of $[BF_4]$-based ionic liquids with various $[C_nmim]^+$ cations (n=2, 3, 6) in the temperature range 298.15-343.15K. These various systems exhibited very small deviations from ideality. In another study, Song and Chen found a near-ideal behavior of the molar volume of the $[eOHmim]BF_4$ – $[C_4mim]BF_4$, $[eOHmim]BF_4$ – $[C_4py]BF_4$ and $[C_4mim]BF_4$ – $[C_4py]BF_4$ common-anion binary systems. The first two systems showed both positive and negative deviations from ideality, while the latter displayed a very small negative deviation.

Clough et al. [11] measured the density of nine binary systems and two ternary reciprocal systems of ionic liquids consisting of imidazolium ($[C_nC_mim]^+$), pyrrolidinium ($[C_nC_mpyrr]^+$), pyrazolium ($[C_nC_mC_ppz]^+$) and diazabicycloundecenium ($[R\text{-}DBU]^+$) as the cations, and of $Cl^-$, $OTf^-$, $MeSO_4^-$, $Me_2PO_4^-$ and $NTf_2^-$ as the anions. The authors reported a close-to-ideal behavior for most of the ionic liquid systems investigated. Two common-cation binary systems such as $[C_4C_1mim]MeSO_4$ – $[C_4C_1mim]NTf_2$ and $[C_4C_1mim]NTf_2$ - $[C_4C_1mim]Me_2PO_4$ as well as the $[C_4C_1mim]NTf_2$ – [Me-

DBU]$MeSO_4$ ternary reciprocal system exhibited deviations from ideality. The authors ascribed this non-ideality to: (i) the loss of fluorophilic interaction between a highly-fluorinated anion ($NTf_2^-$) and another anion with no fluorine atoms ($MeSO_4^-$ or $Me_2PO_4^-$); (ii) the size difference between the ions; (iii) the influence of other interactions such as hydrogen bonding. They also reported that the [$C_4C_1$mim]$NTf_2$ – [Me-DBU]$MeSO_4$ ternary reciprocal system exhibited higher deviations from ideality ($V^E$=1.07 $cm^3.mol^{-1}$ as the highest value) than the other systems owing to the fact that more interactions are involved in the ternary reciprocal system than in the common-cation binary systems; thus involving larger values of the enthalpy and entropy of mixing.

Bharmoria et al. [76] observed at 298.15K a large positive deviation in $V^E$ with a maximum value of about 1.4 $cm^3.mol^{-1}$ for the [HEA]HCOO – [$C_4$mim]Cl ternary reciprocal system. As reported by these authors, this non-ideality is due to improper packing of the dissimilar ions in the liquid solution.

Annat et al. [77] reported a close-to-ideal behavior for the common-anion binary systems consisting of [$C_3$mpyrr]$NTf_2$ with [$C_4$mpyrr]$NTf_2$, [$C_6$mpyrr]$NTf_2$ or [$C_2$mim]$NTf_2$. They observed deviations from ideality for the [$C_3$mpyrr]dca - [$C_3$mpyrr]$NTf_2$ (highest measured $V^E$ value of about 0.5 $cm^3.mol^{-1}$) and the [$P_{6,6,6,14}$]$NTf_2$ - [$C_3$mpyrr]$NTf_2$ binary systems; the latter exhibited the highest deviation, with a $V^E$ value of about 1.5 $cm^3.mol^{-1}$.

Recently, Canongia Lopes et al. [78] investigated the influence of the hydrogen-bonding interaction on the excess molar volume of ammonium-based common-anion binary systems with $NO_3^-$ as the common anion. These authors considered two categories of binary systems: (i) binary systems composed of ethylammonium nitrate ([$N_{0002}$]$NO_3$), propylammonium nitrate ([$N_{0003}$]$NO_3$) and butylammonium nitrate ([$N_{0004}$]$NO_3$), where the cation of each component involves exactly three hydrogen bond donor groups; (ii) binary systems consisting of ethylammonium nitrate (with three hydrogen bond donor groups in the cation) and of various homologous ionic liquids with different numbers of hydrogen bond donor groups: diethylammonium nitrate ([$N_{0022}$]$NO_3$) (two hydrogen bond donors), triethylammonium nitrate ([$N_{0222}$]$NO_3$) (one hydrogen bond donor) and tetraethylammonium nitrate ([$N_{2222}$]$NO_3$) (no hydrogen bond donors). For category (i), Canongia Lopes et al. observed a quasi-ideal behavior with $V^E$ values lying between -0.1 and +0.1 $cm^3.mol^{-1}$. Category (ii) exhibited some deviations from ideality when the difference in the number of carbon atoms present in the cations increased or the number of hydrogen bond donors present in

the cation decreased. A large positive symmetric deviation from ideality (particularly for the $[N_{0222}]NO_3$ - $[N_{0002}]NO_3$ binary system, with a maximum $V^E$ value of about 3 $cm^3.mol^{-1}$) was reported for these binary systems. The authors concluded that interactions such as hydrogen bonding may affect the volumetric properties of ionic liquid mixtures in addition to the expected influence of an increase in the number of carbon atoms in the cation.

# CHAPTER 3 THERMODYNAMIC MODELS, VBT & DENSITY MODEL

This chapter first describes the thermodynamic models applied in this work to the liquid phase and relevant solid solutions. The Modified Quasichemical Model was used for the liquid phase, and the Compound Energy Formalism was employed for the solid solutions. Then, are briefly presented the principles of the Volume-based Thermodynamics from Glasser and Jenkins for the estimation of the missing thermodynamic properties of the pure ionic liquid compounds. The last section of this chapter presents a theoretical model for the density of multicomponent ionic liquid systems, based on the Modified Quasichemical Model.

## 3.1 Thermodynamic model for the liquid phase

In this work, the Modified Quasichemical Model (MQM) for short-range ordering [12-14] is used for the liquid phase. This model considers the distribution of cations and anions on the sites of two different sublattices (cationic and anionic), and each ion occupies exactly one site.

The Modified Quasichemical Model in the Pair Approximation (MQMPA) [12, 13] is used for the liquid phase of common-ion (common-cation or common-anion) systems. Let us consider first the $AX - AY$ (abbreviated as $A//X,Y$) common-cation binary system, where A is the common cation, and X and Y are two anions. In this case, the MQMPA takes into account short-range ordering (SRO) between second-nearest-neighbor (SNN) anion-anion pairs. The following pair-exchange reaction is considered:

$$(X-A-X)_{pair} + (Y-A-Y)_{pair} = 2(X-A-Y)_{pair}; \quad \Delta g_{A_2/XY} \tag{2}$$

where $\Delta g_{A_2/XY}$ is the Gibbs free energy change for the formation of 2 moles of $(X-A-Y)$ pairs. The Gibbs free energy of the binary liquid solution is given by:

$$G = \left(n_{A/X} g^{o}_{A/X} + n_{A/Y} g^{o}_{A/Y}\right) - T\Delta S^{config} + \left(\frac{n_{XY}}{2}\right) \Delta g_{A_2/XY} \tag{3}$$

where $n_{A/X}$ and $n_{A/Y}$ as well as $g^{o}_{A/X}$ and $g^{o}_{A/Y}$ are the number of moles and the molar Gibbs free energies of the AX and AY pure components, respectively; $n_{XY}$ is the number of moles of $(X-A-Y)$ pairs; and $\Delta S^{config}$ is the configurational entropy of mixing given by randomly distributing the $(X-A-X)$, $(Y-A-Y)$, and $(X-A-Y)$ pairs:

$$\Delta S^{\text{config}} = -R(n_X \ln x_X + n_Y \ln x_Y) - R\left[n_{XX}\ln\left(\frac{x_{XX}}{Y_X^2}\right) + n_{YY}\ln\left(\frac{x_{YY}}{Y_Y^2}\right) + n_{XY}\ln\left(\frac{x_{XY}}{2Y_X Y_Y}\right)\right] \quad (4)$$

In Equation (4), R is the gas constant; $x_X$ and $x_Y$ are the anionic site fractions; $Y_X$ and $Y_Y$ are the "coordination-equivalent" fractions; and $x_{XX}$, $x_{YY}$ and $x_{XY}$ are the SNN pair fractions. $Y_X$ and $Y_Y$ are respectively defined as:

$$Y_X = \frac{Z_X . x_X}{Z_X . x_X + Z_Y . x_Y} \quad (5)$$

$$Y_Y = \frac{Z_Y . x_Y}{Z_X . x_X + Z_Y . x_Y} \quad (6)$$

where $Z_X$ and $Z_Y$ are the second-nearest-neighbor coordination numbers of the anions $X$ and $Y$. In the present work, all SNN coordination numbers were set to 6.0. Therefore, $Y_X$ and $Y_Y$ reduce to the mole fractions $x_X$ and $x_Y$, respectively. It should be noted that Eq. (4) is an approximate equation since no exact expression is known for the entropy of this distribution in three dimensions. However, it is an exact expression for a one-dimensional lattice. For a liquid solution close to ideality, it can be shown that $x_{XX} \to Y_X^2$, $x_{YY} \to Y_Y^2$ and $x_{XY} \to 2Y_X Y_Y$. The second term in Equation (4) is then equal to zero, and the configurational entropy thus reduces to the Bragg-Williams (random-mixing) expression. For further details, one is referred to Refs. [12, 13].

The Gibbs free energy change $\Delta g_{A_2/XY}$ is a model parameter, which is expanded in terms of the pair fractions as:

$$\Delta g_{A_2/XY} = \Delta g^{o}_{A_2/XY} + \sum_{i\geq 1} g^{i0}_{A_2/XY} . x^{i}_{XX} + \sum_{j\geq 1} g^{0j}_{A_2/XY} . x^{j}_{YY} \quad (7)$$

where $\Delta g^{o}_{A_2/XY}$, $g^{i0}_{A_2/XY}$ and $g^{0j}_{A_2/XY}$ are empirical coefficients that can be functions of temperature. As $\Delta g_{A_2/XY}$ becomes progressively more negative, reaction (2) is shifted to the right, $(X - A - Y)$ pairs predominate and SNN short-range ordering results.

Let us now consider the $AX - AY - AZ$ (abbreviated as $A//X, Y, Z$) common-cation ternary system, where A is the common cation, and X, Y, and Z are three anions. The Gibbs free energy of the $A//X, Y, Z$ common-cation ternary liquid is given by:

$$G = \left(n_{A/X}g^{o}_{A/X} + n_{A/Y}g^{o}_{A/Y} + n_{A/Z}g^{o}_{A/Z}\right) - T\Delta S^{config} + \left[\left(\frac{n_{XY}}{2}\right)\Delta g_{A_2/XY} + \left(\frac{n_{XZ}}{2}\right)\Delta g_{A_2/XZ} + \left(\frac{n_{YZ}}{2}\right)\Delta g_{A_2/YZ}\right] \quad (8)$$

where $n_{A/X}$, $n_{A/Y}$ and $n_{A/Z}$ as well as $g^{o}_{A/X}$, $g^{o}_{A/Y}$ and $g^{o}_{A/Z}$ are the number of moles and the molar Gibbs free energies of the AX, AY, and AZ pure components, respectively; $n_{XY}$, $n_{XZ}$ and $n_{YZ}$ are the number of moles of $(X-A-Y)$, $(X-A-Z)$, and $(Y-A-Z)$ pairs, respectively; $\Delta g_{A_2/XY}$, $\Delta g_{A_2/XZ}$ and $\Delta g_{A_2/YZ}$ are the Gibbs free energy changes for the formation of 2 moles of $(X-A-Y)$, $(X-A-Z)$, and $(Y-A-Z)$ pairs, respectively, and $\Delta S^{config}$ is the configurational entropy of mixing given by randomly distributing the SNN anion-anion pairs:

$$\Delta S^{config} = -R(n_X \ln x_X + n_Y \ln x_Y + n_Z \ln x_Z) - R\left[n_{XX}\ln\left(\frac{x_{XX}}{Y_X^2}\right) + n_{YY}\ln\left(\frac{x_{YY}}{Y_Y^2}\right) + n_{ZZ}\ln\left(\frac{x_{ZZ}}{Y_Z^2}\right) + n_{XY}\ln\left(\frac{x_{XY}}{2Y_XY_Y}\right) + n_{XZ}\ln\left(\frac{x_{XZ}}{2Y_XY_Z}\right) + n_{YZ}\ln\left(\frac{x_{YZ}}{2Y_YY_Z}\right)\right] \quad (9)$$

In Equation (9), $x_X$, $x_Y$ and $x_Z$ are the anionic site fractions; $Y_X$, $Y_Y$ and $Y_Z$ are the "coordination-equivalent" fractions; and $x_{XX}$, $x_{YY}$, $x_{ZZ}$, $x_{XY}$, $x_{XZ}$ and $x_{YZ}$ are the SNN pair fractions.

The Gibbs free energy of the common-cation ternary liquid is estimated from the optimized binary parameters using a Kohler-like (i.e. symmetric model) or a Kohler-Toop-like (i.e. asymmetric model) interpolation method [25].

In a symmetric model (figure 3.1(a)), the three components are treated in the same way. $\Delta g_{A_2/XY}$ in the common-cation ternary liquid is given by:

$$\Delta g_{A_2/XY} = \Delta g^{o}_{A_2/XY} + \sum_{(i+j)\geq 1} g^{ij}_{A_2/XY}\left(\frac{x_{XX}}{x_{XX}+x_{XY}+x_{YY}}\right)^{i}\left(\frac{x_{YY}}{x_{XX}+x_{XY}+x_{YY}}\right)^{j} + \sum_{\substack{k\geq 1\\ i\geq 0\\ j\geq 0}} g^{ijk}_{A_2/XY(Z)}\left(\frac{x_{XX}}{x_{XX}+x_{XY}+x_{YY}}\right)^{i}\left(\frac{x_{YY}}{x_{XX}+x_{XY}+x_{YY}}\right)^{j} Y_Z^{k} \quad (10)$$

where the second summation in Equation (10) consists of a ternary term which is zero in the $A//X,Y$ binary subsystem, and which gives the effect of the presence of component $AZ$ upon the pair

formation energy $\Delta g_{A_2/XY}$. The empirical ternary coefficient $g^{ijk}_{A_2/XY(Z)}$ is obtained by optimization of experimental ternary data. As $\Delta g_{A_2/XY}$, $\Delta g_{A_2/XZ}$ and $\Delta g_{A_2/YZ}$ become small, the solution approaches ideality, and $x_{XX} \to Y_X^2$, $x_{YY} \to Y_Y^2$, and $x_{XY} \to 2Y_XY_Y$. In this case, $\left(\frac{x_{XX}}{x_{XX}+x_{XY}+x_{YY}}\right) \to \left(\frac{Y_X}{Y_X+Y_Y}\right)^2$ and $\left(\frac{x_{YY}}{x_{XX}+x_{XY}+x_{YY}}\right) \to \left(\frac{Y_Y}{Y_X+Y_Y}\right)^2$. Equation (10) then approaches the Kohler equation (Equation (20) in reference [13]) for symmetric ternary systems. The first term on the right-hand side of Equation (10) is constant along the line $AZ - a$ in figure 3.1(a) and is equal to $\Delta g_{A_2/XY}$ in the $A//X,Y$ binary system at point $a$ (where $Y_X + Y_Y = 1$). That is, it is assumed that the binary $X - A - Y$ pair interaction energy is constant at a constant $\frac{Y_X}{Y_Y}$ ratio. Equations similar to Equation (10) give $\Delta g_{A_2/YZ}$ and $\Delta g_{A_2/XZ}$, with the binary terms equal to their values at points $b$ and $c$, respectively, in figure 3.1(a).

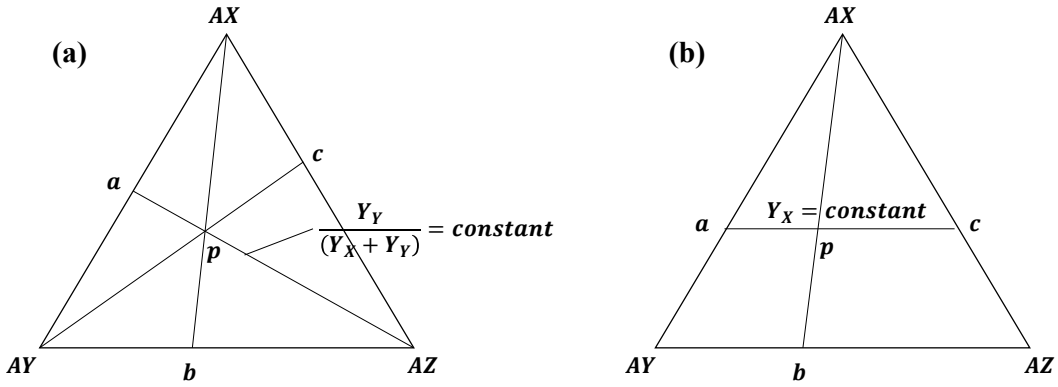


Figure 3.1: Symmetric (left) and asymmetric (right) models for interpolation from binary to ternary solutions.

In an asymmetric model (figure 3.1(b)), one component ($AX$) is treated differently than the other two components. $\Delta g_{A_2/XY}$ in the common-cation ternary liquid is given by:

$$\Delta g_{A_2/XY} = \Delta g^{o}_{A_2/XY} + \sum_{(i+j)\geq 1} g^{ij}_{A_2/XY} x_{XX}^{i} (x_{YY} + x_{YZ} + x_{ZZ})^{j} + \sum_{\substack{k\geq 1 \\ i\geq 0 \\ j\geq 0}} g^{ijk}_{A_2/XY(Z)} x_{XX}^{i} (x_{YY} + x_{YZ} + x_{ZZ})^{j} \left(\frac{Y_Z}{Y_Y + Y_Z}\right)^{k} \quad (11)$$

In the limit of ideality, $x_{XX} \to Y_X^2$ and $(x_{YY} + x_{YZ} + x_{ZZ}) \to (Y_Y + Y_Z)^2 = (1 - Y_X)^2$. Equation (11) then approaches the Kohler-Toop equation (Equation (21) in reference [13]) for asymmetric ternary

systems. The first term on the right-hand side of Equation (11) is constant along the line $ac$ in figure 3.1(b) and is equal to $\Delta g_{A_2/XY}$ in the $A//X,Y$ binary system at point $a$. An equation similar to Equation (11) gives $\Delta g_{A_2/XZ}$, while $\Delta g_{A_2/YZ}$ is given by an equation similar to Equation (10).

The Modified Quasichemical Model in the Quadruplet Approximation (MQMQA) [14] is used for the liquid phase of a ternary reciprocal system $AX - AY - BX - BY$ (abbreviated as $A, B \,||\, X, Y$). The $[C_2py]$, $[C_4py]$ || Cl, Br system is discussed in Chapter 4. This model considers simultaneously first-nearest-neighbor (cation-anion) and second-nearest-neighbor (cation-cation and anion-anion) short-range order. A quadruplet consists of two second-nearest-neighbor cations and two second-nearest-neighbor anions, which are mutual first-nearest-neighbors. Each quadruplet has a Gibbs free energy. The Gibbs free energy of the $A, B \,||\, X, Y$ ternary reciprocal liquid is given by:

$$G = \sum n_{ij/kl} g_{ij/kl} - T\Delta S^{config} \tag{12}$$

where $n_{ij/kl}$ denotes the number of moles of the unary, binary, and reciprocal quadruplets; $g_{ij/kl}$ denotes the Gibbs free energy of the quadruplets; and $\Delta S^{config}$ is the configurational entropy of mixing. In particular, there are four binary quadruplets ($A_2/XY, B_2/XY, AB/X_2, and\ AB/Y_2$) and each Gibbs free energy depends on the corresponding model parameter for the associated common-ion binary subsystem (for instance, $\Delta g_{A_2/XY}$ for the $A_2/XY$ quadruplet). $\Delta S^{config}$ corresponds to the distribution of all quadruplets over "quadruplet sites" considering the overlapping of FNN and SNN pairs. No exact mathematical expression is known for $\Delta S^{config}$, and the entropy of configuration has been approximated by Pelton et al. [14] and then improved [79]. The extent of FNN short-range ordering is related to the Gibbs free energy change for the following exchange reaction:

$$AX + BY = AY + BX\,;\ \Delta g^{exchange}_{AB/XY} \tag{13}$$

$\Delta g^{exchange}_{AB/XY}$ only depends on the Gibbs free energies of the four pure liquid salts AX, $BY$, AY, and BX. If $\Delta g^{exchange}_{AB/XY}$ is negative, then $A - Y$ and $B - X$ FNN pairs predominate.

More details about the MQMQA are given in Chapter 4 (section 4.3).

## 3.2 Thermodynamic model for the solid solutions

The solid solutions relevant for the present work are: the Cl-rich [$C_4$mpyrr](Cl, [Br]) solid solution, the Br-rich [$C_4$mpyrr](Br, [Cl]) solid solution, the [$C_2$py]Cl – [$C_2$py]Br solid solution, the [$C_4$py]Cl-[$C_4$py]Br solid solution, the [$C_3$mpip]$PF_6$ – [$C_3$mpyrr]$PF_6$ low-temperature solid solution, the [$C_3$mpip]$PF_6$ – [$C_3$mpyrr]$PF_6$ intermediate-temperature solid solution, and the [$C_3$mpip]$PF_6$ – [$C_3$mpyrr]$PF_6$ high-temperature solid solution. The Compound Energy Formalism (CEF) is used to model these solid solutions. More details are given in Chapter 4 (section 4.4).

## 3.3 Volume-based Thermodynamics (VBT)

To model the phase diagram of a common-ion system with no existing intermediate compound, only the molar Gibbs free energies of fusion of the pure compounds need to be known. On the other hand, for a $A, B//X, Y$ ternary reciprocal system, the standard thermodynamic properties ($\Delta H^o_{298.15K}$, $S^o_{298.15K}$, and $C_p(T)$) of all four pure compounds must be known or estimated, so that the Gibbs free energy change for the exchange reaction (13) can be assessed. The molar Gibbs free energy of a stoichiometric phase is given by:

$$G_T = \Delta H^o_{298.15K} + \int_{298.15K}^{T} C_p dT - T\left( S^o_{298.15K} + \int_{298.15K}^{T} \frac{C_p}{T} dT \right) \qquad (14)$$

where $\Delta H^o_{298.15K}$ is the standard molar enthalpy at 298.15K (relative to the elements in their stable standard states at 298.15K), $S^o_{298.15K}$ is the standard absolute (third law) molar entropy at 298.15K, and $C_p$ is the molar heat capacity and is a function of the absolute temperature T (K). These quantities thus need to be known for a stoichiometric phase. The limited temperature range of ionic liquid compounds (below T=373.15K, and often below T=298.15K) indicates that $\Delta H^o_{298.15K}$ is by far the most important thermodynamic quantity for these compounds. No compilation tables are currently available for the thermodynamic properties of ionic liquid compounds. It is thus desirable to assess these missing quantities by methods of estimation such as the Volume-based Thermodynamics (VBT) from Glasser and Jenkins [28-33]. This method requires a knowledge of the molecular volume $\nu_m$ (expressed in $nm^3$). The latter can be derived from crystallographic data for the pure solid phases, and from density measurements (using a densimeter) for the pure liquid phases. As emphasized by Jenkins [33], the VBT only takes into account long-range Coulombic

interactions, and short-range interactions such as van der Waals and hydrogen bonding are not yet considered.

Strechan et al. [80] correlated the heat capacity ($C_p$) with the molecular volume ($\nu_m$) at 298.15K for various methyl-imidazolium-based ionic liquids. These authors derived the following linear regression equation:

$$C_p(298.15K)/(J.mol^{-1}.K^{-1}) = 1053.9\nu_m + 37.0 \quad (15)$$

where $\nu_m$ is expressed in $nm^3$. The standard error of a prediction was reported as ±16 $J.mol^{-1}.K^{-1}$. Recently, Robelin [24] tested this equation on various methyl-imidazolium-based ionic liquids. This author reported a relative shift usually lower than 5% between the calculations and the measurements. In the present work, we used Eq. (15) for the estimation of $C_p$ of methyl-imidazolium-based ionic liquids (see Chapter 5). A new $C_p$ correlation from experimental data ($C_p$ and density) was derived for pyridinium-based ionic liquids (see section 4.6.1 in Chapter 4).

Glasser [30] proposed a linear regression equation for the standard absolute entropy ($S^o_{298.15K}$) of ionic liquids. The proposed expression is an average of two linear regression equations, one valid for anhydrous ionic solids [29] and another one valid for organic liquids [81]. This equation is presented in Chapter 4 (section 4.6.2).

Finally, using a thermodynamic cycle, $\Delta H^o_{298.15K}$ for a solid ionic liquid compound can be derived from the standard enthalpies of formation of the cation and of the anion in the gas state, and from the lattice enthalpy. Details are given in Chapter 4 (section 4.6.3).

## 3.4 Density model

A theoretical model based on the Modified Quasichemical Model has been successfully applied to model the density of multicomponent inorganic molten salts such as the NaCl - KCl - $MgCl_2$ - $CaCl_2$ and NaF - $AlF_3$ - $CaF_2$ - $Al_2O_3$ electrolytes. This model is used in the present work for the density of common-ion (common-cation and common-anion) ionic liquid systems. Let us consider the $A//X,Y,Z$ common-cation ternary liquid. The volume V and density ρ of the solution are defined respectively as:

$$V = \left(\frac{\partial G}{\partial P}\right)_{T,n_{A/X},n_{A/Y},n_{A/Z}} \quad (16)$$

$$\rho = \frac{m}{V} \tag{17}$$

where G is the Gibbs free energy of the solution (Eq. (8)) and m is the mass of the solution. Therefore, the volume and the density of the solution can be modeled by introducing pressure-dependent parameters in the Gibbs free energy of the solution.

The molar Gibbs free energy of the pure liquid salt AX can be written as:

$$g^{o}_{A/X}(T,P) = g^{o}_{A/X}(T,1\ \text{bar}) + \int_{1}^{P} V_m^{A/X}(T).dP = g^{o}_{A/X}(T,1\ \text{bar}) + V_m^{A/X}(T).(P-1) \tag{18}$$

where $V_m^{A/X}(T)$ is the molar volume of pure liquid AX at temperature T. It is given by:

$$V_m^{A/X}(T) = V_m^{A/X}(T_{ref}).\exp\left(\int_{T_{ref}}^{T} \alpha(T).dT\right) \tag{19}$$

where $T_{ref}$ and $\alpha(T)$ are a reference temperature (arbitrarily selected) and the thermal expansion, respectively. The latter can be obtained by fitting the experimental volumetric data available for the AX pure liquid salt using the following function of temperature:

$$\alpha(T) = a + bT + cT^{-1} + dT^{-2} \tag{20}$$

where a, b, c and d are constant parameters. From Equations (8, 16, 18), it follows that:

$$\begin{aligned} V = {} & \left(n_{A/X}.V_m^{A/X}(T) + n_{A/Y}.V_m^{A/Y}(T) + n_{A/Z}.V_m^{A/Z}(T)\right) \\ & + \left[\left(\frac{n_{XY}}{2}\right).\left(\frac{\partial \Delta g_{A_2/XY}}{\partial P}\right)_{T,n_{A/X},n_{A/Y},n_{A/Z}}\right. \\ & + \left(\frac{n_{XZ}}{2}\right).\left(\frac{\partial \Delta g_{A_2/XZ}}{\partial P}\right)_{T,n_{A/X},n_{A/Y},n_{A/Z}} \\ & \left. + \left(\frac{n_{YZ}}{2}\right).\left(\frac{\partial \Delta g_{A_2/YZ}}{\partial P}\right)_{T,n_{A/X},n_{A/Y},n_{A/Z}}\right] \end{aligned} \tag{21}$$

The second term in Equation (21) represents the excess molar volume of the common-cation ternary liquid. If the pressure dependent parameters in $\Delta g_{A_2/XY}$, $\Delta g_{A_2/XZ}$ and $\Delta g_{A_2/YZ}$ are all zero,

the melt has an ideal volumetric behavior (i.e. the volumes of the pure liquid salts are simply additive).

For a given common-cation binary liquid such as $A_2/XY$, $\Delta g_{A_2/XY}$ is expanded as a polynomial in the SNN anion-anion pair fractions $x_{XX}$ and $x_{YY}$ (P in bar):

$$\begin{aligned}\Delta g_{A_2/XY} = &\left[\Delta g^{o}_{A_2/XY} + \beta^{o}_{A_2/XY}.(P-1)\right] \\ &+ \sum_{i\geq 1}\left[g^{i0}_{A_2/XY} + \beta^{i0}_{A_2/XY}.(P-1)\right].(x_{XX})^{i} \\ &+ \sum_{j\geq 1}\left[g^{0j}_{A_2/XY} + \beta^{0j}_{A_2/XY}.(P-1)\right].(x_{YY})^{j}\end{aligned} \tag{22}$$

where $\Delta g^{o}_{A_2/XY}$, $g^{i0}_{A_2/XY}$ and $g^{0j}_{A_2/XY}$ represent the parameters of the thermodynamic model (at 1 bar) that may be functions of temperature and that were obtained by least-squares fitting of the experimental thermodynamic properties and phase equilibria available for the $A//X,Y$ common-cation binary system; and $\beta^{o}_{A_2/XY}$, $\beta^{i0}_{A_2/XY}$ and $\beta^{0j}_{A_2/XY}$ are the parameters of the density model that can be functions of temperature and that are obtained by least-squares fitting of the experimental density data available for the $A//X,Y$ common-cation binary liquid. Therefore, the Gibbs free energy change $\Delta g_{A_2/XY}$ now consists of two different terms: one (independent of the hydrostatic pressure) corresponds to the thermodynamic model, and another one (pressure-dependent) is related to the density model. For the latter term, the notation $\Delta g^{P}_{A_2/XY}$ is used. That is:

$$\Delta g^{P}_{A_2/XY} = \left[\beta^{o}_{A_2/XY} + \sum_{i\geq 1}\beta^{i0}_{A_2/XY}.(x_{XX})^{i} + \sum_{j\geq 1}\beta^{0j}_{A_2/XY}.(x_{YY})^{j}\right].(P-1) \tag{23}$$

At 1 bar total pressure, $\Delta g^{P}_{A_2/XY}$ is equal to zero. As discussed previously [16], the parameters $\beta^{o}_{A_2/XY}$, $\beta^{i0}_{A_2/XY}$ and $\beta^{0j}_{A_2/XY}$ in Equations (22) and (23) are always small so that, at given temperature and composition and for pressures not too high (i.e. typically less than 100 bar), the calculated equilibrium anion-anion pair configuration is virtually identical to the one calculated from the (previously developed) thermodynamic model.

Therefore, both the density and the thermodynamic properties of the common-cation ternary liquid can be predicted from the binary excess Gibbs free energy parameters using the standard Kohler-

like and Kohler-Toop-like interpolation methods described previously (section 3.1). Ternary pressure-dependent parameters may be introduced in order to best reproduce the density data available for the ternary liquid. However, such parameters were not used in the present work owing to the lack of ternary density data.

# CHAPTER 4 ARTICLE 1: SOLID-LIQUID EQUILIBRIA FOR A PYRROLIDINIUM-BASED COMMON-CATION TERNARY IONIC LIQUID SYSTEM, AND FOR A PYRIDINIUM-BASED TERNARY RECIPROCAL IONIC LIQUID SYSTEM : EXPERIMENTAL STUDY AND THERMODYNAMIC MODEL

**Meysam Mirarabrazi[1], Olga Stolarska[2,3], Marcin Smiglak[2], Christian Robelin[1,*]**

Article submitted to *Physical Chemistry Chemical Physics*

[1] Centre for Research in Computational Thermochemistry (CRCT), Department of Chemical Engineering, École Polytechnique, C.P. 6079, Succursale "Downtown", Montreal, Quebec, H3C 3A7, Canada
[2] Poznan Science and Technology Park, Adam Mickiewicz University Foundation, Poznań, Poland
[3]Faculty of Chemistry, Adam Mickiewicz University, Poznań, Poland
[*]Corresponding author (E-mail: christian.robelin@polymtl.ca)

## Abstract

The present paper describes an experimental study and a thermodynamic model for the phase diagrams of the common-cation ternary system [$C_4$mpyrr]Cl - [$C_4$mpyrr]Br - [$C_4$mpyrr]$BF_4$ (where [$C_4$mpyrr] refers to 1-butyl-1-methyl-pyrrolidinium) and of the ternary reciprocal system [$C_2$py], [$C_4$py] || Cl, Br (where [$C_n$py] refers to 1-alkyl-pyridinium). Phase equilibria were measured by Differential Scanning Calorimetry (DSC) for two isoplethal sections in the common-cation pyrrolidinium-based ternary system. Phase diagram measurements were recently published for the four common-ion binary subsystems and the two diagonal sections in the pyridinium-based ternary reciprocal system. In each case, the Modified Quasichemical Model was used to model the liquid solution, and the Compound Energy Formalism was used for the relevant solid solutions. For the ternary reciprocal system, the missing thermodynamic properties of the pure compounds were assessed using the Volume-based Thermodynamics (VBT) from Glasser and Jenkins, making it possible to estimate the exchange Gibbs free energy for the reaction [$C_2$py]Br (liquid) + [$C_4$py]Cl (liquid) = [$C_2$py]Cl (liquid) + [$C_4$py]Br (liquid). The experimental diagonal sections [$C_4$py]Br - [$C_2$py]Cl and [$C_4$py]Cl - [$C_2$py]Br were satisfactorily reproduced using solely the optimized model parameters for the four common-ion binary subsystems.

**Keywords:** Ionic liquid mixtures; Pyrrolidinium-based ionic liquids; Pyridinium-based ionic liquids; Thermodynamic modeling; Volume-based Thermodynamics

## 4.1 Introduction

Ionic liquids (ILs) are defined as a class of salts generally composed of a large asymmetric organic cation and an organic or inorganic anion [82], with a melting temperature below 100°C [83]. They possess unique physico-chemical properties such as a very low vapor pressure (i.e. a low volatility), and a high chemical and thermal stability over a broad temperature range (-40 to 200°C) [3]. Over the recent years, ionic liquids have been considered for use in a variety of fields including analytics [4], chemical processing [5], solvents and catalysts [6], electrochemistry [7], biomass processing [8], etc. As reported by Stark and Seddon [9], at a zeroth order approximation, the cation of an ionic liquid controls its physical properties (including density, viscosity, and temperature of fusion), while the anion governs the chemistry and reactivity. Therefore, fine-tuning the properties of ionic liquids may be required to target a specific application.

Over the past several years, a large and growing body of studies has focused on the design of single ionic liquids with "tailor-made" properties. A possible technique to modify the properties of ionic liquids is to add other substances such as molecular solvents, that are broadly accessible and whose properties have been widely investigated. Even though molecular solvents may decrease the viscosity of ionic liquids, they can lead to an increased volatility and consequently to a reduced thermal stability. The combination of single ionic liquids (IL-IL mixtures) may be an interesting alternative. Throughout this paper, the term "ionic liquid mixtures/systems" will refer to the combination of one single ionic liquid with one or more ionic liquid.

So far, there have been relatively few studies dealing with ionic liquid mixtures. Niedermeyer et al. [2] performed a comprehensive review of the mixtures of ionic liquids. These authors investigated thermodynamics, physical and chemical properties, and applications of ionic liquid mixtures. To the best of our knowledge, ternary ionic liquid mixtures have received very little attention until now, thus motivating the present study. As pointed out by Plechkova and Seddon [10], ionic liquid ternary mixtures may be worth considering, where the chemistry of the system would be controlled by the first component, the physical properties (such as density and viscosity) of the system would be adjusted by the second component, and the global cost of the system would be lowered (through a dilution of the other two components) by adding a third component, cheap and chemically inert. The present article describes an experimental study and a thermodynamic model for the phase diagrams of the common-cation ternary system [$C_4$mpyrr]Cl - [$C_4$mpyrr]Br -

[$C_4$mpyrr]$BF_4$ (where [$C_4$mpyrr] refers to 1-butyl-1-methyl-pyrrolidinium) and of the ternary reciprocal system [$C_2$py]Cl - [$C_2$py]Br - [$C_4$py]Cl - [$C_4$py]Br (where [$C_n$py] refers to 1-alkyl-pyridinium) (A ternary reciprocal system is composed of two cations and two anions.). In particular, the minimum liquidus temperature in these two multicomponent ionic liquid systems can be calculated. As part of the present work, a literature review of the phase diagram measurements for ionic liquid systems was conducted (see tables 4.1 to 4.3). Table 4.1 gives an overview of the phase diagram measurements for ionic liquid systems with organic cations. These are almost exclusively binary common-ion (common-cation or common-anion) systems, and the main experimental technique used was Differential Scanning Calorimetry (DSC). As seen in table 4.1, most of these systems are simple eutectic systems; three systems display a eutectic behavior with two terminal solid solutions ([$C_3$mpyrr][$NTf_2$] - [$C_3$mpyrr][FSI], [$C_4$mpyrr][$N(C_4F_9SO_2)_2$] - [$C_4$mpyrr][$C_4F_9SO_3$], and [$C_2$mpyrr][$N(C_4F_9SO_2)_2$] - [$C_2$mpyrr][$CF_3SO_3$]); two systems exhibit an extensive solid solution over the entire composition range ([$C_3$mpyrr][$PF_6$] - [$C_3$mpip][$PF_6$] and [$C_2$mpyrr][$N(C_4F_9SO_2)_2$] - [$C_4$mpyrr][$N(C_4F_9SO_2)_2$]); and one system involves the formation of an intermediate compound ([$N_{1112(OH)}$][$C_4F_9SO_3$] - [$C_4$mpyrr][$C_4F_9SO_3$]). From the thermodynamic modeling viewpoint, Kick et al. [66] modeled the phase diagram of the [$C_2$mim]Cl – [$C_4$mim]Cl common-anion binary system using the Schöder-Van-Laar equation in its simplest form assuming an ideal liquid. Maximo et al. [35] modeled the phase diagrams of nine [$PF_6$]-based binary ionic liquid systems. These authors reported that most of the binary systems investigated are simple eutectic systems with a liquid close to ideal, while one particular binary system ([$C_3$mpyrr][$PF_6$] – [$C_3$mpip][$PF_6$]) displays an extensive solid solution confirmed by powder X-ray diffractometry of the solid phase. Recently, Teles et al. [67] measured the phase diagrams of four binary systems of fluorinated ionic liquids, and modeled three of them. They reported a quasi-ideal eutectic behavior with the presence of two terminal solid solutions for the [$C_4$mpyrr][$N(C_4F_9SO_2)_2$] - [$C_4$mpyrr][$C_4F_9SO_3$] and [$C_2$mpyrr][$N(C_4F_9SO_2)_2$] - [$C_2$mpyrr][$CF_3SO_3$] binary systems. Also, these authors observed a continuous solid solution behavior (confirmed by a X-ray diffraction study of the solid phase) for the [$C_2$mpyrr][$N(C_4F_9SO_2)_2$] - [$C_4$mpyrr][$N(C_4F_9SO_2)_2$] binary common-anion system. Robelin [24] modeled the thermodynamic properties (including the phase diagram) of a binary system consisting of one ionic liquid ([$C_2$mim]Cl) and one inorganic compound ($AlCl_3$) using the Modified Quasichemical Model. Using experimental data from ref. [84], the author calculated two binary eutectics ($T_{eu1}$=231K, $X_{eu1}$=40.1 mol% $AlCl_3$; $T_{eu2}$=166K, $X_{eu2}$=66.2 mol%

$AlCl_3$) along with the formation of the intermediate compound $[C_2mim]AlCl_4$. Robelin [24] reported that this system exhibits extensive short-range ordering owing to the size and charge differences between the inorganic $Al^{3+}$ and organic $[C_2mim]^+$ cations.

The phase diagrams of binary systems of salts with ions commonly used for the preparation of ionic liquids have also been investigated (see table 4.2). These are exclusively common-anion systems. These systems may be simple eutectic systems or may exhibit an intermediate compound or an extensive solid solution over the entire composition range. Robelin [24] modeled the phase diagrams of three binary systems consisting of alkali bis(fluorosulfonyl)amides M[FSA] (with M=Li, K, Cs) using the experimental data reported in ref. [21].

Finally, an overview of the phase diagram measurements available in the literature for ternary systems of salts with ions commonly used for the preparation of ionic liquids is given in table 4.3. These are common-anion ternary systems with different alkali metals. Studies of ionic liquid ternary systems involving organic cations are still lacking. Robelin [24] modeled the phase diagram of the Li[FSA] - K[FSA] - Cs[FSA] system. This author calculated a ternary eutectic ($T_{eu}$=315K with $X_{Li[FSA]}$=0.31, $X_{K[FSA]}$= 0.33, $X_{Cs[FSA]}$=0.36) very close to the experimental eutectic reported in the literature [21, 23]. In another study, Gbassi and Robelin [85] modeled the phase diagram of the $Li[CH_3COO]$ - $K[CH_3COO]$ - $Cs[CH_3COO]$ system. Although the three pure salts have relatively high melting temperatures, a ternary eutectic was calculated at T=368K.

In the present work, the liquid phase of the two multicomponent ionic liquid systems investigated was modeled with the Modified Quasichemical Model for short-range ordering [12-14]. This model has been applied successfully to various inorganic salt systems such as the NaF - $AlF_3$ - $CaF_2$ - $Al_2O_3$ base electrolyte [18] (used to produce aluminum) and fertilizer systems [19, 20]. The liquid model considers the distribution of cations and anions on the sites of two different sublattices, and each ion occupies exactly one site. As mentioned previously [24], this model may have to be modified since the cations in ionic liquid systems are large and may involve long alkyl chains. In particular, it was shown [24] that the current thermodynamic model would fail to reproduce the experimental $[C_2mim]AlCl_4$-$NaAlCl_4$ section in the NaCl - $[C_2mim]Cl$ - $AlCl_3$ phase diagram due to the large size difference between the inorganic $Al^{3+}$ and organic $[C_2mim]^+$ cations (where $[C_2mim]$ refers to 1-ethyl-3-methyl-imidazolium). A large ion such as $[C_2mim]^+$ can occupy several sites on the cationic sublattice. Also, the Modified Quasichemical Model does not yet take

into account specific short-range interactions such as hydrogen bonding, van der Waals and π - π stacking interactions [24]. Despite the fact that coulombic forces are the dominating interaction between the cations and anions of ionic liquids, relatively weak interactions such as hydrogen bonding may affect their physicochemical properties such as melting point, viscosity, etc. [86]. Previous studies have provided evidence for the existence of hydrogen bonds in ionic liquids (mainly imidazolium-based) [87-91]. In particular, it has been found that pyrrolidinium- and pyridinium-based ionic liquids exhibit weaker hydrogen bonding interactions than imidazolium-based compounds [92]. This is due to the fact that the interaction between an anion and a H atom (C-H) on the imidazolium ring makes a stronger H-bond than that between an anion and a H atom (N-$CH_3$) on a non-imidazolium cation.

As explained in section 4.5.1, to model the phase diagram of a common-ion system with no existing intermediate compounds such as [$C_4$mpyrr]Cl - [$C_4$mpyrr]Br - [$C_4$mpyrr]$BF_4$, only the molar Gibbs energies of fusion of the pure compounds need to be known. On the other hand, for a ternary reciprocal system such as [$C_2$py], [$C_4$py] || Cl, Br, the standard thermodynamic properties ($\Delta H^o_{298.15K}$, $S^o_{298.15K}$, and $C_p(T)$) of all four pure compounds must be known or estimated, so that the Gibbs free energy change for the exchange reaction [$C_2$py]Br (liquid) + [$C_4$py]Cl (liquid) = [$C_2$py]Cl (liquid) + [$C_4$py]Br (liquid) can be assessed. Thermodynamic tables such as JANAF [93] and Barin [94] provide recommended values of the standard thermodynamic properties of numerous inorganic compounds. However, no such compilation tables are currently available for ionic liquid compounds. Therefore, methods of estimation such as the Volume-based Thermodynamics (VBT) from Glasser and Jenkins [28-33] need to be used to estimate the missing thermodynamic data for the pure ionic liquid compounds.

The present paper is organised as follows: section 4.2 describes the experimental procedure for the preparation of the various mixtures and for the phase diagram measurements by DSC in the [$C_4$mpyrr]Cl - [$C_4$mpyrr]Br - [$C_4$mpyrr]$BF_4$ ternary system. Sections 4.3 and 4.4 are devoted to the thermodynamic models used for the liquid phase and the relevant solid solutions, respectively. Section 4.5 presents the thermodynamic model developed for the common-cation ternary system [$C_4$mpyrr]Cl - [$C_4$mpyrr]Br - [$C_4$mpyrr]$BF_4$. Section 4.6 briefly describes the principles of the Volume-based Thermodynamics (VBT) with focus on the pyridinium-based compounds of the ternary reciprocal system [$C_2$py], [$C_4$py] || Cl, Br. Finally, section 4.7 is devoted to the thermodynamic model developed for the latter reciprocal system.

Table 4.1: Literature review of the phase diagram measurements for ionic liquid systems with organic cations ($T_{fusion}$: temperature of fusion; $T_g$: glass transition temperature; $T_{eu}$: eutectic temperature; $X_{eu}$: eutectic liquid composition)

| System | Component 1 *($T_{fusion}$ [K])* | Component 2 *($T_{fusion}$ [K])* | Type of phase diagram | Reference |
|---|---|---|---|---|
| Common anion | [$C_2$mim][$PF_6$] *(334)* | [$C_2$pz][$PF_6$] *(352)* | Simple eutectic ($X_{eu}$=47 mol% [$C_2$mim][$PF_6$]; $T_{eu}$=296.15K) | [95] |
| | [$C_3$mpyrr][$NTf_2$] *(282)* | [$C_4$mpyrr][$NTf_2$] *(256)* | Simple eutectic ($X_{eu}$=50 mol% [$C_4$mpyrr][$NTf_2$]; $T_{eu}$=248.15K) | [77] |
| | [$C_3$mpyrr][$NTf_2$] *(282)* | [$C_6$mpyrr][$NTf_2$] *(274)* | Not specified (measurements performed at a few compositions) | |
| | [$C_3$mpyrr][$NTf_2$] *(282)* | [$C_2$mim][$NTf_2$] *(274)* | | |
| | [$C_3$mpyrr][$NTf_2$] *(282)* | [$P_{6,6,6,14}$][$NTf_2$] *($T_g$=198)* | | |
| | [$C_2$mim][Cl] *(361)* | [$C_4$mim][Cl] *(342)* | Simple eutectic ($X_{eu}$=50 mol% [$C_2$mim][Cl]; $T_{eu}$=315K) | [66] |
| | [$C_2$mim][Cl] *(361)* | [$C_4$mim][Cl] *(338)* | Simple eutectic ($X_{eu}$=51.3 mol% [$C_2$mim][Cl]; $T_{eu}$=319K) | [73] |
| | [$C_3$mim][$PF_6$] *(312)* | [$C_3$mpy][$PF_6$] *(312)* | Simple eutectic | [35] |
| | [$C_3$mim][$PF_6$] *(312)* | [$C_3$mpyrr][$PF_6$] *(383)* | Simple eutectic | |
| | [$C_3$mim][$PF_6$] *(312)* | [$C_3$mpip][$PF_6$] *(368)* | Simple eutectic | |
| | [$C_3$mpy][$PF_6$] *(312)* | [$C_3$mpip][$PF_6$] *(368)* | Simple eutectic | |
| | [$C_3$mpy][$PF_6$] *(312)* | [$C_3$mpyrr][$PF_6$] *(383)* | Simple eutectic | |
| | [$C_3$mpyrr][$PF_6$] *(383)* | [$C_3$mpip][$PF_6$] *(368)* | Complete solid solution | |
| | [$C_3$mim][$PF_6$] *(312)* | [$C_{12}$mim][$PF_6$] *(326)* | Simple eutectic | |
| | [$C_3$mim][$PF_6$] *(312)* | [$N_{4444}$][$PF_6$] *(520)* | Simple eutectic | |
| | [$C_3$mim][$PF_6$] *(312)* | [$P_{4444}$][$PF_6$] *(497)* | Simple eutectic | |
| | [$C_1$py][$NTf_2$] *(317)* | [$C_1$mpyrr][$NTf_2$] *(-)* | Simple eutectic ($X_{eu}$=30 mol% [$C_1$mpyrr][$NTf_2$]; $T_{eu}$=306.15K) | [96] |
| | [$C_2$mpyrr][$N(C_4F_9SO_2)_2$] *(431)* | [$C_4$mpyrr][$N(C_4F_9SO_2)_2$] *(374)* | Complete solid solution | [67] |
| | [$N_{1112(OH)}$][$C_4F_9SO_3$] *(449)* | [$C_4$mpyrr][$C_4F_9SO_3$] *(361)* | Formation of an intermediate compound at 33 mol% [$C_4$mpyrr][$C_4F_9SO_3$] | |
| | [$PPh_4$][$NTf_2$] *(407)* | Cs[$NTf_2$] *(398)* | Simple eutectic ($X_{eu}$=32.0 mol% [$PPh_4$][$NTf_2$]; $T_{eu}$=371.75K) | [97] |
| | [$C_3$mpyrr][FSI] *(264)* | [$C_4$mpyrr][FSI] *(255)* | Not specified (measurements performed only at equimolar composition) | [98] |
| | [$C_3$mpyrr][TFSI] *(283)* | [$C_4$mpyrr][TFSI] *(266)* | | |
| Common cation | [$C_2$mim][$PF_6$] *(335)* | [$C_2$mim][Cl] *(361)* | Simple eutectic ($X_{eu}$=37.6 mol% [$C_2$mim][Cl]; $T_{eu}$=312K) | [73] |
| | [$C_2$mim][$PF_6$] *(335)* | [$C_2$mim][$NO_3$] *(316)* | Simple eutectic ($X_{eu}$=60.0 mol% [$C_2$mim][$NO_3$]; $T_{eu}$=292K) | |
| | [1,3-diMeIm][4,5-di$NO_2$-Im] *(372)* | [1,3-diMeIm][4-$NO_2$-Tri] *(359)* | Simple eutectic ($X_{eu}$=64 mol% [1,3-diMeIm][4-$NO_2$-Tri]; $T_{eu}$=339.65K) | [99] |
| | [$C_3$mpyrr][$NTf_2$] *(282)* | [$C_3$mpyrr][dca] *(256)* | Simple eutectic ($X_{eu}$=75 mol% [$C_3$mpyrr][dca]; $T_{eu}$=246.15K) | [77] |
| | [$C_3$mpyrr][$NTf_2$] *(285)*[a] | [$C_3$mpyrr][FSI] *(-)* | Eutectic behavior ($X_{eu}$=70 mol% [$C_3$mpyrr][FSI]; $T_{eu}$=247.15K) with two terminal solid solutions | [100] |
| | [$C_4$mpyrr][Cl] *(474)* | [$C_4$mpyrr][Br] *(477)* | Simple eutectic ($X_{eu}$=35.3 mol% [$C_4$mpyrr][Br]; $T_{eu}$=464K) | |

| | | | | |
|---|---|---|---|---|
| | [$C_4$mpyrr][Cl] *(474)* | [$C_4$mpyrr][$BF_4$] *(425)* | Simple eutectic ($X_{eu}$=44.7 mol% [$C_4$mpyrr][$BF_4$]; $T_{eu}$=366K) | [34] |
| | [$C_4$mpyrr][Br] *(477)* | [$C_4$mpyrr][$BF_4$] *(425)* | Simple eutectic ($X_{eu}$=55.6 mol% [$C_4$mpyrr][$BF_4$]; $T_{eu}$=394K) | |
| | [$C_2$mpyrr][$NTf_2$] *(364)* | [$C_2$mpyrr][$BF_4$] *(339)* | Simple eutectic ($X_{eu}$=40.0 mol% [$C_2$mpyrr][$BF_4$]; $T_{eu}$=322K) | |
| | [$C_4$mpyrr][$N(C_4F_9SO_2)_2$] *(374)* | [$C_4$mpyrr][$C_4F_9SO_3$] *(361)* | Eutectic behavior ($X_{eu}$=48.0 mol% [$C_4$mpyrr][$N(C_4F_9SO_2)_2$]; $T_{eu}$=305K) with two terminal solid solutions | [67] |
| | [$C_2$mpyrr][$N(C_4F_9SO_2)_2$] *(431)* | [$C_2$mpyrr][$CF_3SO_3$] *(384)* | Eutectic behavior ($X_{eu}$=38.0 mol% [$C_2$mpyrr][$N(C_4F_9SO_2)_2$]; $T_{eu}$=357K) with two terminal solid solutions | |
| | [$C_3$mpyrr][FSI] *(264)* | [$C_3$mpyrr][TFSI] *(283)* | Not specified (measurements performed only at equimolar composition) | [98] |
| | [$C_4$mpyrr][FSI] *(255)* | [$C_4$mpyrr][TFSI] *(266)* | | |
| Ternary reciprocal | [$C_2$mpyrr][$NTf_2$] *(364)* | [$C_4$mpyrr][$BF_4$] *(425)* | Simple eutectic ($X_{eu}$=50.8 mol% [$C_4$mpyrr][$BF_4$]; $T_{eu}$=274K) | [34] |
| | [$C_4$mim][Cl] *(338)* | [HEA][HCOO] *(185)* | Simple eutectic | [76] |
| | [$C_3$mpyrr][TFSI] *(283)* | [$C_4$mpyrr][FSI] *(255)* | Not specified (measurements performed only at equimolar composition) | [98] |
| | [$C_3$mpyrr][FSI] *(264)* | [$C_4$mpyrr][TFSI] *(266)* | | |

[a] *Reference [101]*

CATIONS: [$C_n$mim]: 1-alkyl-3-methylimidazolium; [$C_2$pz]: 1-ethyl-2-methylpyrazolium; [$C_n$mpyrr]: 1-alkyl-1-methylpyrrolidinium; [$P_{6,6,6,14}$]: trihexyl(tetradecyl)phosphonium; [$C_3$mpy]: 1-propyl-3-methylpyridinium; [$C_3$mpip]: 1-propyl-1-methyl-piperidinium; [$N_{4444}$]: tetrabutylammonium; [$P_{4444}$]: tetrabutylphosphonium; [1,3-diMeIm]: 1,3-dimethylimidazolium; [$N_{1112(OH)}$]: 2-(hydroxyethyl)trimethylammonium; [$PPh_4$]: tetraphenylphosphonium; [HEA]: 2-hydroxyethylammonium.

ANIONS: [$NTf_2$]: bis(trifluoromethylsulfonyl)imide; [4,5-di$NO_2$-Im]: 4,5-dinitroimidazolate; [4-$NO_2$-Tri]: 4-nitro-1,2,3-triazolate; [dca]: dicyanamide; [FSI]: bis(fluorosulfonyl)imide; [$N(C_4F_9SO_2)_2$]: bis(nonafluorobutylsulfonyl)imide; [$C_4F_9SO_3$]: nonafluorobutanesulfonate; [$CF_3SO_3$]: trifluoromethanesulfonate; [HCOO]: formate; [TFSI]: bis(trifluoromethanesulfonyl)imide.

Table 4.2: Literature review of the phase diagram measurements for common-anion binary systems of salts with ions commonly used for the preparation of ionic liquids ($T_{fusion}$: temperature of fusion; $T_{eu}$: eutectic temperature; $X_{eu}$: eutectic liquid composition)

| Component 1 *($T_{fusion}$ [K])* | Component 2 *($T_{fusion}$ [K])* | Type of phase diagram | Reference |
|---|---|---|---|
| $Li[NTf_2]$ *(506)* | $Na[NTf_2]$ *(530)* | Simple eutectic ($X_{eu}$=67.0 mol% $Li[NTf_2]$; $T_{eu}$=453K) | [102] |
| $Na[NTf_2]$ *(530)* | $Rb[NTf_2]$ *(450)* | Simple eutectic ($X_{eu}$=25.0 mol% $Na[NTf_2]$; $T_{eu}$=431K) | |
| $K[NTf_2]$ *(472)* | $Cs[NTf_2]$ *(395)* | Simple eutectic ($X_{eu}$:not specified; $T_{eu}$=395K) | |
| $Li[NTf_2]$ *(506)* | $Rb[NTf_2]$ *(450)* | Two eutectic reactions ($X_{eu1}$=25.0 mol% $Li[NTf_2]$ and $T_{eu1}$=421K; $X_{eu2}$=60.0 mol% $Li[NTf_2]$ and $T_{eu2}$=426K) with formation of the intermediate compound $LiRb(NTf_2)_2$ | |
| $Li[NTf_2]$ *(506)* | $Cs[NTf_2]$ *(395)* | Two eutectic reactions ($X_{eu1}$=7.0 mol% $Li[NTf_2]$ and $T_{eu1}$=385K; $X_{eu2}$=60.0 mol% $Li[NTf_2]$ and $T_{eu2}$=432K) with formation of the intermediate compound $LiCs(NTf_2)_2$ | |
| $Li[NTf_2]$ *(506)* | $K[NTf_2]$ *(472)* | Eutectic reaction ($X_{eu}$=43.0 mol% $Li[NTf_2]$; $T_{eu}$=423K) with formation of the intermediate compound $Li_3K(NTf_2)_4$ | |
| $Na[NTf_2]$ *(530)* | $K[NTf_2]$ *(472)* | Eutectic reaction ($X_{eu}$=25.0 mol% $Na[NTf_2]$; $T_{eu}$=456K) with formation of the intermediate compound $Na_3K(NTf_2)_4$ | |
| $Na[NTf_2]$ *(530)* | $Cs[NTf_2]$ *(395)* | Eutectic reaction ($X_{eu}$=7.0 mol% $Na[NTf_2]$; $T_{eu}$=383K) with formation of the intermediate compound $Na_3Cs(NTf_2)_4$ | |
| $K[NTf_2]$ *(472)* | $Rb[NTf_2]$ *(450)* | Complete solid solution | |
| $Rb[NTf_2]$ *(450)* | $Cs[NTf_2]$ *(395)* | Complete solid solution | |
| Li[FSA] *(403)* | K[FSA] *(369)* | Simple eutectic ($X_{eu}$=45.0 mol% Li[FSA]; $T_{eu}$=338K) | [21] |
| Li[FSA] *(403)* | Cs[FSA] *(386)* | Simple eutectic ($X_{eu}$=40.0 mol% Li[FSA]; $T_{eu}$=331K) | |
| K[FSA] *(369)* | Cs[FSA] *(386)* | Simple eutectic ($X_{eu}$=60.0 mol% K[FSA]; $T_{eu}$=333K) | |

ANIONS: $[NTf_2]$: bis(trifluoromethylsulfonyl)imide; [FSA]: bis(fluorosulfonyl)amide.

Table 4.3: Literature review of the phase diagram measurements for common-anion ternary systems of salts with ions commonly used for the preparation of ionic liquids ($T_{eu}$: eutectic temperature; $T_p$: peritectic temperature)

| Ternary system | Type of phase diagram | Reference |
|---|---|---|
| $Li[NTf_2]$ - $Na[NTf_2]$ - $K[NTf_2]$ | One ternary eutectic point ($T_{eu}$=427K with $X_{Li[NTf2]}$=0.45, $X_{Na[NTf2]}$= 0.10, $X_{K[NTf2]}$=0.45) and one ternary peritectic point ($T_p$=431K with $X_{Li[NTf2]}$=0.50, $X_{Na[NTf2]}$= 0.10, $X_{K[NTf2]}$=0.40) | [22] |
| $Li[NTf_2]$ - $Na[NTf_2]$ - $Cs[NTf_2]$ | Two ternary eutectic points ($T_{eu1}$=431K with $X_{Li[NTf2]}$=0.60, $X_{Na[NTf2]}$= 0.10, $X_{Cs[NTf2]}$=0.30; $T_{eu2}$=388K with $X_{Li[NTf2]}$=0.05, $X_{Na[NTf2]}$= 0.05, $X_{Cs[NTf2]}$=0.90) | |
| $Li[NTf_2]$ - $K[NTf_2]$ - $Cs[NTf_2]$ | Two ternary peritectic points ($T_{p1}$=421K with $X_{Li[NTf2]}$=0.50, $X_{K[NTf2]}$= 0.25, $X_{Cs[NTf2]}$=0.25; $T_{p2}$=417K with $X_{Li[NTf2]}$=0.30, $X_{K[NTf2]}$= 0.40, $X_{Cs[NTf2]}$=0.30) | |
| $Na[NTf_2]$ - $K[NTf_2]$ - $Cs[NTf_2]$ | No ternary invariant point reported | |
| Li[FSA] - Na[FSA] - K[FSA] | One ternary eutectic point ($T_{eu}$=318K with $X_{Li[FSA]}$=0.30, $X_{Na[FSA]}$= 0.40, $X_{K[FSA]}$=0.30) | [21] |
| Li[FSA] - Na[FSA] - Cs[FSA] | One ternary eutectic point ($T_{eu}$=311K with $X_{Li[FSA]}$=0.30, $X_{Na[FSA]}$= 0.40, $X_{Cs[FSA]}$=0.30) | |
| Na[FSA] - K[FSA] - Cs[FSA] | One ternary eutectic point ($T_{eu}$=309K with $X_{Na[FSA]}$=0.40, $X_{K[FSA]}$= 0.25, $X_{Cs[FSA]}$=0.35) | |
| Li[FSA] - K[FSA] - Cs[FSA] | One ternary eutectic point (ref. [23]: $T_{eu}$=312K with $X_{Li[FSA]}$=0.30, $X_{K[FSA]}$= 0.35, $X_{Cs[FSA]}$=0.35; ref. [21]: $T_{eu}$=309K with $X_{Li[FSA]}$=0.33, $X_{K[FSA]}$= 0.33, $X_{Cs[FSA]}$=0.33) | [21, 23] |

ANIONS: $[NTf_2]$: bis(trifluoromethylsulfonyl)imide; [FSA]: bis(fluorosulfonyl)amide.

## 4.2 Materials and methods

### 4.2.1 Materials

All used ionic liquids were purchased from Iolitec GmbH, with a nominal purity of 99%, were recrystallized from acetonitrile/ethyl acetate (1:10) mixture and dried under high vacuum (p = 0.001 mbar) in order to eliminate the influence of water on the melting point analysis. The water content of the samples was determined by Karl-Fischer titration using a Metrohm 915 KF Ti-Touch instrument with volumetric titration, and kept below 1000 ppm.

### 4.2.2 Preparation of ionic liquid mixtures for DSC analysis

In the case of hygroscopic salts such as pyrrolidinium halides, the procedure for sample preparation for DSC analysis needed to be performed in a glove box, under argon atmosphere with highly reduced humidity. In order to prepare the ternary mixtures of ionic liquids at the different concentrations of each salt, each sample was prepared by weighing out the appropriate amount of each salt and then mixing it together in a vial. Subsequently, each mixture was heated up until complete melting of the solids, cooled down and grinded after solidification. Approximately 6-18 mg of each sample was placed into a tarred aluminium DSC pan, and sealed using a lid of the same material, and submitted for DSC analysis.

### 4.2.3 DSC protocol

Thermal transitions were determined by performing DSC experiments using Mettler-Toledo DSC 1 STARe System differential scanning calorimeter, cooled with a Huber TC100 immersion cooler. The calorimeter was calibrated for temperature and cell constants using high purity indium (melting temperature: 430 K; specific enthalpy of melting: 28.71 $J.g^{-1}$). All data were collected at atmospheric pressure, with nitrogen as a purge gas, and an empty sample pan as the reference. The experiments were conducted in the temperature range from 193.15 to 483.15 K. The samples were initially heated from room temperature, at a rate of 10 $K.min^{-1}$, to the highest temperature. At this temperature, they were held for a 10 min isotherm, prior to two cycles of cooling and heating at rates of 5 $K.min^{-1}$ spaced by 5 min isothermal holding at the lower and upper endpoint temperatures.

### 4.2.4 Transition temperature determination based on the peak position

The data from the DSC thermograms were obtained via analysis with the STARe Evaluation Software by Mettler Toledo. All temperatures reported for the glass transition and melting were established as the onset temperatures for the endothermic changes in heat flow. Uncertainties of 1 K in the temperatures and of 1 % in the enthalpies are estimated.

## 4.3 Thermodynamic model for the liquid phase

The liquid phase of the [$C_2$py], [$C_4$py] || Cl, Br ternary reciprocal system was modeled with the Modified Quasichemical Model in the Quadruplet Approximation (MQMQA), that evaluates coupled 1st-and 2nd-nearest-neighbor short-range order. This is a two-sublattice model, where the cations are assumed to distribute on one sublattice, and the anions are assumed to distribute on another sublattice. A quadruplet consists of two second-nearest-neighbor cations and two second-nearest-neighbor anions, which are mutual first-nearest-neighbors. Each quadruplet has a Gibbs free energy. Quadruplets mix randomly, constrained by an elemental mass balance. The equilibrium quadruplet composition (configuration) is the one that minimizes the Gibbs free energy of the melt at given temperature, pressure and composition, and thus results in an equilibrium configuration that reflects 1st- and 2nd-nearest-neighbor short-range order. The following second-nearest-neighbor pair exchange reactions are taken into account:

$$(A-X-A)_{pair} + (B-X-B)_{pair} = 2(A-X-B)_{pair}; \quad \Delta g_{AB/X_2} \tag{24}$$

$$(X-A-X)_{pair} + (Y-A-Y)_{pair} = 2(X-A-Y)_{pair}; \quad \Delta g_{A_2/XY} \tag{25}$$

where $A$ and $B$ are two different cations ($[C_2py]^+$ and $[C_4py]^+$ in the present case), and $X$ and $Y$ are two different anions ($Cl^-$ and $Br^-$ in the present case). As the Gibbs free energy change $\Delta g_{AB/X_2}$(respectively $\Delta g_{A_2/XY}$) becomes progressively more negative, reaction (24) (respectively (25)) is shifted to the right, $(A-X-B)$ (respectively $(X-A-Y)$) pairs predominate and second-nearest-neighbor cation-cation (respectively anion-anion) short-range ordering results. The Gibbs free energy changes $\Delta g_{AB/X_2}$ and $\Delta g_{A_2/XY}$ are model parameters that can be expressed as a function of composition by empirical polynomial expressions (see equation (11) in reference [13]) in order to reproduce the available experimental data (phase diagram in the present case) for the $A, B \parallel X$ and $A \parallel X, Y$ binary subsystems, respectively. In order to obtain a quantitative fit for the $A, B \parallel X, Y$ system, small empirical "ternary reciprocal parameters" may have to be included. As described previously [13], these parameters represent the Gibbs free energies of formation of the $ABXY$ quadruplets from the binary quadruplets according to:

$$\frac{1}{2}(ABX_2 + ABY_2 + A_2XY + B_2XY) = 2ABXY \;\; ; \;\; \Delta g_{AB/XY} \tag{26}$$

However, such "ternary reciprocal parameters" were not required for the [$C_2$py], [$C_4$py] || Cl, Br system. The extent of first-nearest-neighbor (cation-anion) short-range ordering is related to the Gibbs free energy change for the following exchange reaction:

$$AX + BY = AY + BX\ ;\ \Delta g_{AB/XY}^{exchange} \tag{27}$$

If $\Delta g_{AB/XY}^{exchange}$ is negative, then $A-Y$ and $B-X$ first-nearest-neighbor pairs predominate. For instance, as explained in section 4.7.1, $\Delta g_{[C_2py][C_4py]/ClBr}^{exchange}$ for the exchange reaction [$C_2$py]Br (liquid) + [$C_4$py]Cl (liquid) = [$C_2$py]Cl (liquid) + [$C_4$py]Br (liquid) can be estimated as -1.6 kJ.mol$^{-1}$ at 25°C, -1.9 kJ.mol$^{-1}$ at 100°C, and -2.4 kJ.mol$^{-1}$ at 150°C (i.e. above the highest melting temperature of the four pure ionic liquids). These are relatively small values and thus the [$C_2$py], [$C_4$py] || Cl, Br liquid displays relatively little first-nearest-neighbor (cation-anion) short-range ordering. As will be shown in section 4.7.2, the optimized model parameters $\Delta g_{AB/X_2}$ and $\Delta g_{A_2/XY}$ for the four common-ion binary subsystems are relatively small in amplitude. Therefore, the [$C_2$py], [$C_4$py] || Cl, Br liquid also exhibits relatively little second-nearest-neighbor (cation-cation and anion-anion) short-range ordering. It can be concluded that the investigated ternary reciprocal liquid displays small deviations from ideality, which is due to the fact that the two cations only differ by the length of their alkyl chains (ethyl or butyl) and that the two anions are halides with similar ionic radii.

Values of the second-nearest-neighbor "coordination numbers" of the various ions in the various quadruplets have to be defined. They were all set to 6 for the [$C_2$py], [$C_4$py] || Cl, Br system. In the improved version of the MQMQA [79], the parameter $\zeta_{A/X}$, which is equal to the number of quadruplets emanating from, or containing, a first-nearest-neighbor $A-X$ pair (where $A$ is a cation and $X$ is an anion), is defined as:

$$\zeta_{A/X} = 2Z_{A_2/X_2}^{A} Z_{A_2/X_2}^{X} / \left(Z_{A_2/X_2}^{A} + Z_{A_2/X_2}^{X}\right) \tag{28}$$

where $Z_{A_2/X_2}^{i}$ is the second-nearest-neighbor "coordination number" of the ion $i$ ($i = A, X$) when all $i$ exist in $A_2X_2$ quadruplets. The resulting values of $\zeta_{A/X}$ (equation (28)) for the [$C_2$py], [$C_4$py] || Cl, Br system are all equal to 6.

For the liquid phase of the common-cation ternary system [$C_4$mpyrr]Cl - [$C_4$mpyrr]Br - [$C_4$mpyrr]$BF_4$, the Modified Quasichemical Model in the Pair Approximation (MQMPA) is

sufficient. Since the cationic sublattice is occupied only by one type of cation ($[C_4mpyrr]^+$), only the second-nearest-neighbor anion-anion pairs on the anionic sublattice need to be taken into account, and $\Delta g_{A_2/XY}$ (equation (25)) is the only relevant Gibbs free energy change. For the sake of clarity, this notation will be retained in the present article. (The notation $\Delta g_{A/XY}$ was often used in previous publications.) All second-nearest-neighbor anion-anion "coordination numbers" were set to 6. The [C4mpyrr]Cl - [C4mpyrr]Br - [C4mpyrr]$BF_4$ ternary system is considered to be "asymmetric", with [C4mpyrr]$BF_4$ as the "asymmetric" component. This asymmetry makes the estimation of the thermodynamic properties of the ternary liquid from binary optimized parameters very similar to the Kohler-Toop interpolation method [25]. Under these conditions, the composition variables $\chi_{XY}$, defined previously [13], that are relevant for the present work become:

$$\chi_{Cl(BF_4)} = \chi_{Br(BF_4)} = x_{ClCl} + x_{BrBr} + x_{ClBr} \quad (29)$$

$$\chi_{(BF_4)Cl} = \chi_{(BF_4)Br} = x_{(BF_4)(BF_4)} \quad (30)$$

where $x_{XY}$ is the mole fraction of second-nearest-neighbor $(X - [C_4mpyrr] - Y)$ pairs. Note that, for the binary systems [C4mpyrr]X - [C4mpyrr]$BF_4$ (where X=Cl, Br), equation (29) reduces to:

$$\chi_{X(BF_4)} = x_{XX} \quad (31)$$

As mentioned before, the parameters $\Delta g_{A_2/XY}$ (with A=[C4mpyrr]) of reaction (25) for each anion-anion pair are expanded, through optimization with the available phase diagram data, as empirical polynomials in $\chi_{XY}$ and $\chi_{YX}$. For the ternary system, terms may be added that give the effect of the third component upon the pair-formation energies $\Delta g_{A_2/XY}$ [13]. One ternary term was required for the [C4mpyrr]Cl - [C4mpyrr]Br - [C4mpyrr]$BF_4$ system (see section 4.5.3). As will be shown in section 4.5.2, the optimized model parameters $\Delta g_{A_2/XY}$ for the three binary subsystems are relatively small in amplitude. Therefore, the investigated common-cation ternary liquid displays relatively little second-nearest-neighbor (anion-anion) short-range ordering. Thus, the Bragg-Williams (random-mixing) model could have been used successfully for this liquid. This model is described in detail in reference [103] and is briefly presented in reference [24]. The Modified Quasichemical Model (MQM) was finally preferred since it is suitable for liquids exhibiting either small or extensive short-range ordering, and also for liquids displaying positive deviations from ideality. As a result, the MQM is well adapted for the development of large thermodynamic databases [15, 104, 105].

## 4.4 Thermodynamic model for the solid solutions

The solid solutions relevant for the present work are: the Cl-rich [$C_4$mpyrr](Cl, [Br]) solid solution, the Br-rich [$C_4$mpyrr](Br, [Cl]) solid solution, the [$C_2$py]Cl – [$C_2$py]Br solid solution, and the [$C_4$py]Cl-[$C_4$py]Br solid solution. They were all modeled using the Compound Energy Formalism [26, 27]. Let us consider a solid solution phase such as B(Cl, Br), where B (B=[$C_4$mpyrr]$^+$, [$C_2$py]$^+$ or [$C_4$py]$^+$) resides on the cationic sublattice C, and $Cl^-$ and $Br^-$ reside on the anionic sublattice A. The molar Gibbs free energy of the solution is then given by the following equation:

$$G = y^A_{Cl^-}G^o_{B^+:Cl^-} + y^A_{Br^-}G^o_{B^+:Br^-} + RT(y^A_{Cl^-}lny^A_{Cl^-} + y^A_{Br^-}lny^A_{Br^-}) + G^E \quad (32)$$

The first two terms represent the reference Gibbs free energy of the solution, where $y^A_{Cl^-}$ and $y^A_{Br^-}$ are the site fractions of $Cl^-$ and $Br^-$ on the anionic sublattice A, and $G^o_{B^+:Cl^-}$ and $G^o_{B^+:Br^-}$ are the standard molar Gibbs free energies of the end-member components BCl and BBr, respectively, possibly augmented by a temperature-dependent Gibbs free energy. This latter term is always positive and is a model parameter. For instance, for the Cl-rich [$C_4$mpyrr](Cl, [Br]) high temperature solid solution, the two end-member compositions are [$C_4$mpyrr]Cl($s_2$) and hypothetical [$C_4$mpyrr]Br having the same crystal structure as [$C_4$mpyrr]Cl($s_2$). The Gibbs free energy of this hypothetical [$C_4$mpyrr]Br is that of [$C_4$mpyrr]Br(s) augmented by a constant (and positive) Gibbs free energy. On the other hand, for the [$C_2$py]Cl – [$C_2$py]Br extensive solid solution, the two end-member compositions are [$C_2$py]Cl(s) and [$C_2$py]Br(s) (which have the same crystal structure). The third term in Equation (32) gives the ideal entropy of mixing (Temkin type [106]), assuming a random distribution of the anions on the anionic sublattice. The final term is the molar excess Gibbs free energy and is expressed as follows:

$$G^E = y^A_{Cl^-}y^A_{Br^-}L_{B^+:Cl^-,Br^-} \quad (33)$$

The L factor may depend on the temperature and also on the composition, where Redlich-Kister terms as a function of site fractions are generally used.

## 4.5 The [$C_4$mpyrr]Cl - [$C_4$mpyrr]Br - [$C_4$mpyrr]$BF_4$ system

This section describes a thermodynamic model for the common-cation ternary system [$C_4$mpyrr]Cl - [$C_4$mpyrr]Br - [$C_4$mpyrr]$BF_4$. Figure 4.1 shows the chemical structure of the three pure ionic liquids. The phase diagrams of the three binary subsystems were measured previously by DSC

[34], and these data are used in the present work. As described in section 4.5.3, two isoplethal sections were measured in the ternary system, and these new data are compared to the phase diagrams predicted by using solely the optimized model parameters for the three binary subsystems along with a standard asymmetric interpolation method [13]. Then, one small ternary parameter is included for the liquid phase in order to best reproduce the ternary data.

### 4.5.1 Pure ionic liquids

To model the phase diagram of a common-ion (common-cation or common-anion) system for which measurements are available, only the molar Gibbs free energies of fusion and the molar Gibbs free energies of solid-solid transition (if different allotropes exist) of the pure compounds need to be known. The molar Gibbs free energy of fusion of the pure compound $m$ may be written as:

$$\Delta g^{o}_{fusion\,(m)} = \Delta h^{o}_{fusion\,(m)} \left(1 - \frac{T}{T_{fusion(m)}}\right) \tag{34}$$

where the enthalpy of fusion $\Delta h^{o}_{fusion\,(m)}$ is independent of the temperature to a first approximation. Similarly, the molar Gibbs free energy of solid-solid transition for a compound displaying two different allotropes ($s_1$, $s_2$) may be written as:

$$\Delta g^{o}_{trans\,(s_1)} = \Delta h^{o}_{trans\,(s_1)} \left(1 - \frac{T}{T_{trans(s_1)}}\right) \tag{35}$$

To our knowledge, few thermodynamic data are available in the literature for the three pure compounds [$C_4$mpyrr]Cl, [$C_4$mpyrr]Br and [$C_4$mpyrr]$BF_4$ (see table 4.4). The enthalpy of fusion of [$C_4$mpyrr]$BF_4$ has not been measured, and it was assessed in the present work by using the limiting liquidus slope Equation (36), which assumes no solid solubility:

$$\left(\frac{dT}{dx_m^{liquidus}}\right) = \frac{RT^2_{fusion\,(m)}}{\Delta h^{o}_{fusion(m)}} \quad [at\ x_m = 1] \tag{36}$$

where R is the gas constant, and $T_{fusion(m)}$ and $\Delta h^{o}_{fusion(m)}$ are respectively the temperature of fusion and the molar enthalpy of fusion of the pure salt $m$. Equation (36) was applied to the [$C_4$mpyrr]Cl - [$C_4$mpyrr]$BF_4$, [$C_4$mpyrr]Br - [$C_4$mpyrr]$BF_4$ and [$C_2$mpyrr]$NTf_2$ - [$C_4$mpyrr]$BF_4$ experimental phase diagrams of Stolarska et al. [34] (where [$C_2$mpyrr] and $NTf_2$ refer to 1-ethyl-

1-methyl-pyrrolidinium and bis(trifluoromethylsulfonyl)imide, respectively). An average value of 13725 J.mol$^{-1}$ was obtained for the enthalpy of fusion of [C$_4$mpyrr]BF$_4$. As shown in Table 4.4, experimental values of the enthalpy of fusion of [C$_4$mpyrr]Cl and [C$_4$mpyrr]Br were available and they are used directly in the present work. Finally, for the sake of consistency, the temperatures of fusion of the three pure compounds measured by Stolarska et al. [34] were selected in the present study.

Table 4.4: Enthalpies of fusion and of solid-solid transition measured by DSC in the literature for the pure compounds [C$_4$mpyrr]Cl, [C$_4$mpyrr]Br and [C$_4$mpyrr]BF$_4$

| Cation | Anion | Water content (ppm) | Purity (%) | Melting temperature (K) | Enthalpy of fusion (J.mol$^{-1}$) | Solid-Solid transition | Reference |
|---|---|---|---|---|---|---|---|
| [C$_4$mpyrr]$^+$ | Cl$^-$ | - | >98 | 474 | - | - | [34] |
| | | 7-8 | high | 476 | 13037 | $T_{trans}$=466.45K<br>$\Delta H_{trans}$=1493 J.mol$^{-1}$ | [107] |
| | Br$^-$ | - | >98 | 477 | - | - | [34] |
| | | 3540 | - | 487 | 13120 | - | [108] |
| | BF$_4^-$ | - | >98 | 425 | - | - | [34] |

## 4.5.2 Binary subsystems

### 4.5.2.1 The [C$_4$mpyrr]Br - [C$_4$mpyrr]BF$_4$ binary system

The phase diagram has been measured by DSC [34]. No solid solubility was reported, and there are no reported intermediate compounds. The optimized Gibbs free energy of reaction (25) is:

$$\Delta g_{[C_4mpyrr]_2/Br(BF_4)}/(J.mol^{-1}) = 209.2 + 836.8\chi_{Br(BF_4)} + 1740.5\chi_{(BF_4)Br} \quad (37)$$

The calculated phase diagram is shown along with the measurements in figure 4.2. This is a simple eutectic system. The reported characteristics of the experimental eutectic are {T=394K (i.e. 120.85°C), 55.6 mol% [C$_4$mpyrr]BF$_4$} [34]. The characteristics of the calculated eutectic are {121°C, 55.5 mol% [C$_4$mpyrr]BF$_4$}.

As shown in figure 4.2, a DSC signal for the eutectic reaction was observed only for three binary mixtures. As emphasized by Stolarska et al. [34], owing to the dynamic nature of the experimental technique, thermal transitions that should exist thermodynamically may be kinetically hindered.

Therefore, measuring and interpreting the phase diagrams of ionic liquid systems is expected to be more difficult than for inorganic salt systems. The measured liquidus temperatures in figure 4.2 are somewhat scattered: for instance, at 10 mol% $[C_4mpyrr]BF_4$, the shift between the calculated and experimental liquidus temperatures is almost 10°C. The scattering of the data is more visible in the eutectic temperatures measured for the seven binary mixtures in the $[C_4mpyrr]Cl$ - $[C_4mpyrr]BF_4$ binary system (see figure 4.3).

#### 4.5.2.2 The $[C_4mpyrr]Cl$ - $[C_4mpyrr]BF_4$ binary system

The phase diagram has been measured by DSC [34]. No solid solubility was reported and the measured limiting slope of the $[C_4mpyrr]Cl$ liquidus curve agrees with Equation (36). There are no reported intermediate compounds. The optimized Gibbs free energy of reaction (25) is:

$$\Delta g_{[C_4mpyrr]_2/Cl(BF_4)}/(J.mol^{-1}) = -669.4 - 836.8\chi_{Cl(BF_4)} + 836.8\chi_{(BF_4)Cl} \quad (38)$$

The calculated phase diagram is compared with the measurements in figure 4.3. Again, this is a simple eutectic system. The reported characteristics of the experimental eutectic are {T=366K (i.e. 92.85°C), 47.4 mol% $[C_4mpyrr]BF_4$} [34]. The composition of the eutectic liquid was derived from a Tammann plot, where the specific heat of fusion of the eutectic peak was plotted against the composition [34]. The characteristics of the calculated eutectic are {92°C, 50.4 mol% $[C_4mpyrr]BF_4$}. As reported in Table 4.4, Babushkina [107] measured by DSC a solid-solid transition at 193.3°C for $[C_4mpyrr]Cl$. Therefore, two different allotropes ($s_1$, $s_2$) were introduced for the latter compound in the present work.

#### 4.5.2.3 The $[C_4mpyrr]Cl$ - $[C_4mpyrr]Br$ binary system

The phase diagram has been measured by DSC [34]. No solid solubility was reported, and there are no reported intermediate compounds. As shown in figure 4.4(a), the measured limiting slopes of the $[C_4mpyrr]Cl$ and $[C_4mpyrr]Br$ liquidus curves substantially disagree with Equation (36), and therefore this system exhibits at least some terminal solid solubility. Two thermal transitions were observed only for four binary mixtures. The low-temperature transition at about 190°C was attributed to a binary eutectic [34]. For pure $[C_4mpyrr]Cl$ and most of the $[C_4mpyrr]Cl$ – $[C_4mpyrr]Br$ binary mixtures investigated, another thermal transition was observed in the range 370-390K (i.e. 96.85-116.85°C) [34] (see figure 4.4(b)). As suggested by Stolarska et al., this transition might be associated with $[C_4mpyrr]Cl$ polymorphism, with the existence of two

preferred conformations of the pyrrolidinium ions. However, no such thermal transition was observed for the [C4mpyrr]Cl – [C4mpyrr]$BF_4$ system [34]. Finally, the low-temperature thermal transition reported above was not considered in the present work. Two terminal solid solutions were introduced: a Cl-rich [C4mpyrr](Cl, [Br]) solid solution and a Br-rich [C4mpyrr](Br, [Cl]) solid solution. The reported characteristics of the experimental eutectic are {T=464K (i.e. 190.85°C), 35.3 mol% [C4mpyrr]Br}. The characteristics of the calculated eutectic are {192°C, 35.3 mol% [C4mpyrr]Br}. The low-temperature transitions at about 190°C measured for the binary mixtures containing 60.0 or 80.0 mol% [C4mpyrr]Br are not well reproduced by the model, but this shift may be due to the scattering of the data. Since the $Cl^-$ and $Br^-$ anions have similar ionic radii [109], the binary liquid was assumed to be ideal. That is:

$$\Delta g_{[C_4mpyrr]_2/ClBr} = 0 \tag{39}$$

The two terminal solid solutions were modeled with the Compound Energy Formalism (CEF). Their optimized Gibbs free energies are given by:

$$\begin{aligned} G_{(Cl,[Br])(ss)}/(J.mol^{-1}) & \\ &= y^A_{\mathrm{Cl}^-} G^o_{[C_4\mathrm{mpyrr}]Cl(s_2)} + y^A_{\mathrm{Br}^-}\left(G^o_{[C_4\mathrm{mpyrr}]Br(s)} + 836.8\right) \\ &+ RT\left[y^A_{\mathrm{Cl}^-} ln(y^A_{\mathrm{Cl}^-}) + y^A_{\mathrm{Br}^-} ln(y^A_{\mathrm{Br}^-})\right] \end{aligned} \tag{40}$$

$$\begin{aligned} G_{(Br,[Cl])(ss)}/(J.mol^{-1}) & \\ &= y^A_{\mathrm{Cl}^-}\left(G^o_{[C_4\mathrm{mpyrr}]Cl(s_2)} + 443.5\right) + y^A_{\mathrm{Br}^-} G^o_{[C_4\mathrm{mpyrr}]Br(s)} \\ &+ RT\left[y^A_{\mathrm{Cl}^-} ln(y^A_{\mathrm{Cl}^-}) + y^A_{\mathrm{Br}^-} ln(y^A_{\mathrm{Br}^-})\right] \end{aligned} \tag{41}$$

Recently, the [C4mpyrr]$C_4F_9SO_3$ - [C4mpyrr]$N(C_4F_9SO_2)_2$ phase diagram has been measured by DSC, and it has been interpreted as displaying two terminal solid solutions [67]. A similar assumption was made in the present work for the [C4mpyrr]Cl-[C4mpyrr]Br system, thus implying that [C4mpyrr]Cl($s_2$) and [C4mpyrr]Br do not have the same crystal structure. To our knowledge, no crystal structure information is available. If there was convincing evidence that these two solid compounds have the same crystal structure, then a single solid solution would have to be introduced and the experimental low-temperature transition at about 190°C would be due to a very flat minimum (azeotrope) or to a solid-solid miscibility gap. The introduction of two terminal solid solutions allowed us to best reproduce the experimental phase diagram, in particular the liquidus temperatures which are of primary interest in the present study.

### 4.5.3 The [C4mpyrr]Cl - [C4mpyrr]Br - [C4mpyrr]BF4 ternary system

The calculated liquidus projection of the [C4mpyrr]Cl - [C4mpyrr]Br - [C4mpyrr]BF4 system is shown in figure 4.5. As explained in section 4.3, the thermodynamic properties of the ternary liquid are calculated from the optimized model parameters for the three binary subsystems (Equations (37-39)) using an asymmetric interpolation method. As justified below, a small ternary excess parameter was included for the liquid phase:

$$g^{001}_{[C_4mpyrr]/ClBr(BF_4)}/(J.mol^{-1}) = 3640.1 \quad (42)$$

In figure 4.5, the univariant lines (along which the liquid coexists with two solid phases) are shown as bold lines. By convention, the arrows indicate the directions of decreasing temperature along these lines. The constant temperature lines are called liquidus isotherms, and they are displayed as thin lines. Two ternary invariant reactions are calculated. The ternary eutectic reaction liquid = [C4mpyrr]Cl($s_1$) + [C4mpyrr]BF4 + [C4mpyrr](Cl, [Br]) (ss) occurs at 91°C with a liquid composition of (49.5 mol% [C4mpyrr]BF4 + 49.0 mol% [C4mpyrr]Cl + 1.5 mol% [C4mpyrr]Br). This corresponds to the minimum liquidus temperature in the ternary system. The ternary quasi-peritectic reaction liquid + [C4mpyrr](Br, [Cl]) (ss) = [C4mpyrr](Cl, [Br]) (ss) + [C4mpyrr]BF4 occurs at 98°C with a liquid composition of (52.2 mol% [C4mpyrr]BF4 + 41.9 mol% [C4mpyrr]Cl + 5.9 mol% [C4mpyrr]Br).

In order to test the accuracy of the developed thermodynamic model, two isoplethal sections were measured by DSC: the isoplethal section at constant 50 mol% [C4mpyrr]BF4 and the isoplethal section at constant molar ratio [C4mpyrr]Cl / ([C4mpyrr]Cl + [C4mpyrr]Br) of 0.85. As an example, DSC thermograms for the latter isoplethal section are shown in figure 4.6. The data and the calculations are compared in figures 4.7 and 4.8. A small ternary excess parameter (Equation (42)) was introduced for the liquid in order to best reproduce the measurements. The calculations in presence and in absence of the ternary excess parameter are compared for both isoplethal sections in figures 4.9 and 4.10. As explained previously, thermal transitions that should exist thermodynamically may not be observed by DSC. Therefore, for a given sample, the number of calculated transitions should be equal or higher than the number of experimental transitions. Both situations occur in the isoplethal section shown in figure 4.7. For both of the investigated isoplethal sections, agreement between the calculations and the measurements is satisfactory (figures 4.7 and 4.8). The observed temperature shift is always less than 12°C.

## 4.6 Volume-Based Thermodynamics (VBT)

Since no compilation tables exist currently for the thermodynamic properties ($C_p$ (T), $S^o_{298.15K}$, $\Delta H^o_{298.15K}$) of pure ionic liquids, estimation techniques such as the Volume-Based Thermodynamics (VBT) from Glasser and Jenkins [28-33] are needed to predict the missing thermodynamic data. Recently, Robelin [24] tested the applicability of the VBT to predict the thermodynamic properties of various methyl-imidazolium-based ILs. The VBT only takes into account long-range Coulombic interactions, and short-range interactions such as van der Waals and hydrogen bonding are not yet considered [33]. The VBT requires a knowledge of the molecular volume $\nu_m$ (expressed in $nm^3$). The latter can be derived from crystallographic data for the pure solid phases, and from density measurements (using a densimeter) for the pure liquid phases. The estimation of the relevant thermodynamic properties of a pure ionic liquid is described below.

### 4.6.1 Heat capacity $C_p$ (T)

By analogy with Strechan et al. [80], who correlated the heat capacity ($C_p$) with the molecular volume ($\nu_m$) at 298.15K for various methyl-imidazolium-based ionic liquids, the experimental data ($C_p$ and density) available for twenty one pyridinium-based ILs were collected from the literature (see table 4.5). Only five of the ionic liquids (highlighted in table 4.5) are 1-alkyl-pyridinium-based compounds and have a chemical structure very similar to that of the pyridinium-based ionic liquids studied in the present work. The experimental data available for these five compounds were used to derive the following linear regression equation:

$$C_p(298.15K)/(J.mol^{-1}.K^{-1}) = 1195.2\nu_m + 16.8 \quad (43)$$

where $\nu_m$ is the molecular volume (in $nm^3$). The standard error of a prediction is ±18.4 $J.mol^{-1}.K^{-1}$. Figure 4.11 displays the corresponding linear regression line along with the linear regression line obtained from nineteen pyridinium-based compounds. For the latter, the [4empy]$NTf_2$ and [$O_3$mpy]$BF_4$ compounds (shown as empty circles) were discarded.

### 4.6.2 Standard absolute entropy ($S^o_{298.15K}$)

Glasser [30] proposed the following expression for the standard absolute entropy ($S^o_{298.15K}$) of ionic liquids, which is an average of two linear regression equations (one valid for anhydrous ionic solids [29] and another one valid for organic liquids [81]):

$$S^{o}_{298.15K}/(J.mol^{-1}.K^{-1}) = 29.5 + 1246.5v_m \quad (44)$$

where $v_m$ represents the molecular volume (in $nm^3$).

### 4.6.3 Standard enthalpy $\Delta H^{o}_{298.15K}$

The standard enthalpy of formation ($\Delta H^{o}_{298.15K}$) is the most important thermodynamic quantity for pure ionic liquids. As an example, let us consider solid 1-ethyl-pyridinium chloride (referred to as [$C_2$py]Cl). One can derive the following equation from the thermodynamic cycle shown in figure 4.12:

$$\Delta H^{o}_{298.15K}([C_2py]Cl, s) = \Delta H^{o}_{298.15K}([C_2py]^+, g) + \Delta H^{o}_{298.15K}(Cl^-, g) - \Delta H_L \quad (45)$$

where $\Delta H_L$ is the lattice enthalpy. The values of $\Delta H^{o}_{298.15K}([C_2py]^+, g)$ and $\Delta H^{o}_{298.15K}(Cl^-, g)$ can be assessed from ab initio calculations. The lattice enthalpy is given by the following expression [32]:

$$\Delta H_L = U_{POT} + \sum_{i=1}^{n} n_i \left(\frac{c_i}{2} - 2\right).RT \quad (46)$$

where $U_{POT}$ represents the lattice potential energy, $n$ is the number of ion types in the formula unit, $n_i$ is the number of ions of type $i$, and $c_i$ depends on the type of ion (3 for a monoatomic ion $i$, 5 for a linear polyatomic ion $i$, 6 for a nonlinear polyatomic ion $i$).

The lattice potential energy is calculated as follows [32]:

$$U_{POT} = 2I.\left[\frac{\alpha}{v_m^{\frac{1}{3}}} + \beta\right] \quad (47)$$

where $\alpha$ and $\beta$ are fitted constants obtained by Gutowski et al. [110] for a series of salt compounds containing the organic cations $NH_4^+$, $N_2H_5^+$, $CH_3NH_3^+$, $(CH_3)_2NH_2^+$, $(CH_3)_3NH^+$, $(C_2H_5)_2NH_2^+$ and $(C_2H_5)_3NH^+$:

$$\alpha = 83{,}262\ J.mol^{-1}.nm \quad (48)$$

$$\beta = 157{,}318\ J.mol^{-1} \quad (49)$$

and

$$I = \frac{1}{2}\sum_{i=1}^{n} n_i(z_i)^2 \qquad (50)$$

In Equation (50), $I$ is the ionic strength factor, $n$ is again the number of ion types in the formula unit, $n_i$ is again the number of ions of type $i$, and $z_i$ is the valence of ion $i$. Equation (47) is only valid for lattice potential energy values lower than 5000 kJ.mol$^{-1}$ [32].

Table 4.5: Calculated (Equation (43)) and experimental $C_p$ values at T=298.15K for various pyridinium-based ionic liquids

| Compound | Measured $C_p$ [J.mol$^{-1}$.K$^{-1}$] at 298.15K | Measured density ρ [g.cm$^{-3}$] at 298.15K | $v_m$ [nm$^3$] at 298.15K | Calculated $C_p$ [J.mol$^{-1}$.K$^{-1}$] at 298.15K | Relative shift for $C_p$ (%) | Reference |
|---|---|---|---|---|---|---|
| [bmpy][$C(CN)_3$] | 468.0 | 1.042 | 0.383 | 474.6 | 1.4 | [111] |
| [$b_4$mpy][$NTf_2$] | 636.4 | 1.412 | 0.506 | 621.6 | -2.3 | [112] |
| [$b_3$mpy][$BF_4$] | 412.3 | 1.183 | 0.333 | 414.8 | 0.6 | [113] |
| [$b_4$mpy][$BF_4$] | 413.7 | 1.183 | 0.333 | 414.8 | 0.3 | [113] |
| **[epy][$NTf_2$]** | **522.4** | **1.536** | **0.420** | **518.8** | -0.7 | **[114]** |
| [$b_3$mpy][DCA] | 367.7 | 1.056 | 0.340 | 423.2 | 15.1 | [115] |
| **[ppy][$BF_4$]** | **363.0** | **1.253** | **0.277** | **347.9** | -4.2 | **[116]** |
| [eepy][$eSO_4$] | 412.0 | 1.219 | 0.356 | 442.3 | 7.4 | [117] |
| **[mpy][$mSO_4$]** | **299.0** | **1.346** | **0.253** | **319.2** | 6.8 | **[117]** |
| [$BCN_3$py][$NTf_2$] | 586.0 | 1.479 | 0.495 | 608.4 | 3.8 | [118] |
| [$HCN_3$py][$NTf_2$] | 658.0 | 1.409 | 0.553 | 677.7 | 3.0 | [118] |
| [$HCN_4$py][$NTf_2$] | 633.0 | 1.407 | 0.554 | 678.9 | 7.3 | [118] |
| [$OCN_3$py][$NTf_2$] | 709.0 | 1.355 | 0.609 | 744.7 | 5.0 | [118] |
| [hmpy][$NTf_2$] | 634.0 | 1.362 | 0.559 | 684.9 | 8.0 | [119, 120] |
| [$C_6$py][$NTf_2$] | 612.0 | 1.388 | 0.532 | 652.6 | 6.6 | [120] |
| **[bupy][$BF_4$]** | **395.2** | **1.213** | **0.305** | **381.3** | -3.5 | **[121]** |
| [bmpy][$NTf_2$] | 622.0 | 1.415 | 0.505 | 620.4 | -0.3 | [122, 123] |
| [bmpy][$BF_4$] | 405.0 | 1.183 | 0.333 | 414.8 | 2.4 | [122, 124] |
| **[bupy][$CF_3SO_3$]** | **470.4** | **1.214** | **0.390** | **482.9** | 2.7 | **[125]** |
| [4empy][$NTf_2$] | 630.5 | 1.487 | 0.449 | 553.4 | -12.2 | [126, 127] |
| [$O_3$mpy][$BF_4$] | 450.5 | 1.095 | 0.445 | 548.7 | 21.8 | [128] |

CATIONS: [bmpy]: 1-butyl-3-methylpyridinium; [$b_4$mpy]: 1-butyl-4-methylpyridinium; [$b_3$mpy]: 1-butyl-3-methyl-pyridinium; [epy]: 1-ethylpyridinium; [ppy]: 1-propylpyridinium; [eepy]: 1,2-diethylpyridinium; [mpy]: 1-methylpyridinium; [$BCN_3$py]: 1-butyl-3-cyanopyridinium; [$HCN_3$py]: 1-hexyl-3-cyanopyridinium; [$HCN_4$py]: 1-hexyl-4-cyanopyridinium; [$OCN_3$py]: 1-octyl-3-cyanopyridinium; [hmpy]: 1-hexyl-3-methylpyridinium; [$C_6$py]: 1-hexylpyridinium; [bupy]: 1-butylpyridinium; [4empy]: 1-ethyl-4-methylpyridinium; [$O_3$mpy]: 1-octyl-3-methylpyridinium.

ANIONS: [$C(CN)_3$]: tricyanomethanide; [$NTf_2$]: bis(trifluoromethylsulfonyl)imide; [DCA]: dicyanoamide; [$eSO_4$]: ethylsulfate; [$mSO_4$]: methylsulfate; [$CF_3SO_3$]: triflate.

## 4.7 The [C2py], [C4py] || Cl, Br system

This section describes a thermodynamic model for the ternary reciprocal system [C2py]Cl-[C2py]Br-[C4py]Cl-[C4py]Br. As mentioned previously, the thermodynamic properties of all four pure compounds must be known or estimated, so that the Gibbs free energy change for the exchange reaction [C2py]Br (liquid) + [C4py]Cl (liquid) = [C2py]Cl (liquid) + [C4py]Br (liquid) can be estimated. First of all, the thermodynamic properties ($\Delta H^{o}_{298.15K}$, $S^{o}_{298.15K}$ and $C_p(T)$) of all four pure ionic liquids are assessed by using all available data from the literature and by applying the VBT whenever relevant. Then, the phase diagrams of the four common-ion binary subsystems are modeled. Finally, the liquidus projection of the ternary reciprocal system and the two diagonal sections ([C4py]Br-[C2py]Cl and [C4py]Cl-[C2py]Br) are calculated solely from the optimized model parameters for the four common-ion binary subsystems.

### 4.7.1 Pure ionic liquids

Figure 4.13 presents the chemical structures of the four pure compounds investigated. Table 4.6 gathers all thermodynamic data collected from the literature for the four pyridinium-based pure ionic liquids. All phase diagram measurements in the [C2py], [C4py] || Cl, Br ternary reciprocal system were conducted recently by Stolarska et al. [37]. For the sake of consistency, the temperatures of fusion of the four pure compounds measured by these authors were selected in the present study. The properties of fusion proposed by Verevkin et al. [129] for [C2py]Cl were discarded since these are estimated values. The temperature of fusion was assessed from general trends of ionic liquids as 435K, which is 45K higher than the experimental value of Stolarska et al. [37]. The enthalpy of fusion was estimated as 23,500 $J.mol^{-1}$ using the modified Walden's rule [129]. The properties of fusion of [C2py]Br and [C4py]Br were measured by Verevkin et al. [129], and the ones of [C4py]Cl were measured by Verevkin et al. [130]. The corresponding values of the entropy of fusion are 32.4, 54.0 and 52.6 $J.mol^{-1}.K^{-1}$, respectively. The entropies of fusion of [C4py]Br and [C4py]Cl are very close to each other. Similarly, the entropy of fusion of [C2py]Cl was assumed to be identical to that of [C2py]Br, and the enthalpy of fusion of [C2py]Cl was then estimated as 12,638 $J.mol^{-1}$. The thermodynamic properties ($\Delta H^{o}_{298.15K}$, $S^{o}_{298.15K}$ and $C_p(T)$) of the four pure compounds were assessed using the VBT. The obtained values are discussed in detail below.

As mentioned previously, the VBT requires a knowledge of the molecular volume $\nu_m$ (expressed in $nm^3$). Verevkin et al. [130] measured the density of pure liquid $[C_4py]Cl$ as 1.010 $g.cm^{-3}$ at 418.2K using a pycnometer. To our knowledge, no other experimental density values are available for the solid or liquid phases of $[C_2py]Cl$, $[C_4py]Cl$, $[C_2py]Br$ and $[C_4py]Br$. The molecular volume of each pure solid at 298.15K was finally assessed using the method proposed by Krossing et al. [131]. Based on the cell parameters derived from X-ray diffraction data, these authors determined the molecular volume $\nu_m$ of various ionic liquids in the solid state. Assuming the additivity of the ion volumes (i.e. $\nu_m = \nu_{cation} + \nu_{anion}$), Krossing et al. reported volume values for various ions, which are supposed to be independent of the crystallographic structure. The following values were proposed [131]: 0.047 $nm^3$ for $Cl^-$, 0.056 $nm^3$ for $Br^-$, and 0.198 $nm^3$ for $[C_4py]^+$. Although no volume value was reported for $[C_2py]^+$, an estimation can be made from the volume value reported for $[C_4py]^+$. Krossing et al. [131] proposed the following ion volume values for various methyl-imidazolium-based cations differing from each other by one $-CH_2-$ group: 0.156 $nm^3$ for $[C_2mim]^+$, 0.178 $nm^3$ for $[C_3mim]^+$, 0.196 $nm^3$ for $[C_4mim]^+$ and 0.219 $nm^3$ for $[C_5mim]^+$. Krossing et al. concluded that the addition of one $-CH_2-$ group in the alkyl chain of these various ions corresponds to an average volume increase of 0.021 $nm^3$. The volume of $[C_2py]^+$ may thus be estimated as 0.156 $nm^3$ (i.e. 0.198 - 2×0.021). The derived molar volumes and densities of the four pyridinium-based ionic liquids in the solid state are presented in the Appendix (table A1).

Table 4.6: Thermodynamic data collected from the literature for the pure compounds $[C_2py]Cl$, $[C_2py]Br$, $[C_4py]Cl$ and $[C_4py]Br$

| Cation | Anion | Water content [ppm] | Purity [%] | Experimental technique | $\Delta H°_{298.15K}$ [$kJ.mol^{-1}$] | $C_p$ [$J.mol^{-1}.K^{-1}$] | Temperature of fusion (K) | Enthalpy of fusion ($kJ.mol^{-1}$) | Reference |
|---|---|---|---|---|---|---|---|---|---|
| $[C_2py]^+$ | $Cl^-$ | <100 | 99 | DSC | s:-125.1<br>l: -113.3 | - | 435 | 23.5 | [129] |
| | | - | - | DSC | - | - | 390 | - | [37] |
| | $Br^-$ | <100 | 99 | DSC | s:-82.0<br>l: -77.1 | - | 391.3 | 12.8 | [129] |
| | | - | - | DSC | - | - | 395 | - | [37] |
| | | - | >99.5 | AC | - | 76.4-300.3 $J.mol^{-1}.K^{-1}$ between 77.7 and 409.7K | 391.31 | 12.77 | [132] |
| $[C_4py]^+$ | $Cl^-$ | <100 | 99 | DSC | s:-177.7<br>l: -164.7 | - | 393.3 | 20.7 | [130] |
| | | - | - | DSC | - | - | 408 | - | [37] |
| | $Br^-$ | <100 | 99 | DSC | s:-144.1<br>l: -130.5 | - | 378 | 20.4 | [129] |
| | | - | - | DSC | - | - | 380 | - | [37] |

s and l refer to the solid and liquid phases, respectively.

AC: Adiabatic Calorimetry

In order to assess the density of ionic liquids in the liquid state, Paduszynski and Domanska [133] developed a new method based on generalized empirical correlations and group contributions obtained from a comprehensive database of experimental data for a variety of ionic liquids. These authors considered the organic cations to consist of a core along with alkyl chains or functional groups attached to it, whereas the anions were treated as individual groups. The molar volume of a given ionic liquid in the liquid state is then estimated by adding the molar volumes of its constitutive groups. The molar volumes of the constitutive groups of the four pyridinium-based ionic liquids in the liquid state and the derived densities of the latter are given in the Appendix (table A2). The density of pure liquid [$C_4$py]Cl was calculated to be 1.107 g.cm$^{-3}$ at 298.15K using the group contribution method from Paduszynski and Domanska, and then 1.028 g.cm$^{-3}$ at 418.2K using Equation (26) from Reference [133]. The latter compares reasonably well with the experimental value of 1.010 g.cm$^{-3}$ obtained by Verevkin et al. [130] (relative shift of 1.74%). The same relative shift of 1.74% was finally applied to the original density values estimated at 298.15K (and displayed in table A2 of the Appendix) for the [$C_2$py]Cl, [$C_2$py]Br, [$C_4$py]Cl and [$C_4$py]Br pure liquids.

To our knowledge, no heat capacity measurements are available for the [$C_2$py]Cl, [$C_4$py]Cl and [$C_4$py]Br compounds (solid and liquid). The $C_p$ values at 298.15K were assessed using Equation (43) (valid for 1-alkyl-pyridinium-based compounds) along with our estimated molecular volumes of the solid and liquid phases. Then, an identical procedure (described below) was used to assess the standard absolute entropies $S^o_{298.15K}$ of the solid and liquid phases. As an example, let us consider the [$C_2$py]Cl compound. As a starting point, using Equation (44) $S^o_{298.15K}$ of the solid and liquid phases were estimated as 282.5 and 285.6 J.mol$^{-1}$.K$^{-1}$, respectively. As explained previously, the entropy of fusion of [$C_2$py]Cl is about 32.4 J.mol$^{-1}$.K$^{-1}$. Assuming constant $C_p$ values, one can derive the following expression:

$$\Delta S^o_{fusion} = S^o_{298.15K}(l) - S^o_{298.15K}(s) + \left(C^l_p - C^s_p\right).ln\left(\frac{T_{fusion}}{298.15}\right) \quad (51)$$

It follows that $S^o_{298.15K}(l) - S^o_{298.15K}(s) \approx 31.6\, J\,.mol^{-1}\,.K^{-1}$. Since this term was initially only about 3.1 J.mol$^{-1}$.K$^{-1}$, the shift of (31.6-3.1)=28.5=2×14.2 was equally distributed on the initial values of $S^o_{298.15K}$ for the solid and liquid phases. That is, the $S^o_{298.15K}$ values finally selected for the solid and liquid phases of [$C_2$py]Cl are about 268.3 and 299.9 J.mol$^{-1}$.K$^{-1}$, respectively.

Tong et al. [132] measured the heat capacity of [C2py]Br by adiabatic calorimetry over the temperature range 77-410K. These $C_p$ data were fitted with the following equations:

$$C_p(T)/(J\,.mol^{-1}\,.K^{-1}) = A + BT + CT^2 = 43.0120 + 0.3308T + 0.0008T^2 (T\ in\ K)\ for\ the\ solid\ phase \quad (52)$$

$$C_p(T)/(J\,.mol^{-1}\,.K^{-1}) = a + bT = -23.4290 + 0.7903T\ (T\ in\ K)\ for\ the\ liquid\ phase \quad (53)$$

The calculated $C_p$ values of [C2py]Br are compared to the measurements of Tong et al. [132] in figure 4.14. One can derive the following expression for [C2py]Br:

$$\Delta S^o_{fusion} = S^o_{298.15K}(l) - S^o_{298.15K}(s) + (a-A).ln\left(\frac{T_{fusion}}{298.15}\right) + (b-B)\left(T_{fusion} - 298.15\right) - \frac{C}{2}\left(T^2_{fusion} - 298.15^2\right) \quad (54)$$

As a starting point, using Equation (44) $S^o_{298.15K}$ of the solid and liquid phases of [C2py]Br were estimated as 293.8 and 308.5 J.mol$^{-1}$.K$^{-1}$, respectively. Using a procedure similar to that for [C2py]Cl, the $S^o_{298.15K}$ values finally selected for the solid and liquid phases of [C2py]Br are about 284.4 and 317.9 J.mol$^{-1}$.K$^{-1}$, respectively.

Using an equation similar to Equation (45) along with Equations (46-50), values of $\Delta H^o_{298.15K}$ for the solid phases of [C2py]Cl, [C2py]Br, [C4py]Cl and [C4py]Br were estimated, based on the values $\Delta H^o_{298.15K}([C_2py]^+, g) = 680.1\ kJ.mol^{-1}$ and $\Delta H^o_{298.15K}([C_4py]^+, g) = 633.5\ kJ.mol^{-1}$ reported by Verevkin et al. [129] and the values $\Delta H^o_{298.15K}(Cl^-, g) = -233.954\ kJ.mol^{-1}$ and $\Delta H^o_{298.15K}(Br^-, g) = -219.008\ kJ.mol^{-1}$ taken from the FactSage thermodynamic databases [134]. The standard thermodynamic properties of the four pyridinium-based compounds estimated by the VBT are gathered in table 4.7.

Verevkin et al. [129] measured by DSC $\Delta H^o_{298.15K}$ for the liquid phases of [C2py]Cl, [C2py]Br, [C4py]Cl and [C4py]Br. For each of these four pure liquids, these authors derived $\Delta H^o_{298.15K}$ from the experimental reaction enthalpy $\Delta_r H^o$ related to the formation of the pyridinium-based ionic liquid from precursors (liquid pyridine and liquid $C_4H_9Cl$ in the case of liquid [C4py]Cl). A layer of ionic liquid solvent ([C4mim]$NTf_2$) was used to separate the precursors and to avoid beginning of the chemical reaction outside the DSC apparatus. The reaction enthalpy $\Delta_r H^o$, derived by

integration of the DSC peak, corresponds to the temperature of the peak maximum (about 503K for [$C_4$py]Cl). Verevkin et al. [129] showed that the correction ($\Delta C_p$) required to adjust the reaction enthalpy to the reference temperature 298.15K is within the DSC experimental uncertainties of about 1-3 kJ.mol$^{-1}$. Therefore, the experimental value of $\Delta_r H^o$ was considered to be valid at 298.15K and, using experimental values from the literature for $\Delta H^o_{298.15K}(liquid)$ of the precursors, Verevkin et al. [129] estimated $\Delta H^o_{298.15K}$ for the liquid pyridinium-based compound. These experimental values of $\Delta H^o_{298.15K}(liquid)$ from Verevkin et al. [129] were finally favoured in the present work. The thermodynamic properties finally selected for the four pyridinium-based compounds are displayed in table 4.8. Note that tables 4.7 and 4.8 only differ by the $\Delta H^o_{298.15K}$ values for the solid and liquid phases. In table 4.7, $\Delta H^o_{298.15K}$ $(solid)$ was estimated by the VBT and $\Delta H^o_{298.15K}$ $(liquid)$ was then derived from it using other thermodynamic properties ($C_p$ and properties of fusion). In table 4.8, $\Delta H^o_{298.15K}$ $(liquid)$ was taken directly from Verevkin et al. [129] and $\Delta H^o_{298.15K}$ $(solid)$ was then derived from it using other thermodynamic properties ($C_p$ and properties of fusion). The shifts between the two values of $\Delta H^o_{298.15K}$ $(liquid)$ are about -27.4 kJ.mol$^{-1}$ for [$C_2$py]Cl, -43.8 kJ.mol$^{-1}$ for [$C_2$py]Br, 1.7 kJ.mol$^{-1}$ for [$C_4$py]Cl, and -16.0 kJ.mol$^{-1}$ for [$C_4$py]Br.

Kabo et al. [135] proposed a group contribution method for the assessment of $\Delta H^o_{298.15K}$ of various liquid 1-alkyl-3-methylimidazolium nitrates [$C_n$mim]$NO_3$ (with n = 1, 2, 4). The substitution procedure was described by Emel'yanenko et al. [136], and the group contribution values were determined by Domalski and Hearing [137]. Kabo et al. [135] selected liquid 3-methylimidazolium nitrate [Hmim]$NO_3$ as the starting compound with a known (experimental) $\Delta H^o_{298.15K}$ value. [$C_1$mim]$NO_3$ is obtained from [Hmim]$NO_3$ by substituting the H atom connected to a N atom for a -$CH_3$ group, which corresponds to an enthalpy increment $\Delta H^o_{298.15K}((CH_3)_N) = -0.73\ kJ.mol^{-1}$ [137]. Then, [$C_n$mim]$NO_3$ (with n=2, 4) is obtained from [$C_1$mim]$NO_3$ by substituting one time or three times a H atom connected to a C atom for a -$CH_3$ group, which corresponds to an enthalpy increment $\Delta H^o_{298.15K}((CH_3)_C) = -25.73\ kJ.mol^{-1}$ [137]. In the present work, a similar approach was used for the [$C_2$py]Cl, [$C_2$py]Br, [$C_4$py]Cl and [$C_4$py]Br pure liquids. Liquid [$C_1$py]Cl and [$C_1$py]Br were selected as the starting compounds, since their $\Delta H^o_{298.15K}$ values were measured by Verevkin et al. [129] using DSC.

In table 4.9, for each of the four pyridinium-based compounds, the $\Delta H^{o}_{298.15K}(liquid)$ value derived using the group contribution method from Kabo et al. [135] (series 3) is given along with the experimental value of Verevkin et al. [129] (series 1) displayed in table 4.8, and the value derived from the VBT value of $\Delta H^{o}_{298.15K}(solid)$ (series 2) displayed in table 4.7. As mentioned previously, the shifts between series 1 and 2 lie between -43.8 and +1.7 kJ.mol$^{-1}$, whereas the shifts between series 1 and 3 lie between 5.0 and 8.7 kJ.mol$^{-1}$. The calculated shifts for series 3 are much smaller than those for series 2. This is not surprising since series 3 was obtained with the group contribution method from Kabo et al. [135], which requires the knowledge of $\Delta H^{o}_{298.15K}(liquid)$ for a starting compound similar to the targeted compound. On the other hand, series 2 only required a knowledge of the molecular volumes (for application of the VBT) along with the properties of fusion.

Table 4.7: Standard thermodynamic properties of the pyridinium-based pure compounds estimated by the VBT

| Compound | Molecular volume $v_m$ [nm$^3$] at 298.15K | | $C_p$ [J.mol$^{-1}$.K$^{-1}$] | | $S^o_{298.15K}$ [J.mol$^{-1}$.K$^{-1}$] | | $\Delta H^o_{298.15K}$ [J.mol$^{-1}$] | |
|---|---|---|---|---|---|---|---|---|
| | Solid | Liquid | Solid | Liquid | Solid | Liquid | Solid | Liquid |
| [$C_2$py]Cl | 0.203 | 0.205 | 259.4 | 262.4 | 268.3 | 299.9 | -153072 | -140704 |
| [$C_2$py]Br | 0.212 | 0.224 | $43.0120 + 0.3308T + 0.0008T^2$ | $-23.43 + 0.79T$ | 284.4 | 317.9 | -134058 | -120880 |
| [$C_4$py]Cl | 0.245 | 0.262 | 310.2 | 329.9 | 322.5 | 369.0 | -182293 | -162987 |
| [$C_4$py]Br | 0.254 | 0.280 | 320.4 | 351.9 | 339.5 | 385.5 | -164329 | -146505 |

Table 4.8: Selected thermodynamic properties for the pyridinium-based pure compounds

| Compound | T range [K] | $\Delta H^o_{298.15K}$ [J.mol$^{-1}$] | $S^o_{298.15K}$ [J.mol$^{-1}$.K$^{-1}$] | $C_p$ [J.mol$^{-1}$.K$^{-1}$] |
|---|---|---|---|---|
| [$C_2$py]Cl (s) | 298.15 to 600 | -125668 | 268.3 | 259.4 |
| [$C_2$py]Cl (l) | 298.15 to 600 | -113300 | 299.9 | 262.4 |
| [$C_2$py]Br (s) | 298.15 to 600 | -90278 | 284.4 | $43.0120 + 0.3308T + 0.0008T^2$ |
| [$C_2$py]Br (l) | 298.15 to 600 | -77100 | 317.9 | $-23.43 + 0.79T$ |
| [$C_4$py]Cl (s) | 298.15 to 600 | -184006 | 322.5 | 310.2 |
| [$C_4$py]Cl (l) | 298.15 to 600 | -164700 | 369.0 | 329.9 |
| [$C_4$py]Br (s) | 298.15 to 600 | -148324 | 339.5 | 320.4 |
| [$C_4$py]Br (l) | 298.15 to 600 | -130500 | 385.5 | 351.9 |

Table 4.9: Comparison between experimental and estimated values of $\Delta H^{o}_{298.15K}(liquid)(J.mol^{-1})$ for the pyridinium-based pure compounds

| Compound | From Verevkin et al. (series 1) | From VBT (series 2) | From group contribution method of Kabo et al. [135] (series 3) |
|---|---|---|---|
| [$C_2$py]Cl | -113300 [129] | -140704 | -104630 |
| [$C_2$py]Br | -77100 [129] | -120880 | -72130 |
| [$C_4$py]Cl | -164700 [130] | -162987 | -156090 |
| [$C_4$py]Br | -130500 [129] | -146505 | -123590 |

Kabo et al. [135] also proposed two linear regression equations to assess $\Delta H^{o}_{298.15K}$ for the solid and liquid phases of various 1-butyl-3-methyl-imidazolium compounds with different anionic groups ([$C_4$mim]X) as a function of the known value of $\Delta H^{o}_{298.15K}(solid)$ for the corresponding potassium salt KX, based on the available data for X = Br, I, and $NO_3$. In the present work, a similar approach was used for the liquid phase of 1-butylpyridinium compounds ([$C_4$py]X), using the experimental $\Delta H^{o}_{298.15K}$ values available for X = Cl, Br and $BF_4$ (see table 4.10).

The following linear regression equation was obtained:

$$\Delta H^{o}_{298.15K}([C_4py]X, liquid)/(kJ.mol^{-1}) = 193.4 + 0.82\Delta H^{o}_{298.15K}(KX, solid) \quad (55)$$

where $X$ is an anion. The standard error of a prediction is ± 0.73 kJ.mol$^{-1}$.

Equation (55) can be used to estimate $\Delta H^{o}_{298.15K}(liquid)$ for a given 1-butylpyridinium compound from the known value of $\Delta H^{o}_{298.15K}(solid)$ for the corresponding potassium salt. Owing to the lack of experimental data, no linear regression equation was derived for 1-ethylpyridinium compounds ([$C_2$py]X).

Table 4.10: Experimental values of $\Delta H^{o}_{298.15K}$(liquid or solid) from the literature used to derive Equation (55)

| Anion X | $\Delta H^{o}_{298.15K}([C_4py]X, liquid)$ [kJ.mol$^{-1}$] | $\Delta H^{o}_{298.15K}(KX, solid)$ [kJ.mol$^{-1}$] |
|---|---|---|
| $Cl^-$ | -164.7 [130] | -436.7 [93] |
| $Br^-$ | -130.5 [129] | -393.8 [93] |
| $BF_4^-$ | -1356.3 [138] | -1887.0 [93] |

*Discussion:* Using the selected thermodynamic data in table 4.8, the thermodynamic stability of the [$C_2$py]Cl, [$C_2$py]Br, [$C_4$py]Cl and [$C_4$py]Br pure compounds was examined both in the solid (at 25°C) and liquid (slightly above the melting temperature) states. Each compound is calculated

to decompose into C(graphite, s) and gaseous products. These reactions of decomposition are highly thermodynamically favoured since they have a very negative Gibbs free energy change. However, they are kinetically hindered owing to the necessity to break several bonds. A similar situation occurs for some common organic compounds such as benzene and acetone (both liquid at 25°C) as well as naphthalene and phenol (both solid at 25°C). Although these various compounds are stable at room temperature, they are all calculated to decompose thermodynamically using the FactSage databases [134].

The thermodynamic properties of pure ionic liquids are useful to assess their relative stability. More importantly, they are required to estimate the exchange Gibbs free energy (Equation (27)), which is an important parameter to model the phase diagrams of ternary reciprocal systems such as [$C_2$py], [$C_4$py] || Cl, Br. As mentioned previously, using the selected thermodynamic data in table 4.8, $\Delta g^{exchange}_{[C_2py][C_4py]/ClBr}$ for the exchange reaction [$C_2$py]Br (liquid) + [$C_4$py]Cl (liquid) = [$C_2$py]Cl (liquid) + [$C_4$py]Br (liquid) is estimated as -1.6 kJ.mol$^{-1}$ at 25°C, -1.9 kJ.mol$^{-1}$ at 100°C, and -2.4 kJ.mol$^{-1}$ at 150°C. Using the thermodynamic data in table 4.7 (mainly derived from the VBT), $\Delta g^{exchange}_{[C_2py][C_4py]/ClBr}$ is calculated as -2.9 kJ.mol$^{-1}$ at 25°C, -3.3 kJ.mol$^{-1}$ at 100°C, and -3.7 kJ.mol$^{-1}$ at 150°C. Although these two series of values are very close to each other, this is fortuitous since the shift between the two values of $\Delta H^{o}_{298.15K}(liquid)$ in tables 4.7 and 4.8 is as high as -43.8 kJ.mol$^{-1}$ for [$C_2$py]Br. As reported by Robelin [24], the $\Delta H^{o}_{298.15K}$ value estimated from the VBT for solid [$C_2$mim]$NO_3$ was about 46 kJ.mol$^{-1}$ lower than the experimental value of Emel'yanenko et al. [139] obtained by combustion calorimetry. These shifts are at least partly due to the uncertainty on the value of the standard enthalpy of formation at 298.15K of the organic cation in the gas state, derived from ab initio calculations. It can thus be concluded that, in the general case, the $\Delta H^{o}_{298.15K}$ values assessed from the VBT are not accurate enough to model the phase diagram of reciprocal systems; experimental values of $\Delta H^{o}_{298.15K}$ (such as the data of Verevkin et al. [129] obtained by DSC for the [$C_2$py]Cl, [$C_2$py]Br, [$C_4$py]Cl and [$C_4$py]Br pure liquids) are required.

## 4.7.2 Common-ion binary subsystems

### 4.7.2.1 The [C2py]Br – [C4py]Br binary system

The phase diagram has been measured by DSC [37]. No solid solubility was reported, and the measured limiting slopes of the [C2py]Br and [C4py]Br liquidus curves agree with Equation (36). No intermediate compound has been observed. The optimized Gibbs free energy of reaction (24) is:

$$\Delta g_{[C_2py][C_4py]/Br_2}/(J.mol^{-1}) = 159.0 - 29.3x_{[C_4py][C_4py]} \quad (56)$$

where $x_{[C_4py][C_4py]}$ is the mole fraction of second-nearest-neighbor ($[C_4py] - Br - [C_4py]$) pairs. The calculated phase diagram is shown along with the measurements in figure 4.15. This is a simple eutectic system. The reported characteristics of the experimental eutectic are {T=342K (i.e. 68.85°C), 48.0 mol% [C4py]Br} [37]. The characteristics of the calculated eutectic are {69°C, 48.0 mol% [C4py]Br}.

### 4.7.2.2 The [C2py]Cl – [C4py]Cl binary system

The phase diagram has been measured by DSC [37]. No solid solubility was reported, and the measured limiting slopes of the [C2py]Cl and [C4py]Cl liquidus curves agree with Equation (36). No intermediate compound has been observed. The optimized Gibbs free energy of reaction (24) is:

$$\Delta g_{[C_2py][C_4py]/Cl_2}/(J.mol^{-1}) = 627.6 - 1464.4x_{[C_2py][C_2py]} + 251.0x_{[C_4py][C_4py]} \quad (57)$$

where $x_{ii}$ is the mole fraction of second-nearest-neighbor ($i - Cl - i$) pairs. The calculated phase diagram is compared to the measurements in figure 4.16. Again, this is a simple eutectic system. It was not possible to reproduce the experimental liquidus temperature of 76.1°C at 20.0 mol% [C4py]Cl. If this data point had been favoured, then the calculated eutectic temperature would be significantly lower than the experimental one. The reported characteristics of the experimental eutectic are {T=349K (i.e. 75.85°C), 20.5 mol% [C4py]Cl} [37]. As seen in figure 4.16, the eutectic temperatures measured for the [C2py]Cl – [C4py]Cl binary system are relatively scattered: 75 ± 8°C. The characteristics of the calculated eutectic are {76°C, 27.3 mol% [C4py]Cl}.

#### 4.7.2.3 The [C2py]Cl – [C2py]Br binary system

The phase diagram has been measured by DSC [37]. A full solid solution was reported, and no intermediate compound has been observed. As explained previously, the $Cl^-$ and $Br^-$ anions have similar ionic radii and therefore the binary liquid was assumed to be ideal. That is:

$$\Delta g_{[C_2py]_2/ClBr} = 0 \quad (58)$$

The [C2py]Cl – [C2py]Br extensive solid solution was modeled with the Compound Energy Formalism (CEF). Its optimized Gibbs free energy is given by Equation (32), and the corresponding excess Gibbs free energy is:

$$G^E/(J.mol^{-1}) = y^A_{\mathrm{Cl}^-} y^A_{\mathrm{Br}^-} \left(242.7 - 188.3(y^A_{Cl^-} - y^A_{Br^-})\right) \quad (59)$$

The calculated phase diagram is shown along with the measurements in figure 4.17. Agreement is excellent.

#### 4.7.2.4 The [C4py]Cl – [C4py]Br binary system

The phase diagram has been measured by DSC [37]. Again, a full solid solution was reported, and no intermediate compound has been observed. By analogy with the [C2py]Cl – [C2py]Br system, the binary liquid was assumed to be ideal. That is:

$$\Delta g_{[C_4py]_2/ClBr} = 0 \quad (60)$$

The [C4py]Cl – [C4py]Br extensive solid solution was modeled with the CEF. Its optimized Gibbs free energy is given by Equation (32), with:

$$G^E/(J.mol^{-1}) = y^A_{\mathrm{Cl}^-} y^A_{\mathrm{Br}^-} \left(1292.9 + 292.9(y^A_{Cl^-} - y^A_{Br^-})\right) \quad (61)$$

The calculated phase diagram is compared to the measurements in figure 4.18. Agreement is excellent.

### 4.7.3 The [C2py]Cl – [C2py]Br – [C4py]Cl – [C4py]Br ternary reciprocal system

The [C2py]Cl – [C2py]Br – [C4py]Cl – [C4py]Br ternary reciprocal system has been studied by DSC [37]. Stolarska et al. measured the [C4py]Br – [C2py]Cl and [C4py]Cl – [C2py]Br sections. The corresponding calculated sections are shown along with the measurements in figures 4.19 and 3.20, respectively. (Glass transitions were measured below 250K (i.e. -23°C) in both sections and

are not shown in the figures.) No additional parameters were introduced for the liquid phase. The thermodynamic properties of the latter are calculated solely from the optimized parameters for the four common-ion binary subsystems (Equations (56-58, 60)). As seen in figures 4.19 and 4.20, the measurements are somewhat scattered but agree very satisfactorily with the calculations. The calculated liquidus projection of the $[C_2py]Cl$ – $[C_2py]Br$ – $[C_4py]Cl$ – $[C_4py]Br$ system is shown in figure 4.21. As mentioned previously, the ternary reciprocal liquid exhibits small deviations from ideality, owing to the fact that the two cations only differ by the length of their alkyl chains and that the two anions are halides with similar ionic radii. In the reciprocal square in figure 4.21, the four apices correspond to the pure salts: $[C_2py]Cl$, $[C_4py]Cl$, $[C_2py]Br$ and $[C_4py]Br$. Note that there is a degree of freedom in expressing the compositions in such a system. For example, a solution of one mole of $[C_2py]Cl$ and one mole of $[C_4py]Br$ could equally well be described as a mixture of one mole of $[C_4py]Cl$ and one mole of $[C_2py]Br$. Therefore, the compositions are expressed in terms of cationic and anionic equivalent fractions. The X-axis corresponds to the cationic molar ratio $\frac{n([C_2py])}{n([C_2py])+n([C_4py])}$, and the Y-axis corresponds to the anionic molar ratio $\frac{n_{Cl}}{n_{Cl}+n_{Br}}$ (where $n_i$ is the number of moles of ion $i$).

The $[C_2py]Cl$ – $[C_2py]Br$ – $[C_4py]Cl$ – $[C_4py]Br$ system is indeed a "ternary" system since it consists of four ionic species and the following condition of electroneutrality is respected at any composition inside the reciprocal square:

$$n_{[C_2py]^+} + n_{[C_4py]^+} = n_{Cl^-} + n_{Br^-} \quad (62)$$

In figure 4.21, the univariant line (along which the liquid coexists with the $[C_2py]Cl$ – $[C_2py]Br$ and $[C_4py]Cl$ – $[C_4py]Br$ extensive solid solutions) is shown as a bold line. By convention, the arrow indicates the direction of decreasing temperature along this line. The liquidus isotherms are displayed as thin lines. There are no calculated ternary invariant reactions, and the minimum liquidus temperature in the ternary reciprocal system corresponds to the binary eutectic reaction liquid = $[C_2py]Br$ + $[C_4py]Br$ at 69°C.

## 4.8 Conclusions

For the first time, the phase diagrams of a common-cation ternary system ($[C_4mpyrr]Cl$ – $[C_4mpyrr]Br$ – $[C_4mpyrr]BF_4$) and of a ternary reciprocal system (i.e. a system with two cations

and two anions: [$C_2$py], [$C_4$py] || Cl, Br), both consisting only of pyrrolidinium-based and pyridinium-based ionic liquids, respectively, were modeled successfully. The Modified Quasichemical Model [12-14] was used for the liquid phase, whereas the Compound Energy Formalism (CEF) [26, 27] was used for the relevant solid solutions. The two multicomponent liquids investigated display relatively small deviations from ideality. The Volume-based Thermodynamics (VBT) from Glasser and Jenkins [28-33] was used in conjunction with the available data from the literature to assess the thermodynamic properties of the [$C_2$py]Cl, [$C_2$py]Br, [$C_4$py]Cl and [$C_4$py]Br pure compounds, thus making it possible to estimate the Gibbs free energy change for the exchange reaction [$C_2$py]Br (liquid) + [$C_4$py]Cl (liquid) = [$C_2$py]Cl (liquid) + [$C_4$py]Br (liquid). The optimized parameters form a database for use with the FactSage thermochemical software [134] and may be used, along with Gibbs free energy minimization software, to calculate phase equilibria in the [$C_4$mpyrr]{Cl, Br, $BF_4$} and [$C_2$py], [$C_4$py] || Cl, Br systems.

The phase diagrams of the three binary subsystems of the [$C_4$mpyrr]{Cl, Br, $BF_4$} common-cation system were modeled based on the available DSC measurements [34]. Whereas [$C_4$mpyrr]{Cl, $BF_4$} and [$C_4$mpyrr]{Br, $BF_4$} are simple eutectic systems, [$C_4$mpyrr]{Cl, Br} exhibits a eutectic behavior with two terminal solid solutions. The thermodynamic properties of the ternary liquid were calculated from the optimized model parameters for the three binary subsystems using a standard asymmetric interpolation method with [$C_4$mpyrr]$BF_4$ as the asymmetric component. A small ternary excess parameter was included for the liquid phase in order to best reproduce the two isoplethal sections at constant 50 mol% [$C_4$mpyrr]$BF_4$ and at constant molar ratio [$C_4$mpyrr]Cl / ([$C_4$mpyrr]Cl + [$C_4$mpyrr]Br) of 0.85, which were measured by DSC in the present work. The calculated minimum liquidus temperature in the ternary system corresponds to a ternary eutectic at 91°C, very close to the binary eutectic in the [$C_4$mpyrr]{Cl, $BF_4$} system.

The phase diagrams of the four common-ion binary subsystems of the [$C_2$py], [$C_4$py] || Cl, Br system were modeled based on the available DSC measurements [37]. Whereas {[$C_2$py], [$C_4$py]}Cl and {[$C_2$py], [$C_4$py]}Br are simple eutectic systems, [$C_2$py]{Cl, Br} and [$C_4$py]{Cl, Br} both display an extensive solid solution over the entire composition range. The thermodynamic properties of the ternary reciprocal liquid were calculated solely from the optimized parameters for the four common-ion binary subsystems. The experimental [37] diagonal sections [$C_4$py]Br - [$C_2$py]Cl and [$C_4$py]Cl - [$C_2$py]Br are very satisfactorily reproduced by the model. The calculated

minimum liquidus temperature in the [$C_2$py], [$C_4$py] || Cl, Br system corresponds to the binary eutectic at 69°C in the {[$C_2$py], [$C_4$py]}Br system.

## Acknowledgements

The modeling part of this project was supported by the Natural Sciences and Engineering Research Council of Canada (Discovery Grant RGPIN 435893-2013). The new DSC measurements in the ternary system [$C_4$mpyrr]{Cl, Br, $BF_4$} were supported by the National Science Centre (Poland), project SONATA (Nº 2011/03/D/ST5/06200). Constructive discussions with Prof. Nick Virgilio were much appreciated.

## 4.9 Appendix

Table A1: Molar volume ($V_m$) and density (ρ) of pyridinium-based ionic liquids in the solid state estimated using the method proposed by Krossing et al. [131]

| Compound | $V_m$ ($cm^3.mol^{-1}$) | ρ ($g.cm^{-3}$) |
|---|---|---|
| $[C_2py]Cl$ | 122.3 | 1.174 |
| $[C_2py]Br$ | 127.7 | 1.473 |
| $[C_4py]Cl$ | 147.9 | 1.161 |
| $[C_4py]Br$ | 153.0 | 1.412 |

Table A2: Molar volume ($V_m$) of constitutive groups and density (ρ) of pyridinium-based ionic liquids in the liquid state estimated using the method proposed by Paduszynski and Domanska [133]

| Compound | Constitutive groups | Number | $V_m$ ($cm^3.mol^{-1}$) | ρ ($g.cm^{-3}$) |
|---|---|---|---|---|
| $[C_2py]Cl$ | pyridinium | 1 | 65.95 | 1.181 |
| | $N\text{-}CH_2$ | 1 | 2.88 | |
| | $CH_3$ | 1 | 26.16 | |
| | Cl | 1 | 26.66 | |
| $[C_2py]Br$ | pyridinium | 1 | 65.95 | 1.419 |
| | $N\text{-}CH_2$ | 1 | 2.88 | |
| | $CH_3$ | 1 | 26.16 | |
| | Br | 1 | 37.54 | |
| $[C_4py]Cl$ | pyridinium | 1 | 65.95 | 1.107 |
| | $N\text{-}CH_2$ | 1 | 2.88 | |
| | $CH_2$ | 2 | 16.73 | |
| | $CH_3$ | 1 | 26.16 | |
| | Cl | 1 | 26.66 | |
| $[C_4py]Br$ | pyridinium | 1 | 65.95 | 1.302 |
| | $N\text{-}CH_2$ | 1 | 2.88 | |
| | $CH_2$ | 2 | 16.73 | |
| | $CH_3$ | 1 | 26.16 | |
| | Br | 1 | 37.54 | |

## FIGURE CAPTIONS

**Figure 4.1:** Chemical structure of the pyrrolidinium-based ionic liquids: (a) [$C_4$mpyrr]Cl; (b) [$C_4$mpyrr]Br; (c) [$C_4$mpyrr]$BF_4$.

**Figure 4.2:** Calculated [$C_4$mpyrr]Br - [$C_4$mpyrr]$BF_4$ phase diagram, temperature versus mole fraction of [$C_4$mpyrr]$BF_4$. Experimental data are from Stolarska et al. [34] (●) and from the present work (▲).

**Figure 4.3:** Calculated [$C_4$mpyrr]Cl - [$C_4$mpyrr]$BF_4$ phase diagram, temperature versus mole fraction of [$C_4$mpyrr]$BF_4$. Experimental data are from Stolarska et al. [34] (●) and from the present work (▲).

**Figure 4.4(a):** Calculated [$C_4$mpyrr]Cl - [$C_4$mpyrr]Br phase diagram, temperature versus mole fraction of [$C_4$mpyrr]Br. Experimental data are from Stolarska et al. [34] (●) and from the present work (▲). Notations: A: [$C_4$mpyrr](Cl, [Br]) (ss), B: [$C_4$mpyrr](Br, [Cl]) (ss). The limiting liquidus slopes calculated from Equation (36) are shown as thin red lines.

**Figure 4.4(b)**: Calculated [$C_4$mpyrr]Cl - [$C_4$mpyrr]Br phase diagram over a wider temperature range. Experimental data are from Stolarska et al. [34] (●, ■) and from the present work (▲).

**Figure 4.5:** Calculated liquidus projection of the [$C_4$mpyrr]Cl - [$C_4$mpyrr]Br - [$C_4$mpyrr]$BF_4$ system.

**Figure 4.6:** DSC thermograms of the common-cation ternary system [$C_4$mpyrr]Cl - [$C_4$mpyrr]Br - [$C_4$mpyrr]$BF_4$, for the isoplethal section at constant molar ratio [$C_4$mpyrr]Cl / ([$C_4$mpyrr]Cl + [$C_4$mpyrr]Br) of 0.85. Mole fraction of [$C_4$mpyrr]$BF_4$ in the ternary mixture: (1) 0.00; (2) 0.25; (3) 0.50; (4) 0.75; (5) 0.90; (6) 1.00.

**Figure 4.7:** Calculated section of the [$C_4$mpyrr]Cl - [$C_4$mpyrr]Br - [$C_4$mpyrr]$BF_4$ phase diagram at constant 50.0 mol% [$C_4$mpyrr]$BF_4$. New DSC measurements (●); Stolarska et al. [34] (▲). Notations: A: [$C_4$mpyrr]$BF_4$(s), B: [$C_4$mpyrr]Cl($s_1$), C: [$C_4$mpyrr](Cl, [Br])(ss), D: [$C_4$mpyrr](Br, [Cl])(ss).

**Figure 4.8:** Calculated section of the [$C_4$mpyrr]Cl - [$C_4$mpyrr]Br - [$C_4$mpyrr]$BF_4$ phase diagram at constant molar ratio [$C_4$mpyrr]Cl / ([$C_4$mpyrr]Cl + [$C_4$mpyrr]Br) of 0.85. New DSC measurements (●); Stolarska et al. [34] (▲). Notations: A: [$C_4$mpyrr]$BF_4$(s), B: [$C_4$mpyrr]Cl($s_1$), C: [$C_4$mpyrr](Cl, [Br])(ss), D: [$C_4$mpyrr](Br, [Cl])(ss).

**Figure 4.9:** Calculated section of the [$C_4$mpyrr]Cl - [$C_4$mpyrr]Br - [$C_4$mpyrr]$BF_4$ phase diagram at constant 50.0 mol% [$C_4$mpyrr]$BF_4$, in presence (thick lines) or in absence (thin red lines) of the ternary excess parameter for the liquid phase (Equation (42)).

**Figure 4.10:** Calculated section of the [$C_4$mpyrr]Cl - [$C_4$mpyrr]Br - [$C_4$mpyrr]$BF_4$ phase diagram at constant molar ratio [$C_4$mpyrr]Cl / ([$C_4$mpyrr]Cl + [$C_4$mpyrr]Br) of 0.85, in presence (thick lines) or in absence (thin red lines) of the ternary excess parameter for the liquid phase (Equation (42)).

**Figure 4.11:** Heat capacity ($C_p$) at 298.15K as a function of molecular volume ($\nu_m$) for various pyridinium-based ionic liquids. Experimental data for 1-alkyl-pyridinium-based compounds (▲), experimental data for other types of pyridinium-based compounds (●), discarded experimental data (○). Linear regression equation for compounds shown as ▲: $C_p/(J.mol^{-1}.K^{-1})=1195.2\nu_m+16.8$ (full line). Linear regression equation for compounds shown as ▲ and ●: $C_p/(J.mol^{-1}.K^{-1})=1109.5\nu_m+37.1$ (dashed line).

**Figure 4.12:** Thermodynamic cycle to calculate the standard enthalpy $\Delta H^o_{298.15K}$ of solid [$C_2$py]Cl.

**Figure 4.13:** Chemical structure of the pyridinium-based ionic liquids: (a) [$C_2$py]Cl; (b) [$C_2$py]Br; (c) [$C_4$py]Cl; (d) [$C_4$py]Br.

**Figure 4.14:** Calculated heat capacity of [$C_2$py]Br versus temperature. Experimental data are from Tong et al. [132] (○). $C_p = 43.012 + 0.3308T + 0.0008T^2$ (solid), $C_p = -23.429 + 0.7903T$ (liquid).

**Figure 4.15:** Calculated [$C_2$py]Br - [$C_4$py]Br phase diagram, temperature versus mole fraction of [$C_4$py]Br. Experimental data are from Stolarska et al. [37] (●).

**Figure 4.16:** Calculated [$C_2$py]Cl - [$C_4$py]Cl phase diagram, temperature versus mole fraction of [$C_4$py]Cl. Experimental data are from Stolarska et al. [37] (●).

**Figure 4.17:** Calculated [$C_2$py]Cl - [$C_2$py]Br phase diagram, temperature versus mole fraction of [$C_2$py]Br. Experimental data are from Stolarska et al. [37] (●).

**Figure 4.18:** Calculated [$C_4$py]Cl - [$C_4$py]Br phase diagram, temperature versus mole fraction of [$C_4$py]Br. Experimental data are from Stolarska et al. [37] (●).

**Figure 4.19:** Calculated (predicted) [$C_4$py]Br - [$C_2$py]Cl section of the [$C_2$py]Cl - [$C_2$py]Br - [$C_4$py]Cl - [$C_4$py]Br phase diagram along with measurements from Stolarska et al. [37] (●). Notations: A: ([$C_2$py]Cl – [$C_2$py]Br) (ss), B: ([$C_4$py]Cl – [$C_4$py]Br) (ss).

**Figure 4.20:** Calculated (predicted) [$C_4$py]Cl - [$C_2$py]Br section of the [$C_2$py]Cl - [$C_2$py]Br - [$C_4$py]Cl - [$C_4$py]Br phase diagram along with measurements from Stolarska et al. [37] (●). Notations: A: ([$C_2$py]Cl – [$C_2$py]Br) (ss), B: ([$C_4$py]Cl – [$C_4$py]Br) (ss).

**Figure 4.21:** Calculated (predicted) liquidus projection of the [$C_2$py]Cl - [$C_2$py]Br - [$C_4$py]Cl - [$C_4$py]Br system.

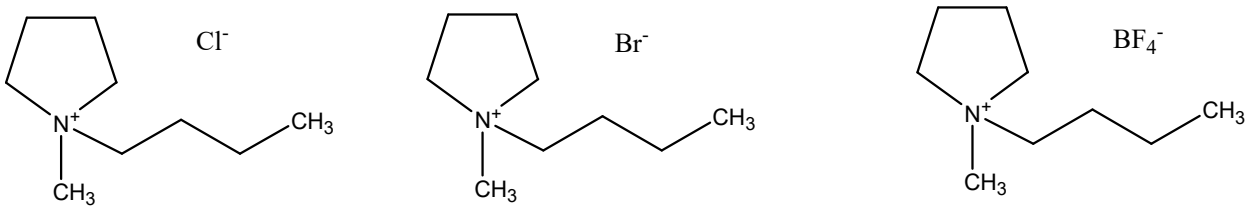


FIGURE 4.1

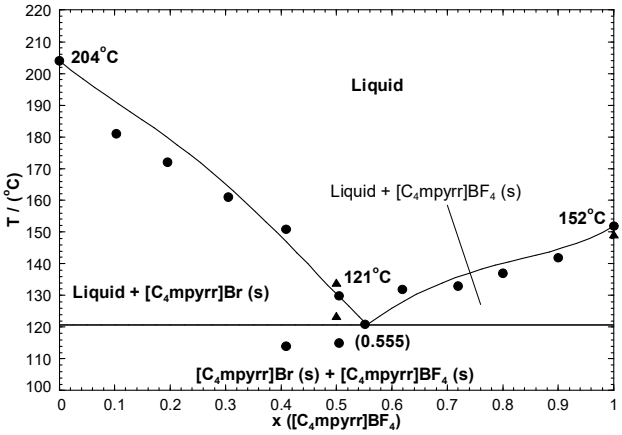


FIGURE 4.2

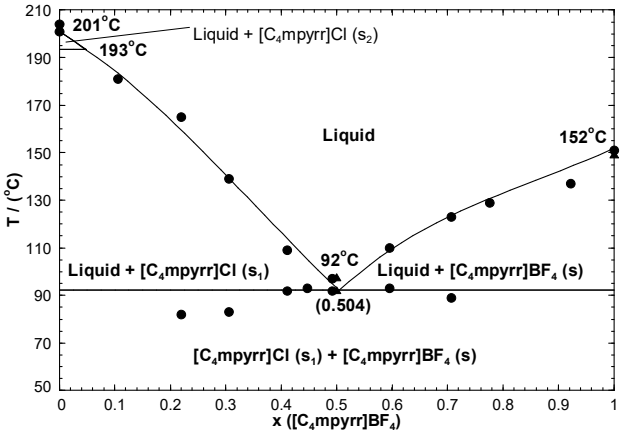


FIGURE 4.3

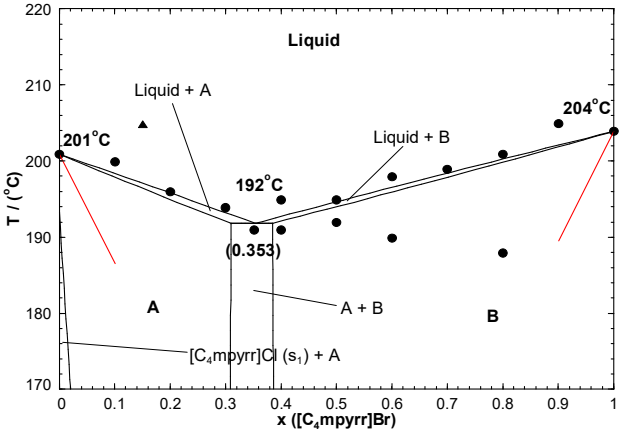


FIGURE 4.4(a)

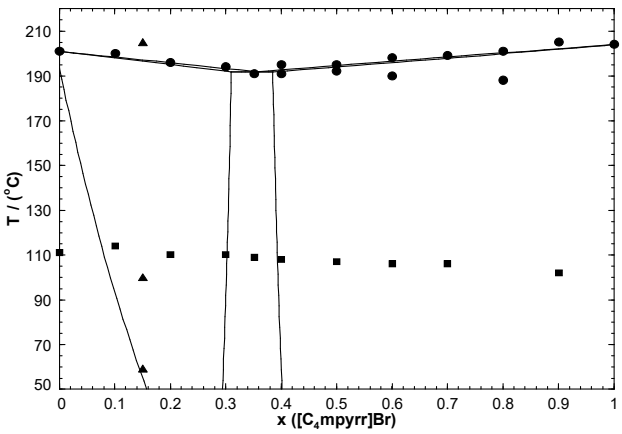


FIGURE 4.4(b)

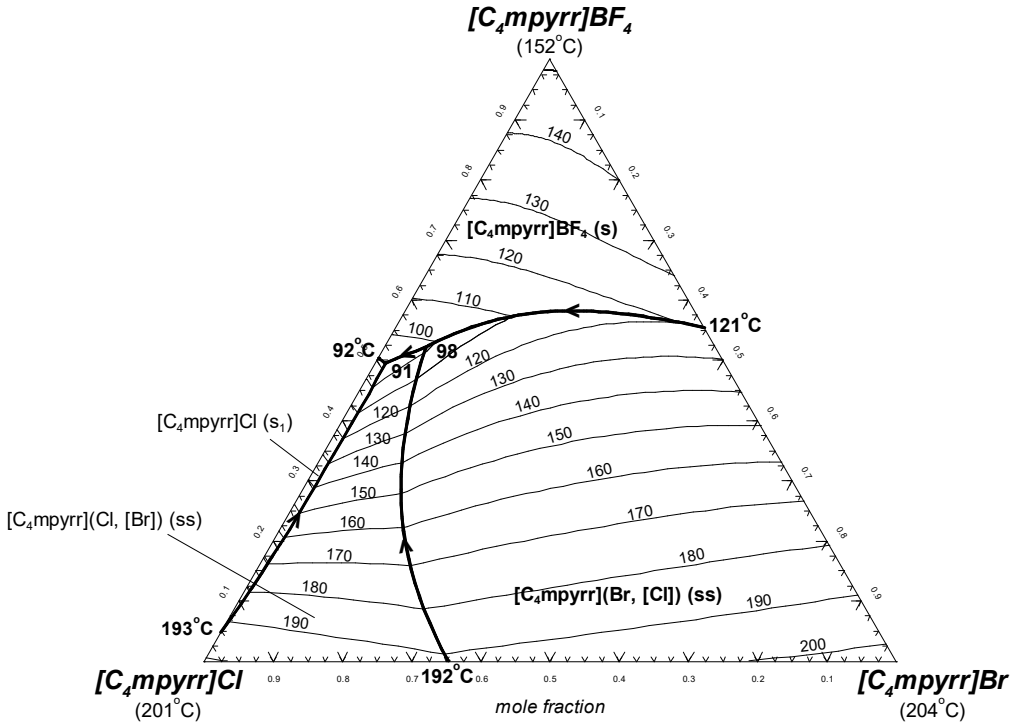


FIGURE 4.5

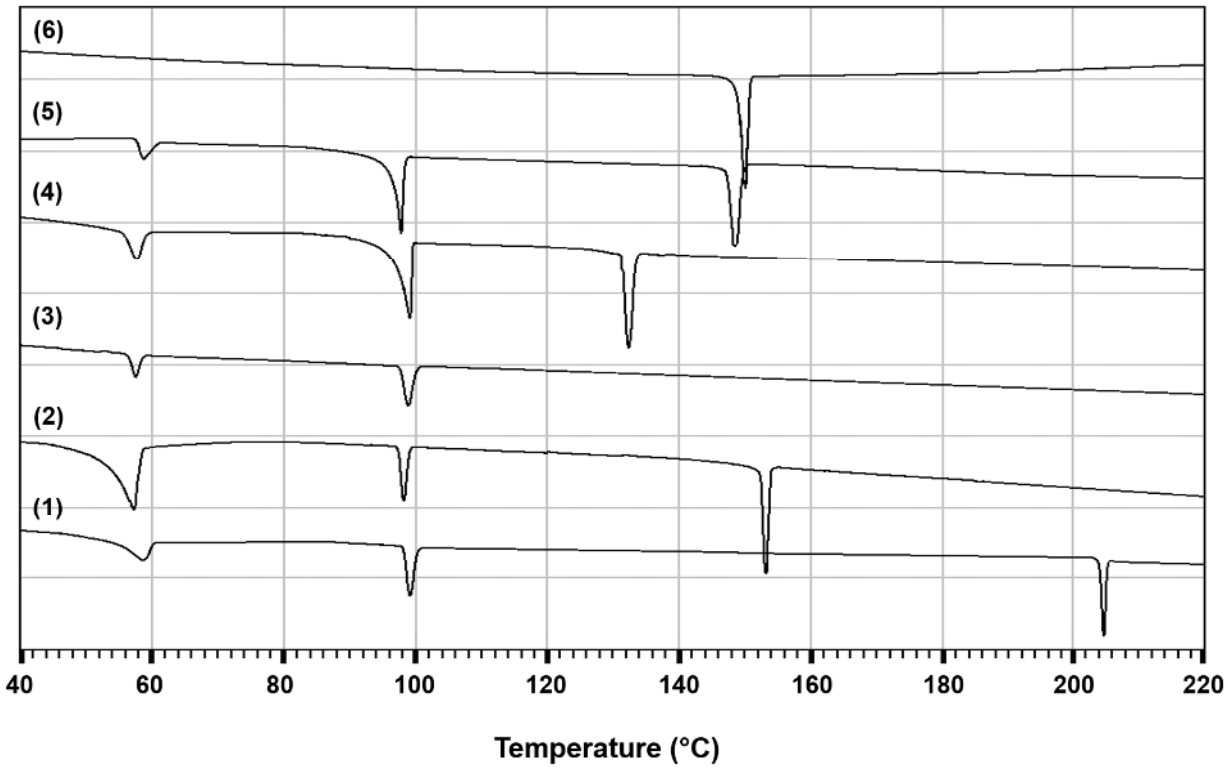


FIGURE 4.6

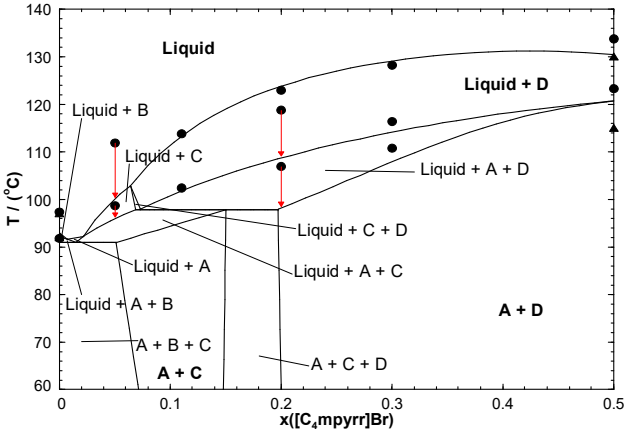


FIGURE 4.7

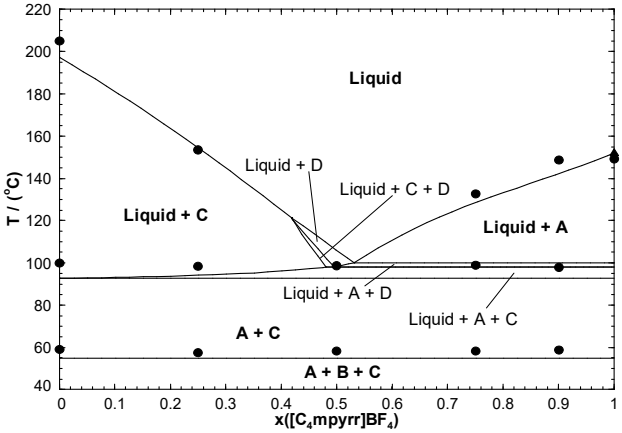


FIGURE 4.8

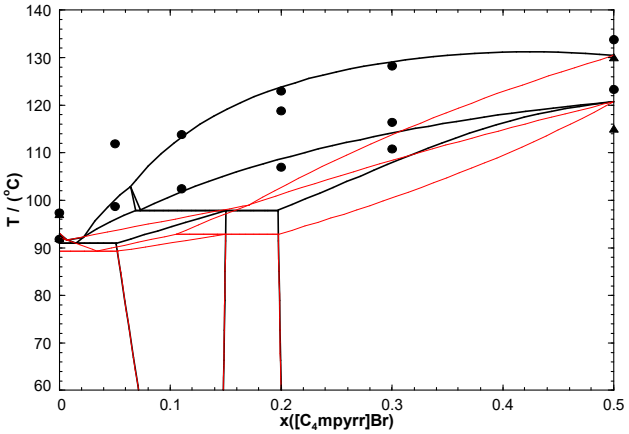


FIGURE 4.9

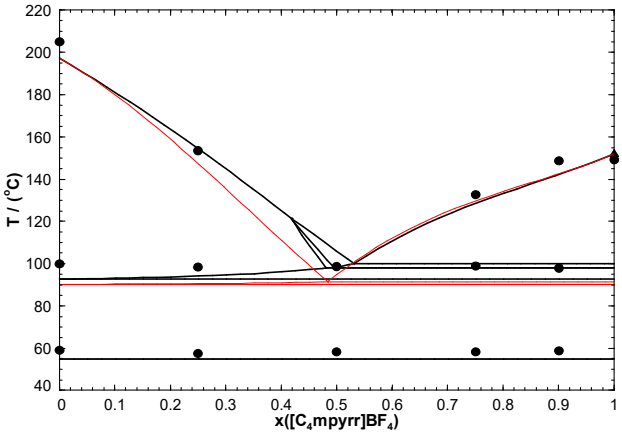


FIGURE 4.10

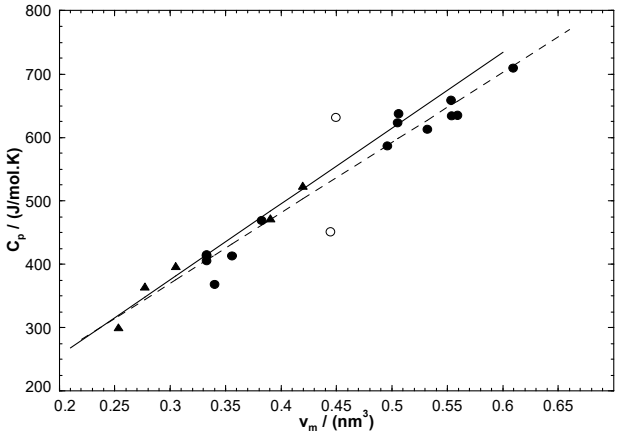


FIGURE 4.11

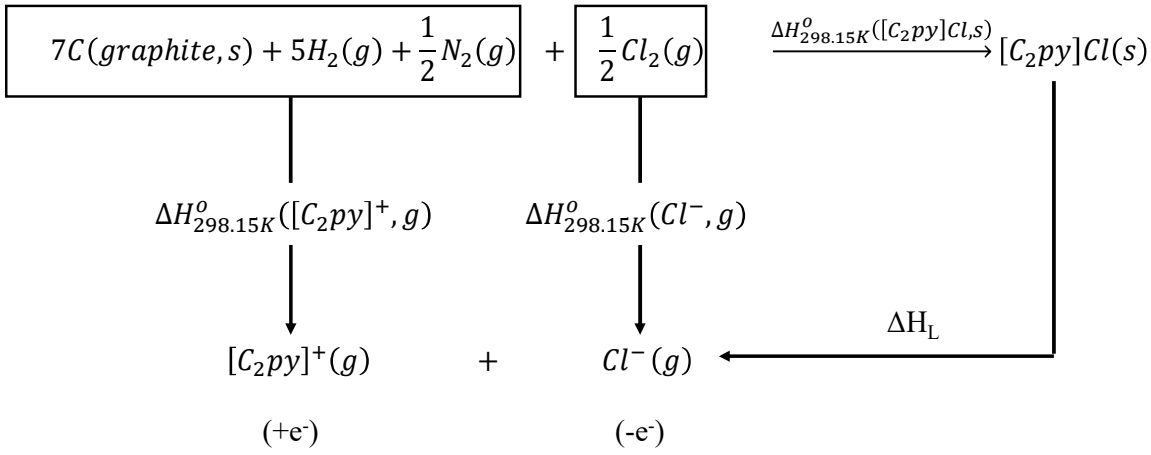


FIGURE 4.12

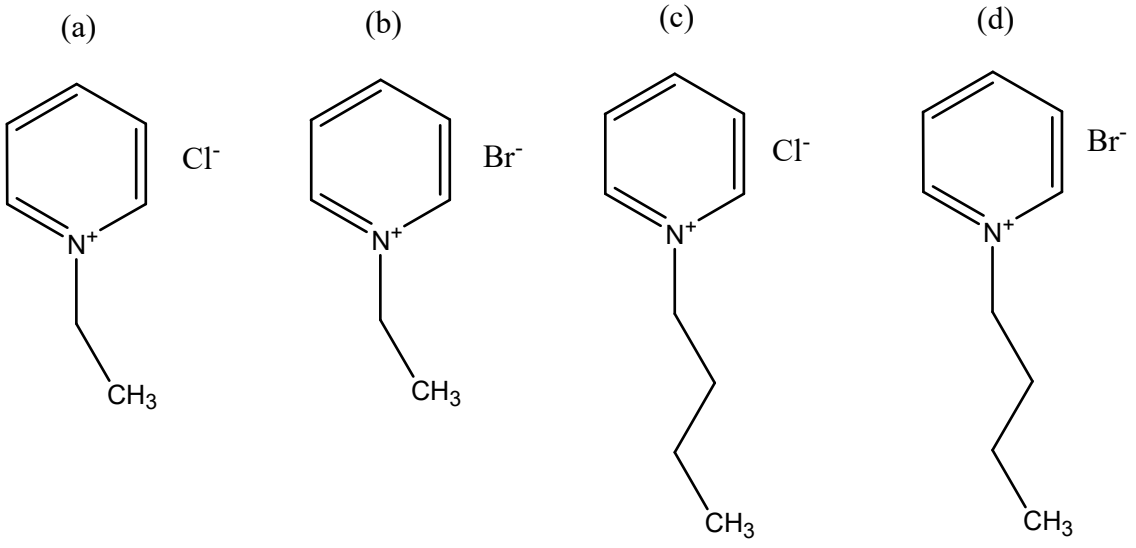


FIGURE 4.13

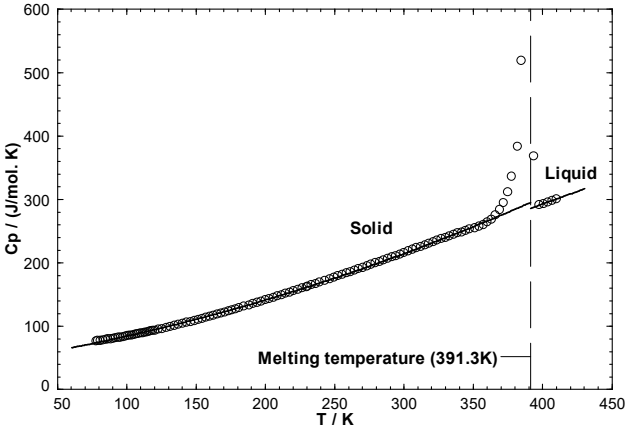


FIGURE 4.14

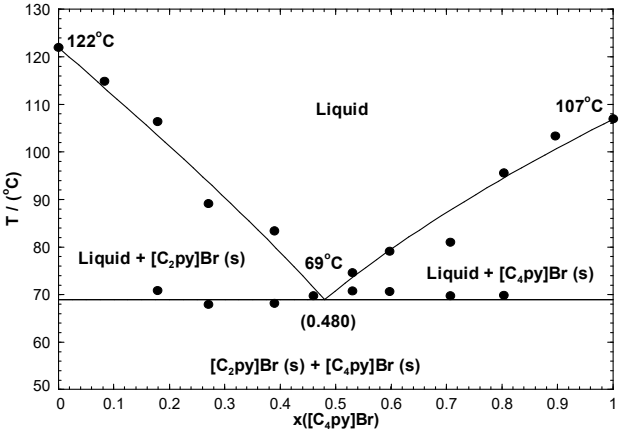


FIGURE 4.15

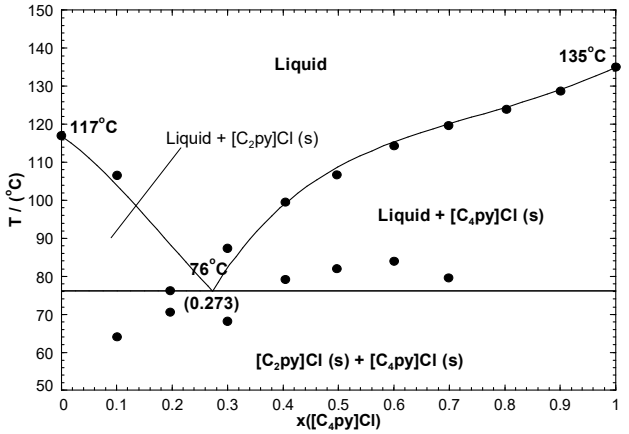


FIGURE 4.16

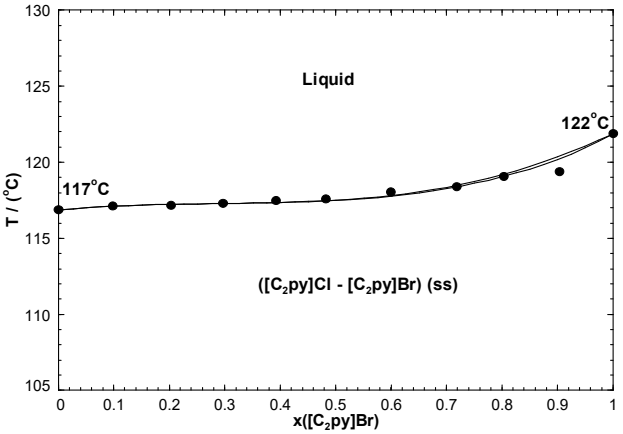


FIGURE 4.17

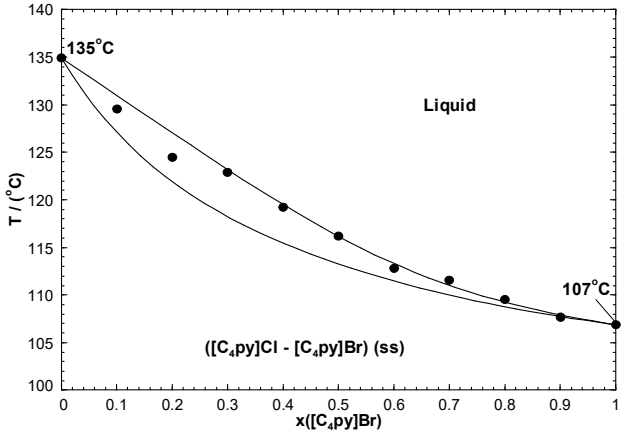


FIGURE 4.18

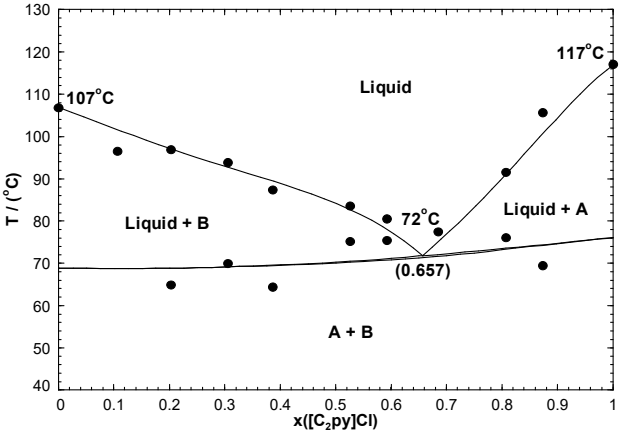


FIGURE 4.19

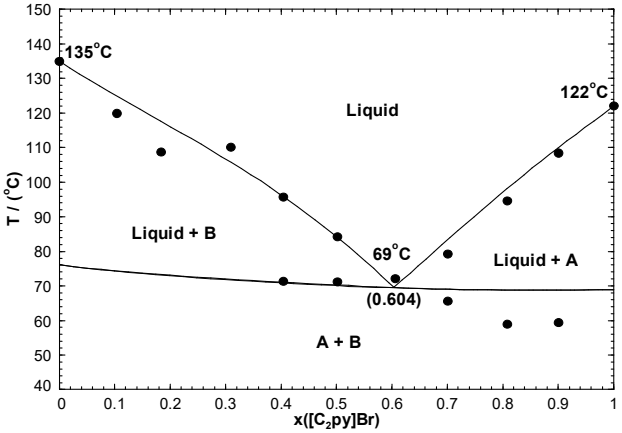


FIGURE 4.20

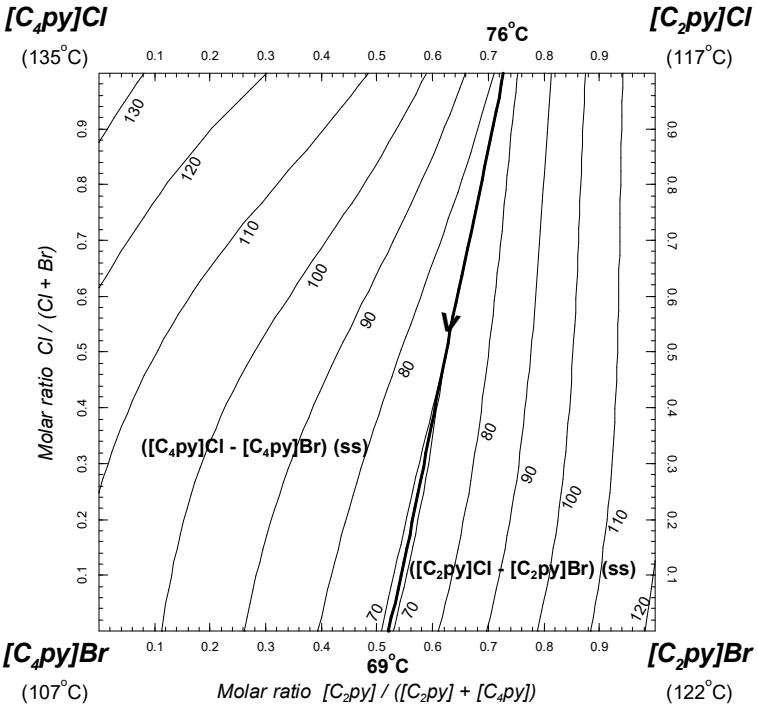


FIGURE 4.21

# CHAPTER 5 PHASE DIAGRAM OF THE COMMON-CATION TERNARY SYSTEM [$C_4$mim]{Cl, $NO_3$, $CH_3SO_3$}

This chapter describes a thermodynamic model for the common-cation ternary system [$C_4$mim]Cl - [$C_4$mim]$NO_3$ - [$C_4$mim]$CH_3SO_3$. DSC measurements were performed by Seddon's group (QUILL) for the three pure compounds and the three binary subsystems. As will be explained later, visual observation along with powder X-ray diffraction were also used to characterize the [$C_4$mim]Cl - [$C_4$mim]$NO_3$ system, owing to severe problems of hygroscopicity. The VBT from Glasser and Jenkins [28-33] is used in conjunction with the available data from the literature to estimate the thermodynamic properties of the pure compounds. Then, the phase diagrams of the three binary subsystems are modeled, and a tentative liquidus projection of the ternary system is calculated, using solely the optimized binary parameters along with a standard symmetric interpolation method.

## 5.1 Pure ionic liquids

In the present work, the [$C_4$mim]Cl - [$C_4$mim]$NO_3$ - [$C_4$mim]$CH_3SO_3$ ternary system was the very first ionic liquid system to be selected, in collaboration with Seddon's group. Imidazolium-based ionic liquids were favoured since they are among the most well-known ionic liquids. Also, they are sufficiently stable, relatively cheap and easy to synthesize. Figure 5.1 presents the chemical structures of the three pure compounds.

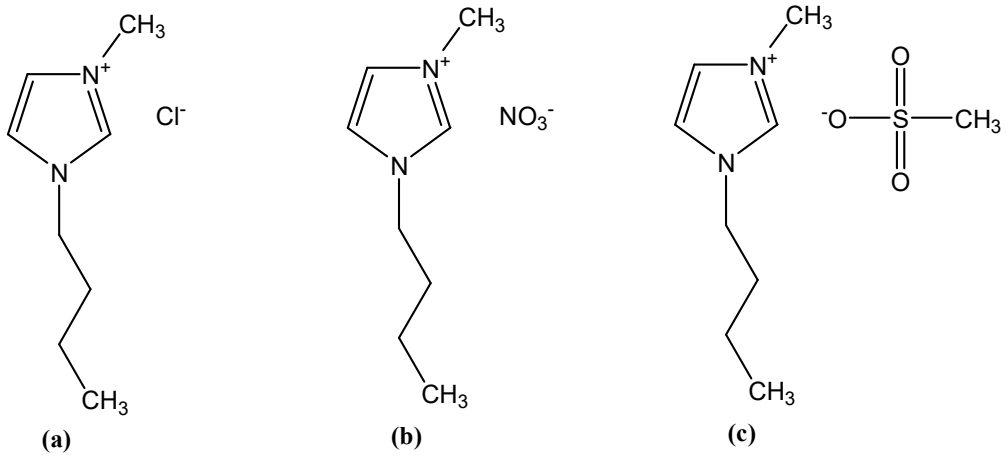


Figure 5.1: Chemical structure of the imidazolium-based ionic liquids: (a) [$C_4$mim]Cl; (b) [$C_4$mim]$NO_3$; (c) [$C_4$mim]$CH_3SO_3$.

*Experimental section:* The thermal behavior of the three pure compounds was studied by Seddon's group using DSC. Prior to the DSC measurements, the three pure ionic liquids were dried *in vacuo* at 70 °C and the water content was measured by the Karl-Fischer technique (between 200 and 1400 ppm). DSC experiments were performed for the three pure compounds using the two following procedures: heating - cooling - heating - cooling - heating and cooling - heating - cooling - heating - cooling cycles. Measurements were carried out at a fixed scan rate of 5°C/min for the heating and cooling cycles, and in the temperature range of -80°C to a temperature higher than the melting point of the pure compounds. The melting points and solid-solid transitions from the second and third heating runs were taken as the top temperatures of the peaks for the endothermic changes in heat flow. As an example, figure 5.2 displays the DSC thermograms for the $[C_4mim]NO_3$ pure compound corresponding to the second heating/cooling cycle according to the two different procedures. As seen in figure 5.2(a), upon heating a glass transition is observed at $T_g$=-78.6°C. Interestingly, an exothermic peak corresponding to a cold crystallization is observed at $T_{cc}$=-40.3°C with an enthalpy change $\Delta h_{cc}$=-13,813 J.mol$^{-1}$. A solid-solid transition is detected at $T_{trans}$=5.5°C with an enthalpy of transition $\Delta h_{trans}$=1,219 J.mol$^{-1}$. Finally, melting occurs at $T_{fusion}$=28.0°C and an enthalpy of fusion $\Delta h_{fusion}$=9,763 J.mol$^{-1}$. Upon cooling, no peak is observed under the measurement conditions. This supercooling behavior depends on variables such as the cooling rate. As seen in figure 5.2(b), upon cooling the pure liquid crystallizes at $T_{crys}$=-28.9°C with an enthalpy change $\Delta h_{crys}$=-9,970 J.mol$^{-1}$. Upon heating, a cold crystallization is detected at $T_{cc}$=-38.5°C with $\Delta h_{cc}$=-1,518 J.mol$^{-1}$. A solid-solid transition is observed at $T_{trans}$=5.6°C with $\Delta h_{trans}$=1,172 J.mol$^{-1}$. Finally, melting occurs at $T_{fusion}$=28.6°C with $\Delta h_{fusion}$=9,620 J.mol$^{-1}$. Table 5.1 gathers the thermal transitions measured by Seddon's group for the $[C_4mim]Cl$, $[C_4mim]NO_3$ and $[C_4mim]CH_3SO_3$ pure compounds along with the thermodynamic data collected from the literature.

As discussed previously, only the molar Gibbs free energies of fusion and the molar Gibbs free energies of solid-solid transition (if different allotropes exist) of the pure compounds need to be known to model the phase diagram of a common-ion (common-cation or common-anion) system for which measurements are available.

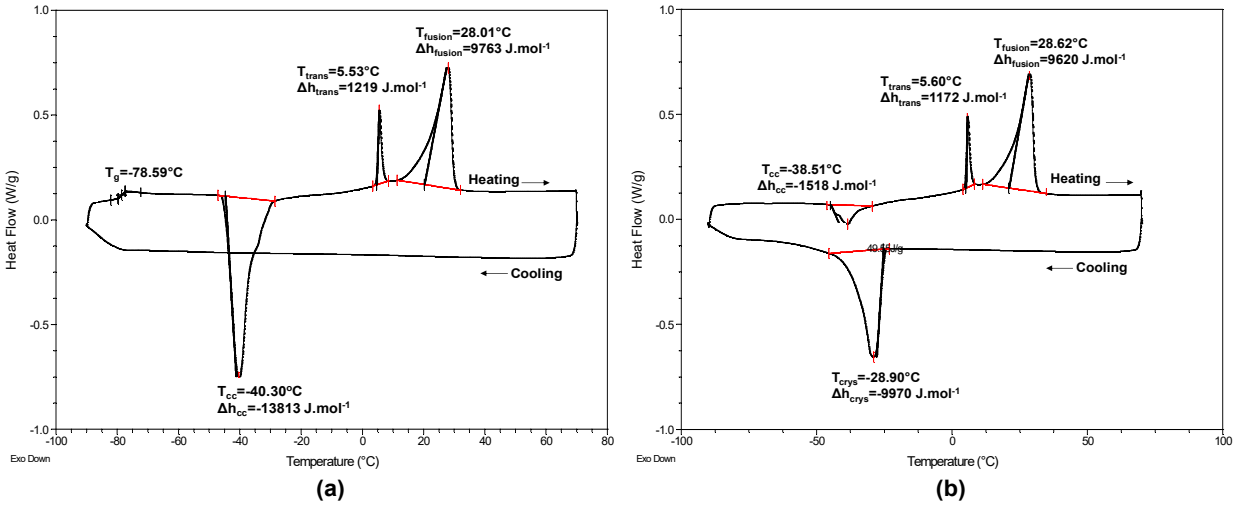


Figure 5.2: DSC thermograms for the $[C_4mim]NO_3$ pure compound starting with a: (a) heating run, or (b) cooling run (obtained by Seddon's group).

Strechan et al. [80] observed three solid-solid transitions by adiabatic calorimetry for the $[C_4mim]NO_3$ compound: $T_{trans1}$=5.65°C and $\Delta h_{trans1}$=2,080 J.mol$^{-1}$; $T_{trans2}$=14.95°C and $\Delta h_{trans2}$=360 J.mol$^{-1}$; $T_{trans3}$=19.05°C and $\Delta h_{trans3}$=150 J.mol$^{-1}$. These authors observed the fusion at $T_{fusion}$=36°C and $\Delta h_{fusion}$=17,990 J.mol$^{-1}$. There is a significant shift between the enthalpy of fusion measured by Seddon's group and that of Strechan et al. There is an excellent agreement between the measurements of Seddon's group and of Strechan et al. regarding the temperature of the first solid-solid transition. However, the corresponding $\Delta h_{trans}$ values are significantly different. The other two solid-solid transitions reported by Strechan et al. correspond to relatively small enthalpy changes and have not been observed by DSC. According to Strechan et al., the various solid-solid transitions are related to the evolution of spatial orientations of the nitrate ion. The temperatures and enthalpies of the three solid-solid transitions, along with the enthalpy of fusion reported by Strechan et al. for the $[C_4mim]NO_3$ compound are used directly in the present work. In particular, as will be explained in section 5.2.1, the enthalpy of fusion from Strechan et al. corresponds to a more reasonable limiting slope of the $[C_4mim]NO_3$ liquidus curve in the $[C_4mim]NO_3$ - $[C_4mim]Cl$ binary phase diagram. Also, it agrees well with the value of 17.4 kJ.mol$^{-1}$ obtained by Emel'yanenko et al. [139] using DSC. For the sake of consistency, the melting temperature of $[C_4mim]NO_3$ measured by Seddon's group was selected in the present work. The properties of fusion measured by Seddon's group (using DSC) for $[C_4mim]Cl$ and $[C_4mim]CH_3SO_3$ are used directly. They agree very satisfactorily with the available data from the literature, as shown in table 5.1.

Table 5.1: Thermodynamic data available in the literature or obtained by Seddon's group for the $[C_4mim]Cl$, $[C_4mim]NO_3$ and $[C_4mim]CH_3SO_3$ pure ionic liquids

| Cation | Anion | Water content (ppm) | Purity (%) | Experimental technique | $C_p$ ($J.mol^{-1}.K^{-1}$) | $\Delta H^o_{298.15K}$ ($J.mol^{-1}$) | Melting temperature (K) | Enthalpy of fusion ($J.mol^{-1}$) | Solid-solid transition | Reference |
|---|---|---|---|---|---|---|---|---|---|---|
| $[C_4mim]^+$ | $Cl^-$ | <0.5 wt% | >99 | DSC | - | - | 347 | 18000 | $T_{trans}$=30°C; $\Delta h_{trans}$=2700 ± 300 $J.mol^{-1}$ | [140] |
| | | - | - | DSC | - | - | 338 | 18500 | - | [141] |
| | | <150 | - | AC | - | - | 342 | 21000 | - | [142] |
| | | - | - | AC | - | - | 341 | 25860 | - | [143] |
| | | - | >98 | DSC | - | - | 342 | 14057 | - | [144] |
| | | <500 | - | DSC | - | - | 327 | 10310 | - | [145] |
| | | <2200 | - | DSC | - | - | 314 | - | - | [68] |
| | | - | - | DSC | - | - | 340 | 22900 | - | [146] |
| | | - | - | DSC | - | s: -214700<br>l: -196100 | 342 | 21700 | - | [147] |
| | | - | - | DSC | - | - | 342 | 20358 | - | Seddon's group |
| | $NO_3^-$ | 0.016 wt% | 99.4 | AC | s: 305.8 at 298.15K<br>l: 353.5 at 360K | s: -278600 | 309 | 17990 | $T_{trans1}$=5.65°C; $\Delta h_{trans1}$=2080 $J.mol^{-1}$<br>$T_{trans2}$=14.95°C; $\Delta h_{trans2}$=360 $J.mol^{-1}$<br>$T_{trans3}$=19.05°C; $\Delta h_{trans3}$=150 $J.mol^{-1}$ | [80] |
| | | <0.2 wt% | >99 | DSC | - | s: -278800<br>l: -261400 | 309 | 17400 | - | [139] |
| | | - | 99 | DSC | - | s: -275000<br>l: -256000 | - | - | - | [135] |
| | | - | - | DSC | - | - | 301 | 9691 | $T_{trans}$=5.60°C; $\Delta h_{trans}$=1196 $J.mol^{-1}$ | Seddon's group |
| | $CH_3SO_3^-$ | - | 99 | BC | - | - | 347 | 22000 | - | [148] |
| | | 0.29 wt% | 96 | DSC | l: 449.9 at 358.15K | - | 353 | - | - | [149] |
| | | - | - | DSC | - | - | 350 | - | - | [150] |
| | | - | - | DSC | - | - | 348 | 21278 | - | Seddon's group |

s and l refer to the solid and liquid phases, respectively.

AC: Adiabatic Calorimetry; BC: Bomb Calorimetry.

The thermodynamic properties ($\Delta H^{o}_{298.15K}$, $S^{o}_{298.15K}$ and $C_p(T)$) of the three pure compounds were assessed using the VBT in conjunction with the available data from the literature. The obtained values are discussed in detail below.

As mentioned previously, the VBT requires a knowledge of the molecular volume $v_m$ (expressed in $nm^3$). The densities of the $[C_4mim]Cl$, $[C_4mim]NO_3$ and $[C_4mim]CH_3SO_3$ pure liquids were measured by Seddon's group as discussed in Chapter 7. Since these compounds are all solid at room temperature, the densities of the three pure liquids at 298.15K were estimated by linear extrapolation of the data from Seddon's group. The obtained density values are 1.067 $g.cm^{-3}$ for liquid $[C_4mim]Cl$, 1.156 $g.cm^{-3}$ for liquid $[C_4mim]NO_3$, and 1.153 $g.cm^{-3}$ for liquid $[C_4mim]CH_3SO_3$. Using single crystal X-ray diffraction, Holbrey et al. [151] observed two crystalline polymorphs for $[C_4mim]Cl$, which differ only in the conformation of the butyl chain: an orthorhombic form (more thermodynamically stable) formed upon cooling the pure ionic liquid; and a monoclinic form formed via crystallization in the presence of an organic solvent or another ionic liquid. Only the orthorhombic form is considered in the present work. Based on the reported cell parameters, a density value of 1.207 $g.cm^{-3}$ at 298.15K is derived for solid $[C_4mim]Cl$. Using X-ray diffraction, Abe et al. [152] observed two crystalline polymorphs for $[C_4mim]NO_3$: an orthorhombic form stable at room temperature, and a monoclinic form stable at lower temperatures. Based on their measured cell parameters, these authors reported a density of 1.357 $g.cm^{-3}$ at 298.15K for the orthorhombic form of $[C_4mim]NO_3$. To our knowledge, no experimental density value is available in the literature for solid $[C_4mim]CH_3SO_3$. The molecular volume of solid $[C_4mim]CH_3SO_3$ at 298.15K was assessed in the present work using the method proposed by Krossing et al. [131] and described in Chapter 4 (section 4.7.1). These authors reported an ion volume of 0.196 $nm^3$ for $[C_4mim]^+$. Ye and Shreeve [153] reported an ion volume of 0.099 $nm^3$ for $CH_3SO_3^-$. The molecular volume of solid $[C_4mim]CH_3SO_3$ can thus be estimated as 0.295 $nm^3$, which corresponds to a density of 1.319 $g.cm^{-3}$.

For the solid and liquid phases of $[C_4mim]Cl$ and $[C_4mim]CH_3SO_3$, the $C_p$ values at 298.15K were assessed using Equation (15) from Chapter 3 (valid for methyl-imidazolium-based ionic liquids) along with the available molecular volume values.

Hu et al. [154] and Holbrey et al. [155] measured by DSC the heat capacity of liquid [C4mim]Cl over the temperature ranges 343-403K and 338-448K, respectively. These measurements were fitted with the two following equations:

$$C_p(T)/(J\,.mol^{-1}\,.K^{-1}) = a + bT = 106.8200 + 0.6711T\ (T\ in\ K) \quad (63)$$

$$C_p(T)/(J\,.mol^{-1}\,.K^{-1}) = 115.5500 + 0.5271T\ (T\ in\ K) \quad (64)$$

The $C_p$ values of liquid [C4mim]Cl extrapolated at 298.15K from Equations (63) and (64) were compared to the $C_p$ values assessed by the VBT. The corresponding shifts are about 16.6 J.mol$^{-1}$.K$^{-1}$ (5.4 %) and 50.9 J.mol$^{-1}$.K$^{-1}$ (18.6 %) for the measurements of Hu et al. and Holbrey et al., respectively. As discussed previously [24], the relative shift for methyl-imidazolium-based ionic liquids is expected to be usually lower than 5%. Therefore, Equation (63), derived from the $C_p$ data of Hu et al. [154], is finally preferred in the present work for liquid [C4mim]Cl. The calculated $C_p$ values of liquid [C4mim]Cl are compared to the measurements of Hu et al. [154] and Holbrey et al. [155] in figure 5.3.

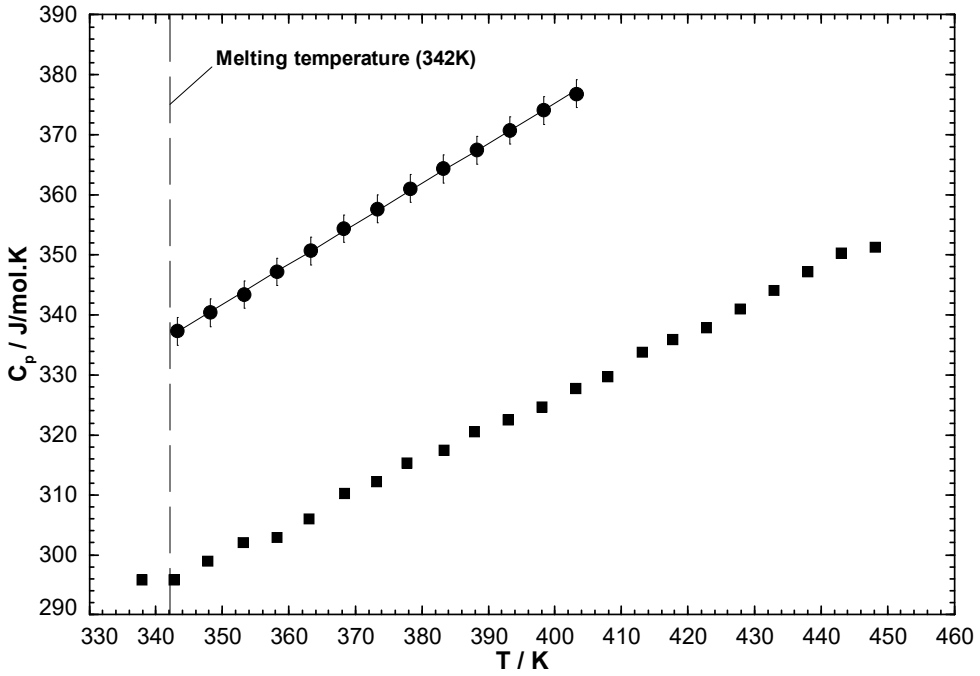


Figure 5.3: Calculated heat capacity of liquid [C4mim]Cl versus temperature. Experimental data are from Hu et al. [154] (●) and Holbrey et al. [155] (■).

Strechan et al. [80] measured the heat capacity of $[C_4mim]NO_3$ by adiabatic calorimetry over the temperature range 5-370K. These $C_p$ data were fitted with the following equations:

$$C_p/(J\,.mol^{-1}\,.K^{-1}) = -289.5157 - 2.8058T + 0.0035T^2 + 63.8467T^{0.5} + 366.8009T^{-0.5}\ (T\ in\ K) until\ 200K, for\ the\ solid\ phase \quad (65)$$

$$C_p(T)/(J\,.mol^{-1}\,.K^{-1}) = A + BT = 42.3390 + 0.8811T\ (T\ in\ K)\ above\ 200K\ for\ the\ solid\ phase \quad (66)$$

$$C_p(T)/(J\,.mol^{-1}\,.K^{-1}) = a + bT = 229.4500 + 0.4140T\ (T\ in\ K) for\ the\ liquid\ phase \quad (67)$$

The calculated $C_p$ values of $[C_4mim]NO_3$ are compared to the measurements of Strechan et al. [80] in figure 5.4.

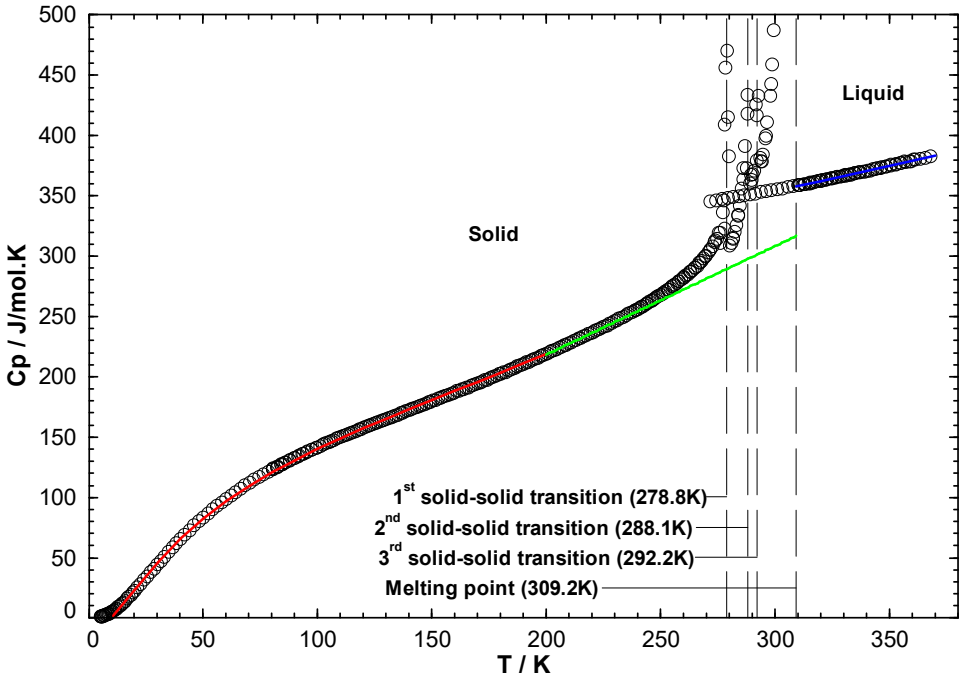


Figure 5.4: Calculated heat capacity of $[C_4mim]NO_3$ versus temperature. Experimental data are from Strechan et al. [80] (○). $C_p = -289.5157 - 2.8058T + 0.0035T^2 + 63.8467T^{0.5} + 366.8009T^{-0.5}$ (red line); $C_p = 42.3390 + 0.8811T$ (green line); $C_p = 229.4500 + 0.4140T$ (blue line).

As a starting point, the standard absolute entropies $S^o_{298.15K}$ of the solid and liquid phases of [C4mim]Cl, [C4mim]$NO_3$ and [C4mim]$CH_3SO_3$ were estimated using Equation (44) from Chapter 4. $S^o_{298.15K}$ was then adjusted using a procedure similar to the one described for [C2py]Br in Chapter 4 (section 4.7.1). Equation (54) was used with $B = C = 0$ for [C4mim]Cl, $C = 0$ for [C4mim]$NO_3$, and $B = C = b = 0$ for [C4mim]$CH_3SO_3$. The $S^o_{298.15K}$ value obtained for the allotrope ($s_4$) of [C4mim]$NO_3$ (stable form at 298.15K) was about 333.4 J.mol$^{-1}$.K$^{-1}$. It was finally adjusted to the value of 365.8 J.mol$^{-1}$.K$^{-1}$ derived by Strechan et al. [80] from their $C_p$ measurements at low temperatures. $S^o_{298.15K}$ for liquid [C4mim]$NO_3$ was then adjusted accordingly, using the relevant thermodynamic properties ($C_p$ and properties of fusion).

Using an equation similar to Equation (45) along with Equations (46-50) from Chapter 4 (section 4.6.3), values of $\Delta H^o_{298.15K}$ for the solid phases of [C4mim]Cl and [C4mim]$NO_3$ were estimated, based on an average value of 590,839 J.mol$^{-1}$ for $\Delta H^o_{298.15K}([C_4mim]^+, g)$ obtained from the two values 586,100 J.mol$^{-1}$ [129] and 595,579 J.mol$^{-1}$ [24], and on the values $\Delta H^o_{298.15K}(Cl^-, g) = -233{,}954\ \mathrm{J.mol^{-1}}$ and $\Delta H^o_{298.15K}(NO_3^-, g) = -310{,}779\ \mathrm{J.mol^{-1}}$ taken from the FactSage thermodynamic databases [134]. To our knowledge, no values of $\Delta H^o_{298.15K}(CH_3SO_3^-, g)$ are available in the literature. The standard thermodynamic properties of the three imidazolium-based compounds estimated by the VBT are gathered in table 5.2.

Verevkin et al. [129] measured by DSC $\Delta H^o_{298.15K} = -196{,}100\ \mathrm{J.mol^{-1}}$ for liquid [C4mim]Cl. The experimental procedure is similar to that described for the pyridinium-based compounds in Chapter 4 (section 4.7.1). The shift between this measured value and that derived from the VBT is about -11.8 kJ.mol$^{-1}$. Strechan et al. [80] measured $\Delta H^o_{298.15K} = -278{,}600\ \mathrm{J.mol^{-1}}$ for solid [C4mim]$NO_3$ using combustion calorimetry. There is a shift of about -26.6 kJ.mol$^{-1}$ between this measured value and that assessed by the VBT. The experimental values of $\Delta H^o_{298.15K}$ from Verevkin et al. [129] for liquid [C4mim]Cl and from Strechan et al. [80] for solid [C4mim]$NO_3$ (allotrope ($s_4$)) were finally favoured in the present work. The thermodynamic properties finally selected for the three imidazolium-based compounds are displayed in table 5.3. Note that tables 5.2 and 4.3 display some differences. In table 5.2, $\Delta H^o_{298.15K}$ $(solid)$ was estimated by the VBT and $\Delta H^o_{298.15K}$ $(liquid)$ was then derived from it using other thermodynamic properties ($C_p$ and properties of fusion). In table 5.3, $\Delta H^o_{298.15K}$ $(liquid)$ of [C4mim]Cl was taken directly from Verevkin et al. [129] and $\Delta H^o_{298.15K}$ $(solid)$ was then derived from it using other thermodynamic

properties ($C_p$ and properties of fusion). Also, $S^o_{298.15K}\,(solid)$ and $\Delta H^o_{298.15K}\,(solid)$ of $[C_4mim]NO_3$ (allotrope ($s_4$)) were directly taken from Strechan et al. [80], and $S^o_{298.15K}\,(liquid)$ and $\Delta H^o_{298.15K}\,(liquid)$ were then derived from them using other thermodynamic properties ($C_p$ and properties of fusion). Since $\Delta H^o_{298.15K}(CH_3SO_3^-, g)$ is unknown, $\Delta H^o_{298.15K}(solid)$ for $[C_4mim]CH_3SO_3$ was arbitrarily set to zero (table 5.3). As explained previously, only the molar Gibbs free energies of fusion and of solid-solid transition need to be known to model the phase diagram of a common-cation system such as $[C_4mim]Cl$ – $[C_4mim]NO_3$ – $[C_4mim]CH_3SO_3$. Therefore, the arbitrary value of $\Delta H^o_{298.15K}$ for solid $[C_4mim]CH_3SO_3$ will have no impact.

Verevkin et al. [129] measured by DSC $\Delta H^o_{298.15K} = -100{,}700\ J.mol^{-1}$ for liquid $[C_1mim]Cl$. Using the group contribution method proposed by Kabo et al. [135], and described in Chapter 4 (section 4.7.1), $\Delta H^o_{298.15K}$ of liquid $[C_4mim]Cl$ can be assessed as -177,890 J.mol$^{-1}$. The shift between the experimental value of $\Delta H^o_{298.15K}$ for liquid $[C_4mim]Cl$ from Verevkin et al. and the value estimated by the group contribution method from Kabo et al. is about +18.2 kJ.mol$^{-1}$.

Using the selected thermodynamic data in table 5.3, the thermodynamic stability of the $[C_4mim]Cl$ and $[C_4mim]NO_3$ pure compounds was examined both in the solid (at 25°C) and liquid (slightly above the melting temperature) states. Each compound is calculated to decompose into C (graphite, s) and gaseous products. As explained before in Chapter 4 for the pyridinium-based compounds, although these reactions of decomposition are highly thermodynamically favoured, they are kinetically hindered owing to the necessity to break several bonds.

Table 5.2: Standard thermodynamic properties of the imidazolium-based pure compounds estimated by the VBT

| Compound | Molecular volume $v_m$ [nm$^3$] at 298.15K | | $C_p$ [J.mol$^{-1}$.K$^{-1}$] | | $S^o_{298.15K}$ [J.mol$^{-1}$.K$^{-1}$] | | $\Delta H^o_{298.15K}$ [J.mol$^{-1}$] | |
|---|---|---|---|---|---|---|---|---|
| | Solid | Liquid | Solid | Liquid | Solid | Liquid | Solid | Liquid |
| $[C_4mim]Cl$ | 0.240[a] | 0.272 | 290.2 | $106.8200 + 0.6711T$ | 321.1 | 376.3 | -226867 | -207895 |
| $[C_4mim]NO_3$ | 0.246[b] | 0.289 | $-289.5157 - 2.8058T + 0.0035T^2 + 63.8467T^{0.5} + 366.8009T^{-0.5}$ *(A)* | $229.4500 + 0.4140T$ | - ($s_1$) | 392.7 | - ($s_1$) | -287395 |
| | | | $42.3390 + 0.8811T$ *(B)* | | 324.2 ($s_1$) | | -307834 ($s_1$) | |
| | | | | | 331.7 ($s_2$) | | -305754 ($s_2$) | |
| | | | | | 332.9 ($s_3$) | | -305394 ($s_3$) | |
| | | | | | 333.4 ($s_4$) | | -305244 ($s_4$) | |
| $[C_4mim]CH_3SO_3$ | 0.295 | 0.337 | 347.9 | 392.6 | 396.6 | 450.7 | 21094 + $\Delta H^o_{298.15K}(CH_3SO_3^-, g)$ | 40137 + $\Delta H^o_{298.15K}(CH_3SO_3^-, g)$ |

[a] *Reference* [151]; [b] *Reference* [152]. *(A)*: until 200K for ($s_1$, $s_2$, $s_3$, $s_4$); *(B)*: above 200K for ($s_1$, $s_2$, $s_3$, $s_4$).

Table 5.3: Selected thermodynamic properties for the imidazolium-based pure compounds

| Compound | T range [K] | $\Delta H^{o}_{298.15K}$ [J.mol$^{-1}$] | $S^{o}_{298.15K}$ [J.mol$^{-1}$.K$^{-1}$] | $C_p$ [J.mol$^{-1}$.K$^{-1}$] |
|---|---|---|---|---|
| [C$_4$mim]Cl (s) | 298.15 to 600 | -215072 | 321.1 | 290.2 |
| [C$_4$mim]Cl (l) | 298.15 to 600 | -196100 | 376.3 | $106.8200 + 0.6711T$ |
| [C$_4$mim]NO$_3$ (s$_1$, s$_2$, s$_3$, s$_4$) | 10 to 200 | - (s$_1$) | - (s$_1$) | $-289.5157 - 2.8058T + 0.0035T^2 + 63.8467T^{0.5} + 366.8009T^{-0.5}$ |
| | 200 to 301.15 | -281190 (s$_1$) | 356.6 (s$_1$) | $42.3390 + 0.8811T$ |
| | | -279110 (s$_2$) | 364.0 (s$_2$) | |
| | | -278750 (s$_3$) | 365.3 (s$_3$) | |
| | | -278600 (s$_4$) | 365.8 (s$_4$) | |
| [C$_4$mim]NO$_3$ (l) | 10 to 200 | - | - | $-289.5157 - 2.8058T + 0.0035T^2 + 63.8467T^{0.5} + 366.8009T^{-0.5}$ |
| | 200 to 600 | -260751 | 425.1 | $229.4500 + 0.4140T$ |
| [C$_4$mim]CH$_3$SO$_3$ (s) | 298.15 to 600 | 0 | 396.6 | 347.9 |
| [C$_4$mim]CH$_3$SO$_3$ (l) | 298.15 to 600 | +19043 | 450.7 | 392.6 |

## 5.2 Binary subsystems

The binary phase diagrams were measured by DSC using three consecutive heating and cooling cycles with scan rates of 2.5°C/min (heating) and 5°C/min (cooling), respectively. The binary mixtures were dried in the freeze dryer prior to the DSC experiments.

### 5.2.1 The [C$_4$mim]NO$_3$ – [C$_4$mim]Cl binary system

This is the first binary system that was studied in the present work. Substantial problems of hygroscopicity were encountered and, for some compositions, it was not possible to measure their liquidus temperature by DSC (absence of peak). Therefore, visual observation (upon heating) along with powder X-ray diffraction at room temperature were also used to characterize the [C$_4$mim]NO$_3$ – [C$_4$mim]Cl phase diagram. The optimized Gibbs free energy of reaction (25) in Chapter 4 is:

$$\Delta g_{[C_4mim]_2/(NO_3)Cl}(J.mol^{-1}) = 418.4 + 543.9x_{(NO_3)(NO_3)} \quad (68)$$

where $x_{(NO_3)(NO_3)}$ is the mole fraction of second-nearest-neighbor $(NO_3 - [C_4mim] - NO_3)$ pairs. The calculated phase diagram is compared to the measurements in figure 5.5. As seen in this figure, the data are rather scattered. Stolarska et al. [73] reported that they were unable to obtain reproducible DSC measurements for the phase diagram of the [C$_2$mim]NO$_3$ – [C$_2$mim]Cl binary

system, owing to the very hygroscopic nature of this combination of ionic liquids. Note that the $[C_4mim]^+$ and $[C_2mim]^+$ cations only differ by the length of their alkyl chains (butyl or ethyl). The calculated (tentative) $[C_4mim]NO_3$ – $[C_4mim]Cl$ phase diagram is a simple eutectic system. The characteristics of the calculated eutectic are {T=21°C, 21.8 mol% $[C_4mim]Cl$}.

The calculated limiting slope of the $[C_4mim]NO_3$ liquidus curve agrees reasonably well with the available data. If the experimental enthalpy of fusion of $[C_4mim]NO_3$ measured by Seddon's group had been favoured, then the corresponding limiting slope would be even steeper (see figure 5.5) and agreement in the $[C_4mim]NO_3$-rich region would be much less satisfactory. The calculated eutectic composition of 21.8 mol% $[C_4mim]Cl$ agrees reasonably well with the powder X-ray diffraction data (shown in figure 5.6), which suggest that the experimental eutectic composition is close to 30 mol% $[C_4mim]Cl$.

The diffractogram (0) of pure $[C_4mim]NO_3$ displays two distinctive peaks at $2\theta\approx15°$ and $2\theta\approx22°$. According to Strechan et al. [80], there are four different allotropes, and the high-temperature form is formed at about 19°C. Since all temperatures measured by Seddon's group are above 20°C, only the allotrope ($s_4$) should be observed.

The diffractogram (10) of pure $[C_4mim]Cl$ exhibits two distinctive peaks at $2\theta\approx10°$ and $2\theta\approx20°$. For 10 and 20 mol% $[C_4mim]Cl$, only the peaks related to pure $[C_4mim]NO_3$ are observed. For 60, 70, 80 and 90 mol% $[C_4mim]Cl$, only the peaks related to pure $[C_4mim]Cl$ are observed. For 30 mol% $[C_4mim]Cl$, the peaks related to both pure compounds are observed (in particular, the peak at $2\theta\approx20°$ for pure $[C_4mim]Cl$). For 40 and 50 mol% $[C_4mim]Cl$, the diffractograms are not very conclusive and difficult to interpret.

For the X-ray diffraction experiments, the various samples were prepared in a glove box and protected from the environment using a Kapton film. The measurements were performed at room temperature (i.e. very close to the calculated eutectic temperature). The diffractograms related to the binary mixtures at 10, 20, 60, 70, 80 and 90 mol% $[C_4mim]Cl$ only display the peaks corresponding to pure $[C_4mim]NO_3$ or pure $[C_4mim]Cl$. Therefore, thermodynamic equilibrium has not been reached and only the peaks for the primary solid phase precipitating are observed. Although the formation of solid solutions cannot be excluded, it is very unlikely. Indeed, the experimental ACl – $ANO_3$ binary phase diagrams (with A=Li, Na, K) display a negligible solid solubility.

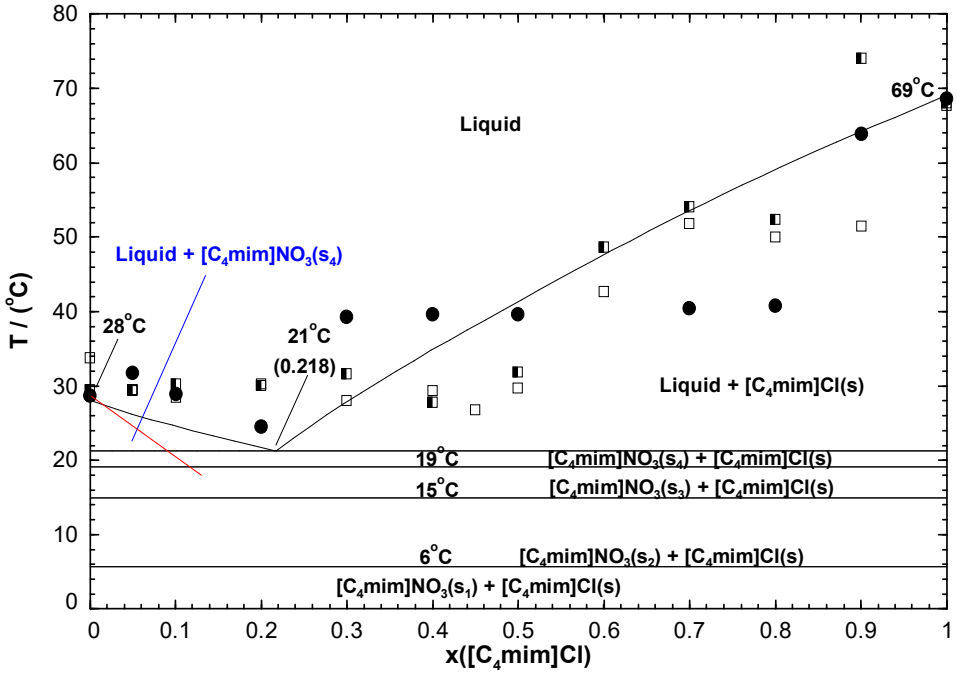


Figure 5.5: Calculated (tentative) $[C_4mim]NO_3$ - $[C_4mim]Cl$ phase diagram, temperature versus mole fraction of $[C_4mim]Cl$. Experimental data are from Seddon's group. (●): DSC measurements; (□): first series of visual observation data; (◧): second series of visual observation data. The limiting slope of the $[C_4mim]NO_3$ liquidus curve calculated with the experimental enthalpy of fusion from Seddon's group is shown as a red line.

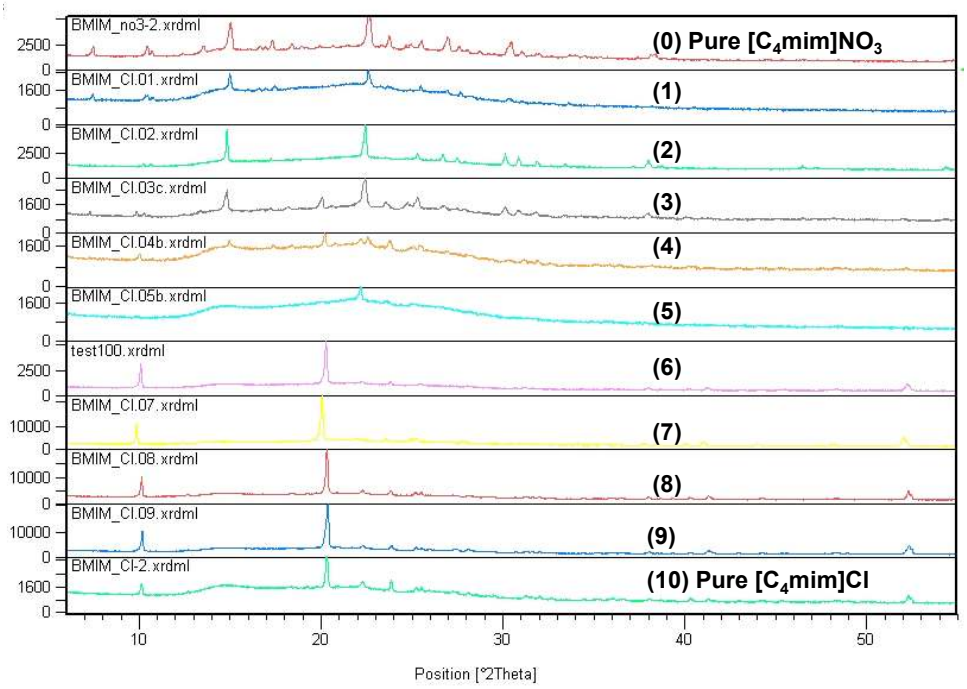


Figure 5.6: X-ray diffractograms for the $[C_4mim]NO_3$ - $[C_4mim]Cl$ binary system (obtained by Seddon's group). Mole fraction of $[C_4mim]Cl$ in the binary mixture: (0) 0; (1) 0.1; (2) 0.2; (3) 0.3; (4) 0.4; (5) 0.5; (6) 0.6; (7) 0.7; (8) 0.8; (9) 0.9; (10) 1.

### 5.2.2 The $[C_4mim]CH_3SO_3$ – $[C_4mim]Cl$ binary system

The phase diagram has been measured by DSC. No solid solubility was observed, and the measured limiting slope of the $[C_4mim]CH_3SO_3$ liquidus curve agrees with Equation (36) in Chapter 4. No intermediate compound has been observed. The optimized Gibbs free energy of reaction (25) in Chapter 4 is:

$$\Delta g_{[C_4mim]_2/(CH_3SO_3)Cl}/(J.mol^{-1}) = 694.5 - 418.4x_{ClCl} \quad (69)$$

where $x_{ClCl}$ is the mole fraction of second-nearest-neighbor $(Cl - [C_4mim] - Cl)$ pairs. The calculated phase diagram is compared to the measurements in figure 5.7. This is a simple eutectic system. The measured liquidus temperatures in the $[C_4mim]Cl$-rich region are somewhat scattered: for instance, at 80 mol% $[C_4mim]Cl$, the shift between the calculated and experimental liquidus temperatures is almost 5°C. Also, the measured eutectic temperature at 80 mol% $[C_4mim]Cl$ is about 6°C lower than the calculated eutectic temperature. The characteristics of the calculated eutectic are {T=47°C, 59.3 mol% $[C_4mim]Cl$}.

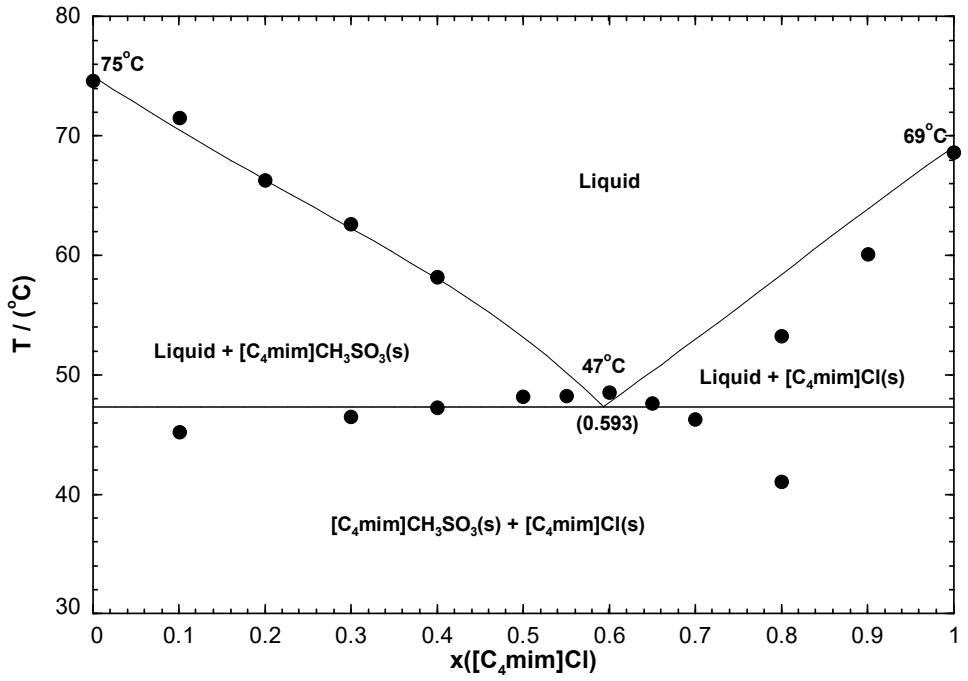


Figure 5.7: Calculated $[C_4mim]CH_3SO_3$ - $[C_4mim]Cl$ phase diagram, temperature versus mole fraction of $[C_4mim]Cl$. Experimental data are from Seddon's group (●).

### 5.2.3 The $[C_4mim]CH_3SO_3$ – $[C_4mim]NO_3$ binary system

The phase diagram has been measured by DSC. No solid solubility was observed, and there are no intermediate compounds. The measured limiting slope of the $[C_4mim]CH_3SO_3$ liquidus curve agrees with Equation (36) in Chapter 4. The optimized Gibbs free energy of reaction (25) in Chapter 4 is:

$$\Delta g_{[C_4mim]_2/(CH_3SO_3)NO_3}/(J.mol^{-1}) = 736.4 + 795.0x_{(NO_3)(NO_3)} \quad (70)$$

where $x_{(NO_3)(NO_3)}$ is the mole fraction of second-nearest-neighbor $(NO_3 - [C_4mim] - NO_3)$ pairs. The calculated phase diagram is compared with the measurements in figure 5.8. Again, this is a simple eutectic system. The characteristics of the calculated eutectic are {T=25°C, 90.4 mol% $[C_4mim]NO_3$}. The calculated eutectic temperature is very close to the melting temperature of pure $[C_4mim]NO_3$.

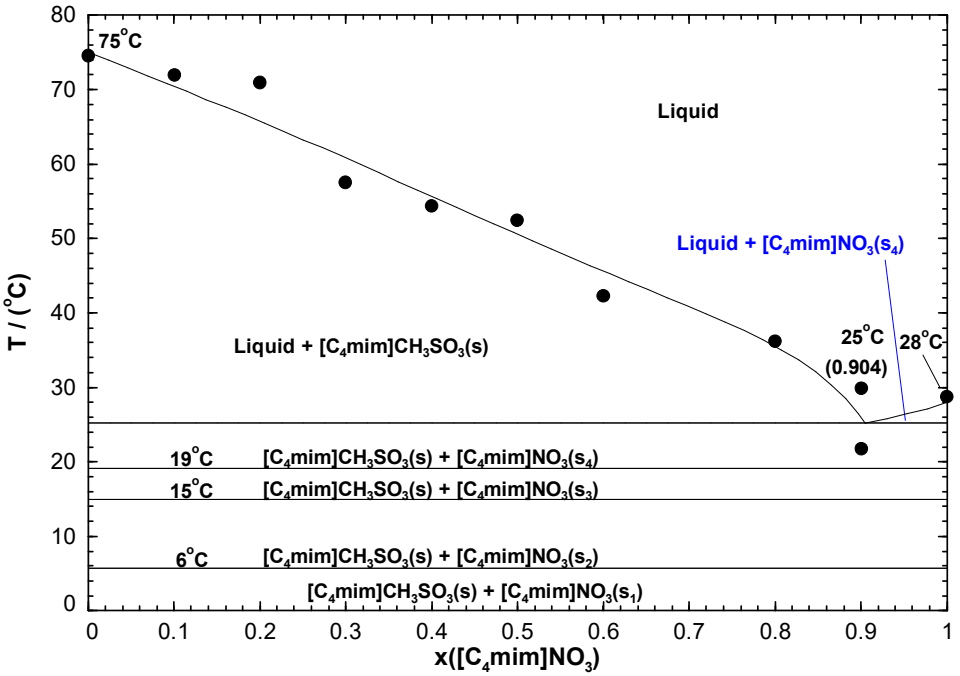


Figure 5.8: Calculated $[C_4mim]CH_3SO_3$ - $[C_4mim]NO_3$ phase diagram, temperature versus mole fraction of $[C_4mim]NO_3$. Experimental data are from Seddon's group (●).

## 5.3 The [C4mim]Cl – [C4mim]NO3 – [C4mim]CH3SO3 ternary system

The calculated (tentative) liquidus projection of the [C4mim]Cl - [C4mim]$NO_3$ - [C4mim]$CH_3SO_3$ system is shown in figure 5.9. The thermodynamic properties of the ternary liquid are calculated solely from the optimized model parameters for the three binary subsystems (Equations (68-70)) using a Kohler-like symmetric interpolation method. The ternary eutectic reaction liquid = [C4mim]Cl + [C4mim]$NO_3$($s_3$) + [C4mim]$CH_3SO_3$ is calculated at 18°C with a liquid composition of (24.0 mol% [C4mim]Cl + 64.4 mol% [C4mim]$NO_3$ + 11.6 mol% [C4mim]$CH_3SO_3$). This corresponds to the minimum liquidus temperature in the ternary system. Owing to the large uncertainty in the [C4mim]$NO_3$ – [C4mim]Cl binary subsystem, no phase diagram measurements were conducted in the ternary system.

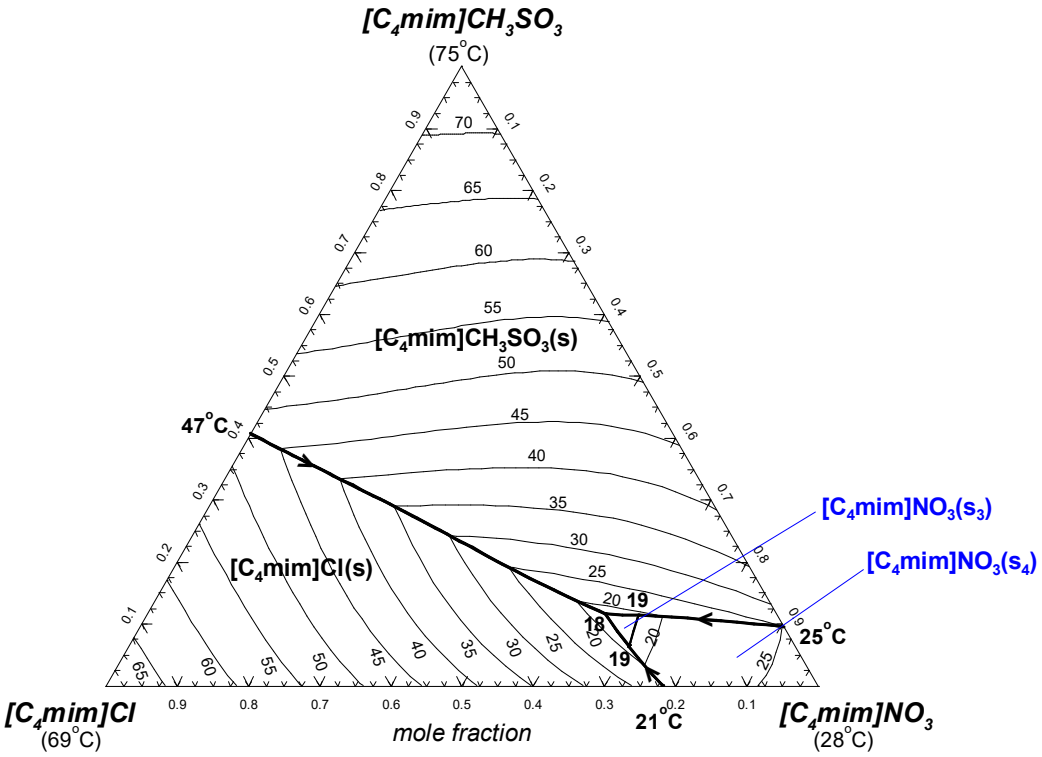


Figure 5.9: Calculated (tentative) liquidus projection of the [C4mim]Cl - [C4mim]$NO_3$ - [C4mim]$CH_3SO_3$ system.

# CHAPTER 6 PHASE DIAGRAM OF THE COMMON-ANION QUATERNARY SYSTEM {[$C_3$mim], [$C_3$mpy], [$C_3$mpyrr], [$C_3$mpip]}$PF_6$

This chapter describes a thermodynamic model for the common-anion quaternary system [$C_3$mim]$PF_6$ - [$C_3$mpy]$PF_6$ - [$C_3$mpyrr]$PF_6$ – [$C_3$mpip]$PF_6$. DSC measurements have been performed by Maximo et al. [35] for the pure compounds, and optical microscopy measurements have been conducted by the same authors for the six binary subsystems [35]. The phase diagrams of the various binary subsystems are modeled, and then the liquidus projections of the four ternary subsystems are predicted: (1) [$C_3$mim]$PF_6$ – [$C_3$mpip]$PF_6$ – [$C_3$mpyrr]$PF_6$, (2) [$C_3$mpip]$PF_6$ – [$C_3$mpy]$PF_6$ – [$C_3$mim]$PF_6$, (3) [$C_3$mpy]$PF_6$ – [$C_3$mpip]$PF_6$ – [$C_3$mpyrr]$PF_6$, and (4) [$C_3$mpyrr]$PF_6$ – [$C_3$mpy]$PF_6$ – [$C_3$mim]$PF_6$. The thermodynamic properties of each ternary liquid are calculated using solely the optimized binary parameters along with a standard symmetric (for systems (2) and (4)) or asymmetric (for systems (1) and (3)) interpolation method. In order to test the accuracy of the developed thermodynamic model, two isoplethal sections were measured in each of the ternary systems (1) and (2) by Coutinho's group using DSC. The thermodynamic model is slightly adjusted, and then the composition in the quaternary system corresponding to a global minimum of the liquidus temperature is calculated using the programme FactOptimal [36].

## 6.1 Pure ionic liquids

Figure 6.1 displays the chemical structures of the four $PF_6$-based pure compounds. Maximo et al. [35] measured their thermal transitions by DSC. These authors performed three repeated cycles of cooling and heating at 1 $K.min^{-1}$ from 183.15K to a temperature higher than the melting point. They measured the properties in the last heating run, and the melting temperatures were taken as the peak top values in the DSC thermograms. Maximo et al. [35] also measured the melting temperatures of the pure compounds using optical microscopy, by exploring temperatures between 243.15K and 393.15K. Finally, the crystal structures of the pure compounds were also determined by single crystal X-ray diffraction at 180K. Table 6.1 gives the thermal transition data from Maximo et al. [35] along with the data available in the literature for the pure compounds. For the sake of consistency, the data of Maximo et al. are used in the present work. In particular, [$C_3$mpyrr]$PF_6$ and [$C_3$mpip]$PF_6$ both have three allotropes ($s_1$, $s_2$, $s_3$).

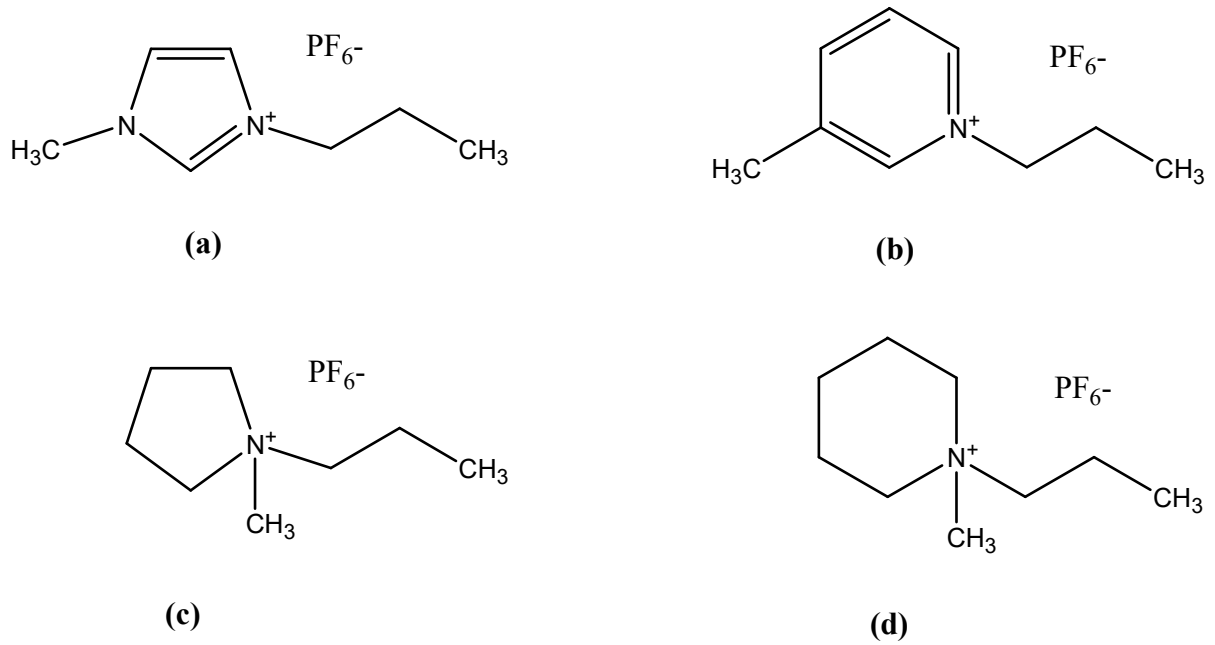


Figure 6.1: Chemical structures of the $PF_6$-based ionic liquids: (a) 1-methyl-3-propylimidazolium hexafluorophosphate ($[C_3mim]PF_6$), (b) 1-methyl-3-propylpyridinium hexafluorophosphate ($[C_3mpy]PF_6$), (c) 1-methyl-1-propylpyrrolidinium hexafluorophosphate ($[C_3mpyrr]PF_6$), (d) 1-methyl-1-propylpiperidinium hexafluorophosphate ($[C_3mpip]PF_6$).

Table 6.1: Enthalpies of fusion and of solid-solid transition measured by DSC in the literature for the pure compounds $[C_3mim]PF_6$, $[C_3mpy]PF_6$, $[C_3mpyrr]PF_6$ and $[C_3mpip]PF_6$.

| Cation | Anion | Water content (wt.%) | Purity (%) | Melting temperature (K) | Enthalpy of fusion ($J.mol^{-1}$) | Solid-Solid transition | Reference |
|---|---|---|---|---|---|---|---|
| $[C_3mim]^+$ | $PF_6^-$ | <0.5 | >99 | 312 | 14260 | - | [35] |
| | | <20 ppm | - | 313 | - | - | [43] |
| $[C_3mpy]^+$ | | <0.5 | >99 | 312 | 12640 | - | [35] |
| $[C_3mpyrr]^+$ | | <0.5 | >99 | 383 | 3410 | $T_{trans1}$=346.6K, $\Delta h_{trans1}$=2810 $J.mol^{-1}$<br>$T_{trans2}$=359.5K, $\Delta h_{trans2}$=2310 $J.mol^{-1}$ | [35] |
| | | - | - | 386 | 6565 | $T_{trans1}$=355.2K<br>$T_{trans2}$=370.2K | [156] |
| $[C_3mpip]^+$ | | <0.5 | >99 | 368 | 5110 | $T_{trans1}$=311.7K, $\Delta h_{trans1}$=8080 $J.mol^{-1}$<br>$T_{trans2}$=352.4K, $\Delta h_{trans2}$=2740 $J.mol^{-1}$ | [35] |

## 6.2 Binary subsystems

The phase diagrams of the six binary subsystems have been measured by Maximo et al. [35] using mainly optical microscopy. According to these authors, the melting temperatures of the binary mixtures measured by optical microscopy are accurate (reported uncertainty of 1.30K) since the mean absolute deviations between the two techniques were always lower than the summation of the uncertainties related to the melting temperatures determined by optical microscopy or DSC. No intermediate compound has been observed. As explained in Chapter 2, Maximo et al. [35] modeled the various binary phase diagrams using Equation (1), taking into account that the binary system has a simple eutectic behavior with no solid solubility ($a_i^S = x_i^S . \gamma_i^S = 1$) and neglecting the differences in heat capacity ($\Delta_{fus} C_p = 0$). In the case of an ideal liquid phase, they considered that $\gamma_i^L = 1$. Our calculated phase diagrams are described below.

### 6.2.1 Phase diagrams with a simple eutectic behavior

Figures 6.2 to 6.6 display the calculated phase diagrams for the $[C_3mpy]PF_6$ - $[C_3mim]PF_6$, $[C_3mpip]PF_6$ - $[C_3mim]PF_6$, $[C_3mpyrr]PF_6$ - $[C_3mim]PF_6$, $[C_3mpy]PF_6$ - $[C_3mpyrr]PF_6$ and $[C_3mpip]PF_6$ - $[C_3mpy]PF_6$ binary subsystems along with the experimental data from Maximo et al. [35] These are simple eutectic systems with negligible solid solubility. The characteristics of the calculated binary eutectic (temperature and composition) are shown in each figure. Agreement between the calculations and the measurements is satisfactory. Table 6.2 gives the optimized Gibbs free energy of reaction (24) in Chapter 4 for each binary liquid.

Table 6.2: Optimized Gibbs free energy of reaction (24) in Chapter 4 for the eutectic-type phase diagrams ($x_{ii}$ is the mole fraction of second-nearest-neighbor ($i - PF_6 - i$) pairs)

| Binary system | Optimized $\Delta g_{AB/(PF_6)_2}$ (J.mol$^{-1}$) |
|---|---|
| $[C_3mpy]PF_6$ - $[C_3mim]PF_6$ | $205.0 - 163.2x_{(C_3mpy)(C_3mpy)}$ |
| $[C_3mpip]PF_6$ - $[C_3mim]PF_6$ | $-460.2 + 677.8x_{(C_3mpip)(C_3mpip)} + 602.5x_{(C_3mim)(C_3mim)}$ |
| $[C_3mpyrr]PF_6$ - $[C_3mim]PF_6$ | $-598.3 + 661.1x_{(C_3mpyrr)(C_3mpyrr)} + 623.4x_{(C_3mim)(C_3mim)}$ |
| $[C_3mpy]PF_6$ - $[C_3mpyrr]PF_6$ | $-192.5 + 272.0x_{(C_3mpy)(C_3mpy)} + 502.1x_{(C_3mpyrr)(C_3mpyrr)}$ |
| $[C_3mpip]PF_6$ - $[C_3mpy]PF_6$ | $715.5x_{(C_3mpip)(C_3mpip)}$ |

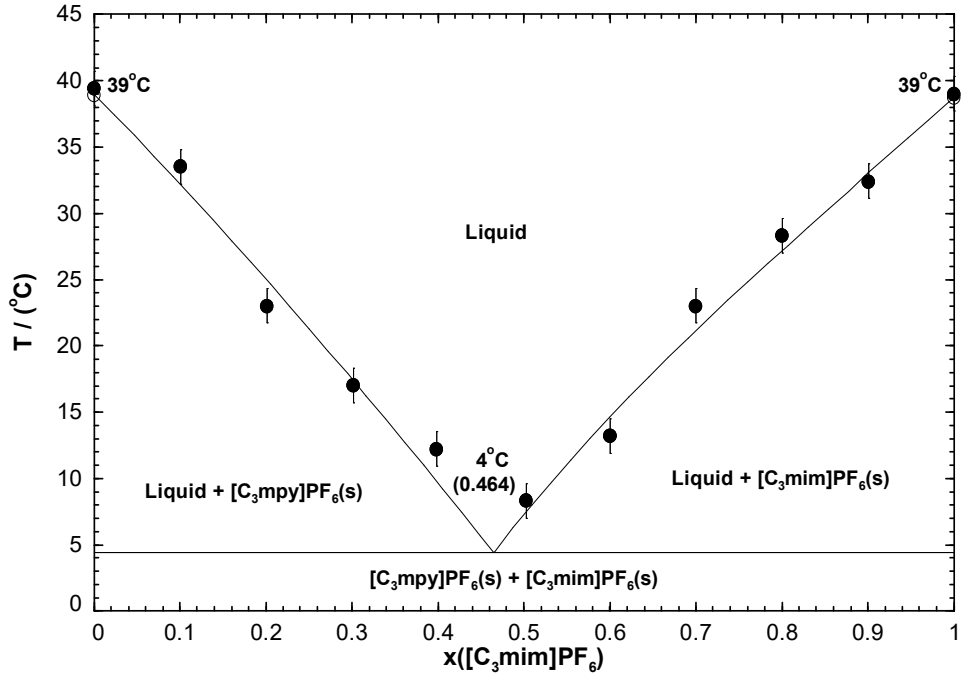


Figure 6.2: Calculated $[C_3mpy]PF_6$ - $[C_3mim]PF_6$ phase diagram, temperature versus mole fraction of $[C_3mim]PF_6$. Experimental data are from Maximo et al. [35] (optical microscopy (●), DSC (○)).

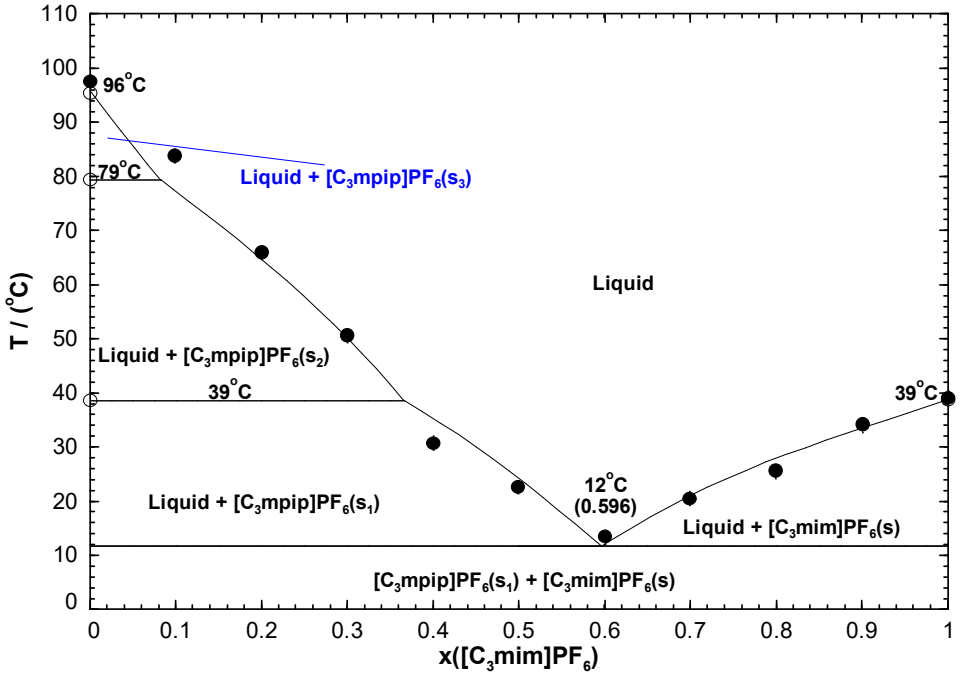


Figure 6.3: Calculated $[C_3mpip]PF_6$ - $[C_3mim]PF_6$ phase diagram, temperature versus mole fraction of $[C_3mim]PF_6$. Experimental data are from Maximo et al. [35] (optical microscopy (●), DSC (○)).

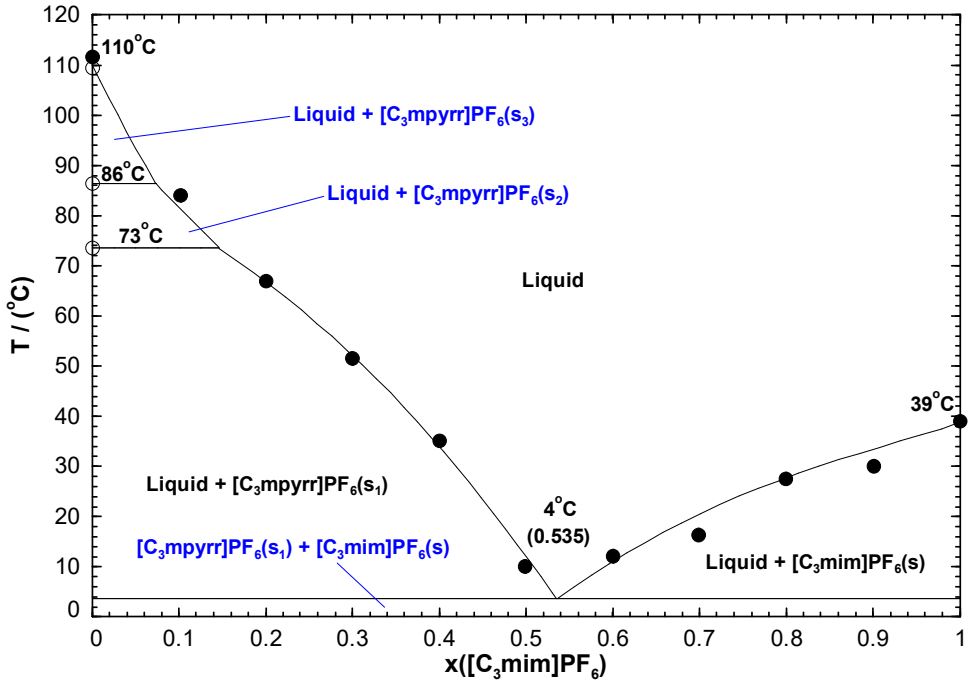


Figure 6.4: Calculated $[C_3mpyrr]PF_6$ - $[C_3mim]PF_6$ phase diagram, temperature versus mole fraction of $[C_3mim]PF_6$. Experimental data are from Maximo et al. [35] (optical microscopy (●), DSC (○)).

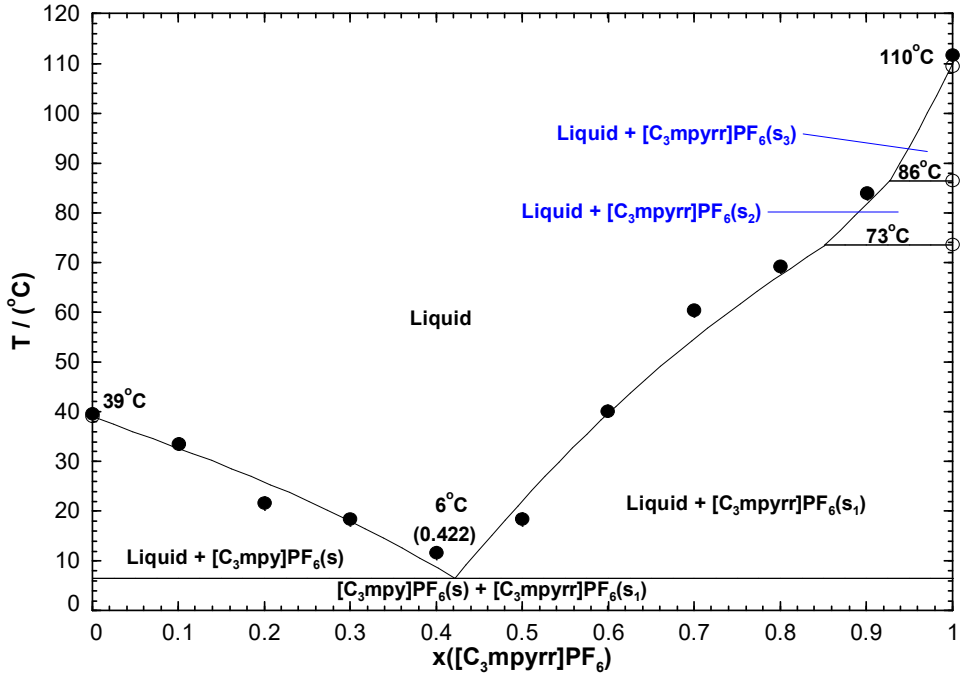


Figure 6.5: Calculated $[C_3mpy]PF_6$ - $[C_3mpyrr]PF_6$ phase diagram, temperature versus mole fraction of $[C_3mpyrr]PF_6$. Experimental data are from Maximo et al. [35] (optical microscopy (●), DSC (○)).

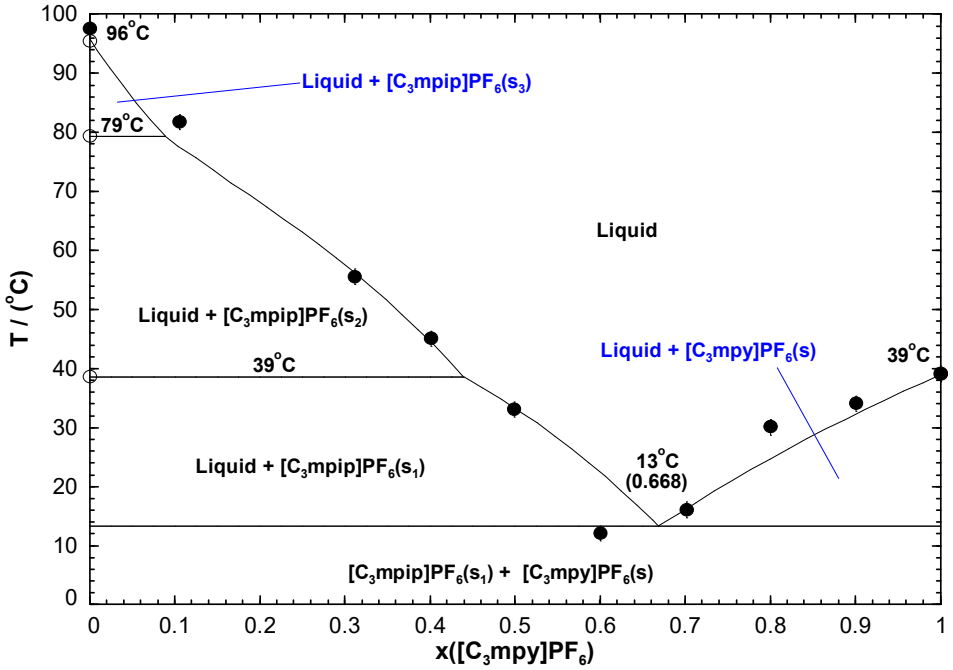


Figure 6.6: Calculated $[C_3mpip]PF_6$ - $[C_3mpy]PF_6$ phase diagram, temperature versus mole fraction of $[C_3mpy]PF_6$. Experimental data are from Maximo et al. [35] (optical microscopy (●), DSC (○)).

### 6.2.2 Phase diagram with complete solid solution

The phase diagram of the $[C_3mpip]PF_6$ – $[C_3mpyrr]PF_6$ binary system has been measured by Maximo et al. [35] using optical microscopy, DSC and powder X-ray diffractometry of the solid phase. No intermediate compound has been observed. As shown in figure 6.7(a), the measured limiting slopes (thin red lines) of the $[C_3mpip]PF_6$ and $[C_3mpyrr]PF_6$ liquidus curves substantially disagree with Equation (36) in Chapter 4, and therefore this system exhibits at least some terminal solid solubility. Maximo et al. [35] reported an extensive solid solution over the entire composition range for the $[C_3mpip]PF_6$ – $[C_3mpyrr]PF_6$ binary system. Common-anion ionic liquid binary systems that exhibit full solid solutions are rather uncommon. More recently, Teles et al. [67] observed an extensive solid solution for the $[C_2mpyrr]N(C_4F_9SO_2)_2$ - $[C_4mpyrr]N(C_4F_9SO_2)_2$ binary system. Maximo et al. [35] observed on their DSC thermograms a single endothermic transition upon heating, which suggests the presence of a continuous solid solution. These authors verified the formation of a monophasic solid phase by powder X-ray diffraction at 298.15K (solid solution *C* ($s_3$-$s_3$) in figure 6.7). They also determined the crystallographic structure of the

$[C_3mpip]PF_6$ pure compound by single crystal X-ray diffraction at 180K (allotrope ($s_1$)). This compound is monoclinic (space group $P2_1/c$) with 8 formula units per unit cell and unit cell angles $\alpha = 90°, \beta = 109.466°, \gamma = 90°$. Golding et al. [156] reported crystallographic data for the $[C_3mpyrr]PF_6$ pure compound at 123K (allotrope ($s_1$)). This compound is monoclinic (space group C 2/c) with 36 formula units per unit cell and unit cell angles $\alpha = 90°, \beta = 109.797°, \gamma = 90°$. Thus, the low-temperature allotropes ($s_1$) of $[C_3mpip]PF_6$ and $[C_3mpyrr]PF_6$ have monoclinic unit cells with very similar crystallographic axes angles. Maximo et al. [35] suggested that the crystalline structure of $[C_3mpyrr]PF_6$, which corresponds to a bigger crystal volume, may act as a host-structure to accommodate the crystal structure of $[C_3mpip]PF_6$, thus leading to the formation of a continuous solid solution. It can thus be concluded that the high-temperature allotropes ($s_3$) of $[C_3mpip]PF_6$ and $[C_3mpyrr]PF_6$ form an extensive solid solution over the entire composition range, and that the low-temperature allotropes ($s_1$) most likely have the same behavior. Therefore, it is reasonable to assume that the intermediate-temperature allotropes ($s_2$) are also fully miscible. In order to check this hypothesis, two different scenarios are considered in the present work to model the phase diagram of the $[C_3mpip]PF_6$ – $[C_3mpyrr]PF_6$ binary system. The first scenario assumes a negligible solid solubility between the low-temperature allotropes ($s_1$-$s_1$) and also between the intermediate-temperature allotropes ($s_2$-$s_2$) (figure 6.7(a)). The second scenario assumes a continuous solid solution between the low-temperature allotropes ($s_1$-$s_1$) and also between the intermediate-temperature allotropes ($s_2$-$s_2$) (figure 6.7(b)). As a first approximation, in the latter scenario, the same interaction parameter as for the high-temperature ($s_3$-$s_3$) solid solution (which was optimized based on the experimental data of Maximo et al. [35]) is used for both the low-temperature ($s_1$-$s_1$) and the intermediate-temperature ($s_2$-$s_2$) solid solutions. The two pure compounds have very similar cation structures (only differing by one carbon atom) and also similar crystal structures. Thus, the binary liquid is assumed to be ideal. That is:

$$\Delta g_{[C_3mpip][C_3mpyrr]/(PF_6)_2} = 0 \quad (71)$$

The various solid solutions are modeled with the Compound Energy Formalism (CEF). Figure 6.7 displays the calculated phase diagram along with the measurements from Maximo et al., according to the first scenario (figure 6.7(a)) and the second scenario (figure 6.7(b)). The calculated phase diagram for the first scenario displays the high-temperature ($s_3$-$s_3$) solid solution along with the eutectoid reaction $\{[C_3mpip]PF_6(s_3) – [C_3mpyrr]PF_6(s_3)\}(ss) = [C_3mpip]PF_6(s_1) + [C_3mpyrr]PF_6(s_1)$ at -5°C and 56.6 mol% $[C_3mpyrr]PF_6$. On the other hand, there are three distinct

areas corresponding to the high-temperature ($s_3$-$s_3$), intermediate-temperature ($s_2$-$s_2$) and low-temperature ($s_1$-$s_1$) solid solutions in the calculated phase diagram for the second scenario. As will be shown later, the second scenario allows to best reproduce the DSC measurements performed by Coutinho's group in the $[C_3mim]PF_6$ - $[C_3mpip]PF_6$ - $[C_3mpyrr]PF_6$ ternary system. The final optimized excess Gibbs free energy ($G^E$) of each solid solution is given in table 6.3. These are small positive regular interaction parameters. The final calculated phase diagram of the $[C_3mpip]PF_6$ – $[C_3mpyrr]PF_6$ binary system with the interaction parameters from table 6.3 is shown in figure 6.8. There is an azeotrope at 95°C and 22 mol% $[C_3mpyrr]PF_6$. The temperature of the azeotrope is lower than the melting points of the pure compounds.

Table 6.3: Optimized excess Gibbs free energies of the solid solutions in the $[C_3mpip]PF_6$ – $[C_3mpyrr]PF_6$ binary system ($y_i^C$ is the site fraction of species $i$ on the cationic sublattice $C$)

| Solid solution | Optimized $G^E$ (J.mol$^{-1}$) |
|---|---|
| High-temperature ($s_3$-$s_3$) | $217.6\times y^C_{[C_3\mathrm{mpip}]^+}\times y^C_{[C_3\mathrm{mpyrr}]^+}$ |
| Intermediate-temperature ($s_2$-$s_2$) | $83.7\times y^C_{[C_3\mathrm{mpip}]^+}\times y^C_{[C_3\mathrm{mpyrr}]^+}$ |
| Low-temperature ($s_1$-$s_1$) | $502.1\times y^C_{[C_3\mathrm{mpip}]^+}\times y^C_{[C_3\mathrm{mpyrr}]^+}$ |

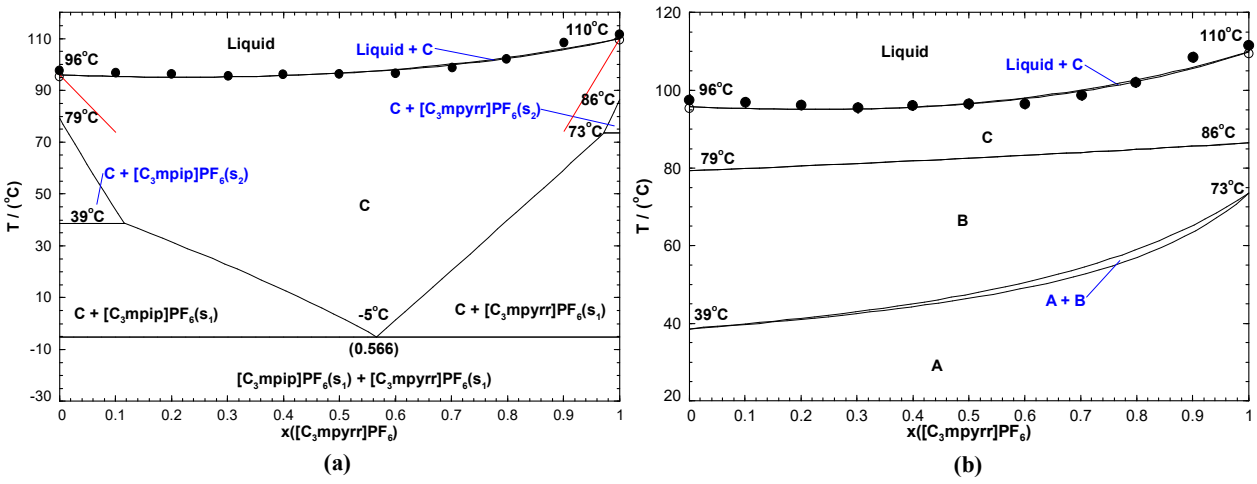


Figure 6.7: Calculated $[C_3mpip]PF_6$ - $[C_3mpyrr]PF_6$ phase diagram, temperature versus mole fraction of $[C_3mpyrr]PF_6$: (a) first scenario, (b) second scenario. Experimental data are from Maximo et al. [35] (optical microscopy (●), DSC (○)). Notations: A={$[C_3mpip]PF_6(s_1)$ – $[C_3mpyrr]PF_6(s_1)$}(ss); B={$[C_3mpip]PF_6(s_2)$ – $[C_3mpyrr]PF_6(s_2)$}(ss); C={$[C_3mpip]PF_6(s_3)$ – $[C_3mpyrr]PF_6(s_3)$}(ss). In figure (a), the limiting liquidus slopes calculated from Equation (36) (Chapter 4) are shown as thin red lines.

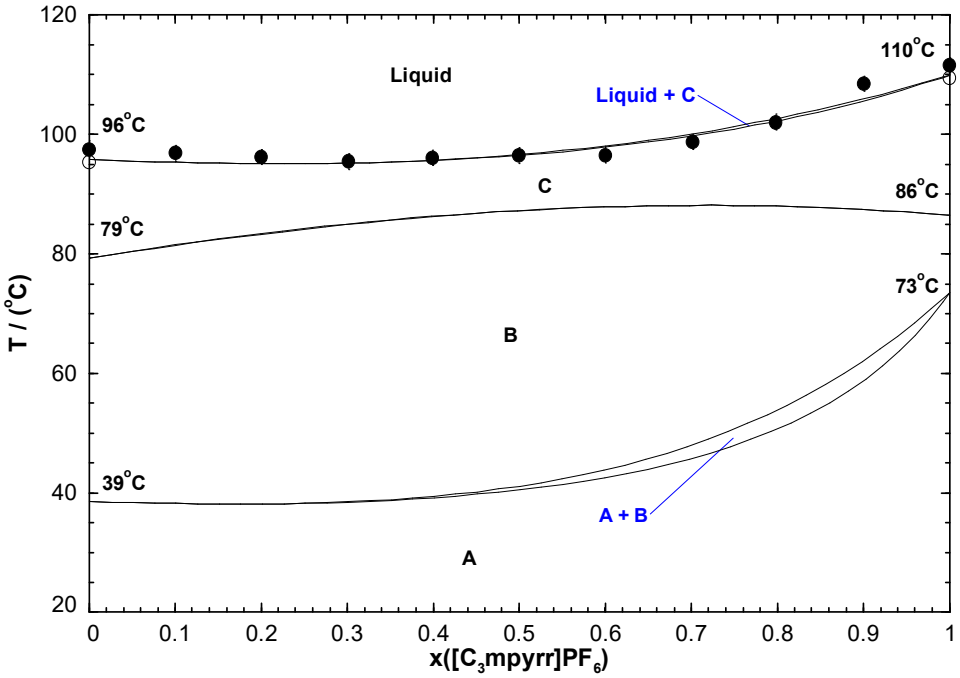


Figure 6.8: Final calculated $[C_3mpip]PF_6$ - $[C_3mpyrr]PF_6$ phase diagram, temperature versus mole fraction of $[C_3mpyrr]PF_6$. Experimental data are from Maximo et al. [35] (optical microscopy (●), DSC (○)). Notations: A={$[C_3mpip]PF_6(s_1)$ – $[C_3mpyrr]PF_6(s_1)$}(ss); B={$[C_3mpip]PF_6(s_2)$ – $[C_3mpyrr]PF_6(s_2)$}(ss); C={$[C_3mpip]PF_6(s_3)$ – $[C_3mpyrr]PF_6(s_3)$}(ss).

## 6.3 Ternary subsystems

The quaternary system investigated consists of the four following ternary subsystems: (1) $[C_3mim]PF_6$ - $[C_3mpip]PF_6$ - $[C_3mpyrr]PF_6$, (2) $[C_3mpy]PF_6$ - $[C_3mpip]PF_6$ - $[C_3mpyrr]PF_6$, (3) $[C_3mpip]PF_6$ - $[C_3mpy]PF_6$ - $[C_3mim]PF_6$, and (4) $[C_3mpyrr]PF_6$ - $[C_3mpy]PF_6$ - $[C_3mim]PF_6$. Since systems (1) and (2) both include the $[C_3mpip]PF_6$ and $[C_3mpyrr]PF_6$ components, they will display at least a complete high temperature binary solid solution ($s_3$-$s_3$). On the other hand, systems (3) and (4) do not exhibit any solid solubility. Two isoplethal sections were measured in each of the ternary systems (1) and (3) by Coutinho's group using DSC. Experimental details are given below.

*Experimental section:* The $[C_3mim]PF_6$, $[C_3mpy]PF_6$, $[C_3mpyrr]PF_6$, and $[C_3mpip]PF_6$ pure compounds were purchased from Iolitec with a purity of 99%. Compounds were dried under vacuum at room temperature during at least three days and the purity of each sample was

additionally confirmed by $^{1}H$, $^{13}C$, $^{19}F$ and $^{31}P$ NMR spectra. A Metrohm 831 Karl Fischer coulometer using the analyte Hydranal® - Coulomat AG, from Riedel-de Haën, was used to determine the water content of the compounds, which was found to be less than 900 ppm. Ternary mixtures were prepared inside a dry argon glove-box, at room temperature using an analytical balance model ALS 220-4N from Kern with an accuracy of ±0.002 g. Vials with mixtures were heated under stirring until complete melting and then recrystallized at room temperature. Samples (2 – 5 mg) of mixtures of pure compounds were hermetically sealed in aluminum pans inside the glovebox and then weighed in a micro analytical balance AD6 (PerkinElmer, USA, precision=$2\times10^{-6}$g). The melting properties were determined using a Hitachi DSC7000X model working at atmospheric pressure. For most of the DSC measurements, one cooling run at 5K.min$^{-1}$ followed by one heating run at 2K.min$^{-1}$ were performed (the minimum temperature reached upon cooling was -100°C for the {[$C_3$mim], [$C_3$mpip], [$C_3$mpyrr]}$PF_6$ ternary system and -180ºC for the {[$C_3$mim], [$C_3$mpip], [$C_3$mpy]}$PF_6$ ternary system). For a few ternary mixtures, three consecutive heating/cooling cycles were used with rates of 2 K.min$^{-1}$ (heating) and 5 K.min$^{-1}$ (cooling), respectively. The equipment was previously calibrated with several standards with weight fraction purities higher than 99%.

Liquidus projections of the various ternary subsystems are calculated. As discussed previously, [$C_3$mpip]$PF_6$ and [$C_3$mpyrr]$PF_6$ have very similar cation structures and also similar crystal structures. Thus, the thermodynamic properties of the ternary liquids (1) and (2) (which include both components) are calculated from the optimized model parameters for the three binary subsystems using a Kohler-Toop-like (asymmetric) interpolation method, with the third component as the asymmetric component. For the ternary liquids (3) and (4), a Kohler-like (symmetric) interpolation method is used.

Figures 6.9 and 6.10 display the calculated liquidus projection of the [$C_3$mim]$PF_6$ - [$C_3$mpip]$PF_6$ - [$C_3$mpyrr]$PF_6$ system corresponding to the first and second scenarios, respectively. The calculated liquidus projection with the first scenario exhibits a ternary eutectic reaction at -9°C (see figure 6.9), while the one with the second scenario displays no ternary invariant reaction (see figure 6.10). In order to select the most probable scenario, two isoplethal sections were measured by Coutinho's group using DSC: the isoplethal section at constant 40 mol% [$C_3$mim]$PF_6$ (red dashed line in figures 6.9 and 6.10) and the isoplethal section at constant molar ratio [$C_3$mpyrr]$PF_6$ / ([$C_3$mpyrr]$PF_6$ + [$C_3$mpip]$PF_6$) of 0.60 (blue dashed line in figures 6.9 and 6.10). The liquidus lines

of both isoplethal sections according to the two scenarios are also calculated. For the isoplethal section at constant 40 mol% $[C_3mim]PF_6$ (see figure 6.11(a)), the first scenario gives two liquidus lines (in black), corresponding to the precipitation of $[C_3mpip]PF_6(s_1)$ or $[C_3mpyrr]PF_6(s_1)$, while there is an almost flat liquidus line corresponding to the precipitation of the $[C_3mpip]PF_6(s_1)$ - $[C_3mpyrr]PF_6(s_1)$ solid solution for the second scenario (blue line). For the isoplethal section at constant molar ratio $[C_3mpyrr]PF_6$ / ($[C_3mpyrr]PF_6$ + $[C_3mpip]PF_6$) of 0.60 (see figure 6.11(b)), the first scenario (in black) gives a liquidus line corresponding to the successive precipitation of {$[C_3mpip]PF_6(s_3)$ - $[C_3mpyrr]PF_6(s_3)$}(ss), $[C_3mpip]PF_6(s_1)$ and $[C_3mim]PF_6$. For the second scenario (in blue), the solid phases precipitating are successively {$[C_3mpip]PF_6(s_3)$ - $[C_3mpyrr]PF_6(s_3)$}(ss), {$[C_3mpip]PF_6(s_2)$ - $[C_3mpyrr]PF_6(s_2)$}(ss), {$[C_3mpip]PF_6(s_1)$ - $[C_3mpyrr]PF_6(s_1)$}(ss) and $[C_3mim]PF_6$. While investigating the isoplethal sections at constant 40 mol% $[C_3mim]PF_6$ and at constant molar ratio $[C_3mpyrr]PF_6$ / ($[C_3mpyrr]PF_6$ + $[C_3mpip]PF_6$) of 0.60, Coutinho's group performed two series of DSC measurements (first series and second series) with the same samples but at different times, in order to check the reproducibility of their results. The experimental procedure was always the same: one cooling run followed by one heating run. Following our request, they studied again a few ternary mixtures (third series) using three consecutive heating / cooling cycles (i.e. an experimental procedure very similar to that of Smiglak's group: see Chapter 4). Figures 6.12 and 6.13 display the measured and calculated isoplethal sections at constant 40 mol% $[C_3mim]PF_6$ and at constant molar ratio $[C_3mpyrr]PF_6$ / ($[C_3mpyrr]PF_6$ + $[C_3mpip]PF_6$) of 0.60, respectively. These are the final calculated isoplethal sections. The second scenario has finally been favoured based on the available ternary experimental data. As seen in figure 6.12, the measured liquidus temperatures virtually do not change as a function of the mole fraction of $[C_3mpyrr]PF_6$ in the ternary mixture. This is consistent with the second scenario (see figure 6.11(a)). No ternary excess parameter was included for the liquid phase. That is, as explained previously, the thermodynamic properties of the ternary liquid $[C_3mim]PF_6$ - $[C_3mpip]PF_6$ -$[C_3mpyrr]PF_6$ are calculated solely from the optimized binary model parameters using an asymmetric interpolation method, with $[C_3mim]PF_6$ as the asymmetric component. Also, the excess Gibbs free energies of the low temperature ($s_1$-$s_1$) and intermediate-temperature ($s_2$-$s_2$) solid solutions were adjusted (see table 6.3) in order to best reproduce the ternary data. The interpretation of the measured isoplethal section at constant 40 mol% $[C_3mim]PF_6$ (figure 6.12) is not straightforward. This section has been divided into three different temperature zones (zones 1,

2 and 3). Zone 1 corresponds to the measured liquidus temperatures: in principle, for a given sample, the last thermal arrest upon heating should be the liquidus temperature. The only exceptions are the ternary mixtures at 50 mol% $[C_3mpyrr]PF_6$ (second series) and at 55 mol% $[C_3mpyrr]PF_6$ (second series). In the former case, the highest temperature measured is believed to belong to zone 2 (which will be discussed below). In the latter case, the highest temperature measured (56°C) should be discarded: as shown by the third series of data at 55 mol% $[C_3mpyrr]PF_6$, the intermediate thermal arrest (second series) is the true liquidus temperature. In figure 6.12, the binary data from Maximo et al. [35] at 0 and 60 mol% $[C_3mpyrr]PF_6$ are also shown. The shift between the calculated and measured (first series) liquidus temperatures is usually lower than 5°C, which is the corresponding shift for the binary mixture at 0 mol% $[C_3mpyrr]PF_6$. The shift between the calculated and measured (second series) liquidus temperatures is usually lower than 9°C. Note that the thermal arrests measured at 37.5 mol% $[C_3mim]PF_6$ (and at 37.5 mol% $[C_3mpyrr]PF_6$) (see the isoplethal section at constant molar ratio $[C_3mpyrr]PF_6$ / ($[C_3mpyrr]PF_6$ + $[C_3mpip]PF_6$) of 0.60 in figure 6.13) are also displayed in figure 6.12 along with the corresponding calculated liquidus line (shown as a dashed green line). The lens-shaped region calculated at low temperatures remains virtually unchanged at 37.5 mol% $[C_3mim]PF_6$.

Zone 3 corresponds to the measured low-temperature thermal arrests. Depending on the ternary mixture studied, there may be zero, one or two thermal transitions measured in this zone. Agreement between these data points and the calculated lens-shaped region is satisfactory.

Zone 2 corresponds to the measured thermal arrests observed in the intermediate temperature range and possibly associated with metastable phase equilibria. These data points are not reproduced by the thermodynamic model. Such thermal arrests are present with certainty at 40 mol% $[C_3mpyrr]PF_6$ (second series), at 50 mol% $[C_3mpyrr]PF_6$ (first series), and at 55 mol% $[C_3mpyrr]PF_6$ (third series). These thermal arrests might be associated with $[C_3mpyrr]PF_6$ polymorphism, with the existence of two preferred conformations of the pyrrolidinium cations. As reported in Chapter 4, for pure $[C_4mpyrr]Cl$ and most of the $[C_4mpyrr]Cl$ – $[C_4mpyrr]Br$ binary mixtures investigated, a thermal transition was observed by Stolarska et al. [34] in the range 97-117°C and it was attributed to a possible polymorphism of $[C_4mpyrr]Cl$. However, no such thermal transition had been observed in the $[C_4mpyrr]Cl$ – $[C_4mpyrr]BF_4$ system. Interestingly, the thermal transitions measured at 37.5 mol% $[C_3mim]PF_6$ (and at 37.5 mol% $[C_3mpyrr]PF_6$), and taken from the isoplethal section in figure 6.13, agree very satisfactorily with the model; no metastable phase

equilibria are observed at this particular composition. For the isoplethal section at constant molar ratio $[C_3mpyrr]PF_6$ / ($[C_3mpyrr]PF_6$ + $[C_3mpip]PF_6$) of 0.60 (see figure 6.13), the binary and unary experimental data from Maximo et al. [35] are also displayed at 0 and 100 mol% $[C_3mim]PF_6$, respectively. For each ternary mixture investigated, the number of thermal transitions observed for the first and second series is not always the same. However, when one thermal transition is observed in both cases, the temperature shift between the two measurements is always relatively small. A very high liquidus temperature of about 118°C is observed at 12.5 mol% $[C_3mim]PF_6$. While performing three consecutive heating / cooling cycles, Coutinho's group measured a liquidus temperature of about 70°C, which agrees well with the model. Therefore, the previous measurement is not reliable and must be discarded. Agreement between the calculations and the ternary data is satisfactory (see figure 6.13). The final calculated liquidus projection of the $[C_3mim]PF_6$ - $[C_3mpip]PF_6$ - $[C_3mpyrr]PF_6$ system is displayed in figure 6.14. The minimum liquidus temperature corresponds to the binary eutectic reaction liquid = $[C_3mim]PF_6$ + $[C_3mpyrr]PF_6(s_1)$ at 4°C.

Figures 6.15 and 6.16 show the calculated liquidus projection of the $[C_3mpy]PF_6$ - $[C_3mpip]PF_6$ - $[C_3mpyrr]PF_6$ system according to the first scenario and second scenario, respectively. These two figures are very similar to the corresponding figures calculated for the $[C_3mim]PF_6$ - $[C_3mpip]PF_6$ - $[C_3mpyrr]PF_6$ system (figures 6.9 and 6.10). No ternary DSC data are available for the $[C_3mpy]PF_6$ - $[C_3mpip]PF_6$ - $[C_3mpyrr]PF_6$ system. Again, the second scenario was favoured, and the optimized excess Gibbs free energies of the low-temperature ($s_1$-$s_1$) and intermediate-temperature ($s_2$-$s_2$) solid solutions remain unchanged (see table 6.3). By analogy with the $[C_3mim]PF_6$ - $[C_3mpip]PF_6$ - $[C_3mpyrr]PF_6$ system, no ternary excess parameter was included for the liquid phase. That is, the thermodynamic properties of the ternary liquid $[C_3mpy]PF_6$ - $[C_3mpip]PF_6$ - $[C_3mpyrr]PF_6$ are calculated solely from the optimized binary model parameters using an asymmetric interpolation method, with $[C_3mpy]PF_6$ as the asymmetric component. The final calculated liquidus projection is shown in figure 6.17 and is expected to be reasonably accurate. The minimum liquidus temperature corresponds to the binary eutectic reaction liquid = $[C_3mpy]PF_6$ + $[C_3mpyrr]PF_6(s_1)$ at 6°C.

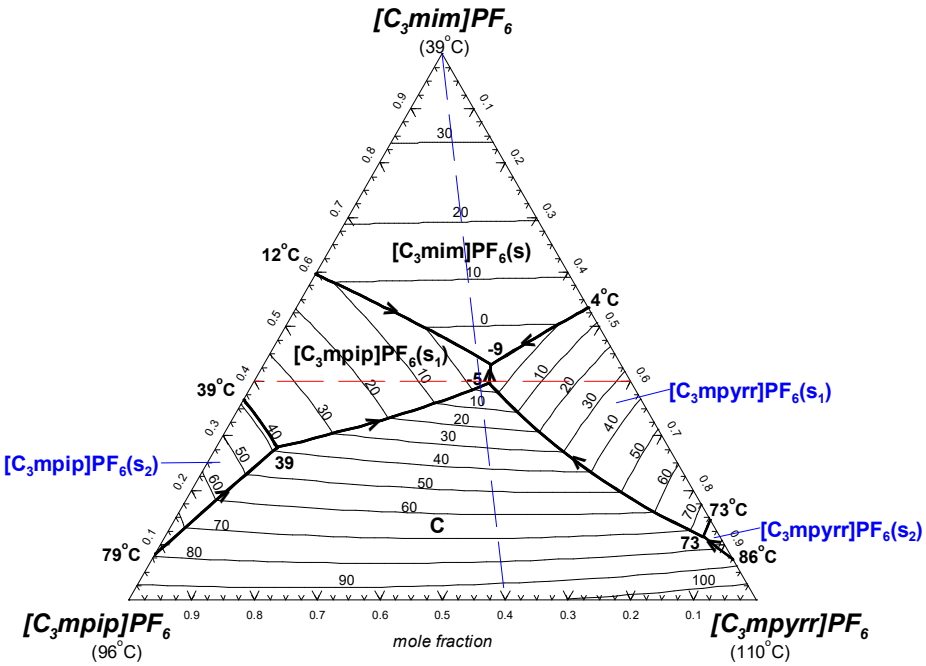


Figure 6.9: Calculated liquidus projection of the $[C_3mim]PF_6$ - $[C_3mpip]PF_6$ - $[C_3mpyrr]PF_6$ system with the first scenario. Notations: C={$[C_3mpip]PF_6(s_3)$ – $[C_3mpyrr]PF_6(s_3)$}(ss). Isoplethal section at constant 40 mol% $[C_3mim]PF_6$ (red dashed line), isoplethal section at constant molar ratio $[C_3mpyrr]PF_6$ / ($[C_3mpyrr]PF_6$ + $[C_3mpip]PF_6$) of 0.60 (blue dashed line).

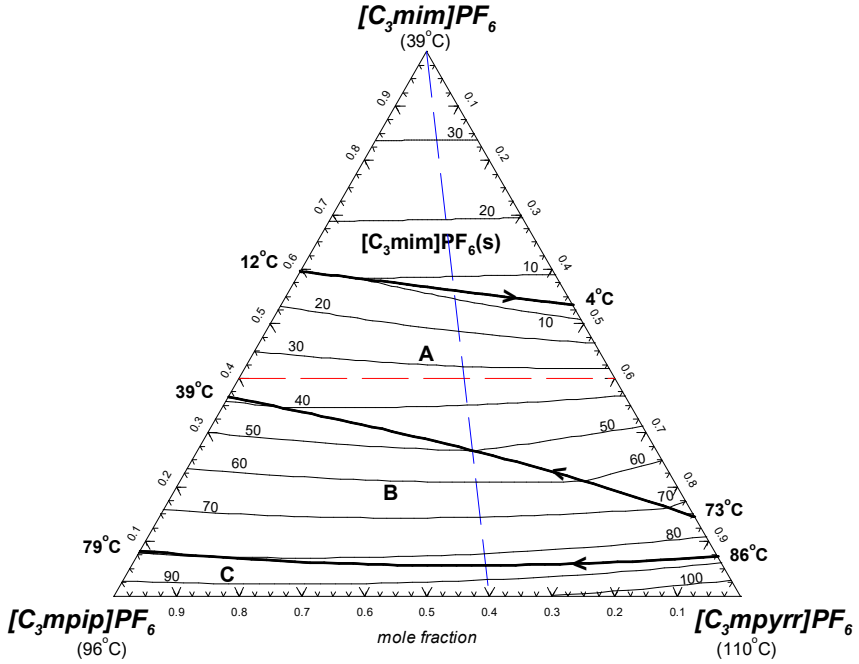


Figure 6.10: Calculated liquidus projection of the $[C_3mim]PF_6$ - $[C_3mpip]PF_6$ - $[C_3mpyrr]PF_6$ system with the second scenario. Notations: A={$[C_3mpip]PF_6(s_1)$ – $[C_3mpyrr]PF_6(s_1)$}(ss); B={$[C_3mpip]PF_6(s_2)$ – $[C_3mpyrr]PF_6(s_2)$}(ss); C={$[C_3mpip]PF_6(s_3)$ – $[C_3mpyrr]PF_6(s_3)$}(ss). Isoplethal section at constant 40 mol% $[C_3mim]PF_6$ (red dashed line), isoplethal section at constant molar ratio $[C_3mpyrr]PF_6$ / ($[C_3mpyrr]PF_6$ + $[C_3mpip]PF_6$) of 0.60 (blue dashed line).

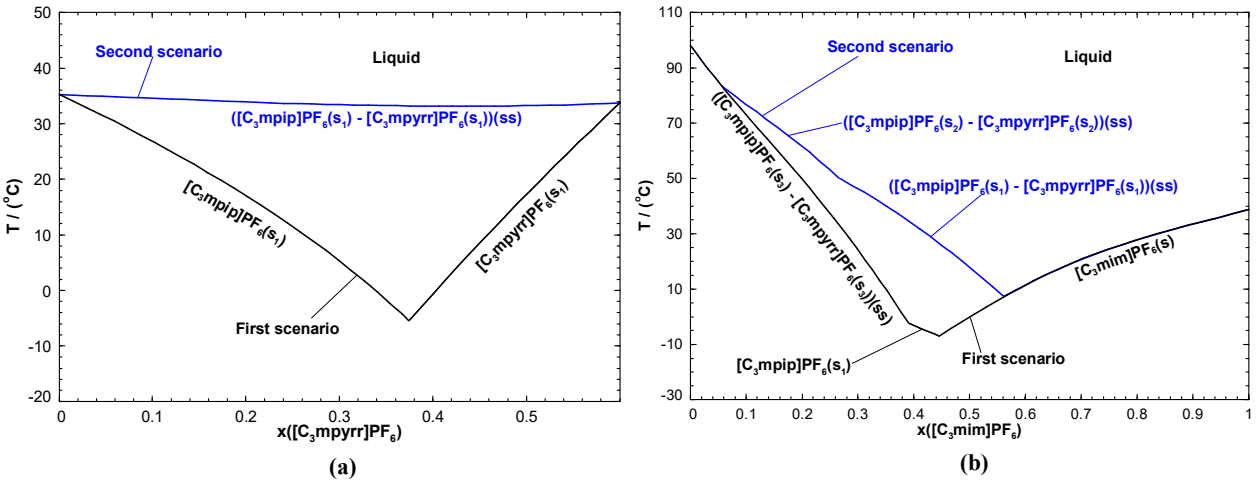


Figure 6.11: Calculated liquidus lines for the two isoplethal sections in the $[C_3mim]PF_6$ - $[C_3mpip]PF_6$ - $[C_3mpyrr]PF_6$ ternary system with the first (black line) and second (blue line) scenarios: (a) constant 40 mol% $[C_3mim]PF_6$, (b) constant molar ratio $[C_3mpyrr]PF_6$ / ($[C_3mpyrr]PF_6$ + $[C_3mpip]PF_6$) of 0.60.

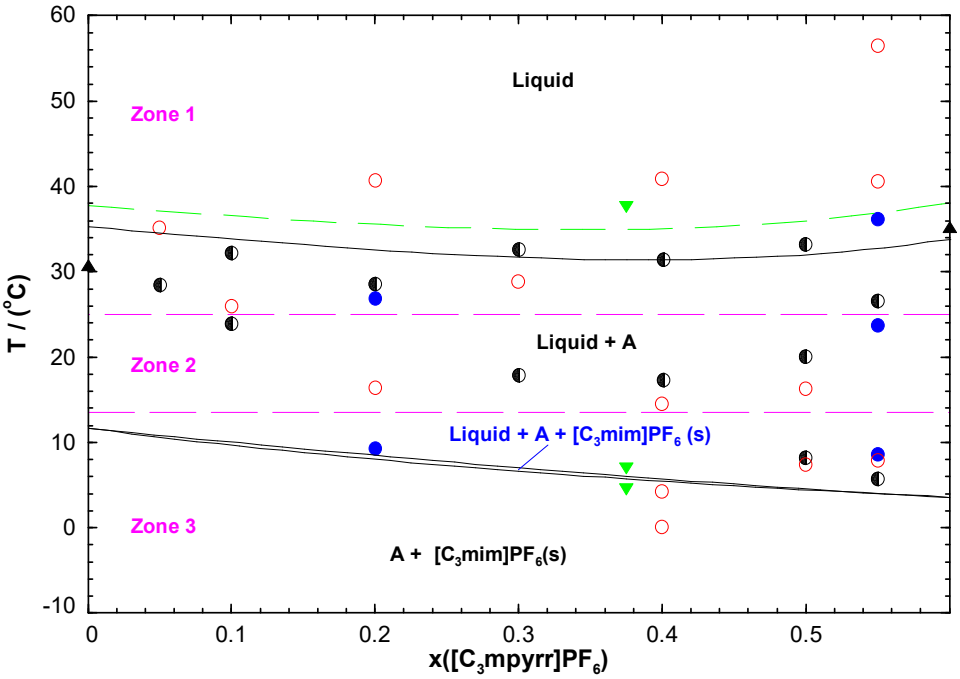


Figure 6.12: Calculated isoplethal section at 40 mol% $[C_3mim]PF_6$. The calculated liquidus line at 37.5 mol% $[C_3mim]PF_6$ is also shown as a dashed green line. Experimental data are from Coutinho's group: first series (◐), second series (○), third series (●), and from Maximo et al. [35] (▲). The thermal transitions measured at 37.5 mol% $[C_3mim]PF_6$ and taken from figure 6.13 are also shown (▼). Notations: A={$[C_3mpip]PF_6(s_1)$ – $[C_3mpyrr]PF_6(s_1)$}(ss).

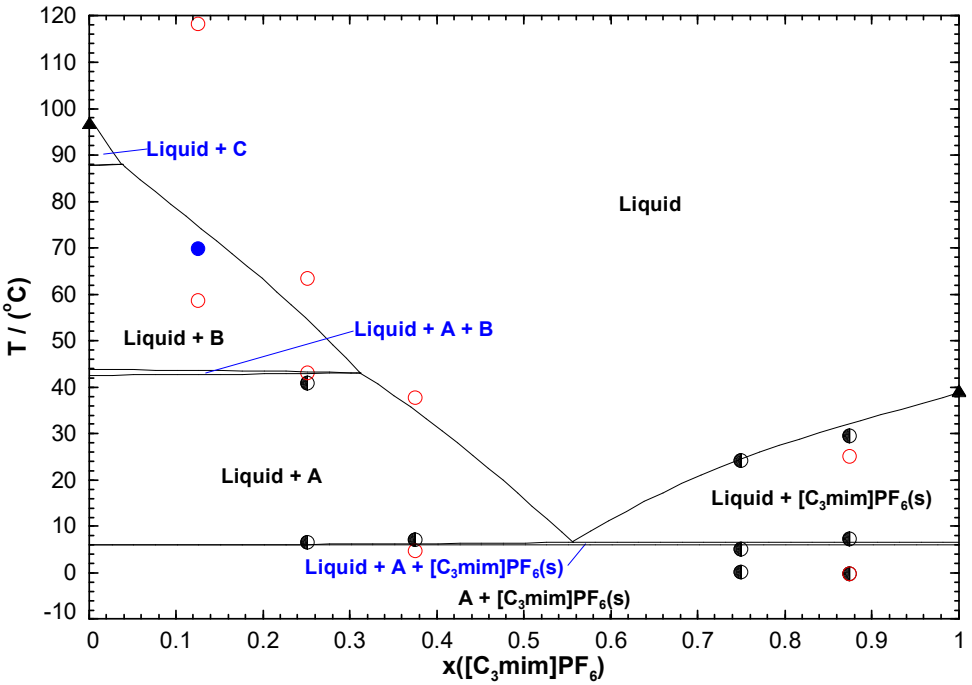


Figure 6.13: Calculated isoplethal section at constant molar ratio $[C_3mpyrr]PF_6$ / ($[C_3mpyrr]PF_6$ + $[C_3mpip]PF_6$) of 0.60. Experimental data are from Coutinho's group: first series (◐), second series (○), third series (●), and from Maximo et al. [35] (▲, △). Notations: A={$[C_3mpip]PF_6(s_1)$ – $[C_3mpyrr]PF_6(s_1)$}(ss); B={$[C_3mpip]PF_6(s_2)$ – $[C_3mpyrr]PF_6(s_2)$}(ss); C={$[C_3mpip]PF_6(s_3)$ – $[C_3mpyrr]PF_6(s_3)$}(ss).

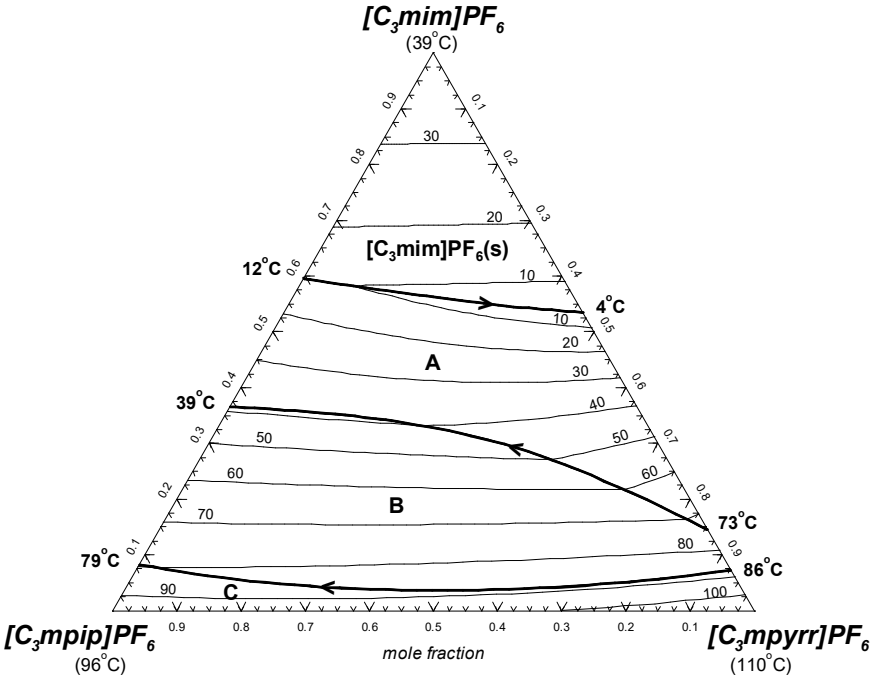


Figure 6.14: Final calculated liquidus projection of the $[C_3mim]PF_6$ - $[C_3mpip]PF_6$ - $[C_3mpyrr]PF_6$ system. Notations: A={$[C_3mpip]PF_6(s_1)$ – $[C_3mpyrr]PF_6(s_1)$}(ss); B={$[C_3mpip]PF_6(s_2)$ – $[C_3mpyrr]PF_6(s_2)$}(ss); C={$[C_3mpip]PF_6(s_3)$ – $[C_3mpyrr]PF_6(s_3)$}(ss).

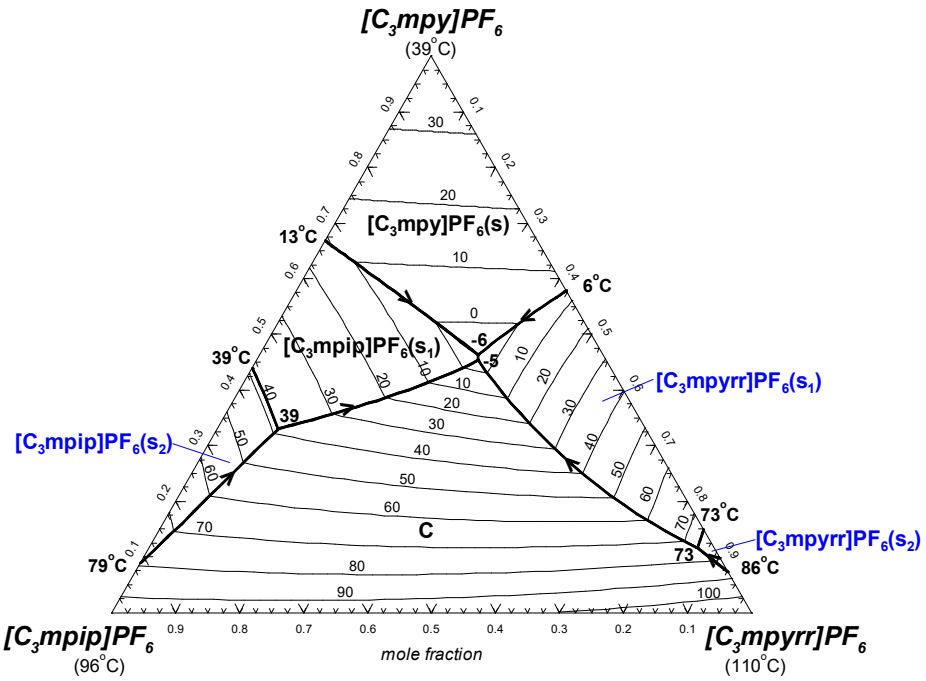


Figure 6.15: Calculated liquidus projection of the $[C_3mpy]PF_6$ - $[C_3mpip]PF_6$ - $[C_3mpyrr]PF_6$ system with the first scenario. Notations: C={$[C_3mpip]PF_6(s_3)$ – $[C_3mpyrr]PF_6(s_3)$}(ss).

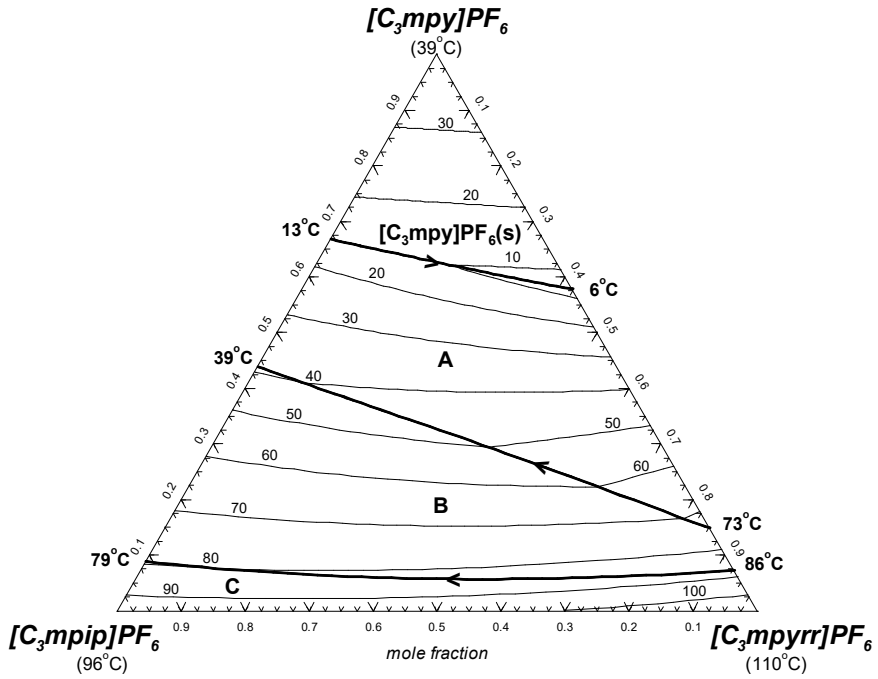


Figure 6.16: Calculated liquidus projection of the $[C_3mpy]PF_6$ - $[C_3mpip]PF_6$ - $[C_3mpyrr]PF_6$ system with the second scenario. Notations: A={$[C_3mpip]PF_6(s_1)$ – $[C_3mpyrr]PF_6(s_1)$}(ss); B={$[C_3mpip]PF_6(s_2)$ – $[C_3mpyrr]PF_6(s_2)$}(ss); C={$[C_3mpip]PF_6(s_3)$ – $[C_3mpyrr]PF_6(s_3)$}(ss).

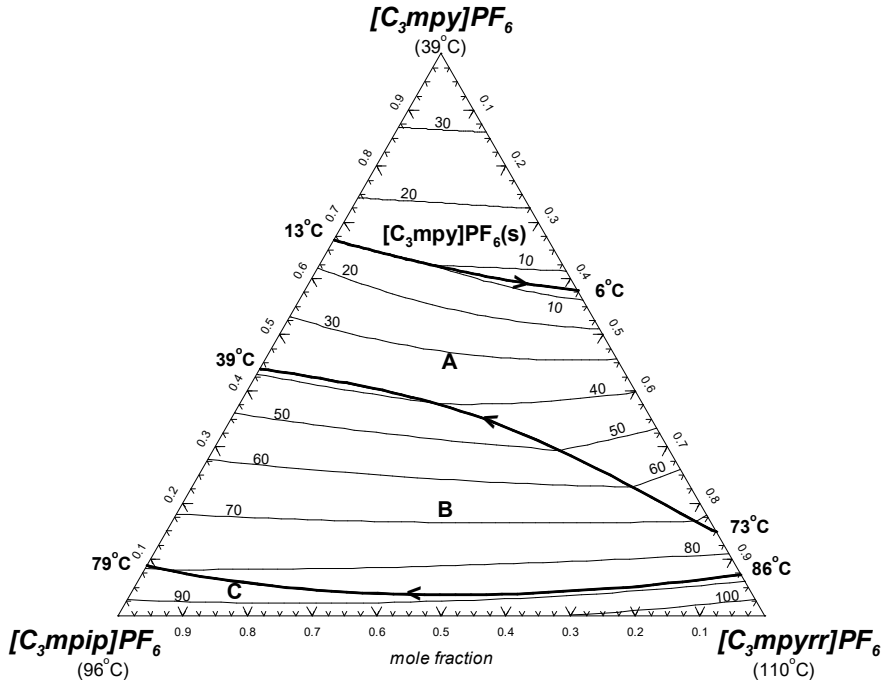


Figure 6.17: Final calculated liquidus projection of the $[C_3mpy]PF_6$ - $[C_3mpip]PF_6$ - $[C_3mpyrr]PF_6$ system. Notations: A={$[C_3mpip]PF_6(s_1)$ – $[C_3mpyrr]PF_6(s_1)$}(ss); B={$[C_3mpip]PF_6(s_2)$ – $[C_3mpyrr]PF_6(s_2)$}(ss); C={$[C_3mpip]PF_6(s_3)$ – $[C_3mpyrr]PF_6(s_3)$}(ss).

The calculated liquidus projection of the $[C_3mpip]PF_6$ - $[C_3mpy]PF_6$ - $[C_3mim]PF_6$ system is displayed in figure 6.18. No ternary excess parameter was introduced for the liquid. The thermodynamic properties of the ternary liquid are calculated solely from the optimized binary model parameters, using a symmetric interpolation method. The ternary eutectic reaction liquid = $[C_3mpip]PF_6(s_1)$ + $[C_3mpy]PF_6$ + $[C_3mim]PF_6$ is calculated at -8°C with a liquid composition of (22.6 mol% $[C_3mpip]PF_6$ + 41.5 mol% $[C_3mpy]PF_6$ + 35.9 mol% $[C_3mim]PF_6$). This corresponds to the minimum liquidus temperature in the ternary system. In order to test the accuracy of the developed thermodynamic model, two isoplethal sections were measured by Coutinho's group using DSC: the isoplethal section at constant 40 mol% $[C_3mpy]PF_6$ (red dashed line in figure 6.18) and the isoplethal section at constant molar ratio $[C_3mpy]PF_6$ / ($[C_3mpy]PF_6$ + $[C_3mim]PF_6$) of 0.60 (blue dashed line in figure 6.18). Figures 6.19 and 6.20 display the measured and calculated isoplethal sections. In each case, Coutinho's group performed one series of DSC measurements, with one cooling run followed by one heating run. Following our request, they studied again two ternary mixtures (second series) using three consecutive heating / cooling cycles. In figure 6.19, the binary data from Maximo et al. [35] at 0 and 60 mol% $[C_3mpip]PF_6$ are also shown. Note that

the thermal arrests measured at 45.2 mol% $[C_3mpy]PF_6$ (and at 25.5 mol% $[C_3mpip]PF_6$) and at 37.6 mol% $[C_3mpy]PF_6$ (and at 37.9 mol% $[C_3mpip]PF_6$), both taken from the isoplethal section at constant molar ratio $[C_3mpy]PF_6$ / ($[C_3mpy]PF_6$ + $[C_3mim]PF_6$) of 0.60 in figure 6.20, are also displayed in figure 6.19. The corresponding calculated liquidus temperatures are virtually identical to those calculated at 40 mol% $[C_3mpy]PF_6$ and displayed in figure 6.19. For the ternary mixture at 5 mol% $[C_3mpip]PF_6$, the very high liquidus temperature of about 47°C (first series) should be discarded: the three thermal arrests measured during the third heating run of the second series of data agree very well with the calculations; and the corresponding liquidus temperature is about 10°C. For the ternary mixture at 27.7 mol% $[C_3mpip]PF_6$ (second series), two thermal arrests were measured during the first heating run, and no thermal arrests were observed during the second and third heating runs. Although the two thermal arrests from the first heating run (second series) occur at temperatures significantly lower than those from the first series of data, they are still substantially higher than the calculations. Apart from the results for the ternary mixture with 27.7 mol% $[C_3mpip]PF_6$, the shift between the calculated and measured temperatures is always lower than 14°C. In figure 6.20, the binary and unary data from Maximo et al. [35] are also shown at 0 and 100 mol% $[C_3mpip]PF_6$, respectively. The shift between the calculated and measured temperatures is always lower than 15°C.

Overall, the experimental isoplethal sections at constant 40 mol% $[C_3mpy]PF_6$ and at constant molar ratio $[C_3mpy]PF_6$ / ($[C_3mpy]PF_6$ + $[C_3mim]PF_6$) of 0.60 are satisfactorily reproduced by the model. Therefore, the calculated liquidus projection of the $[C_3mpip]PF_6$ - $[C_3mpy]PF_6$ - $[C_3mim]PF_6$ system (figure 6.18) is expected to be reasonably accurate.

No ternary DSC data are available for the $[C_3mpyrr]PF_6$ - $[C_3mpy]PF_6$ - $[C_3mim]PF_6$ system. By analogy with the $[C_3mpip]PF_6$ - $[C_3mpy]PF_6$ - $[C_3mim]PF_6$ system, no ternary excess parameter was introduced for the liquid and a symmetric interpolation method was used. The calculated liquidus projection is shown in figure 6.21 and is expected to be reasonably accurate. The ternary eutectic reaction liquid = $[C_3mpyrr]PF_6(s_1)$ + $[C_3mpy]PF_6$ + $[C_3mim]PF_6$ is calculated at -16°C with a liquid composition of (33.9 mol% $[C_3mpyrr]PF_6$ + 33.9 mol% $[C_3mpy]PF_6$ + 32.2 mol% $[C_3mim]PF_6$). This is the minimum liquidus temperature in the ternary system.

Using the programme FactOptimal [36], which is a coupling of the FactSage thermochemical software with the powerful Mesh Adaptive Direct Search (MADS) algorithm, we identified the

global minimum liquidus temperature in the quaternary system $[C_3mim]PF_6$ - $[C_3mpyrr]PF_6$ - $[C_3mpy]PF_6$ - $[C_3mpip]PF_6$. This global minimum is very close to the ternary eutectic in the $[C_3mpyrr]PF_6$ - $[C_3mpy]PF_6$ - $[C_3mim]PF_6$ system (figure 6.21). This is a true minimum, where three solid phases coexist ($[C_3mpy]PF_6$, $[C_3mim]PF_6$, and a $[C_3mpyrr]PF_6(s_1)$ - $[C_3mpip]PF_6(s_1)$ solid solution which is almost pure $[C_3mpyrr]PF_6(s_1)$); and the quaternary liquid contains only about 0.003 mol% $[C_3mpipPF_6$.

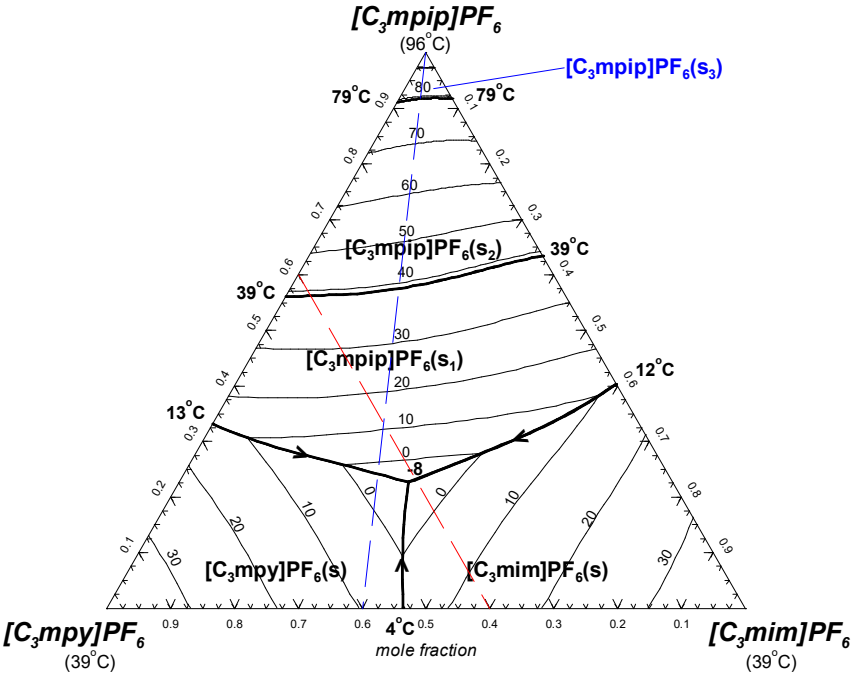


Figure 6.18: Calculated liquidus projection of the $[C_3mpip]PF_6$ - $[C_3mpy]PF_6$ - $[C_3mim]PF_6$ system. Isoplethal section at constant 40 mol% $[C_3mpy]PF_6$ (red dashed line), isoplethal section at constant molar ratio $[C_3mpy]PF_6$ / ($[C_3mpy]PF_6$ + $[C_3mim]PF_6$) of 0.60 (blue dashed line).

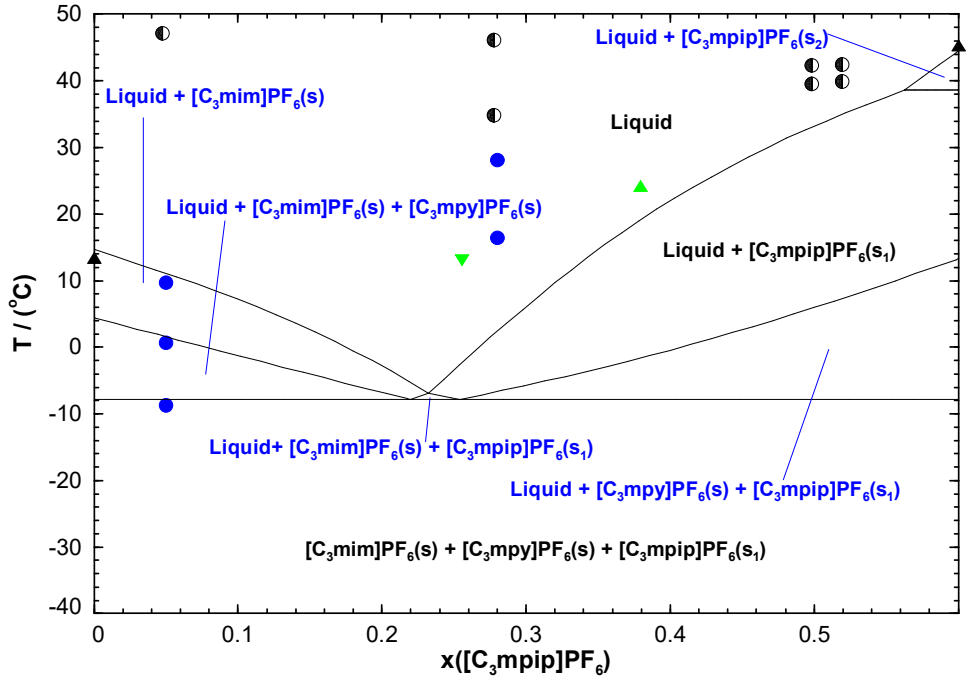


Figure 6.19: Calculated isoplethal section at constant 40 mol% $[C_3mpy]PF_6$. Experimental data are from Coutinho's group: first series (◐), second series (●), and from Maximo et al. [35] (▲). The thermal transitions measured at 45.2 mol% $[C_3mpy]PF_6$ (▼) and at 37.6 mol% $[C_3mpy]PF_6$ (▲), and taken from figure 6.20, are also shown.

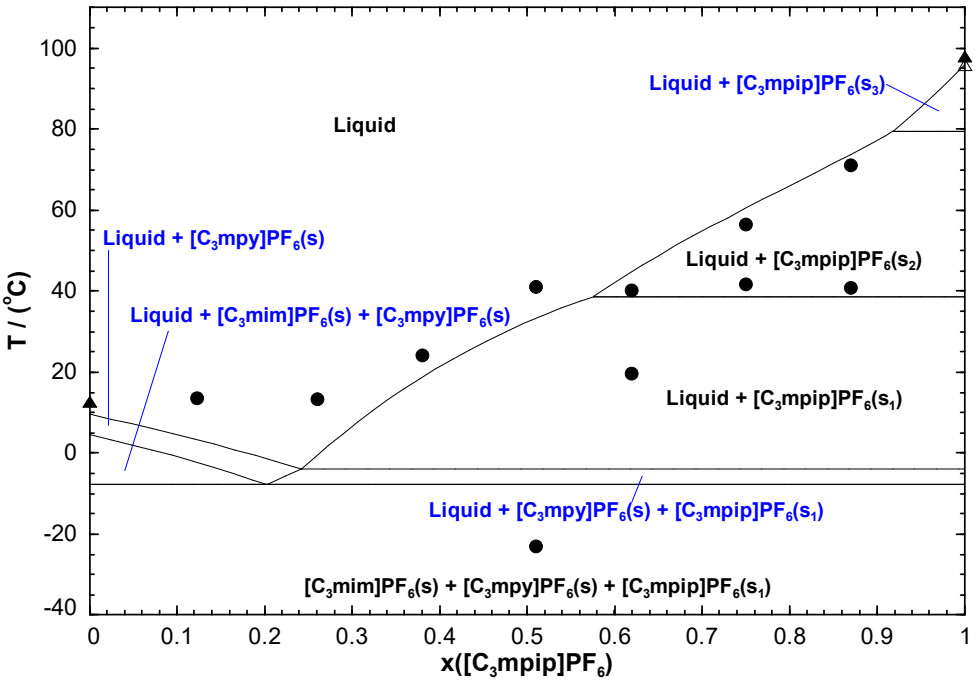


Figure 6.20: Calculated isoplethal section at constant molar ratio $[C_3mpy]PF_6$ / ($[C_3mpy]PF_6$ + $[C_3mim]PF_6$) of 0.60. Experimental data are from Coutinho's group (●) and Maximo et al. [35] (▲, △).

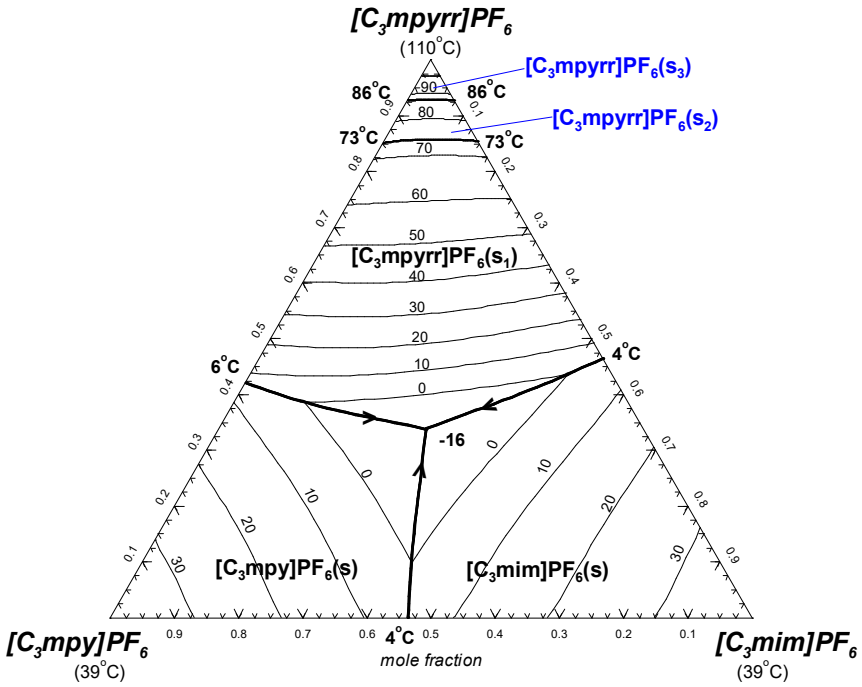


Figure 6.21: Calculated liquidus projection of the $[C_3mpyrr]PF_6$ - $[C_3mpy]PF_6$ - $[C_3mim]PF_6$ system.

# CHAPTER 7 DENSITY OF IONIC LIQUID SYSTEMS

This chapter describes a density model for common-ion (common-cation and common-anion) ionic liquid ternary systems. Two common-cation ternary systems were studied in the present work: [$C_4$mim]{Cl, $NO_3$, $CH_3SO_3$} in collaboration with Seddon's group (QUILL), and [$C_4$mim]{$BF_4$, $PF_6$, $NTf_2$} based on the published density data from Canongia Lopes et al. [38]. Two common-anion ternary systems were also investigated: {[$C_2$mim], [$C_8$mim], [$C_{10}$mim]}$NTf_2$ and {[$C_4$mim], [$C_8$mim], [$C_{10}$mim]}$NTf_2$, again based on the published density data from Canongia Lopes et al. [38]. The densities of the pure liquids and of the binary liquids are modeled, based on the available data. For the three common-ion ternary systems based on the work of Canongia Lopes et al., the density is predicted from the optimized density model parameters for the binary liquids using a standard symmetric interpolation method.

## 7.1 Common-cation ternary system [$C_4$mim]{Cl, $NO_3$, $CH_3SO_3$}

In the present work, the density of the [$C_4$mim]Cl, [$C_4$mim]$NO_3$ and [$C_4$mim]$CH_3SO_3$ pure ionic liquids and of the corresponding binary liquids was investigated by Seddon's group (QUILL). The density of the three pure liquids and of the [$C_4$mim]$CH_3SO_3$ - [$C_4$mim]Cl and [$C_4$mim]$NO_3$ - [$C_4$mim]Cl binary liquids was measured with a U-tube density meter DM 40 from Mettler Toledo. The experimental error for the DM 40 density measurements is typically 0.1K for the temperature and 0.0001 $g.cm^{-3}$ for the density. All samples were then sent by QUILL to a Portuguese group (Rebelo's group), who has a more accurate equipment than that of QUILL. Rebelo's group measured the density of the three pure liquids and of the three binary liquids using SVM 3000 or DMA 5000 densimeters. As will be shown later, for the [$C_4$mim]$CH_3SO_3$ - [$C_4$mim]Cl and [$C_4$mim]$NO_3$ - [$C_4$mim]Cl binary liquids, the excess molar volumes ($V^E$) measured by the two research groups show opposite trends (i.e. positive or negative values). Thus, the density of these two binary liquids is finally not modeled, and a prediction of the density of the [$C_4$mim]Cl - [$C_4$mim]$NO_3$ - [$C_4$mim]$CH_3SO_3$ ternary liquid is not possible. Only the density of the [$C_4$mim]$CH_3SO_3$ - [$C_4$mim]$NO_3$ binary liquid is modeled. For the sake of consistency, the densities measured by Rebelo's group for the three pure liquids are favoured in the present work.

### 7.1.1 Pure ionic liquids

Table 7.1 presents the expressions for the optimized thermal expansion (Eq. (20) in Chapter 3) of the [C4mim]Cl, [C4mim]$NO_3$ and [C4mim]$CH_3SO_3$ pure liquids. These expressions were derived from the density data of Rebelo's group. In the present work, the reference temperature $T_{ref}$ was arbitrarily set to 298.15K. Hence, the reference molar volume ($V_m^{liquid}$) is extrapolated at 298.15K from the optimized molar volume values at high temperatures, using the optimized thermal expansion expression.

Table 7.1: Molar volume at 298.15K and thermal expansion of the pure liquids

| Liquid | $V_m^{liquid}(298.15K)$ ($cm^3.mol^{-1}$) | Thermal expansion $\alpha(T)$ ($K^{-1}$) |
|---|---|---|
| [C4mim]Cl | 161.4 | $0.420\times10^{-3} + 2.959\times10^{-7}T$ |
| [C4mim]$NO_3$ | 174.3 | $0.433\times10^{-3} + 3.245\times10^{-7}T$ |
| [C4mim]$CH_3SO_3$ | 200.1 | $0.437\times10^{-3} + 3.321\times10^{-7}T$ |

Figures 7.1, 7.2 and 7.3 compare the calculated and measured densities from Rebelo's group for the three pure ionic liquids. The experimental densities from Seddon's group along with the data available from the literature are also shown. The shifts between the data of Seddon's group and of Rebelo's group are about +0.00066 $g.cm^{-3}$ for liquid [C4mim]Cl, -0.00049 $g.cm^{-3}$ for liquid [C4mim]$NO_3$, and +0.00024 $g.cm^{-3}$ for liquid [C4mim]$CH_3SO_3$. The densities of the [C4mim]Cl, [C4mim]$NO_3$ and [C4mim]$CH_3SO_3$ pure liquids were calculated over the temperature range -60°C to 300°C, using the thermal expansions in table 7.1 extrapolated well below and well above the melting temperatures of the pure ionic liquids. The calculations are shown in figure 7.4. It can be seen that each calculated density exhibits a linear temperature dependence over a large temperature range.

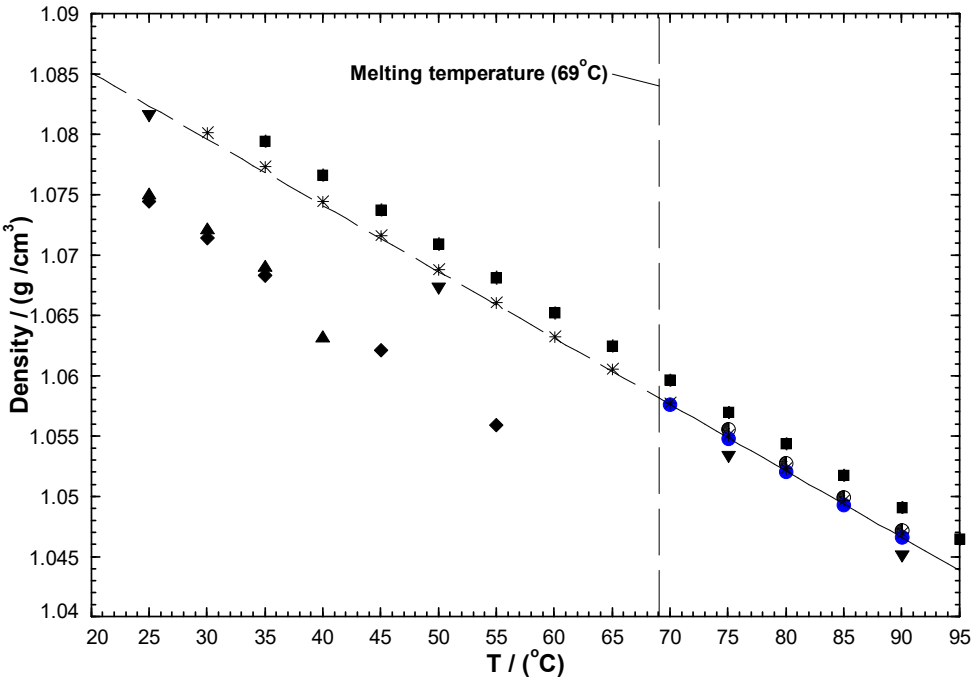


Figure 7.1: Calculated density of pure liquid [C4mim]Cl. Experimental data are from Rebelo's group (●), Seddon's group (◐), Martins et al. [157] (■), Kavitha et al. [158] (▲), Govinda et al. [159] (▼), He et al. [160] (◆), and Dowell et al. [161] (✳).

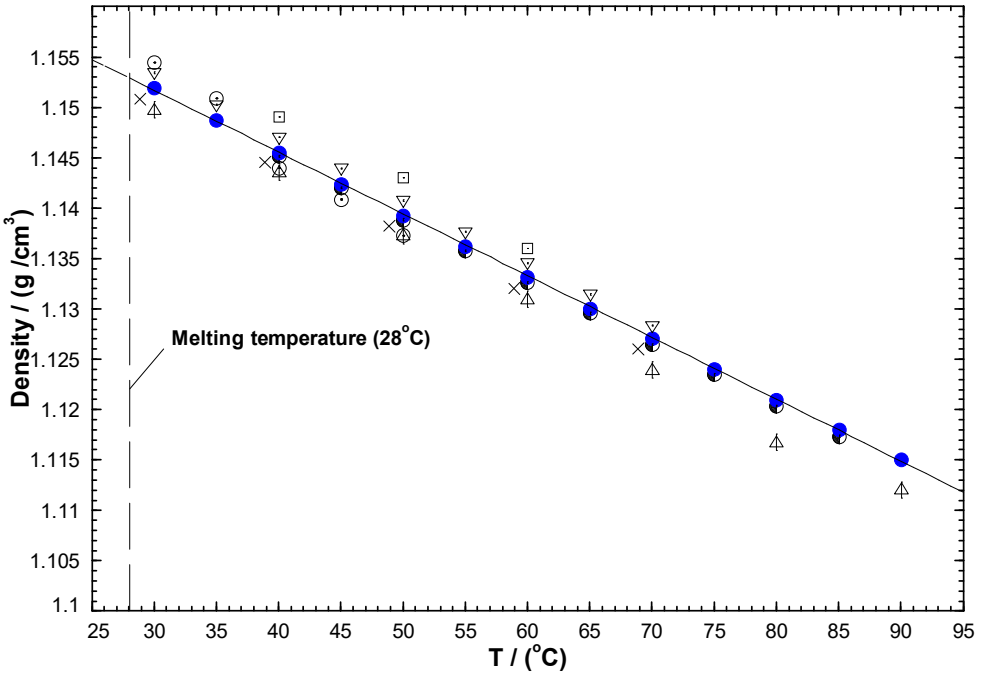


Figure 7.2: Calculated density of pure liquid [C4mim]$NO_3$. Experimental data are from Rebelo's group (●), Seddon's group (◐), Moosavi et al. [162] (○), Mokhtarani et al. [163] (▽), Seddon et al. [164] (△), Bermejo et al. [165] (╳), and Blanchard et al. [166] (□).

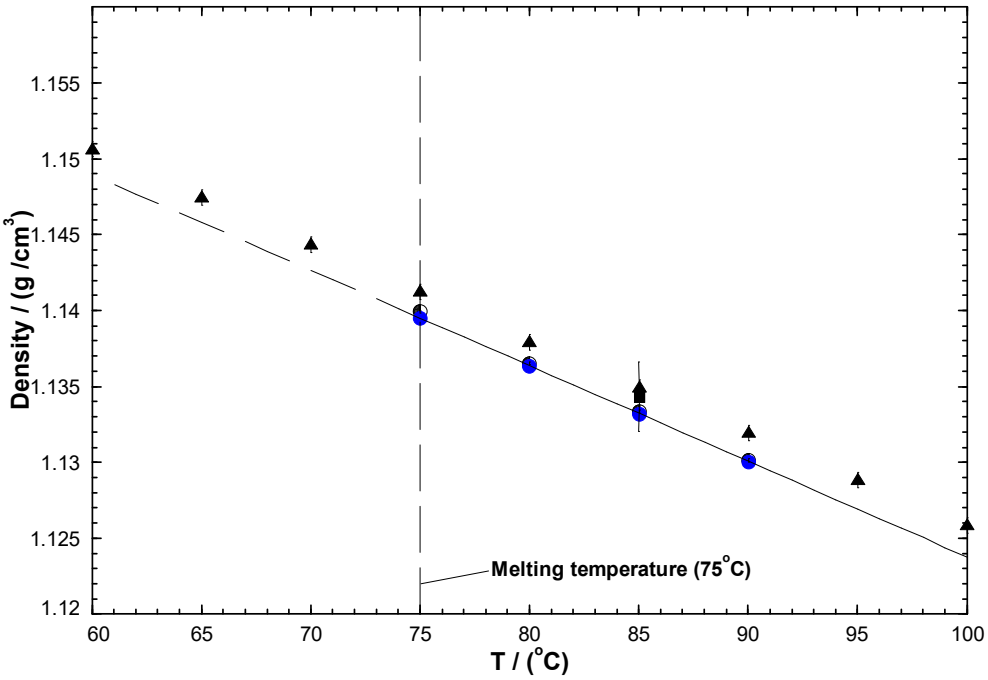


Figure 7.3: Calculated density of pure liquid [C4mim]$CH_3SO_3$. Experimental data are from Rebelo's group (●), Seddon's group (◐), Stark et al. [149] (■), and Martins et al. [157] (▲).

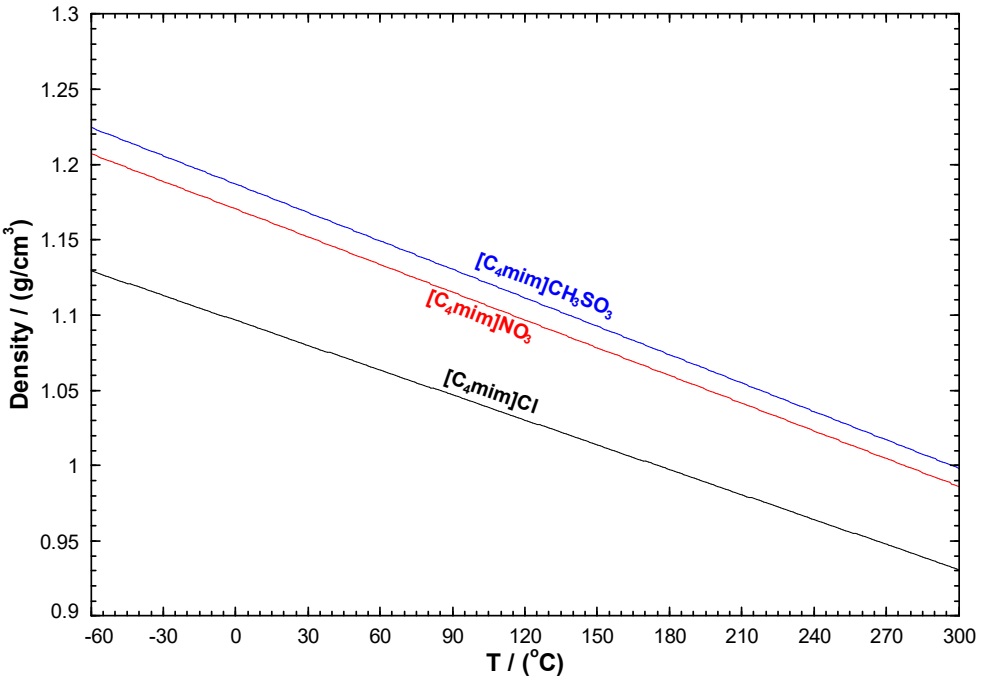


Figure 7.4: Calculated density of the [C4mim]Cl, [C4mim]$NO_3$ and [C4mim]$CH_3SO_3$ pure liquids between -60°C and 300°C.

## 7.1.2 Binary subsystems

### 7.1.2.1 The $[C_4mim]CH_3SO_3$ – $[C_4mim]NO_3$ binary liquid

The density of the $[C_4mim]CH_3SO_3$ – $[C_4mim]NO_3$ binary liquid was measured by Rebelo's group over the entire composition range and over the temperature range 50-90°C, using a DMA 5000 densimeter. Canongia Lopes et al. [38] measured the density of various common-ion (common-cation or common-anion) binary liquids of the methyl-imidazolium type. They reported a density precision lower than 0.001%, and an estimated uncertainty of about ±0.02 $cm^3.mol^{-1}$ for the excess molar volume ($V^E$) values. The latter uncertainty is assumed to be valid for all density data obtained with the DMA 5000 densimeter. The excess molar volume ($V^E$) is defined as follows:

$$V^E = V_{mix} - V_{ideal} = V_{mix} - x_1V_1 - x_2V_2 \quad (72)$$

where $V_{mix}$, $V_{ideal}$, $V_1$ and $V_2$ are the molar volumes of the binary mixture, of the hypothetical ideal mixture, and of the two pure ionic liquids, respectively, and $x_i$ $(i = 1\ or\ 2)$ are the corresponding mole fractions.

Figure 7.5 compares the calculated and measured $V^E$ values at 75°C and 90°C. There are very small negative deviations from ideality (maximum value of about -0.2 $cm^3.mol^{-1}$) over the entire composition range. The measured $V^E$ values are somewhat scattered and are almost identical at 75°C and 90°C.

As explained in Chapter 3, the density model is linked to the thermodynamic model. The optimized pressure-independent term of the Gibbs free energy of reaction (25) in Chapter 4 was given in Chapter 5. The optimized pressure-dependent term is:

$$\Delta g^P_{[C_4mim]_2/(CH_3SO_3)NO_3}/(J.mol^{-1}) = -0.017(P-1) \quad (73)$$

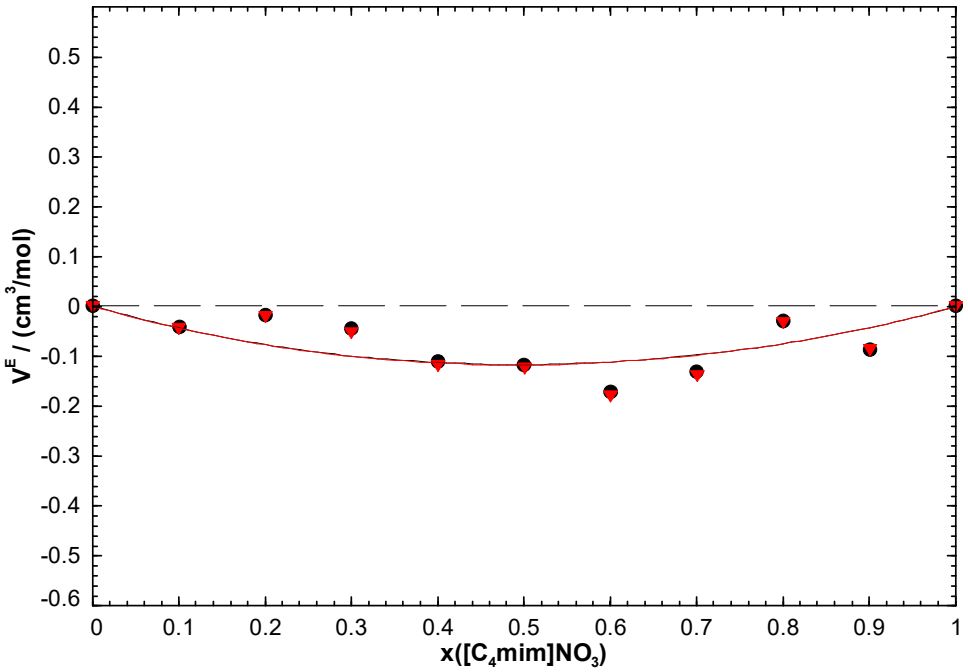


Figure 7.5: Calculated excess molar volume ($V^E$) of the [$C_4$mim]$CH_3SO_3$ - [$C_4$mim]$NO_3$ binary liquid at 75°C (black line) and 90°C (red line). Experimental data are from Rebelo's group: 75°C (●), 90°C (▼).

### 7.1.2.2 The [$C_4$mim]$CH_3SO_3$ – [$C_4$mim]Cl binary liquid

The density of the [$C_4$mim]$CH_3SO_3$ – [$C_4$mim]Cl binary liquid was measured by Seddon's group over the entire composition range and over the temperature range 55-90°C, using a DM 40 densimeter. Rebelo's group performed their measurements over the temperature range 50-90°C, using a SVM 3000 densimeter. Figure 7.6 displays the measured $V^E$ values at 75°C and 90°C. There are zero or small positive deviations from ideality (maximum value of about 0.3 $cm^3.mol^{-1}$) for the $V^E$ values measured by Seddon's group. On the other hand, there are small negative deviations from ideality (maximum value of about -0.4 $cm^3.mol^{-1}$) for the $V^E$ values measured by Rebelo's group. Owing to these opposite trends displayed by the two series of $V^E$ values, the density of the [$C_4$mim]$CH_3SO_3$ – [$C_4$mim]Cl binary liquid was finally not modeled.

At 75°C and for a given binary composition, the original densities measured by Rebelo's group are always higher than those of Seddon's group. The largest density shift $\Delta\rho_{MAX} = \rho_2 - \rho_1$ is about 0.00173 $g.cm^{-3}$ and is observed at 70 mol% [$C_4$mim]Cl. Pure liquid water is less dense than liquid [$C_4$mim]$CH_3SO_3$ or liquid [$C_4$mim]Cl (it has a density of 0.97468 $g.cm^{-3}$ at 75°C). If we assume

that the decrease in density is only due to the presence of water, then the estimated weight fraction of water is about $\frac{\Delta\rho_{MAX}\cdot\rho_{H_2O}}{(\rho_2)^2} \approx 1430$ ppm. This is very close to the maximum water content of 1400 ppm reported by Seddon's group. Therefore, the shifts between the two series of density measurements are at least partly due to the presence of water.

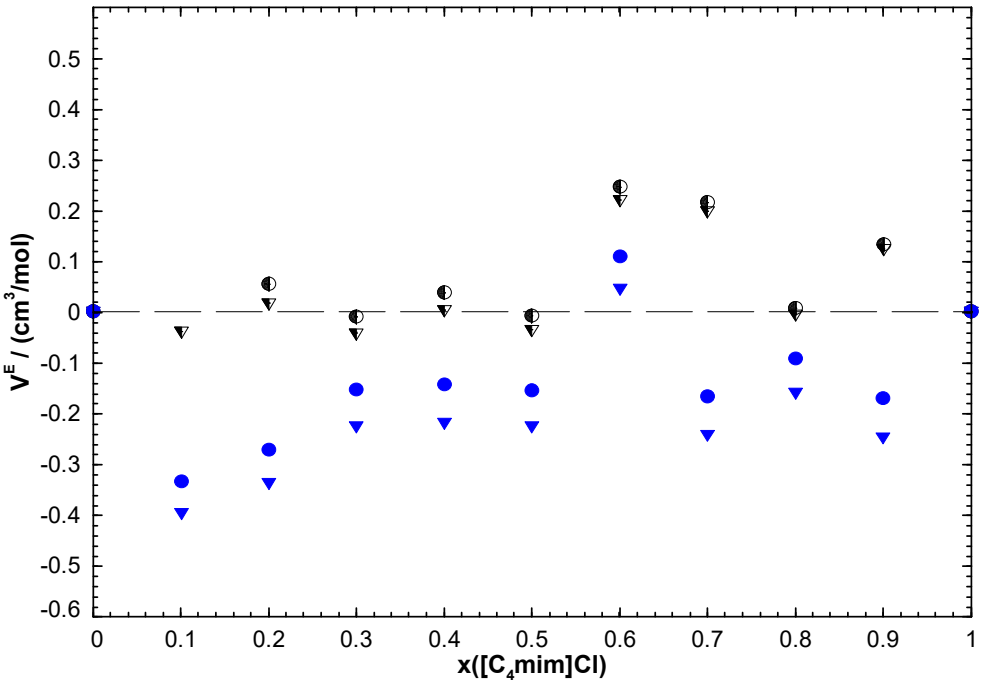


Figure 7.6: Measured excess molar volume ($V^E$) values of the $[C_4mim]CH_3SO_3$ - $[C_4mim]Cl$ binary liquid at 75°C and 90°C . Experimental data are from Seddon's group (75°C (◐), 90°C (▼)) and Rebelo's group (75°C (●), 90°C (▼)).

### 7.1.2.3 The $[C_4mim]NO_3$ – $[C_4mim]Cl$ binary liquid

The density of the $[C_4mim]NO_3$ – $[C_4mim]Cl$ binary liquid was measured by Seddon's group (through two series of experiments) over the entire composition range and over the temperature range 40-85°C, using a DM 40 densimeter. Rebelo's group conducted their measurements over the temperature range 40-90°C, using SVM 3000 or DMA 5000 densimeters. Figure 7.7 displays the measured $V^E$ values at 75°C and 85°C for Seddon's group, and at 75°C and 90°C for Rebelo's group. There are negative deviations from ideality (maximum value of about -0.5 $cm^3.mol^{-1}$) for

the $V^E$ values measured by Seddon's group. (The second series of data at 20 mol% [C4mim]Cl are rather doubtful). On the other hand, except for the binary mixture with 40 mol% [C4mim]Cl which exhibits $V^E \approx +0.2$ $cm^3.mol^{-1}$, there are almost zero deviations from ideality for the $V^E$ values measured by Rebelo's group. Again, due to these rather different trends displayed by the two series of $V^E$ values, the density of the $[C_4mim]NO_3$ – [C4mim]Cl binary liquid was finally not modeled.

At 75°C and for a given binary composition, the original densities measured by Seddon's group are always higher than those of Rebelo's group, except for the binary liquid at 20 mol% [C4mim]Cl. The largest density shift is about 0.00235 $g.cm^{-3}$ and is observed at 80 mol% [C4mim]Cl. Again, if we assume that the decrease in density is only due to the presence of water, then the estimated water content of this sample would be about $\frac{\Delta\rho_{MAX}.\rho_{H_2O}}{(\rho_2)^2} \approx 2000$ ppm. This is significantly more than the maximum water content of 1400 ppm reported by Seddon's group. Again, it seems very likely that the shifts between the two series of density measurements are at least partly due to the presence of water.

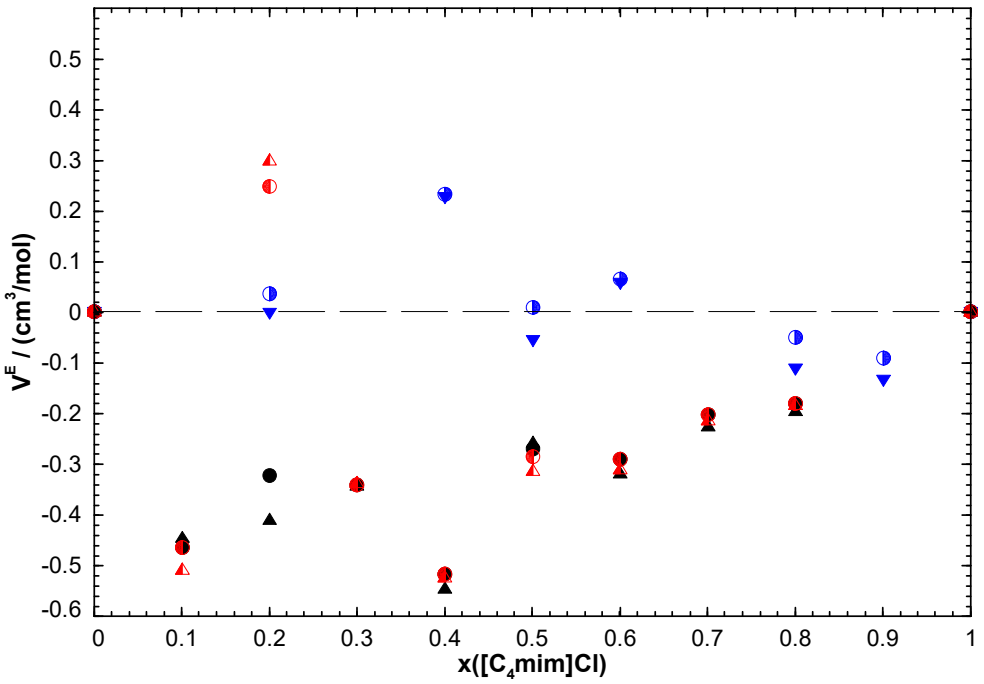


Figure 7.7: Measured excess molar volume ($V^E$) values of the $[C_4mim]NO_3$ - [C4mim]Cl binary liquid at 75°C, 85°C and 90°C . Experimental data are from Seddon's group: first series of data (75°C (●), 85°C (▲)), second series of data (75°C (◐), 85°C (◭)), and from Rebelo's group (75°C (◑), 90°C (▼)).

## 7.2 Common-cation ternary system [C4mim]{BF4, PF6, NTf2}

Canongia Lopes et al. [38] measured the density of the common-cation ionic liquid system [C4mim]{BF4, PF6, NTf2}. ($NTf_2$ is the notation used for $N(CF_3O_2S)_2$.) These authors measured the density of the three pure liquids and of the three binary liquids at 298.15K, 303.15K and 333.15K, using a DMA 5000 densimeter. As already mentioned, they reported a density precision lower than 0.001% and an estimated uncertainty of ±0.02 $cm^3.mol^{-1}$ for the $V^E$ values.

### 7.2.1 Pure ionic liquids

Table 7.2 presents the expressions for the optimized thermal expansion (Eq. (20) in Chapter 3) and the reference molar volume ($V_m^{liquid}$) extrapolated at 298.15K for the [C4mim]BF4, [C4mim]PF6 and [C4mim]NTf2 pure ionic liquids. These expressions were derived from the density data of Canongia Lopes et al. [38].

Table 7.2: Molar volume at 298.15K and thermal expansion of the pure liquids

| Liquid | $V_m^{liquid}(298.15K)$ ($cm^3.mol^{-1}$) | Thermal expansion $\alpha(T)$ ($K^{-1}$) |
|---|---|---|
| [C4mim]BF4 | 187.6 | $0.461\times10^{-3} + 3.911\times10^{-7}T$ |
| [C4mim]PF6 | 207.9 | $0.473\times10^{-3} + 4.256\times10^{-7}T$ |
| [C4mim]NTf2 | 292.3 | $0.504\times10^{-3} + 5.262\times10^{-7}T$ |

Figures 7.8, 7.9 and 7.10 compare the calculated and measured densities from Canongia Lopes et al. [38] for the three pure ionic liquids. The available data from the literature are also shown. The densities of the [C4mim]BF4, [C4mim]PF6 and [C4mim]NTf2 pure liquids were calculated over the temperature range -60°C to 300°C, using the thermal expansions in table 7.2 extrapolated well below and well above the melting temperatures of the pure ionic liquids (see figure 7.11). Each calculated density has a linear temperature dependence over a large temperature range.

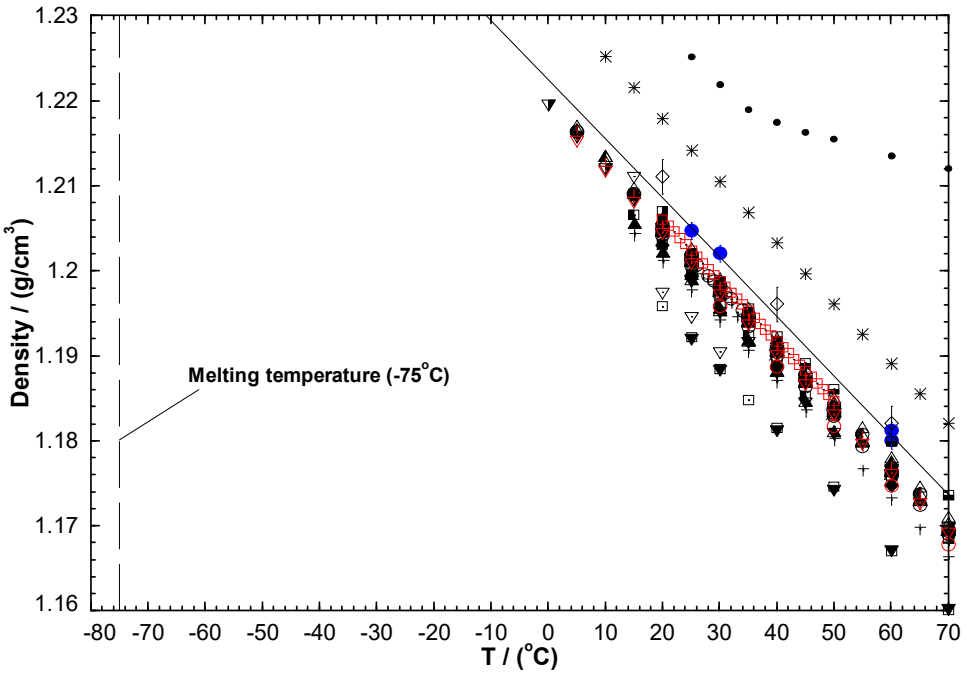


Figure 7.8: Calculated density of pure liquid [$C_4$mim]$BF_4$. Experimental data are from Canongia Lopes et al. [38] (●), Navia et al. [74] (○), Huo et al. [167] (□), Salgado et al. [168] (△), Qi et al. [169] (▽), Tomida et al. [170] (◇), Soriano et al. [171] (+), Afzal et al. [172] (†), Kumar et al. [173] (✳), Jacquemin et al. [174] (×), Montalbán et al. [175] (°), Tokuda et al. [176] (■), Zhang et al. [177] (▲), Huo et al. [178] (▼), Tariq et al. [179] (◆), Song & Chen [180] (◓), Iglesias-Otero et al. [181] (◒), Nikitina et al. [182] (◐), Ciocirlan et al. [183] (◑), Ge et al. [184] (•), Taib & Murugesan [185] (⬒), Zhou et al. [186] (⬓), Pal & Kumar [187] (◧), Santos et al. [188] (◨), Vercher et al. [189] (▪), Currás et al. [190] (◭), Rao et al. [191] (◭), Krishna et al. [192] (▼), Harris et al. [193] (▼), Iglesias-Otero et al. [194] (◈), Zafarani-Moattar & Shekaari [195] (◈), Wu et al. [196] (◈), Singh et al. [197] (◈), Zhao et al. [198] (○), Sanmamed et al. [199] (□), Neves et al. [200] (△), Vakili-Nezhaad et al. [201] (▽), Klomfar et al. [202] (◊), and Soriano et al. [171] (+).

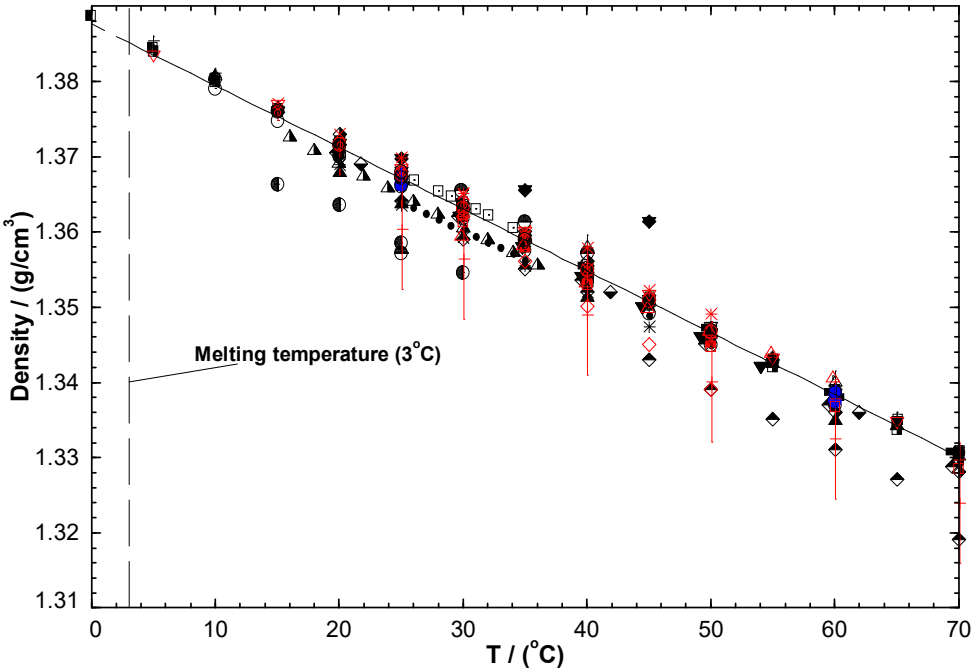


Figure 7.9: Calculated density of pure liquid [$C_4$mim]$PF_6$. Experimental data are from Canongia Lopes et al. [38] (●), Fan et al. [203] (○), Navia et al. [74] (□), Qiao et al. [204] (△), Geng et al. [205] (▽), Huo et al. [167] (◇), Salgado et al.[168] (+), Vaid et al. [206] (†), Yanfang et al. [207] (✳), Krishna et al. [208] (×), Zafarani-Moattar et al. [209] (°), Vaid et al. [210] (■), Kumar et al. [211] (▲), Singh & Kumar [212] (▼), Zhong et al. [213] (◆), Pereiro & Rodríguez [214] (◓), Qi & Wang [169] (◒), Tomida et al.[170] (◐), Soriano et al. [171] (◑), Rocha et al. [215] (◔), Afzal et al. [172] (◘), Harris et al. [216] (⬓), Pereiro et al. [217] (◧), Jacquemin et al. [218] (◨), Kumar [173] (◾), Kumełan et al. [219] (◭), Kabo et al. [220] (◮), Li et al. [221] (▼), Jacquemin et al. [174] (▼), Troncoso et al. [53] (◆), AlTuwaim et al. [222] (◆), Seddon et al. [223] (◆), Chaudhary et al. [224] (◆), Reyes et al. [225] (○), Singh et al. [226] (□), Zech et al. [227] (△), Dzyuba et al. [228] (▽), Gu & Brennecke [229] (◊), Montalbán et al. [175] (+), Moosavi et al. [230] (†), Tokuda et al. [176] (✳), Zhang et al. [177] (×), Tariq et al. [179] (°), and Huo et al. [178] (■).

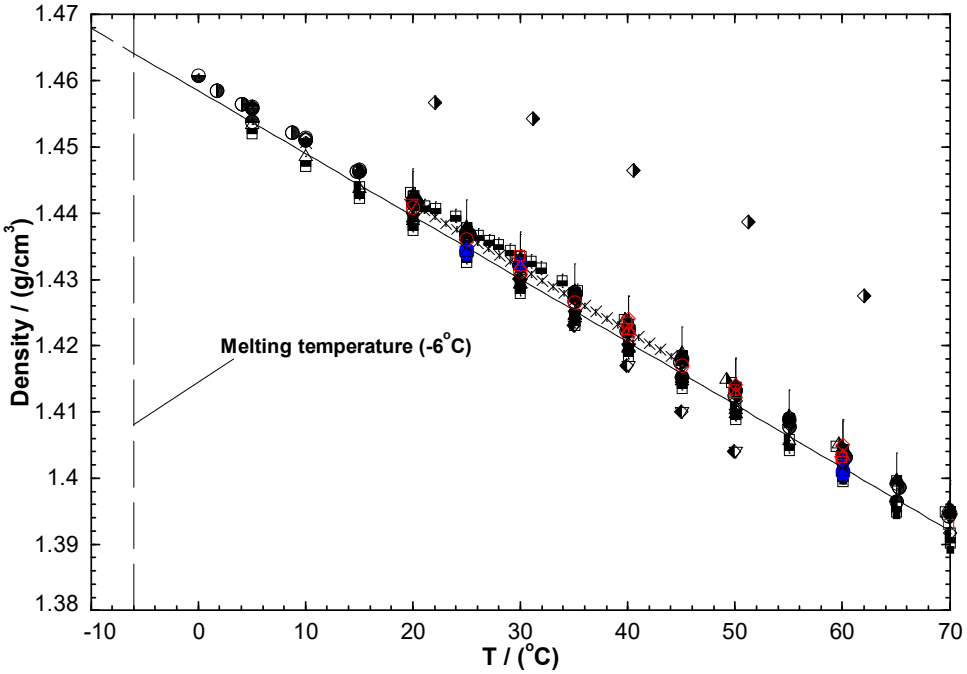


Figure 7.10: Calculated density of pure liquid [$C_4$mim]$NTf_2$. Experimental data are from Canongia Lopes et al. [38] (●), Salgado et al. [168] (○), Jacquemin et al. [174] (□), Troncoso et al. [53] (△), Dzyuba and Bartsch [228] (▽), Montalbán et al. [175] (◇), Zhang et al. [177] (+), Tariq et al. [179] (†), Currás et al. [231] (✳), de Castro et al. [232] (×), Hamidova et al. [233] (°), De Azevedo et al. [234] (■), Vraneš et al. [235] (▲), Malek and Ijardar [236] (▼), Geppert-Rybczyńska et al. [237] (◆), Salinas et al. [238] (◓), Kanakubo et al. [239] (◒), Kanakubo & Harris [240] (◐), Batista et al. [241] (◑), Součková et al. [242] (•), Tariq et al. [243] (▬), Rocha et al. [244] (▬), Katsuta et al. [245] (◧), Santos et al. [188] (◨), Krummen et al. [246] (▪), Vranes et al. [247] (◭), Jacquemin et al. [248] (◭), Jacquemin et al. [249] (▼), Hiraga et al. [250] (▼), Vraneš et al. [251] (◆), Wandschneider et al. [252] (◆), Xue et al. [253] (◆), Fredlake et al. [44] (◆), Pal et al. [254] (○), Gomes et al. [255] (□), Bahadur et al. [256] (△), Liu et al. [257] (▽), and Palgunadi et al. [258] (◊).

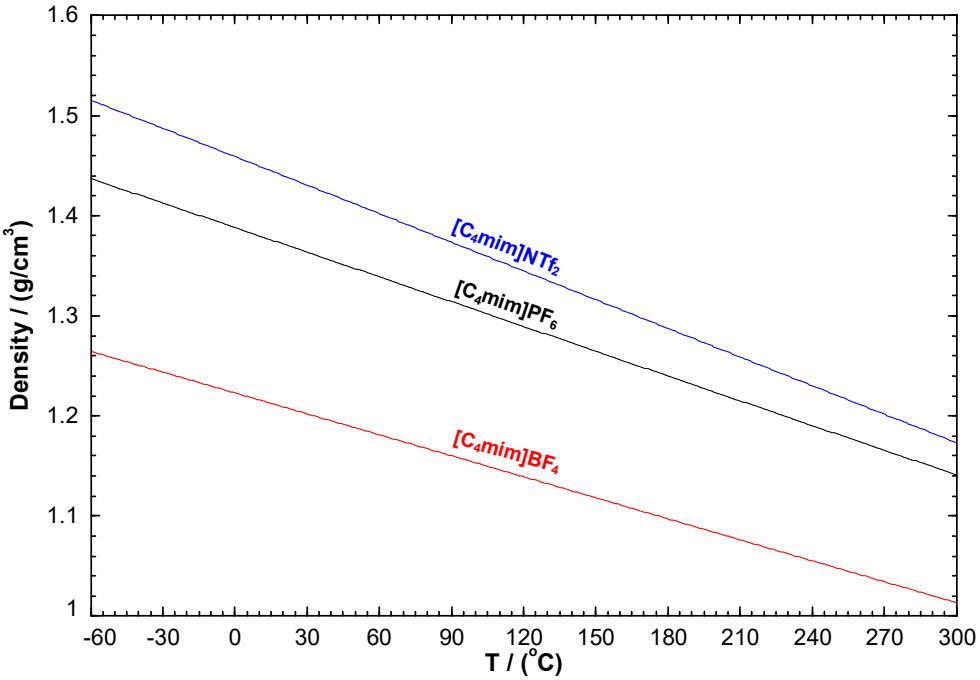


Figure 7.11: Calculated density of the $[C_4mim]PF_6$, $[C_4mim]BF_4$ and $[C_4mim]NTf_2$ pure liquids between -60°C and 300°C.

### 7.2.2 Binary liquids

As already explained, the density model is linked to the thermodynamic model. The three binary liquids are assumed to be ideal (that is, $\Delta g_{[C_4mim]_2/XY} = 0$ where $X, Y = BF_4, PF_6 \; and \; NTf_2$). This is a reasonable assumption since the phase diagrams of the three binary subsystems of $[C_4mim]\{Cl, NO_3, CH_3SO_3\}$ showed that the corresponding binary liquids are close to ideal (Chapter 5).

Canongia Lopes et al. [38] measured the density of the $[C_4mim]BF_4$ – $[C_4mim]PF_6$, $[C_4mim]NTf_2$ – $[C_4mim]PF_6$ and $[C_4mim]NTf_2$ – $[C_4mim]BF_4$ binary liquids at 298.15K, 303.15K and 333.15K. Navia et al. [74] measured the density of the $[C_4mim]BF_4$ - $[C_4mim]PF_6$ binary liquid at 298.15K and 308.15K. The excess molar volume ($V^E$) is calculated using Eq. (72). For each binary liquid, a small and constant positive parameter is introduced in the pressure-dependent term of the Gibbs free energy of reaction (25) in Chapter 4. Table 7.3 presents the optimized pressure-dependent terms for the three binary liquids. Figures 7.12 to 7.14 display the calculated and measured $V^E$ values. There is a symmetric behavior with small positive deviations from ideality for the three binary liquids. The density model reproduces well the density data within experimental error limits.

Figure 7.15 compares the calculated $V^E$ values of the three binary liquids. Canongia Lopes et al. [38] reported that $V^E$ increases as the size difference between the two anions in the common-cation binary system increases. The $[C_4mim]NTf_2$ - $[C_4mim]PF_6$ and $[C_4mim]BF_4$ - $[C_4mim]PF_6$ binary liquids exhibit $V^E$ values lower than about 0.14 $cm^3.mol^{-1}$, while the $[C_4mim]NTf_2$ - $[C_4mim]BF_4$ binary liquid displays $V^E$ values lower than about 0.33 $cm^3.mol^{-1}$. This is consistent with the size difference between the anions, where $NTf^-_2 > PF^-_6 > BF^-_4$ (e.g. 158.7, 73.7, and 53.4 $cm^3.mol^{-1}$, respectively [259]).

Table 7.3: Optimized pressure-dependent term of the Gibbs free energy of reaction (25) (Chapter 4) for the common-cation binary liquids

| Binary liquid | Optimized $\Delta g^P_{A_2/XY}$ (J.mol$^{-1}$) |
|---|---|
| $[C_4mim]BF_4$ - $[C_4mim]PF_6$ | $0.018(P-1)$ |
| $[C_4mim]NTf_2$ - $[C_4mim]PF_6$ | $0.018(P-1)$ |
| $[C_4mim]NTf_2$ - $[C_4mim]BF_4$ | $0.044(P-1)$ |

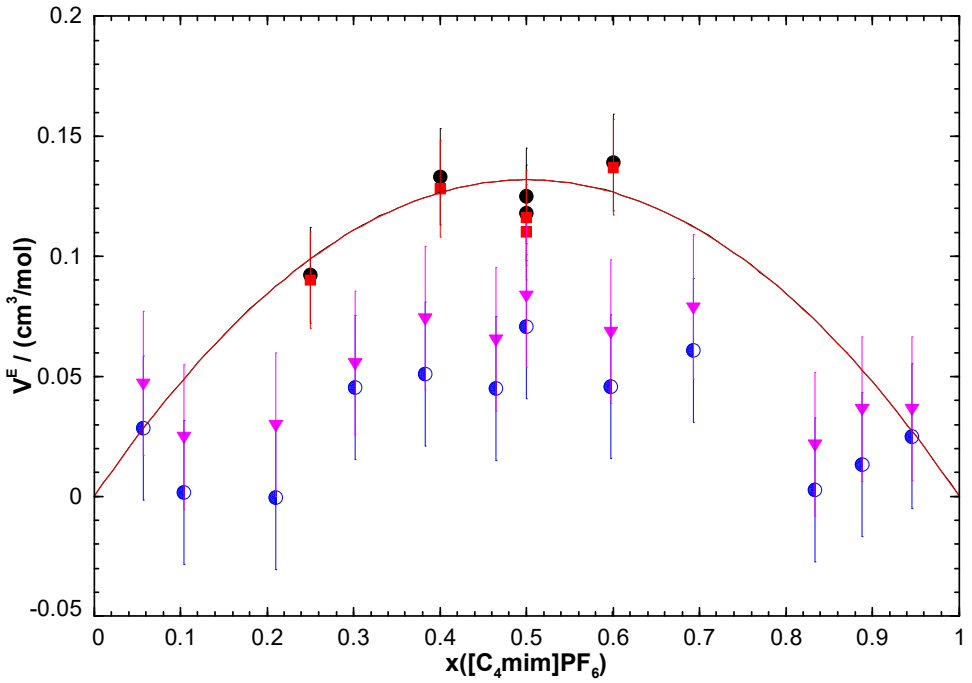


Figure 7.12: Calculated excess molar volume ($V^E$) of the $[C_4mim]BF_4$ - $[C_4mim]PF_6$ binary liquid at 298.15K (black line) and 333.15K (red line). Experimental data are from Canongia Lopes et al. [38] (298.15K (●), 333.15K (■)) and Navia et al. [74] (298.15K (◑), 308.15K (▼)).

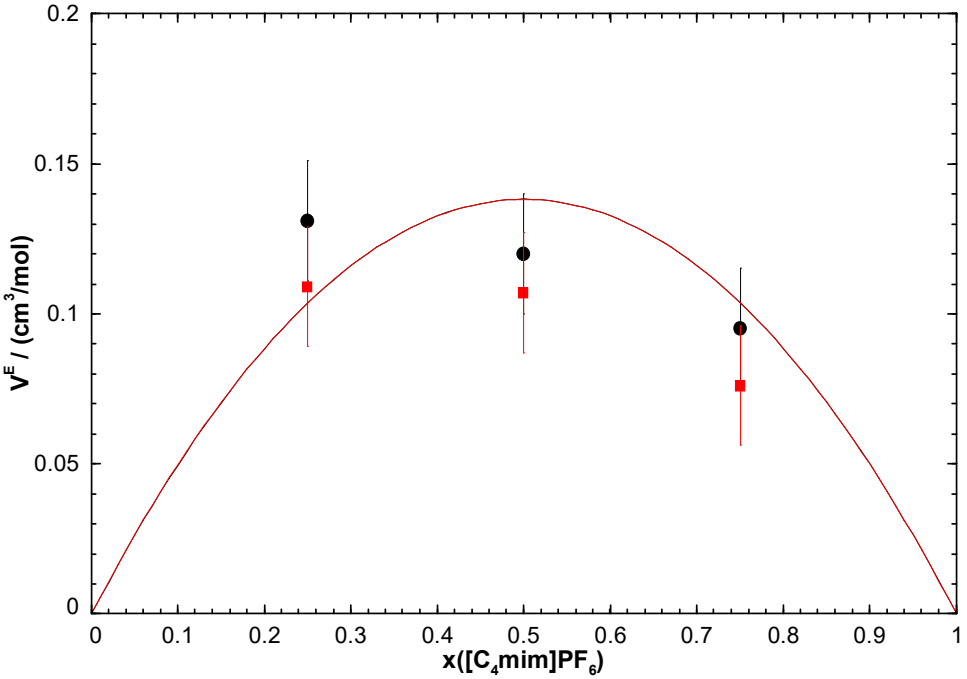


Figure 7.13: Calculated excess molar volume ($V^E$) of the [$C_4$mim]$NTf_2$ - [$C_4$mim]$PF_6$ binary liquid at 298.15K (black line) and 333.15K (red line). Experimental data are from Canongia Lopes et al. [38] (298.15K (●), 333.15K (■)).

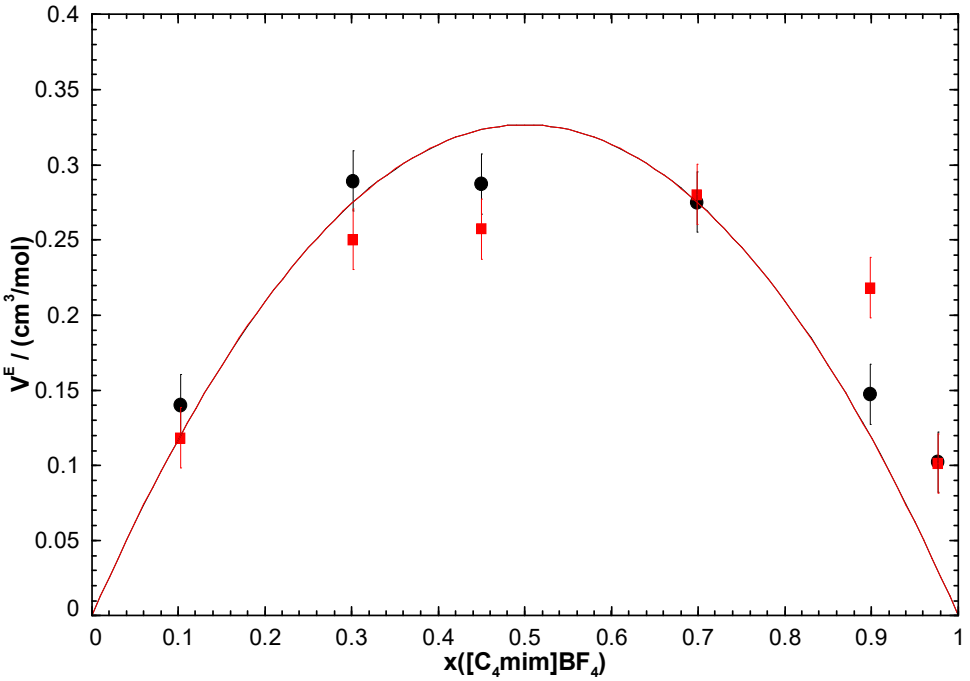


Figure 7.14: Calculated excess molar volume ($V^E$) of the [$C_4$mim]$NTf_2$ - [$C_4$mim]$BF_4$ binary liquid at 303.15K (black line) and 333.15K (red line). Experimental data are from Canongia Lopes et al. [38] (303.15K (●), 333.15K (■)).

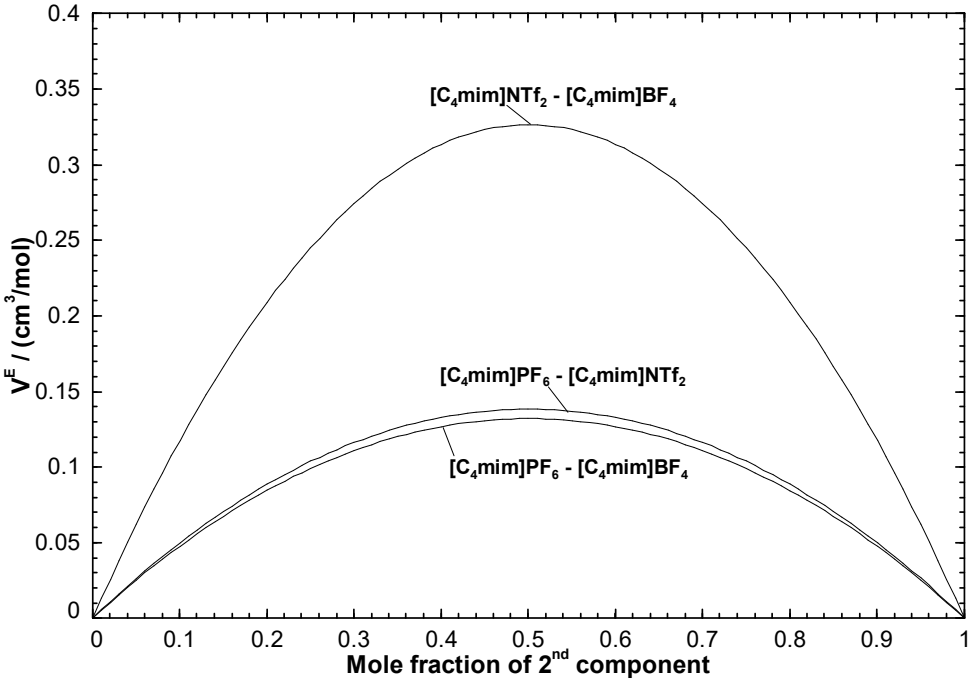


Figure 7.15: Calculated excess molar volume ($V^E$) of the common-cation binary liquids at 298.15K.

### 7.2.3 The $[C_4mim]BF_4$ - $[C_4mim]PF_6$ - $[C_4mim]NTf_2$ ternary liquid

To our knowledge, there are no density data available for the $[C_4mim]BF_4$ - $[C_4mim]PF_6$ - $[C_4mim]NTf_2$ ternary liquid. Figure 7.16 displays the calculated iso-excess molar volume lines at 298.15K for the latter. The molar volume of the ternary liquid is predicted from the optimized temperature-dependent expansivities and molar volumes at 298.15K of the pure liquids (table 7.2), and from the optimized binary pressure-dependent parameters (table 7.3) using a standard symmetric interpolation method. As shown in figure 7.16, the $V^E$ values increase as the composition of the ternary liquid approaches the $[C_4mim]NTf_2$ - $[C_4mim]BF_4$ binary liquid, in which the greatest $V^E$ values were observed (see figure 7.15).

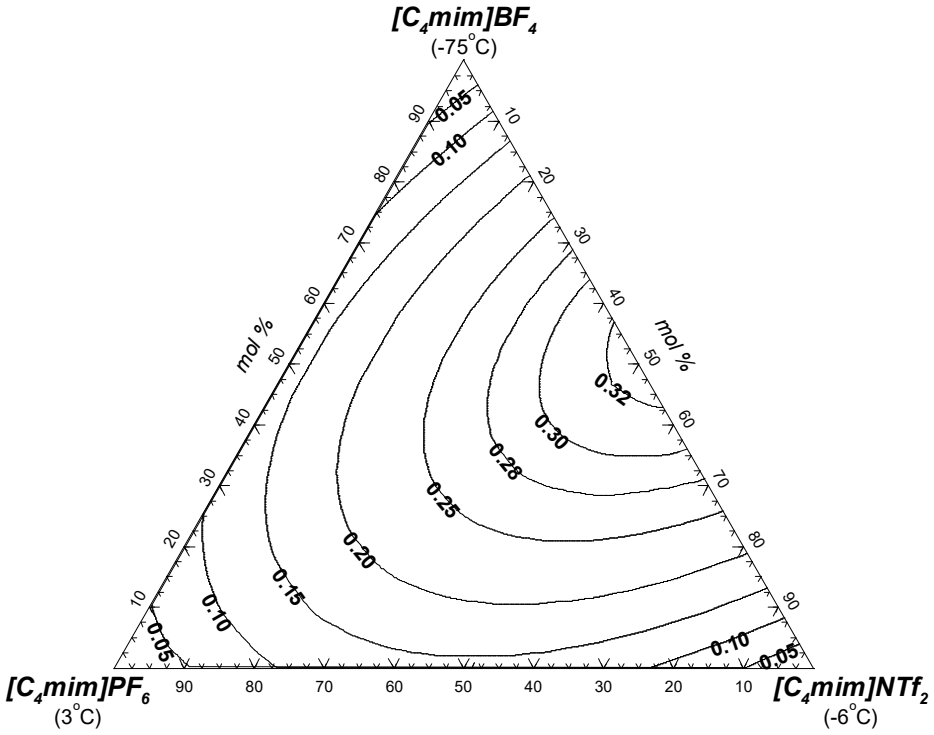


Figure 7.16: Calculated iso-$V^E$ lines in the $[C_4mim]BF_4$ - $[C_4mim]PF_6$ - $[C_4mim]NTf_2$ ternary liquid at 298.15K.

## 7.3 Common-anion ternary systems {$[C_2mim]$, $[C_8mim]$, $[C_{10}mim]$}$NTf_2$ and {$[C_4mim]$, $[C_8mim]$, $[C_{10}mim]$}$NTf_2$

Canongia Lopes et al. [38] measured the density of common-anion ionic liquid systems with $NTf_2^-$ as the common anion and a series of 1-alkyl-3-methylimidazolium cations ($[C_nmim]^+$ with n = 2, 4, 8, 10). They measured the density of the pure liquids and of five binary liquids at 298.15K and 333.15K, using a DMA 5000 densimeter. Again, they reported a density precision lower than 0.001% and an estimated uncertainty of ±0.02 $cm^3.mol^{-1}$ for the $V^E$ values. In the present work, the densities of the $[C_2mim]NTf_2$ - $[C_8mim]NTf_2$ - $[C_{10}mim]NTf_2$ and $[C_4mim]NTf_2$ - $[C_8mim]NTf_2$ - $[C_{10}mim]NTf_2$ ternary liquids are predicted.

Based on the elemental mass balance, the following equilibrated reactions can occur thermodynamically:

$$4[C_8mim]^+ = [C_2mim]^+ + 3[C_{10}mim]^+ \quad (74)$$

$$3[C_8mim]^+ = [C_4mim]^+ + 2[C_{10}mim]^+ \quad (75)$$

However, the cations $[C_2mim]^+$, $[C_4mim]^+$, $[C_8mim]^+$ and $[C_{10}mim]^+$ are all stable. In the FactSage thermochemical software, any reaction that is kinetically hindered cannot be prevented from occurring. Therefore, in order to inhibit reactions (74) and (75), the real chemical formula ($C_{14}H_{23}N_3S_2O_4F_6$) of the compound $[C_8mim]NTf_2$ was replaced with the "hypothetical" chemical formula $C_{17}H_{41}N_3OF_3Na_5$. That is, $S_2O_3F_3$ was replaced with $C_3H_{18}Na_5$. These two groups of atoms have virtually the same molecular weight (169.123 g.mol$^{-1}$), making it possible to perform correct density calculations for the $\{[C_2mim], [C_8mim], [C_{10}mim]\}NTf_2$ and $\{[C_4mim], [C_8mim], [C_{10}mim]\}NTf_2$ ternary liquids.

### 7.3.1 Pure ionic liquids

The density of pure liquid $[C_4mim]NTf_2$ was modeled previously (see section 7.2.1). Table 7.4 presents the expressions for the optimized thermal expansion (Eq. (20) in Chapter 3) and the reference molar volume ($V_m^{liquid}$) extrapolated at 298.15K of the $[C_2mim]NTf_2$, $[C_8mim]NTf_2$ and $[C_{10}mim]NTf_2$ pure ionic liquids. These expressions were derived from the density data of Canongia Lopes et al. [38].

Table 7.4: Molar volume at 298.15K and thermal expansion of the pure liquids

| Liquid | $V_m^{liquid}(298.15K)$ (cm$^3$.mol$^{-1}$) | Thermal expansion $\alpha(T)$ (K$^{-1}$) |
|---|---|---|
| $[C_2mim]NTf_2$ | 257.9 | $0.501\times10^{-3} + 5.160\times10^{-7}T$ |
| $[C_8mim]NTf_2$ | 362.2 | $0.507\times10^{-3} + 5.359\times10^{-7}T$ |
| $[C_{10}mim]NTf_2$ | 404.1 | $0.505\times10^{-3} + 5.289\times10^{-7}T$ |

Figures 7.17 to 7.19 compare the calculated and measured densities from Canongia Lopes et al. [38] for the pure ionic liquids. The densities of the $[C_2mim]NTf_2$, $[C_4mim]NTf_2$, $[C_8mim]NTf_2$ and $[C_{10}mim]NTf_2$ pure liquids were calculated over the temperature range -60°C to 300°C, using the thermal expansions in table 7.4 extrapolated well below and well above the melting temperatures of the pure ionic liquids (see figure 7.20). Each calculated density exhibits a linear temperature dependence over a large temperature range.

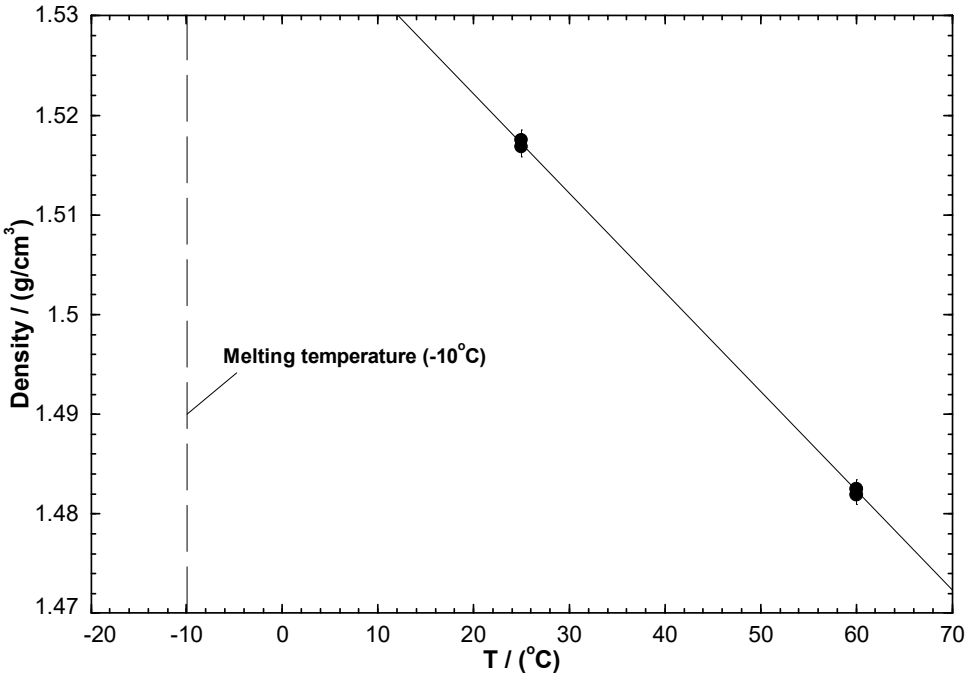


Figure 7.17: Calculated density of pure liquid [$C_2$mim]$NTf_2$. Experimental data are from Canongia Lopes et al. [38] (●).

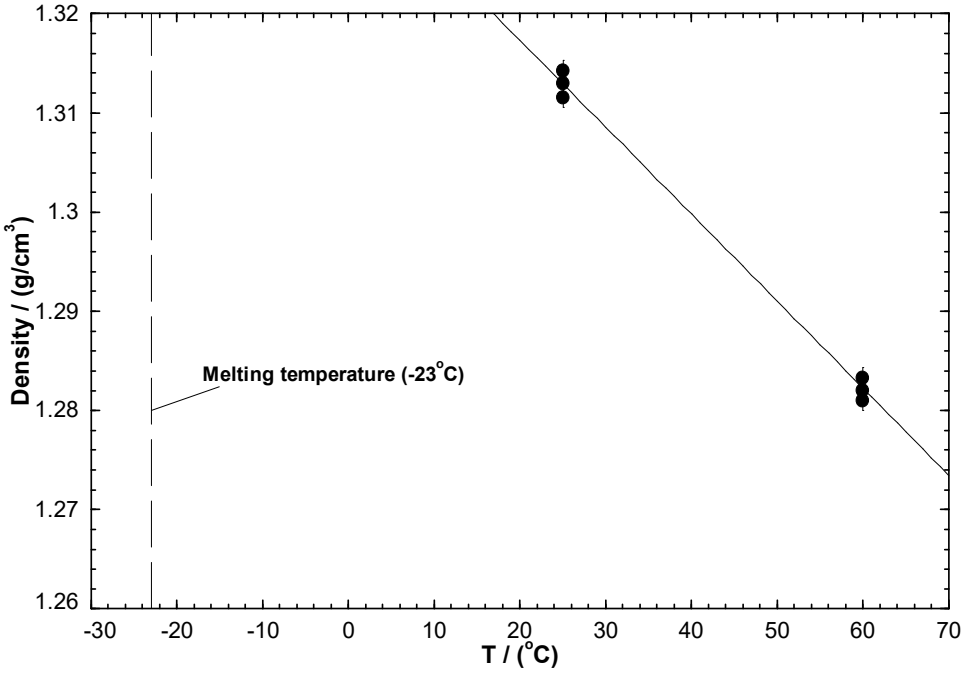


Figure 7.18: Calculated density of pure liquid [$C_8$mim]$NTf_2$. Experimental data are from Canongia Lopes et al. [38] (●).

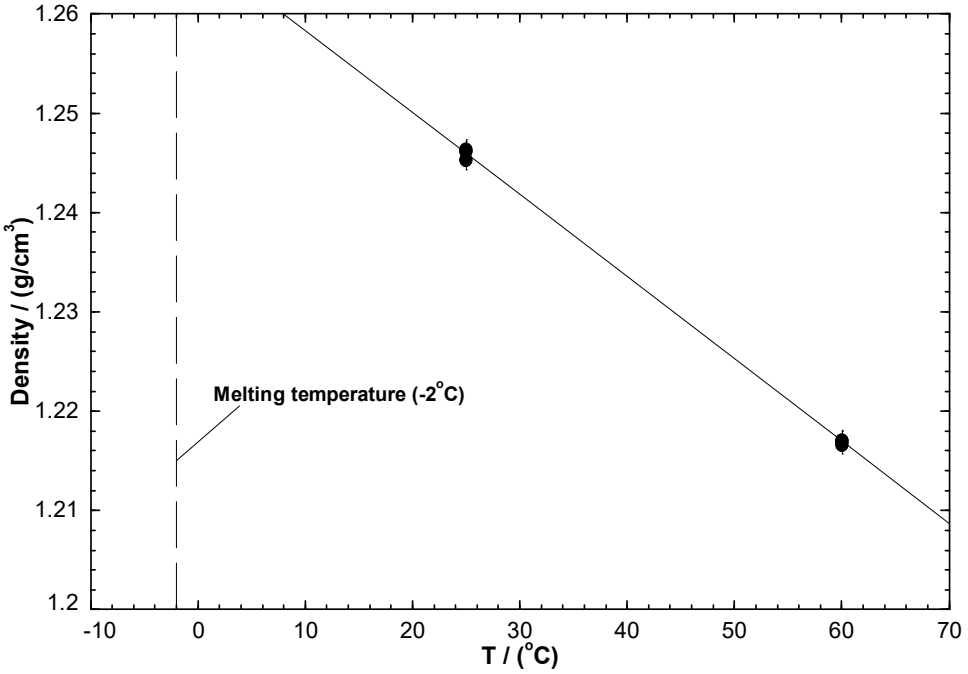


Figure 7.19: Calculated density of pure liquid $[C_{10}mim]NTf_2$. Experimental data are from Canongia Lopes et al. [38] (●).

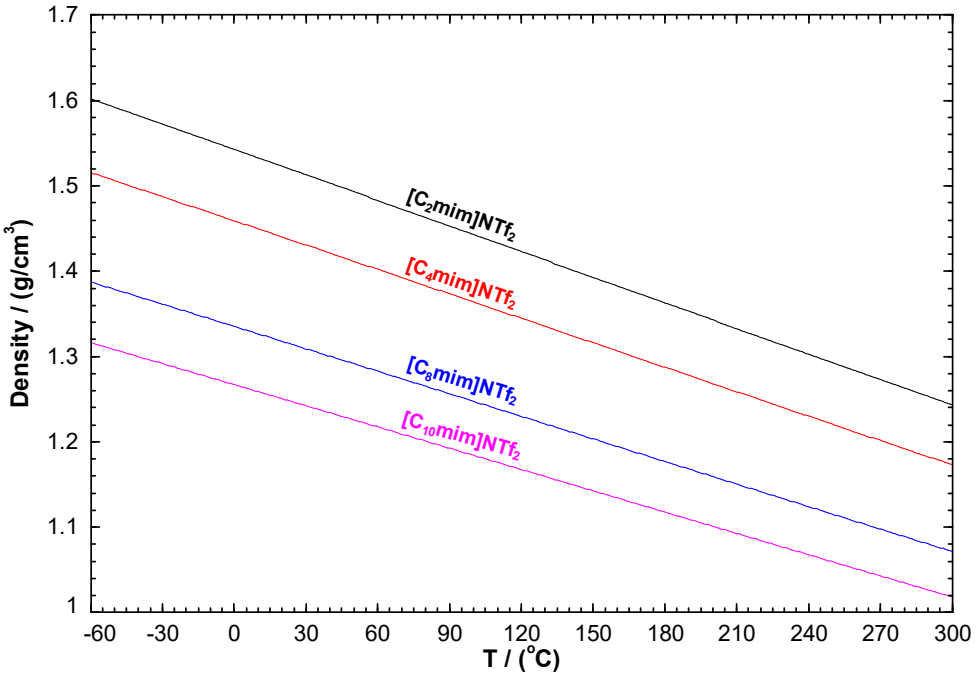


Figure 7.20: Calculated density of the $[C_2mim]NTf_2$, $[C_4mim]NTf_2$, $[C_8mim]NTf_2$ and $[C_{10}mim]NTf_2$ pure liquids between -60°C and 300°C.

### 7.3.2 Binary liquids

As already mentioned, the density model is linked to the thermodynamic model. Using Flory's theory, Canongia Lopes et al. [38] calculated the enthalpy of mixing of the five binary liquids related to the {[$C_2$mim], [$C_8$mim], [$C_{10}$mim]}$NTf_2$ and {[$C_4$mim], [$C_8$mim], [$C_{10}$mim]}$NTf_2$ ternary liquids at 298.15K and at the equimolar composition. Flory's theory correlates the molar enthalpy of mixing with the excess molar volume, but it does not take into account hydrogen bonds and strong electrostatic interactions. This method has been used successfully to predict the excess properties of alcohol systems [260] and also of mixtures containing ionic liquids [261, 262].

For each binary liquid, a constant parameter is introduced in the Gibbs free energy of reaction (24) (Chapter 4) in order to reproduce the enthalpy of mixing value estimated by Canongia Lopes et al. [38]. The optimized pressure-independent terms are given in table 7.5. Figure 7.21 compares our calculated enthalpies of mixing at 298.15K with the estimated values from Canongia Lopes et al. [38]. Canongia Lopes et al. [38] measured the density of the five binary liquids at 303.15K and 333.15K. The excess molar volume ($V^E$) is calculated using Eq. (72). For each binary liquid, a small and constant positive parameter is introduced in the pressure-dependent term of the Gibbs free energy of reaction (24) in Chapter 4. Table 7.5 presents the optimized pressure-dependent terms for the various binary liquids. Figures 7.22 to 7.26 display the calculated and measured $V^E$ values. There is a symmetric behavior with small positive deviations from ideality for all binary liquids investigated. Figure 7.27 compares the calculated $V^E$ values at 298.15K for the five binary liquids. As seen in figures 7.21 and 7.27, both the enthalpy of mixing and the excess molar volume ($V^E$) increase as the difference between the alkyl chain lengths of the two cations increases.

Table 7.5: Optimized pressure-independent ($\Delta g^{th}_{AB/NTf_2}$) and pressure-dependent ($\Delta g^{P}_{AB/NTf_2}$) terms of the Gibbs free energy of reaction (24) (Chapter 4) for the common-anion binary liquids

| Binary liquid | Optimized $\Delta g^{th}_{AB/NTf_2}$(J.mol$^{-1}$) | Optimized $\Delta g^{P}_{AB/NTf_2}$(J.mol$^{-1}$) |
|---|---|---|
| [$C_2$mim]$NTf_2$ – [$C_8$mim]$NTf_2$ | 432.2 | $0.020(P-1)$ |
| [$C_2$mim]$NTf_2$ – [$C_{10}$mim]$NTf_2$ | 813.2 | $0.035(P-1)$ |
| [$C_4$mim]$NTf_2$ – [$C_8$mim]$NTf_2$ | 403.0 | $0.018(P-1)$ |
| [$C_4$mim]$NTf_2$ – [$C_{10}$mim]$NTf_2$ | 718.7 | $0.032(P-1)$ |
| [$C_8$mim]$NTf_2$ – [$C_{10}$mim]$NTf_2$ | 246.1 | $0.011(P-1)$ |

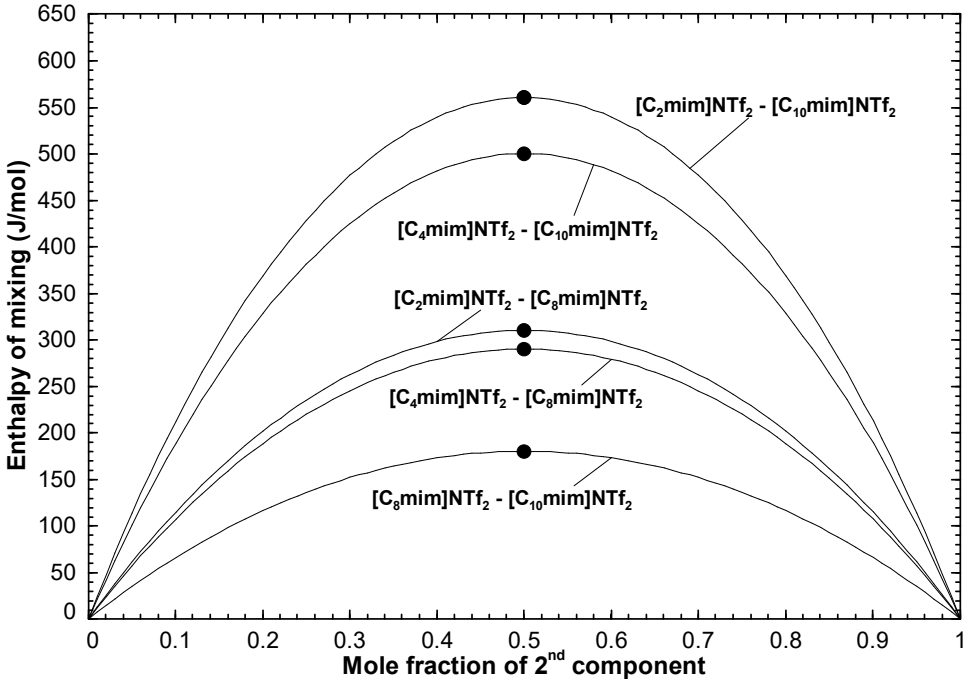


Figure 7.21: Calculated enthalpy of mixing of the common-anion binary liquids at 298.15K along with the values (●) estimated by Canongia Lopes et al. [38] using Flory's theory.

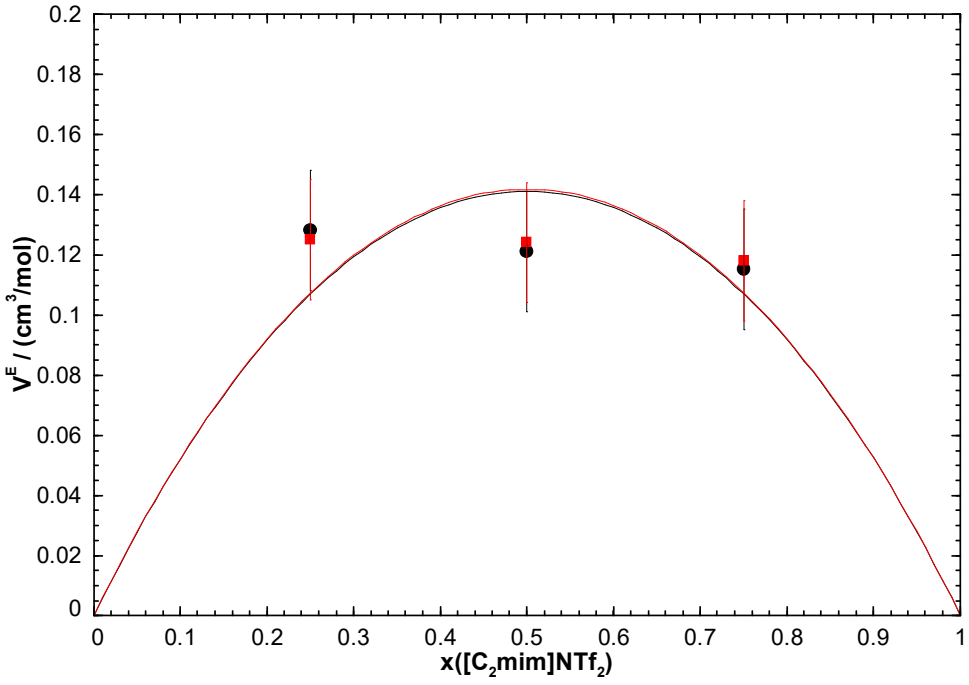


Figure 7.22: Calculated excess molar volume ($V^E$) of the $[C_2mim]NTf_2$ - $[C_8mim]NTf_2$ binary liquid at 298.15K (black line) and 333.15K (red line). Experimental data are from Canongia Lopes et al. [38] (298.15K (●), 333.15K (■)).

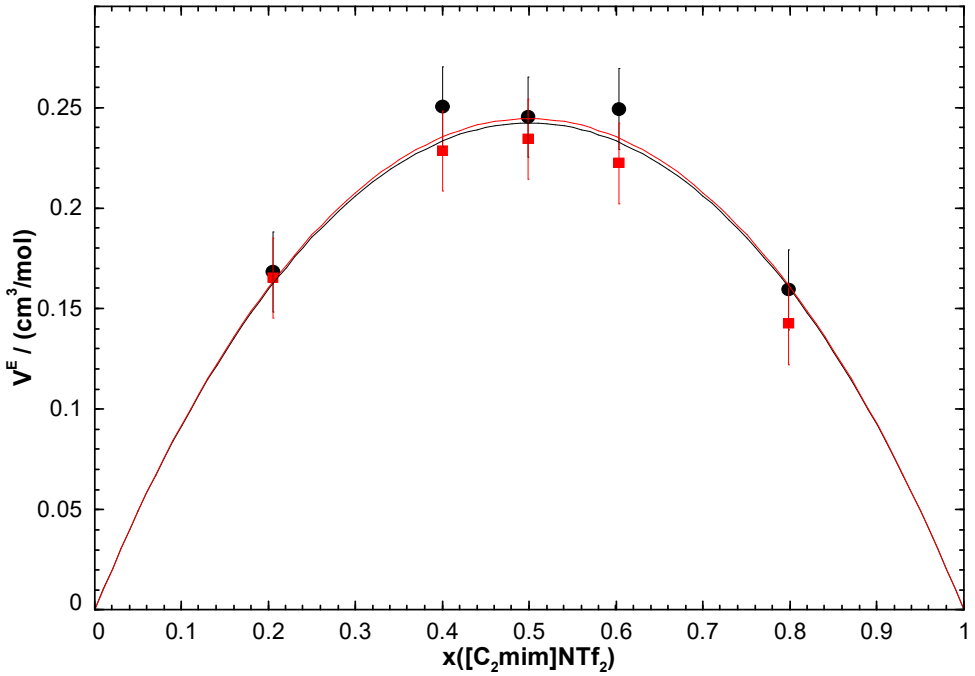


Figure 7.23: Calculated excess molar volume ($V^E$) of the $[C_2mim]NTf_2$ - $[C_{10}mim]NTf_2$ binary liquid at 298.15K (black line) and 333.15K (red line). Experimental data are from Canongia Lopes et al. [38] (298.15K (●), 333.15K (■)).

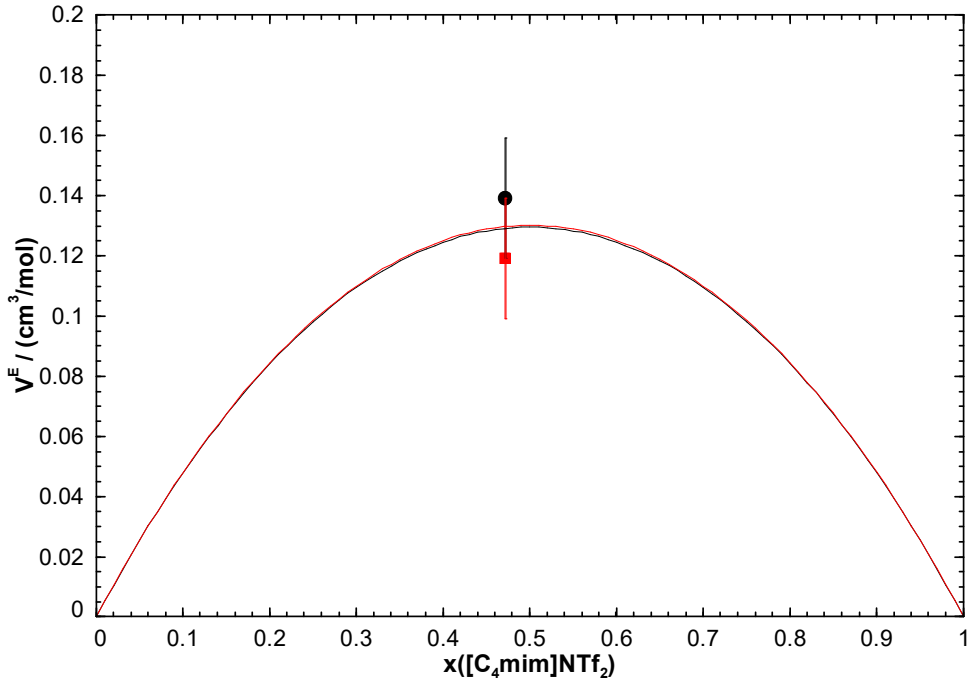


Figure 7.24: Calculated excess molar volume ($V^E$) of the $[C_4mim]NTf_2$ - $[C_8mim]NTf_2$ binary liquid at 298.15K (black line) and 333.15K (red line). Experimental data are from Canongia Lopes et al. [38] (298.15K (●), 333.15K (■)).

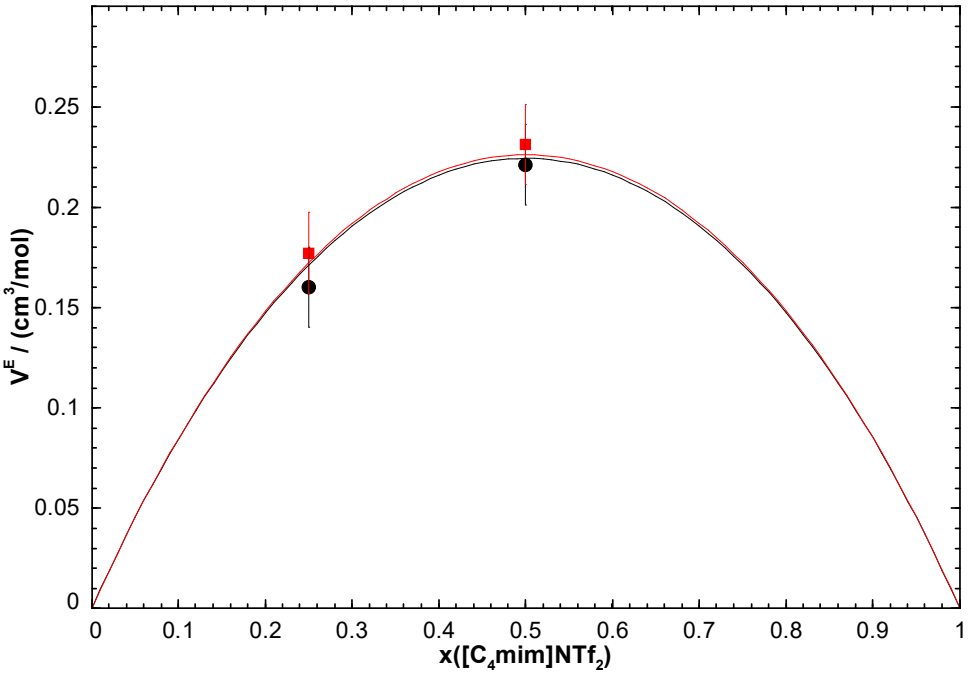


Figure 7.25: Calculated excess molar volume ($V^E$) of the [$C_4$mim]$NTf_2$ - [$C_{10}$mim]$NTf_2$ binary liquid at 298.15K (black line) and 333.15K (red line). Experimental data are from Canongia Lopes et al. [38] (298.15K (●), 333.15K (■)).

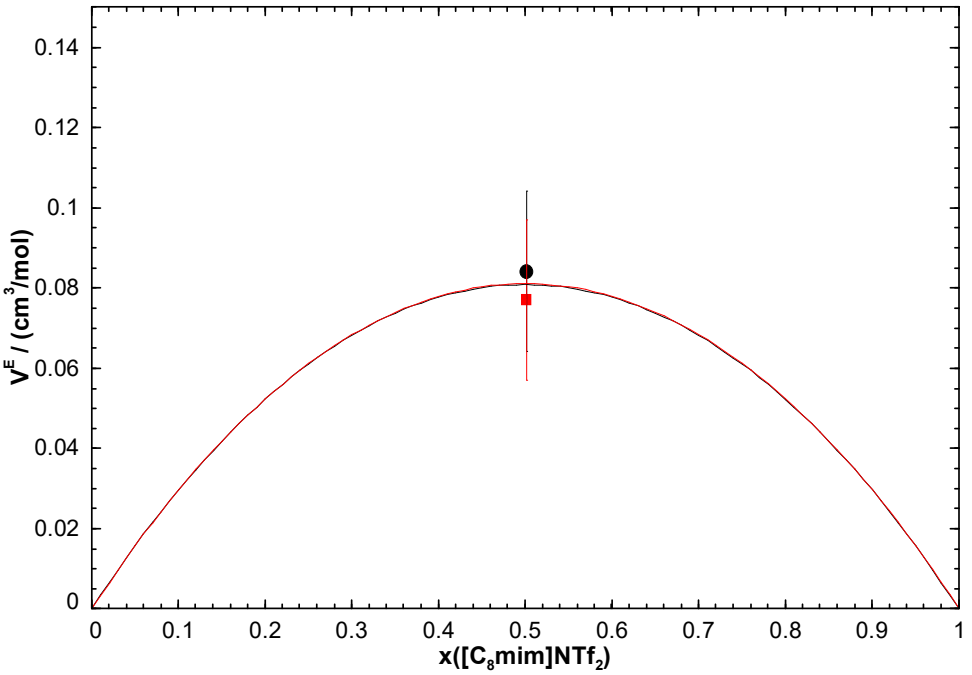


Figure 7.26: Calculated excess molar volume ($V^E$) of the [$C_8$mim]$NTf_2$ - [$C_{10}$mim]$NTf_2$ binary liquid at 298.15K (black line) and 333.15K (red line). Experimental data are from Canongia Lopes et al. [38] (298.15K (●), 333.15K (■)).

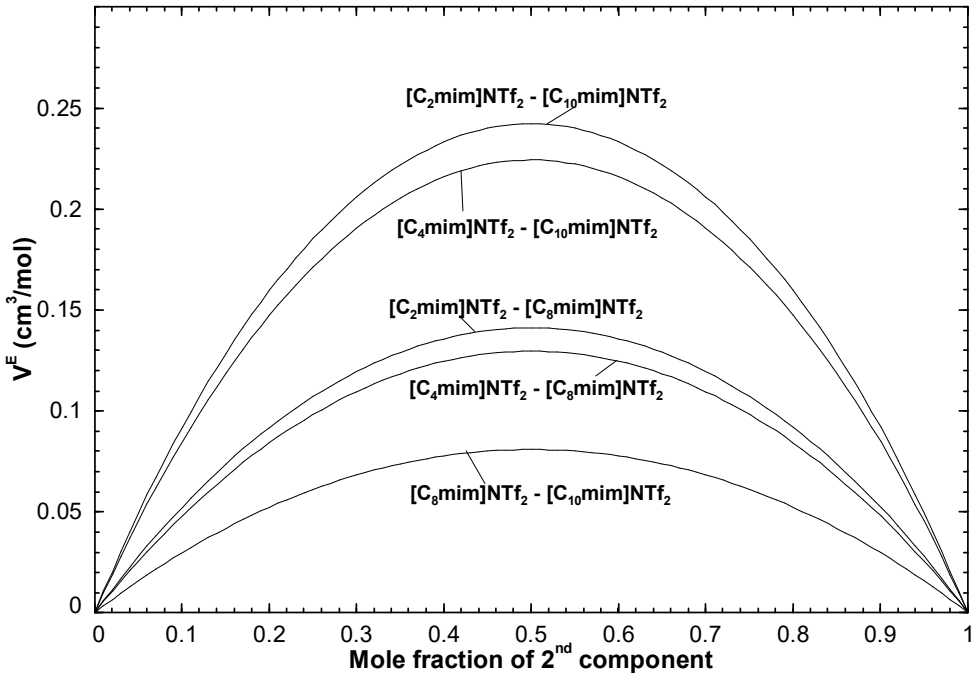


Figure 7.27: Calculated excess molar volume ($V^E$) of the common-anion binary liquids at 298.15K.

### 7.3.3 The $[C_2mim]NTf_2$ – $[C_8mim]NTf_2$ – $[C_{10}mim]NTf_2$ and $[C_4mim]NTf_2$ – $[C_8mim]NTf_2$ – $[C_{10}mim]NTf_2$ ternary liquids

To our knowledge, there are no density data available for the {[$C_2$mim], [$C_8$mim], [$C_{10}$mim]}$NTf_2$ and {[$C_4$mim], [$C_8$mim], [$C_{10}$mim]}$NTf_2$ ternary liquids. Figures 7.28 and 7.29 display the calculated iso-excess molar volume lines at 298.15K for these two liquids. The molar volume of each ternary liquid is predicted from the optimized temperature-dependent expansivities and molar volumes at 298.15K of the pure liquids (tables 7.2 and 7.4), and from the optimized pressure-dependent parameters (table 7.5) using a standard symmetric interpolation method. For each ternary liquid, the $V^E$ values increase as the composition of the liquid approaches the binary liquid in which the greatest $V^E$ values were observed ([$C_2$mim]$NTf_2$ - [$C_{10}$mim]$NTf_2$ in figure 7.28, and [$C_4$mim]$NTf_2$ - [$C_{10}$mim]$NTf_2$ in figure 7.29).

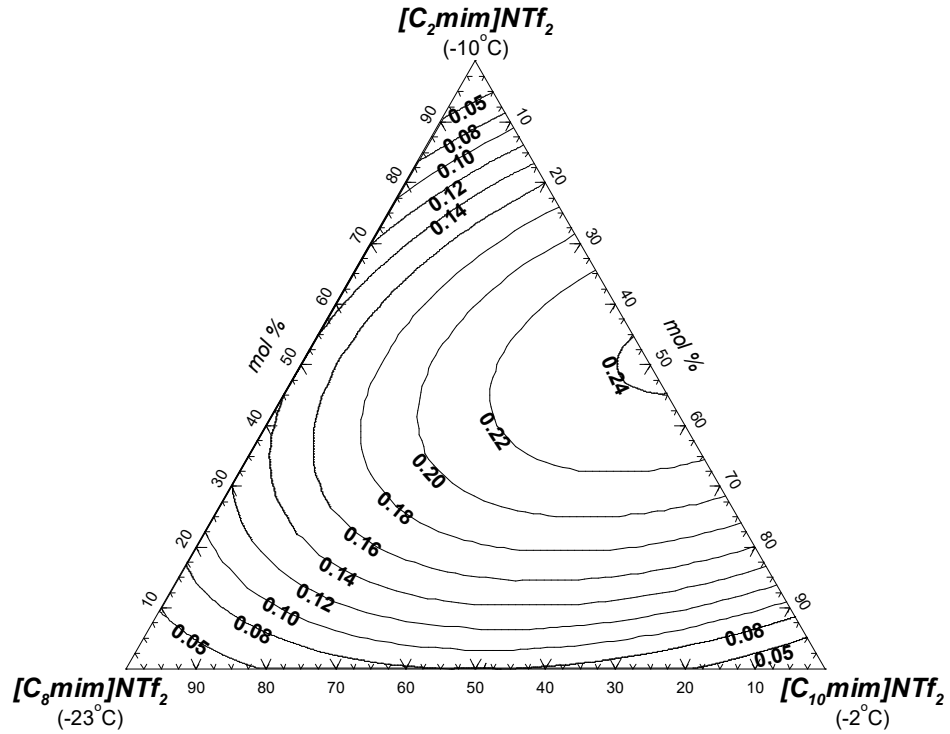


Figure 7.28: Calculated iso-$V^E$ lines in the $[C_2mim]NTf_2$ - $[C_8mim]NTf_2$ - $[C_{10}mim]NTf_2$ ternary liquid at 298.15K.

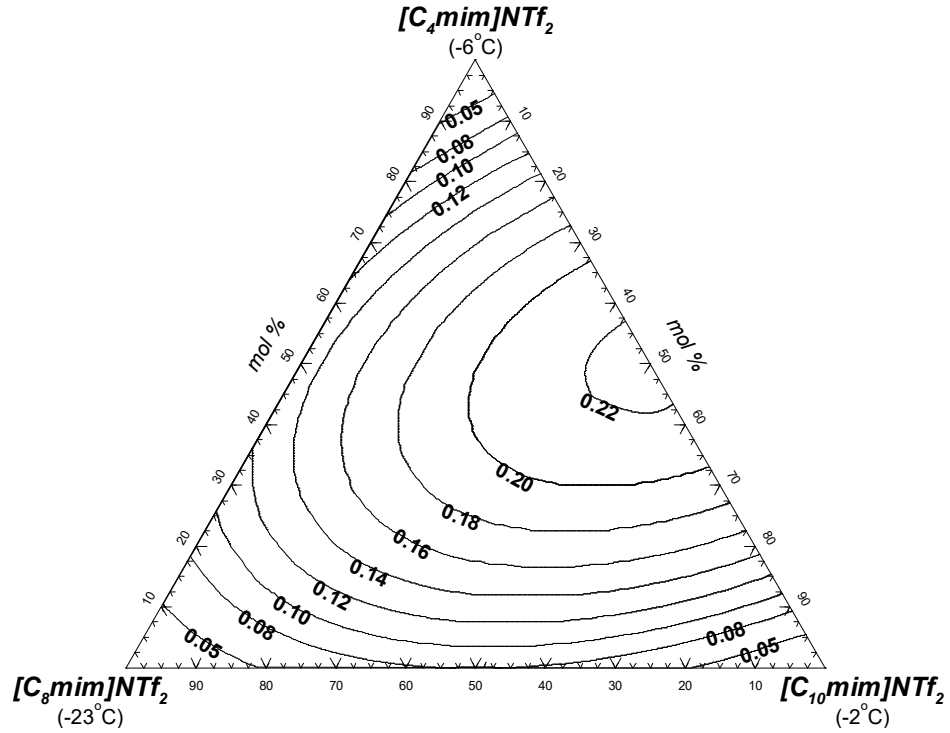


Figure 7.29: Calculated iso-$V^E$ lines in the $[C_4mim]NTf_2$ - $[C_8mim]NTf_2$ - $[C_{10}mim]NTf_2$ ternary liquid at 298.15K.

# CHAPTER 8 GENERAL DISCUSSION

Water is an important source of impurity in ionic liquids. As a matter of fact, almost all ionic liquids are known to be hygroscopic and may absorb water from the atmosphere to some extent [263, 264]. It may arise from the water interactions with anions owing to the fact that strong hydrogen bonds can form between water and the anion of ionic liquids [265]. Efficient drying is necessary for moisture sensitive ionic liquids [266]. The presence of water in an ionic liquid may have a significant influence on its stability, thermal properties (melting point) and physicochemical properties (density, viscosity, etc.) [68-72]. For example, the thermal transitions measured by DSC for the $[C_2mim]NO_3$ - $[C_2mim]Cl$ common-cation binary ionic liquid system were found to be unreliable with a very poor reproducibility due to the highly hygroscopic character of this system [73]. Similarly, the thermal transitions measured by Seddon's group for the $[C_4mim]NO_3$ - $[C_4mim]Cl$ common-cation binary system, using both DSC and visual observation, were rather scattered. Consequently, only a tentative calculated liquidus projection of the $[C_4mim]Cl$ – $[C_4mim]NO_3$ – $[C_4mim]CH_3SO_3$ common-cation system was presented in the present work.

In the existing literature, researchers have applied different methodologies and equipment to examine the thermal behavior (e.g. melting point, heat capacity) of ionic liquids (pure or mixtures). Factors such as the sample preparation method, the thermal history of the sample, the heating and cooling scan rates and the number of repeated heating and cooling cycles have a significant impact on the thermal transitions measured by DSC [267]. Smiglak's group measured the thermal transitions of $[C_4mpyrr]\{Cl, Br, BF_4\}$ common-cation ternary mixtures by DSC: each sample was initially heated from room temperature to the highest temperature at a scan rate of 10 $K \cdot min^{-1}$, prior to two cycles of cooling and heating at scan rates of 5 $K \cdot min^{-1}$. Seddon's group measured the thermal transitions of the three binary subsystems of the $[C_4mim]\{Cl, NO_3, CH_3SO_3\}$ common-cation ternary system by DSC using three consecutive heating and cooling cycles with scan rates of 2.5 $K.min^{-1}$ (heating) and 5 $K.min^{-1}$ (cooling), respectively. Finally, Coutinho's group measured by DSC the thermal transitions of $\{[C_3mim], [C_3mpip], [C_3mpyrr]\}PF_6$ and $\{[C_3mpip], [C_3mpy], [C_3mim]\}PF_6$ common-anion ternary mixtures by performing one cooling run at 5 $K.min^{-1}$ followed by one heating run at 2 $K.min^{-1}$. For some selected ternary mixtures, the DSC measurements were repeated by using three consecutive heating / cooling cycles with scan rates of 2 $K.min^{-1}$ (heating) and 5 $K.min^{-1}$ (cooling). Interestingly, the thermal transitions measured with this latter DSC protocol were in closer agreement with the calculations from the thermodynamic

model. It is thus essential to standardize the experimental DSC procedure in order to obtain high quality and reliable experimental data. The use of three consecutive heating / cooling cycles, usually applied by Smiglak's group, seems to be desirable: the thermal transitions measured upon the second and third heating runs are favoured and should in principle be consistent with each other.

The Modified Quasichemical Model (MQM) [12-14] has been applied successfully to various high temperature inorganic salt systems and it was applied for the first time in the present work to ternary ionic liquid systems. The MQM was used because it is suitable for liquids exhibiting either small or extensive short-range ordering, and also for liquids displaying positive deviations from ideality [24]. In the case of common-ion liquids, the Bragg-Williams model can also be used when the Gibbs free energy change of the quasichemical reaction is small. In this case, the degree of short-range ordering is small, and the solution approximates a random mixture of ions on the corresponding sublattice. The MQM may have to be modified since the cations in ionic liquid systems are large and may involve long alkyl chains. The size difference between the cations in ionic liquid systems can have a significant influence on the degree of nonideality. For example, Maximo et al. [35] measured and modeled the phase diagrams of the $[C_3mim]PF_6$ – $[C_{12}mim]PF_6$, $[C_3mim]PF_6$ – $[N_{4444}]PF_6$ and $[C_3mim]PF_6$ – $[P_{4444}]PF_6$ common-anion binary systems and observed larger deviations from ideality of the liquid phase for these three systems than for those discussed in Chapter 6. As a matter of fact, the molecular structures of the $[C_3mim]PF_6$, $[C_3mpy]PF_6$, $[C_3mpyrr]PF_6$ and $[C_3mpip]PF_6$ compounds are very similar, considering the size of ring, differing by one carbon atom, and position of the radical. Maximo et al. [35] ascribed the ideal or almost ideal thermodynamic behavior of the binary liquids discussed in Chapter 6 to these structural similarities. On the other hand, in the case of the binary mixtures of $[C_{12}mim]PF_6$, $[N_{4444}]PF_6$ and $[P_{4444}]PF_6$ with $[C_3mim]PF_6$, the entropic contributions arising from the size differences between the cations of the two compounds led to marked deviations from ideality. Robelin [24] reported that the current thermodynamic model would fail to reproduce the experimental $[C_2mim]AlCl_4$ - $NaAlCl_4$ section in the NaCl - $[C_2mim]Cl$ - $AlCl_3$ phase diagram due to the large size difference between the inorganic $Al^{3+}$ and organic $[C_2mim]^+$ cations. A large ion such as $[C_2mim]^+$ can occupy several sites on the cationic sublattice. However, in the current version of the MQM, each ion occupies exactly one site.

Many studies existing in the literature have emphasized the influence of hydrogen bonding on the physicochemical properties of ionic liquids such as the melting point, density, viscosity, etc. [86].

For example, Canongia Lopes et al. [78] observed a large degree of deviation from ideality for the excess molar volume ($V^E$ values up to 3 $cm^3.mol^{-1}$) of ammonium-based common-anion binary liquids with $NO_3^-$ as the common anion. These authors attributed this significant non-ideal behavior to the existence of hydrogen-bonding interactions in the system. It has also been reported that imidazolium-based compounds possess stronger hydrogen bonding interactions than other families of ionic liquids such as pyrrolidinium- and pyridinium-based compounds [92].

To our knowledge, this is the first time that a ternary reciprocal ionic liquid system was investigated experimentally and thermodynamically. In the present work, in order to model the phase diagram of the [$C_2$py], [$C_4$py] || Cl, Br ternary reciprocal system, the standard thermodynamic properties ($\Delta H^o_{298.15K}$, $S^o_{298.15K}$, and $C_p(T)$) of the four pure compounds had to be known with good accuracy. For this system, the extent of first-nearest-neighbor (cation-anion) short-range ordering is related to the exchange Gibbs free energy $\Delta g^{\text{exchange}}_{[C_2py][C_4py]/\text{ClBr}}$ for the reaction [$C_2$py]Br (liquid) + [$C_4$py]Cl (liquid) = [$C_2$py]Cl (liquid) + [$C_4$py]Br (liquid), which only depends on the Gibbs free energies of the [$C_2$py]Cl, [$C_2$py]Br, [$C_4$py]Cl and [$C_4$py]Br pure liquids. Currently, there are no compilation tables for the standard thermodynamic properties of pure ionic liquid compounds. The Volume-based Thermodynamics (VBT) estimation technique from Glasser and Jenkins [28-33] was used in conjunction with the available data from the literature to assess the thermodynamic properties of the four pyridinium-based pure compounds. The values estimated from the VBT may be in significant error. For instance, for the pyridinium-based pure liquids, the shifts between the $\Delta H^o_{298.15K}$ measured by Verevkin et al. [129] using DSC and the values estimated from the VBT lie between -43.8 and +1.7 $kJ.mol^{-1}$. For solid [$C_2$mim]$NO_3$, Robelin [24] reported a shift of about 46 $kJ.mol^{-1}$ between the $\Delta H^o_{298.15K}$ value estimated from the VBT and the experimental value from Emel'yanenko et al. [139]. As highlighted by this author, this shift arises at least partly from the uncertainty on the $\Delta H^o_{298.15K}$ value of the organic cation in the gaseous state, derived from ab initio calculations. The VBT assumes that the Coulombic forces are the dominant long-range interactions between the ions, and does not yet consider short-range interactions such as van der Waals and hydrogen bonding [33]. It is an estimation technique easy to apply, which mainly requires a knowledge of the molecular volume $\nu_m$. However, it is not accurate enough to model successfully the phase diagrams of reciprocal systems.

The capability of the MQM to predict the phase diagrams of ternary ionic liquid systems solely from the optimized parameters for the common-ion binary subsystems was also tested in the present work. No ternary reciprocal parameter was required to reproduce the experimental diagonal sections in the [$C_2$py], [$C_4$py] || Cl, Br ternary reciprocal system. No ternary excess parameter was introduced for the liquid phase of the {[$C_3$mim], [$C_3$mpip], [$C_3$mpyrr]}$PF_6$ and {[$C_3$mpip], [$C_3$mpy], [$C_3$mim]}$PF_6$ common-anion ternary systems, and the two isoplethal sections measured in each of them were reasonably well reproduced. In the former case, the excess Gibbs free energies of the low-temperature ($s_1$-$s_1$) and intermediate-temperature ($s_2$-$s_2$) binary solid solutions between [$C_3$mpyrr]$PF_6$ and [$C_3$mpip]$PF_6$ had to be adjusted. Finally, for the [$C_4$mpyrr]{Cl, Br, $BF_4$} common-cation ternary system, a small ternary excess parameter was introduced in the liquid model in order to best reproduce the ternary data.

The good capability of prediction of the MQM is most likely due to the fact that all ionic liquid systems considered in the present work do not display large deviations from ideality. For each ternary ionic liquid system investigated, the deviation from ideality was quantified by calculating the activity coefficients (relative to liquid standard state) of the components along the isoplethal sections measured by DSC. A temperature of 100°C was selected since it corresponds to the average of the melting temperatures of the various pure ionic liquids. Let us first consider the case of a common-cation ternary liquid $AX - AY - AZ$, where $A$ is the common cation and $X$, $Y$, and $Z$ are the anions. The activity coefficient of $AX$ in the ternary liquid can be defined as:

$$\gamma_{AX} = \frac{a_{AX}}{(a_{AX})^{ideal}} \qquad (i.e. \gamma_{AX} = 1 \; in \; the \; ideal \; case) \tag{76}$$

$(a_{AX})^{ideal}$ is the activity of $AX$ in the ideal case, when the anions are randomly distributed on the anionic sublattice. Thus:

$$(a_{AX})^{ideal} = Y_A . Y_X = Y_X = x_X = \frac{n_X}{n_X + n_Y + n_Z} = \frac{n_{AX}}{n_{AX} + n_{AY} + n_{AZ}} = x_{AX} \tag{77}$$

($Y_A = 1$ since there is only one type of cation on the cationic sublattice.)

Finally: $\gamma_{AX} = \frac{a_{AX}}{x_{AX}}$ (where $x_{AX}$ is the mole fraction of $AX$ in the common-cation ternary liquid).

An identical expression is obtained for a common-anion ternary liquid $AX - BX - CX$.

Let us now consider a ternary reciprocal liquid $AX - BX - AY - BY$, where $A$ and $B$ are two cations, and $X$ and $Y$ are two anions. Let us consider for instance the $AX - BY$ diagonal section. Thus:

$$(a_{AX})^{ideal} = Y_A . Y_X = x_A x_X = \left(\frac{n_A}{n_A+n_B}\right).\left(\frac{n_X}{n_X+n_Y}\right) = \left(\frac{n_{AX}}{n_{AX}+n_{BY}}\right)^2 = (x_{AX})^2 \quad (78)$$

Finally: $\gamma_{AX} = \frac{a_{AX}}{(x_{AX})^2}$.

(i) For the [C4mpyrr]{Cl, Br, $BF_4$} common-cation ternary liquid, the activity coefficients were calculated at 100°C along the isoplethal sections at constant 50 mol% [C4mpyrr]$BF_4$ and at constant molar ratio [C4mpyrr]Cl / ([C4mpyrr]Cl + [C4mpyrr]Br) of 0.85 (figure 8.1). Along the former section (see figure 8.1(a)), very small positive and negative deviations from ideality are observed for [C4mpyrr]$BF_4$ and [C4mpyrr]Cl, respectively, while [C4mpyrr]Br exhibits a significant positive deviation with activity coefficient values of up to 3.2. Along the latter isoplethal section (see figure 8.1(b)), a marked positive deviation from ideality is again observed for [C4mpyrr]Br with activity coefficient values of up to 6.3, whereas [C4mpyrr]$BF_4$ and [C4mpyrr]Cl behave almost ideally. At 0 mol% [C4mpyrr]$BF_4$, the activity coefficients of [C4mpyrr]Cl and [C4mpyrr]Br are both equal to 1 since the corresponding binary liquid was assumed to be ideal at all compositions.

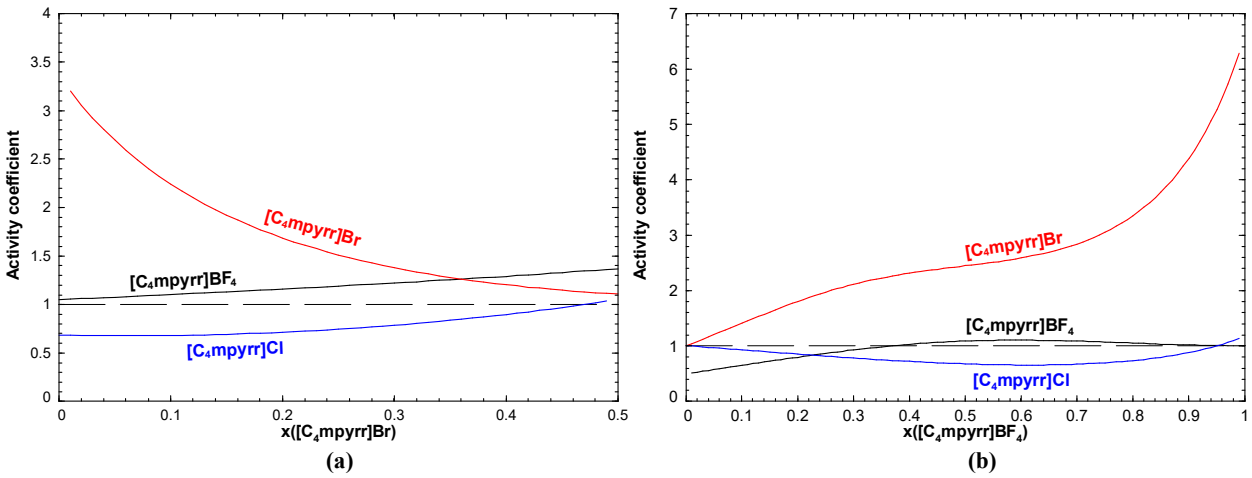


Figure 8.1: Calculated activity coefficients at 100°C of the components (liquid standard state) in the [C4mpyrr]Cl - [C4mpyrr]Br - [C4mpyrr]$BF_4$ ternary liquid along the isoplethal sections at: (a) constant 50 mol% [C4mpyrr]$BF_4$, and (b) constant molar ratio [C4mpyrr]Cl / ([C4mpyrr]Cl + [C4mpyrr]Br) of 0.85.

(ii) For the [$C_2$py], [$C_4$py] || Cl, Br ternary reciprocal liquid, the activity coefficients were calculated at 100°C along the diagonal sections [$C_4$py]Cl – [$C_2$py]Br and [$C_4$py]Br – [$C_2$py]Cl (figure 8.2). Along the former diagonal section, [$C_4$py]Cl and [$C_2$py]Br display both small positive deviations and negative deviations from ideality, depending on the composition. Along the latter diagonal section, again there are positive and negative deviations from ideality for [$C_4$py]Br and [$C_2$py]Cl with activity coefficient values of up to 2.1 (for [$C_2$py]Cl).

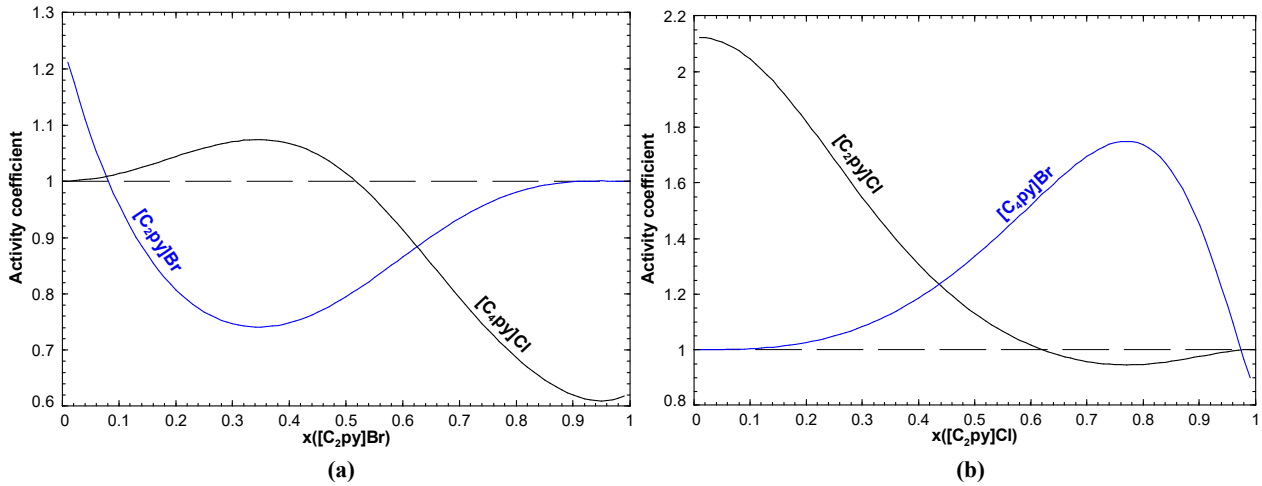


Figure 8.2: Calculated activity coefficients at 100°C of the components (liquid standard state) in the [$C_2$py], [$C_4$py] || Cl, Br ternary reciprocal liquid along the diagonal sections: (a) [$C_4$py]Cl – [$C_2$py]Br, and (b) [$C_4$py]Br – [$C_2$py]Cl.

(iii) For the {[$C_3$mim], [$C_3$mpip], [$C_3$mpyrr]}$PF_6$ common-anion ternary liquid, the activity coefficients were calculated at 100°C along the isoplethal sections at constant 40 mol% [$C_3$mim]$PF_6$ and at constant molar ratio [$C_3$mpyrr]$PF_6$ / ([$C_3$mpyrr]$PF_6$ + [$C_3$mpip]$PF_6$) of 0.60 (figure 8.3). Along the former isoplethal section, [$C_3$mpip]$PF_6$ exhibits very small positive deviations from ideality, while there are small negative deviations for both [$C_3$mpyrr]$PF_6$ and [$C_3$mim]$PF_6$. Along the latter isoplethal section, the three components display both very small positive and negative deviations from ideality depending on the composition. At 0 mol% [$C_3$mim]$PF_6$, the activity coefficients of [$C_3$mpip]$PF_6$ and [$C_3$mpyrr]$PF_6$ are both equal to 1 since the corresponding binary liquid was assumed to be ideal at all compositions.

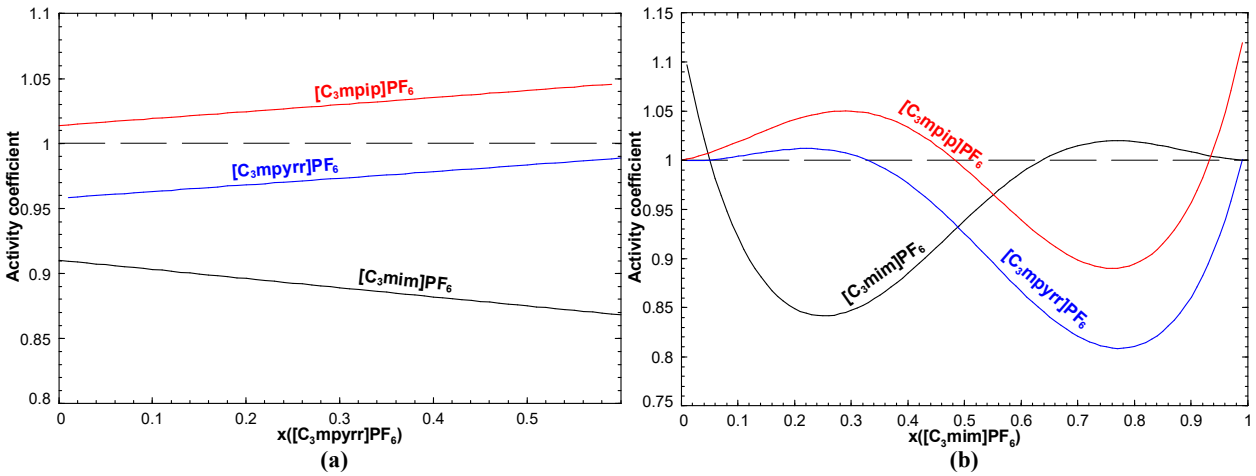


Figure 8.3: Calculated activity coefficients at 100°C of the components (liquid standard state) in the $[C_3mim]PF_6$ - $[C_3mpip]PF_6$ - $[C_3mpyrr]PF_6$ ternary liquid along the isoplethal sections at: (a) constant 40 mol% $[C_3mim]PF_6$, and (b) constant molar ratio $[C_3mpyrr]PF_6$ / ($[C_3mpyrr]PF_6$ + $[C_3mpip]PF_6$) of 0.60.

(iv) For the {$[C_3mpip]$, $[C_3mpy]$, $[C_3mim]$}$PF_6$ common-anion ternary liquid, the activity coefficients were calculated at 100°C along the isoplethal sections at constant 40 mol% $[C_3mpy]PF_6$ and at constant molar ratio $[C_3mpy]PF_6$ / ($[C_3mpy]PF_6$ + $[C_3mim]PF_6$) of 0.60 (figure 8.4). Along the former isoplethal section, the three components exhibit an almost ideal behavior. Along the latter isoplethal section, there are slight deviations from ideality for $[C_3mim]PF_6$ and $[C_3mpip]PF_6$, while $[C_3mpy]PF_6$ displays positive deviations with activity coefficient values of up to 1.95. Overall, small deviations from ideality are observed in the two common-anion ternary systems investigated by Coutinho's group using DSC. As discussed previously, this is most probably due to the very similar molecular structures of the $[C_3mim]PF_6$, $[C_3mpy]PF_6$, $[C_3mpyrr]PF_6$ and $[C_3mpip]PF_6$ compounds.

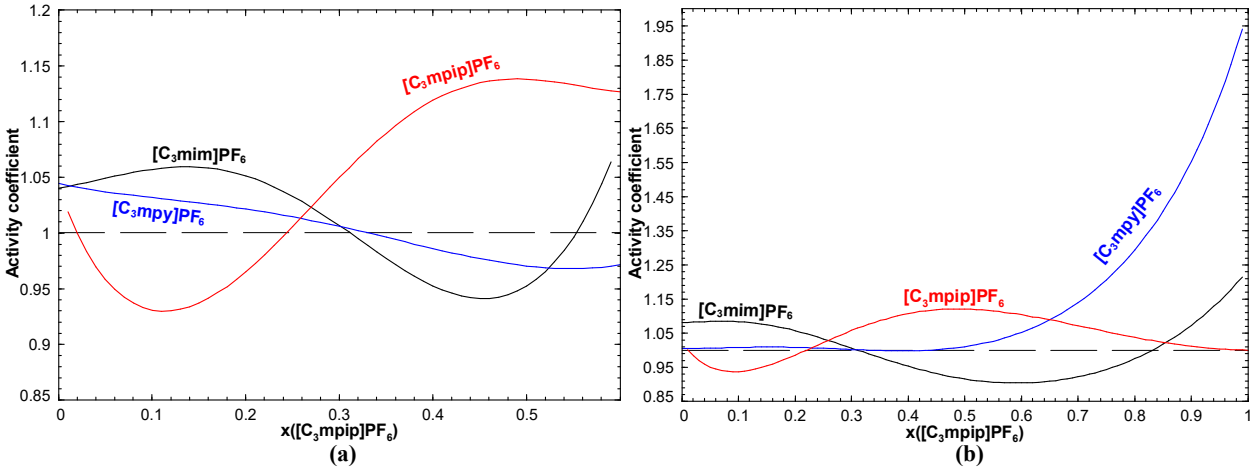


Figure 8.4: Calculated activity coefficients at 100°C of the components (liquid standard state) in the $[C_3mpip]PF_6$ - $[C_3mpy]PF_6$ - $[C_3mim]PF_6$ ternary liquid along the isoplethal sections at: (a) constant 40 mol% $[C_3mpy]PF_6$, and (b) constant molar ratio $[C_3mpy]PF_6$ / ($[C_3mpy]PF_6$ + $[C_3mim]PF_6$) of 0.60.

(v) For the $[C_4mim]${Cl, $NO_3$, $CH_3SO_3$}$ common-cation ternary liquid, the activity coefficients were calculated at 100°C along the isoplethal sections at constant 50 mol% $[C_4mim]CH_3SO_3$ and at constant molar ratio $[C_4mim]Cl$ / ($[C_4mim]Cl$ + $[C_4mim]NO_3$) of 0.85 (figure 8.5). Along the former isoplethal section, the three components exhibit positive deviations from ideality with activity coefficient values of up to 1.8 (for $[C_4mim]Cl$). Along the latter isoplethal section, there are again positive deviations for all components with activity coefficient values of up to 2.1 (for $[C_4mim]NO_3$).

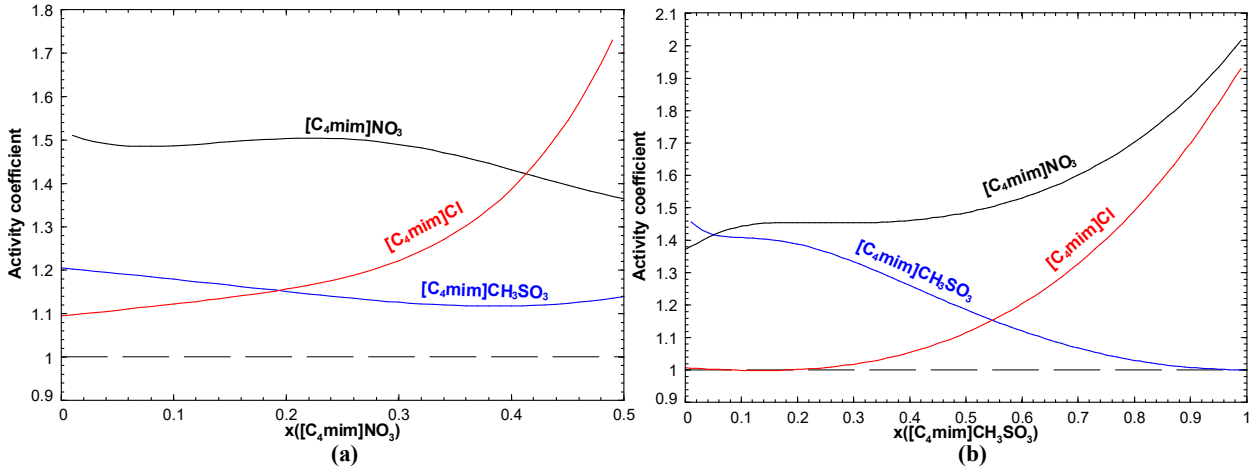


Figure 8.5: Calculated activity coefficients at 100°C of the components (liquid standard state) in the $[C_4mim]Cl$ - $[C_4mim]NO_3$ - $[C_4mim]CH_3SO_3$ ternary liquid along the isoplethal sections at: (a) constant 50 mol% $[C_4mim]CH_3SO_3$, and (b) constant molar ratio $[C_4mim]Cl$ / ($[C_4mim]Cl$ + $[C_4mim]NO_3$) of 0.85.

Some of the investigated common-ion ternary ionic liquid systems display a global minimum of the liquidus temperature lower than the melting temperatures of the three pure compounds. For the $[C_4mpyrr]Cl$ – $[C_4mpyrr]Br$ – $[C_4mpyrr]BF_4$, $[C_3mpip]PF_6$ – $[C_3mpy]PF_6$ – $[C_3mim]PF_6$ and $[C_3mpyrr]PF_6$ – $[C_3mpy]PF_6$ – $[C_3mim]PF_6$ ternary systems, a ternary eutectic reaction is calculated at 91, -8 and -16°C, respectively. Moreover, the calculated (tentative) liquidus projection of the $[C_4mim]Cl$ – $[C_4mim]NO_3$ – $[C_4mim]CH_3SO_3$ system displays a ternary eutectic at 18°C.

The present work was limited to ionic liquid systems in which the cations have short alkyl chains (ethyl, propyl or butyl). The compounds involving long alkyl chains have low melting temperatures, often below room temperature. Modeling the phase diagrams of systems involving such compounds would not be of great interest. Also, the current thermodynamic model may fail to reproduce the phase diagram of a system involving organic cations with a large size difference.

Although pure ionic liquids are stable compounds at room temperature, they may not be stable from the thermodynamic viewpoint. Using our selected thermodynamic properties estimated by the VBT in conjunction with the available data from the literature, it was found that the pyridinium-based (discussed in Chapter 4) and imidazolium-based (discussed in Chapter 5) pure compounds are calculated to decompose into C(graphite, s) and gaseous products, both in the solid (at 25°C) and liquid (slightly above the melting temperature) states. These reactions of decomposition are highly thermodynamically favoured (i.e. they have a very negative Gibbs free energy change) but are kinetically hindered. The same phenomenon occurs for some common organic compounds such as benzene, acetone, naphthalene and phenol.

For the $\{[C_2mim], [C_8mim], [C_{10}mim]\}NTf_2$ and $\{[C_4mim], [C_8mim], [C_{10}mim]\}NTf_2$ common-anion ternary liquids, two equilibrated reactions involving the decomposition of the cation $[C_8mim]^+$ occur thermodynamically. However, the four imidazolium-based cations are all stable. In order to inhibit these reactions of decomposition, the real chemical formula $C_{14}H_{23}N_3S_2O_4F_6$ of the $[C_8mim]NTf_2$ compound was replaced with the "hypothetical" chemical formula $C_{17}H_{41}N_3OF_3Na_5$ with the same molecular weight, thus permitting correct density calculations for the two ternary liquids. This trick had to be used owing to a current limitation of the FactSage thermochemical software: any reaction that is in reality kinetically hindered cannot be prevented from occurring.

The deviations from ideality of the experimental excess molar volumes ($V^E$) of Seddon's group and Rebelo's group for the $[C_4mim]Cl$ – $[C_4mim]CH_3SO_3$ and $[C_4mim]Cl$ – $[C_4mim]NO_3$ binary liquids show opposite trends. The density measurements were conducted on the same samples. The discrepancies between the $V^E$ values measured by the two research groups may be due to the different apparatuses used and also to the different water contents of the samples. (The presence of water decreases the density of the ionic liquid binary mixture owing to the lower density of water.)

# CHAPTER 9 CONCLUSIONS AND RECOMMENDATIONS

The main goal of this work was to develop thermodynamic models for the phase diagrams of various ternary ionic liquid systems (common-cation, common-anion, and ternary reciprocal with two cations and two anions). Density models were also developed for a few ternary ionic liquid systems (common-cation and common-anion). The experimental data necessary to calibrate and validate the models were both taken from the literature and obtained through a scientific collaboration with the following research groups: Seddons's group at Queen's University Ionic Liquid Laboratories (QUILL) in Belfast (UK); Smiglak's group at Poznań Science and Technology Park, Adam Mickiewicz University Foundation in Poznań (Poland); and Coutinho's group at University of Aveiro in Aveiro (Portugal). The new data obtained by these three groups were the thermal transitions measured for some binary and ternary ionic liquid mixtures using DSC, and the densities of a few binary ionic liquid systems (including the pure liquids).

Thermodynamic models were developed for the phase diagrams of the following ionic liquid systems: the [$C_4$mpyrr]{Cl, Br, $BF_4$} and [$C_4$mim]{Cl, $NO_3$, $CH_3SO_3$} common-cation ternary systems, the {[$C_3$mim], [$C_3$mpy], [$C_3$mpyrr], [$C_3$mpip]}$PF_6$ common-anion quaternary system, and the [$C_2$py]Cl – [$C_2$py]Br – [$C_4$py]Cl – [$C_4$py]Br ternary reciprocal system.

Density models were developed for the following ionic liquid systems: the [$C_4$mim]{Cl, $NO_3$, $CH_3SO_3$} (still in progress) and [$C_4$mim]{$BF_4$, $PF_6$, $NTf_2$} common-cation ternary liquids, and the {[$C_2$mim], [$C_8$mim], [$C_{10}$mim]}$NTf_2$ and {[$C_4$mim], [$C_8$mim], [$C_{10}$mim]}$NTf_2$ common-anion ternary liquids.

The MQMQA [13], which considers coupled 1st- and 2nd-nearest-neighbor short-range ordering, was used to model the liquid phase of the [$C_2$py], [$C_4$py] || Cl, Br ternary reciprocal system. This liquid displays relatively little first-nearest-neighbor (cation-anion) short-range ordering. For example, $\Delta g^{\text{exchange}}_{[C_2py][C_4py]/ClBr}$ for the exchange reaction [$C_2$py]Br (liquid) + [$C_4$py]Cl (liquid) = [$C_2$py]Cl (liquid) + [$C_4$py]Br (liquid) was estimated as -2.4 kJ.mol$^{-1}$ at 150°C. The liquid also exhibits relatively little second-nearest-neighbor (cation-cation and anion-anion) short-range ordering, based on the small optimized binary common-ion model parameters ($\Delta g_{AB/X_2}$ and $\Delta g_{A_2/XY}$). It was thus concluded that the studied ternary reciprocal liquid displays small deviations from ideality owing to the similarity of the two cations and of the two anions. While [$C_2$py]Cl –

[C4py]Cl and [C2py]Br – [C4py]Br are simple eutectic systems, [C2py]Cl – [C2py]Br and [C4py]Cl – [C4py]Br both exhibit an extensive solid solution over the entire composition range. The thermodynamic properties of the ternary reciprocal liquid were calculated solely from the optimized parameters for the four common-ion binary subsystems. The experimental diagonal sections [C4py]Br – [C2py]Cl and [C4py]Cl – [C2py]Br are very satisfactorily reproduced by the model. No ternary reciprocal parameter was required.

The MQMPA [12, 13], which takes into account only 2nd-nearest-neighbor short-range ordering, was used to model the phase diagrams of the common-ion ternary ionic liquid systems. In the [C4mpyrr]{Cl, Br, $BF_4$} common-cation system, [C4mpyrr]Br - [C4mpyrr]$BF_4$ and [C4mpyrr]Cl - [C4mpyrr]$BF_4$ are simple eutectic systems, while [C4mpyrr]Cl - [C4mpyrr]Br displays two terminal solid solutions. The thermodynamic properties of the ternary liquid were calculated solely from the optimized binary model parameters along with an asymmetric interpolation method, with [C4mpyrr]$BF_4$ as the "asymmetric" component. A small ternary parameter was included for the liquid in order to best reproduce the experimental isoplethal sections at constant 50 mol% [C4mpyrr]$BF_4$ and at constant molar ratio [C4mpyrr]Cl / ([C4mpyrr]Cl + [C4mpyrr]Br) of 0.85. The calculated minimum liquidus temperature in the ternary system corresponds to a ternary eutectic at 91°C, very close to the binary eutectic in the [C4mpyrr]Cl - [C4mpyrr]$BF_4$ system.

The three binary subsystems of the [C4mim]{Cl, $NO_3$, $CH_3SO_3$} common-cation system are all simple eutectic systems. Very scattered data were obtained for the [C4mim]$NO_3$ - [C4mim]Cl binary subsystem using both DSC and visual observation. This was attributed to the very hygroscopic nature of this particular binary system. A tentative liquidus projection of the ternary system was calculated using a symmetric interpolation method. The predicted minimum liquidus temperature corresponds to a ternary eutectic reaction at 18°C.

The phase diagrams of the six binary subsystems and four ternary subsystems of the {[C3mim], [C3mpy], [C3mpyrr], [C3mpip]}$PF_6$ common-anion quaternary system were modeled. The binary phase diagrams were modeled based on the experimental data of Maximo et al. [35]. All binary subsystems display a simple eutectic behaviour, except for the [C3mpip]$PF_6$ - [C3mpyrr]$PF_6$ binary system. The latter exhibits an extensive high-temperature ($s_3$-$s_3$) solid solution over the entire composition range. Two different scenarios were considered in the present work: the first scenario assumed a negligible solid solubility between the low-temperature allotropes ($s_1$-$s_1$) and also

between the intermediate-temperature allotropes ($s_2$-$s_2$) of $[C_3mpip]PF_6$ and $[C_3mpyrr]PF_6$; the second scenario assumed a continuous solid solution between the low-temperature allotropes ($s_1$-$s_1$) and also between the intermediate-temperature allotropes ($s_2$-$s_2$). The second scenario was finally favoured in order to best reproduce the experimental isoplethal sections at constant 40 mol% $[C_3mim]PF_6$ and at constant molar ratio $[C_3mpyrr]PF_6$ / ($[C_3mpyrr]PF_6$ + $[C_3mpip]PF_6$) of 0.60 in the $[C_3mim]PF_6$ - $[C_3mpip]PF_6$ - $[C_3mpyrr]PF_6$ ternary system. The thermodynamic properties of the ternary liquid were calculated solely from the binary optimized parameters using an asymmetric interpolation method, with $[C_3mim]PF_6$ as the asymmetric component. No ternary excess parameter was included for the liquid phase, and the excess Gibbs free energies of the low-temperature ($s_1$-$s_1$) and intermediate-temperature ($s_2$-$s_2$) binary solid solutions were adjusted. The model does not reproduce the measured thermal arrests observed in the intermediate temperature range, in the isoplethal section at 40 mol% $[C_3mim]PF_6$. These thermal arrests might be associated with $[C_3mpyrr]PF_6$ polymorphism, with the existence of two preferred conformations of the pyrrolidinium cations. Similarly, for the $[C_3mpy]PF_6$ - $[C_3mpip]PF_6$ - $[C_3mpyrr]PF_6$ ternary system, an asymmetric interpolation method was used, with $[C_3mpy]PF_6$ as the asymmetric component. Again, no ternary excess parameter was introduced in the liquid model.

For the $[C_3mpip]PF_6$ - $[C_3mpy]PF_6$ - $[C_3mim]PF_6$ ternary system, the experimental sections at constant 40 mol% $[C_3mpy]PF_6$ and at constant molar ratio $[C_3mpy]PF_6$ / ($[C_3mpy]PF_6$ + $[C_3mim]PF_6$) of 0.60 were satisfactorily reproduced. A symmetric interpolation method was used, and no ternary excess parameter was required for the liquid. The calculated minimum liquidus temperature in the ternary system corresponds to a ternary eutectic at -8°C. Similarly, for the $[C_3mpyrr]PF_6$ - $[C_3mpy]PF_6$ - $[C_3mim]PF_6$ ternary system, a symmetric interpolation method was used, and no ternary excess parameter was introduced in the liquid model. A ternary eutectic reaction was calculated at -16°C. This is the global minimum liquidus temperature in the entire common-anion quaternary system.

All ternary ionic liquid systems studied in the present work display small deviations from ideality, owing to the similarities in size (and sometimes also in the molecular structure) of the ionic species distributing on the same sublattice.

The Volume-based Thermodynamics (VBT) from Glasser and Jenkins [28-33] was used in conjunction with the available data from the literature to assess the thermodynamic properties

($\Delta H^{o}_{298.15K}$, $S^{o}_{298.15K}$, and $C_p(T)$) of the pyridinium- and imidazolium-based pure ionic liquids considered in the present work. The VBT is not accurate enough to model the phase diagrams of reciprocal systems.

The densities of some common-ion ternary ionic liquid systems were also modeled in the present work. For the [$C_4$mim]{Cl, $NO_3$, $CH_3SO_3$} common-cation ternary liquid, only densities of the three pure liquids and of the [$C_4$mim]$CH_3SO_3$ – [$C_4$mim]$NO_3$ binary liquid were modeled. The calculated excess molar volume ($V^E$) values for this binary liquid exhibit very small negative deviations from ideality. For the [$C_4$mim]Cl – [$C_4$mim]$CH_3SO_3$ and [$C_4$mim]Cl – [$C_4$mim]$NO_3$ binary liquids, the deviations from ideality of the experimental $V^E$ values from two different research groups display opposite trends. Therefore, new density measurements need to be conducted. The densities of the [$C_4$mim]{$BF_4$, $PF_6$, $NTf_2$} common-cation ternary liquid, and {[$C_2$mim], [$C_8$mim], [$C_{10}$mim]}$NTf_2$ and {[$C_4$mim], [$C_8$mim], [$C_{10}$mim]}$NTf_2$ common-anion ternary liquids were modeled based on the experimental data from Canongia Lopes et al. [38]. In each case, the molar volume of the ternary liquid was predicted from the optimized temperature-dependent expansivities and molar volumes at 298.15K of the pure liquids, and from the optimized binary pressure-dependent parameters using a standard symmetric interpolation method. Iso-excess molar volume ($V^E$) lines were predicted. For each ternary liquid, the calculated $V^E$ values increase as the composition of the liquid approaches the binary liquid in which the greatest $V^E$ values were observed.

Here are some recommendations and suggestions for future work:

1) Complete the density measurements and the density model for the [$C_4$mim]{Cl, $NO_3$, $CH_3SO_3$} common-cation ternary liquid,
2) Develop a density model that considers both the short-range hydrogen-bonding interactions and the long-range Coulombic interactions for ionic liquid systems with a high level of hydrogen-bonding, such as the ammonium-based common-anion binary systems recently studied by Canongia Lopes et al. [78],
3) Model the viscosity of ionic liquid systems by trying to apply the viscosity model previously developed for inorganic salt systems [268] (this model depends on both the thermodynamic model and the density model) or by developing a new viscosity model,

4) Study the phase diagrams of ternary reciprocal systems of ionic liquids with two very different organic cations and two different anions. (The exchange Gibbs free energy $\Delta g_{AB/XY}^{exchange}$ for the exchange reaction $AX + BY = AY + BX$ would then be higher in amplitude and the system would be more difficult to model.),
5) Perform further research on the VBT method in order to test its applicability to a wide range of families of ionic liquids,
6) Model the phase diagrams of "mixed" ternary systems, consisting of one or two quaternary ammonium salts and one or two polyols, and which may serve as Deep Eutectic Solvents (DES).

# BIBLIOGRAPHY


[1] S. J. Pas, M. S. Dargusch, and D. R. MacFarlane, "Crystallisation kinetics of some archetypal ionic liquids: isothermal and non-isothermal determination of the Avrami exponent," *Physical Chemistry Chemical Physics,* vol. 13, pp. 12033-12040, 2011.

[2] H. Niedermeyer, J. P. Hallett, I. J. Villar-Garcia, P. A. Hunt, and T. Welton, "Mixtures of ionic liquids," *Chemical Society Reviews,* vol. 41, pp. 7780-7802, 2012.

[3] J. J. Raj, C. D. Wilfred, S. N. Shah, M. Pranesh, M. A. Mutalib, and K. C. Lethesh, "Physicochemical and thermodynamic properties of imidazolium ionic liquids with nitrile and ether dual functional groups," *Journal of Molecular Liquids,* vol. 225, pp. 281-289, 2017.

[4] M. Koel, *Ionic liquids in chemical analysis*: CRC press, 2008.

[5] J. F. Brennecke and E. J. Maginn, "Ionic liquids: innovative fluids for chemical processing," *AIChE Journal,* vol. 47, pp. 2384-2389, 2001.

[6] C. Hardacre and V. Parvulescu, *Catalysis in Ionic Liquids: From Catalyst Synthesis to Application* vol. 15: Royal society of chemistry, 2014.

[7] A. Martinelli, A. Matic, P. Johansson, P. Jacobsson, L. Börjesson, A. Fernicola*, et al.*, "Conformational evolution of $TFSI^-$ in protic and aprotic ionic liquids," *Journal of Raman Spectroscopy,* vol. 42, pp. 522-528, 2011.

[8] Z. Fang, *Production of biofuels and chemicals with ionic liquids, Diss. Tohoku University, Japan,* 2014.

[9] A. Stark and K. R. Seddon, "Ionic liquids," *Kirk-Othmer encyclopedia of chemical technology,* 2007.

[10] N. V. Plechkova and K. R. Seddon, "Applications of ionic liquids in the chemical industry," *Chemical Society Reviews,* vol. 37, pp. 123-150, 2008.

[11] M. T. Clough, C. R. Crick, J. Gräsvik, P. A. Hunt, H. Niedermeyer, T. Welton*, et al.*, "A physicochemical investigation of ionic liquid mixtures," *Chemical Science,* vol. 6, pp. 1101-1114, 2015.

[12] A. Pelton, S. Degterov, G. Eriksson, C. Robelin, and Y. Dessureault, "The modified quasichemical model I-binary solutions," *Metallurgical and Materials Transactions B,* vol. 31, pp. 651-659, 2000.

[13] A. D. Pelton and P. Chartrand, "The modified quasi-chemical model: Part II. Multicomponent solutions," *Metallurgical and Materials Transactions A,* vol. 32, pp. 1355-1360, 2001.

[14] A. D. Pelton, P. Chartrand, and G. Eriksson, "The modified quasi-chemical model: Part IV. Two-sublattice quadruplet approximation," *Metallurgical and Materials Transactions A,* vol. 32, pp. 1409-1416, 2001.

[15] A. D. Pelton and P. Chartrand, "Thermodynamic evaluation and optimization of the LiCl-NaCl-KCl-RbCl-CsCl-$MgCl_2$-$CaCl_2$ system using the modified quasi-chemical model," *Metallurgical and Materials transactions A,* vol. 32, pp. 1361-1383, 2001.

[16] C. Robelin, P. Chartrand, and G. Eriksson, "A density model for multicomponent liquids based on the modified quasichemical model: Application to the NaCl-KCl-$MgCl_2$-$CaCl_2$ system," *Metallurgical and Materials Transactions B,* vol. 38, pp. 869-879, 2007.

[17] S. Mizani, "Modeling the viscosity of liquid solutions used in aluminum alloys production," Mémoire de maîtrise, Département de génie chimique, École polytechnique de Montréal, Montréal, 2008.

[18] P. Chartrand and A. D. Pelton, "A predictive thermodynamic model for the Al-NaF-$AlF_3$-$CaF_2$-$Al_2O_3$ system," *Light Metals, Warrendale, Proceedings,* pp. 245-252, 2002.

[19] P. Chartrand, F. Gemme, and C. Robelin, "A Thermodynamic Model for the $NH_4$, K//$H_2PO_4$, $H_2P_2O_{72}$, $NO_3$, Cl-$H_2O$ System," *Procedia Engineering,* vol. 83, pp. 250-258, 2014.

[20] C. Robelin, P. Chartrand, and A. D. Pelton, "Thermodynamic evaluation and optimization of the ($NaNO_3$+$KNO_3$+$Na_2SO_4$+$K_2SO_4$) system," *The Journal of Chemical Thermodynamics,* vol. 83, pp. 12-26, 2015.

[21] K. Kubota, T. Nohira, G. Takuya, and R. Hagiwara, "Binary and ternary mixtures of MFSA (M= Li, K, Cs) as new inorganic ionic liquids," *ECS Transactions,* vol. 16, pp. 91-98, 2009.

[22] K. Kubota, T. Nohira, T. Goto, and R. Hagiwara, "Ternary phase diagrams of alkali bis (trifluoromethylsulfonyl) amides," *Journal of Chemical & Engineering Data,* vol. 53, pp. 2144-2147, 2008.

[23] K. Kubota, T. Nohira, and R. Hagiwara, "New inorganic ionic liquids possessing low melting temperatures and wide electrochemical windows: Ternary mixtures of alkali bis (fluorosulfonyl) amides," *Electrochimica Acta,* vol. 66, pp. 320-324, 2012.

[24] C. Robelin, "Models for the thermodynamic properties of molten salt systems: Perspectives for ionic liquids," *Fluid Phase Equilibria,* vol. 409, pp. 482-494, 2016.

[25] G. Toop, "Predicting ternary activities using binary data," *Transactions of the Metallurgical Society of AIME,* vol. 233, pp. 850-854, 1965.

[26] B. Sundman and J. Ågren, "A regular solution model for phases with several components and sublattices, suitable for computer applications," *Journal of Physics and Chemistry of Solids,* vol. 42, pp. 297-301, 1981.

[27] M. Hillert, "The compound energy formalism," *Journal of Alloys and Compounds,* vol. 320, pp. 161-176, 2001.

[28] H. D. B. Jenkins, H. K. Roobottom, J. Passmore, and L. Glasser, "Relationships among ionic lattice energies, molecular (formula unit) volumes, and thermochemical radii," *Inorganic Chemistry,* vol. 38, pp. 3609-3620, 1999.

[29] H. D. B. Jenkins and L. Glasser, "Standard Absolute Entropy, Values from Volume or Density. 1. Inorganic Materials," *Inorganic Chemistry,* vol. 42, pp. 8702-8708, 2003.

[30] L. Glasser, "Lattice and phase transition thermodynamics of ionic liquids," *Thermochimica Acta,* vol. 421, pp. 87-93, 2004.

[31] L. Glasser and H. D. B. Jenkins, "Ambient Isobaric Heat Capacities, $C_{p,m}$, for Ionic Solids and Liquids: An Application of Volume-Based Thermodynamics (VBT)," *Inorganic Chemistry,* vol. 50, pp. 8565-8569, 2011.

[32] L. Glasser and H. D. B. Jenkins, "Volume-based thermodynamics: a prescription for its application and usage in approximation and prediction of thermodynamic data," *Journal of Chemical & Engineering Data,* vol. 56, pp. 874-880, 2010.

[33] H. D. B. Jenkins, "Ionic liquids–an overview," *Science progress,* vol. 94, pp. 265-297, 2011.

[34] O. Stolarska, H. Rodríguez, and M. Smiglak, "Eutectic mixtures of pyrrolidinium-based ionic liquids," *Fluid Phase Equilibria,* vol. 408, pp. 1-9, 2016.

[35] G. J. Maximo, R. J. Santos, P. Brandao, J. M. Esperança, M. C. Costa, A. J. Meirelles*, et al.*, "Generating Ionic Liquids from Ionic Solids: An Investigation of the Melting Behavior of Binary Mixtures of Ionic Liquids," *Crystal Growth & Design,* vol. 14, pp. 4270-4277, 2014.

[36] A. E. Gheribi, C. Robelin, S. Le Digabel, C. Audet, and A. D. Pelton, "Calculating all local minima on liquidus surfaces using the factsage software and databases and the mesh adaptive direct search algorithm," *The Journal of Chemical Thermodynamics,* vol. 43, pp. 1323-1330, 2011.

[37] O. Stolarska, A. Soto, H. Rodríguez, and M. Smiglak, *Physical Chemistry Chemical Physics,* 2017.

[38] J. N. Canongia Lopes, T. C. Cordeiro, J. M. Esperança, H. J. Guedes, S. Huq, L. P. Rebelo*, et al.*, "Deviations from ideality in mixtures of two ionic liquids containing a common ion," *The Journal of Physical Chemistry B,* vol. 109, pp. 3519-3525, 2005.

[39] P. Walden, "Molecular weights and electrical conductivity of several fused salts," *Bull. Acad. Imper. Sci.(St. Petersburg),* vol. 8, pp. 405-422, 1914.

[40] K. Seddon, "Ionic liquids: designer solvents," in *The International George Papatheodorou Symposium: Proceedings, ed. S. Boghosian, V. Dracopoulos, CG Kontoyannis and GA Voyiatzis, Institute of Chemical Engineering and High Temperature Chemical Processes, Patras*, 1999, pp. 131-135.

[41] D. Paschek, B. Golub, and R. Ludwig, "Hydrogen bonding in a mixture of protic ionic liquids: a molecular dynamics simulation study," *Physical Chemistry Chemical Physics,* vol. 17, pp. 8431-8440, 2015.

[42] R. Gusain, P. S. Bakshi, S. Panda, O. P. Sharma, R. Gardas, and O. P. Khatri, "Physicochemical and tribophysical properties of trioctylalkylammonium bis (salicylato) borate (N888 n-BScB) ionic liquids: effect of alkyl chain length," *Physical Chemistry Chemical Physics,* vol. 19, pp. 6433-6442, 2017.

[43] H. L. Ngo, K. LeCompte, L. Hargens, and A. B. McEwen, "Thermal properties of imidazolium ionic liquids," *Thermochimica Acta,* vol. 357, pp. 97-102, 2000.

[44] C. P. Fredlake, J. M. Crosthwaite, D. G. Hert, S. N. Aki, and J. F. Brennecke, "Thermophysical properties of imidazolium-based ionic liquids," *Journal of Chemical & Engineering Data,* vol. 49, pp. 954-964, 2004.

[45] J. D. Holbrey and K. R. Seddon, "The phase behaviour of 1-alkyl-3-methylimidazolium tetrafluoroborates; ionic liquids and ionic liquid crystals," *Journal of the Chemical Society, Dalton Transactions,* pp. 2133-2140, 1999.

[46] T. L. Greaves and C. J. Drummond, "Protic ionic liquids: properties and applications," *Chemical reviews,* vol. 108, pp. 206-237, 2008.

[47] J. Huang and A. F. Hollenkamp, "Thermal behavior of ionic liquids containing the FSI anion and the Li+ cation," *The Journal of Physical Chemistry C,* vol. 114, pp. 21840-21847, 2010.

[48] M. Kosmulski, J. Gustafsson, and J. B. Rosenholm, "Thermal stability of low temperature ionic liquids revisited," *Thermochimica Acta,* vol. 412, pp. 47-53, 2004.

[49] D. MacFarlane, S. Forsyth, J. Golding, and G. Deacon, "Ionic liquids based on imidazolium, ammonium and pyrrolidinium salts of the dicyanamide anion," *Green Chemistry,* vol. 4, pp. 444-448, 2002.

[50] C. Nieto de Castro, M. Lourenço, A. Ribeiro, E. Langa, S. Vieira, P. Goodrich*, et al.*, "Thermal properties of ionic liquids and ionanofluids of imidazolium and pyrrolidinium liquids," *Journal of Chemical & Engineering Data,* vol. 55, pp. 653-661, 2009.

[51] M. E. Van Valkenburg, R. L. Vaughn, M. Williams, and J. S. Wilkes, "Thermochemistry of ionic liquid heat-transfer fluids," *Thermochimica Acta,* vol. 425, pp. 181-188, 2005.

[52] R. E. Del Sesto, C. Corley, A. Robertson, and J. S. Wilkes, "Tetraalkylphosphonium-based ionic liquids," *Journal of Organometallic Chemistry,* vol. 690, pp. 2536-2542, 2005.

[53] J. Troncoso, C. A. Cerdeiriña, Y. A. Sanmamed, L. Romaní, and L. P. N. Rebelo, "Thermodynamic properties of imidazolium-based ionic liquids: densities, heat capacities, and enthalpies of fusion of [bmim][$PF_6$] and [bmim][$NTf_2$]," *Journal of Chemical & Engineering Data,* vol. 51, pp. 1856-1859, 2006.

[54] R. Mackenzie, "Nomenclature for thermal analysis-IV (Recommendations 1985)," *Pure and Applied Chemistry,* vol. 57, pp. 1737-1740, 1985.

[55] S. Handy, *Ionic Liquids-Current State of the Art*: InTech, 2015.

[56] A. P. De Los Rios and F. J. H. Fernandez, *Ionic Liquids in Separation Technology*: Elsevier, 2014.

[57] Z.-C. Tan, D.-W. Fang, P.-F. Yan, Q.-S. Liu, and U. Welz-Biermann, *Thermodynamic properties of ionic liquids-Measurements and predictions*: INTECH Open Access Publisher, 2011.

[58] G. Klančnik, J. Medved, and P. Mrvar, "Differential thermal analysis (DTA) and differential scanning calorimetry (DSC) as a method of material investigation Diferenčna termična analiza (DTA) in diferenčna vrstična kalorimetrija (DSC) kot metoda za raziskavo materialov," *RMZ–Materials and Geoenvironment,* vol. 57, pp. 127-142, 2010.

[59] K. R. Basudeb Karmakar, Andrey Stepanov, *Glass Nanocomposites : Synthesis, Properties and Applications*: Elsevier 2016.

[60] E. Gómez, N. Calvar, Á. Domínguez, and E. n. A. Macedo, "Thermal Analysis and Heat Capacities of 1-Alkyl-3-methylimidazolium Ionic Liquids with $NTf_2^-$, $TFO^-$, and $DCA^-$ Anions," *Industrial & Engineering Chemistry Research,* vol. 52, pp. 2103-2110, 2013.

[61] P. J. Dyson and T. J. Geldbach, *Metal catalysed reactions in ionic liquids* vol. 29: Springer, 2005.

[62] B. Kirchner, *Ionic liquids* vol. 290: Springer, 2009.

[63] J. M. Lopes, F. A. Sánchez, S. B. R. Reartes, M. D. Bermejo, Á. Martín, and M. J. Cocero, "Melting point depression effect with $CO_2$ in high melting temperature cellulose dissolving ionic liquids. Modeling with group contribution equation of state," *The Journal of Supercritical Fluids,* vol. 107, pp. 590-604, 2016.

[64] J. O. Valderrama and P. F. Arce, "Modeling the melting temperature depression of ionic liquids caused by supercritical carbon dioxide," *Fluid Phase Equilibria,* vol. 341, pp. 1-6, 2013.

[65] A. Kokorin, *Ionic liquids: Applications and perspectives*: InTech, 2011.

[66] M. Kick, P. Keil, and A. König, "Solid–liquid phase diagram of the two Ionic Liquids EMIMCl and BMIMCl," *Fluid Phase Equilibria,* vol. 338, pp. 172-178, 2013.

[67] A. R. R. Teles, H. Correia, G. J. Maximo, L. P. Rebelo, M. G. Freire, A. B. Pereiro*, et al.*, "Solid–liquid equilibria of binary mixtures of fluorinated ionic liquids," *Physical Chemistry Chemical Physics,* vol. 18, pp. 25741-25750, 2016.

[68] J. G. Huddleston, A. E. Visser, W. M. Reichert, H. D. Willauer, G. A. Broker, and R. D. Rogers, "Characterization and comparison of hydrophilic and hydrophobic room temperature ionic liquids incorporating the imidazolium cation," *Green chemistry,* vol. 3, pp. 156-164, 2001.

[69] K. R. Seddon, A. Stark, and M.-J. Torres, "Influence of chloride, water, and organic solvents on the physical properties of ionic liquids," *Pure and Applied Chemistry,* vol. 72, pp. 2275-2287, 2000.

[70] V. L. Martins, B. G. Nicolau, S. M. Urahata, M. C. Ribeiro, and R. M. Torresi, "Influence of the water content on the structure and physicochemical properties of an ionic liquid and its Li+ mixture," *The Journal of Physical Chemistry B,* vol. 117, pp. 8782-8792, 2013.

[71] E. Grishina, L. Ramenskaya, M. Gruzdev, and O. Kraeva, "Water effect on physicochemical properties of 1-butyl-3-methylimidazolium based ionic liquids with inorganic anions," *Journal of Molecular Liquids,* vol. 177, pp. 267-272, 2013.

[72] L. Ramenskaya, E. Grishina, A. Pimenova, and M. Gruzdev, "The influence of water on the physicochemical characteristics of 1-butyl-3-methylimidazolium bromide ionic liquid," *Russian Journal of Physical Chemistry A, Focus on Chemistry,* vol. 82, pp. 1098-1103, 2008.

[73] O. Stolarska, A. Soto, H. Rodríguez, and M. Smiglak, "Properties modification by eutectic formation in mixtures of ionic liquids," *RSC Advances,* vol. 5, pp. 22178-22187, 2015.

[74] P. Navia, J. Troncoso, and L. Romaní, "Excess magnitudes for ionic liquid binary mixtures with a common ion," *Journal of Chemical & Engineering Data,* vol. 52, pp. 1369-1374, 2007.

[75] D. Song and J. Chen, "Density and Viscosity Data for Mixtures of Ionic Liquids with a Common Anion," *Journal of Chemical & Engineering Data,* vol. 59, pp. 257-262, 2014.

[76] P. Bharmoria, K. Damarla, T. J. Trivedi, N. I. Malek, and A. Kumar, "A reciprocal binary mixture of protic/aprotic ionic liquids as a deep eutectic solvent: physicochemical behavior and application towards agarose processing," *RSC Advances,* vol. 5, pp. 99245-99252, 2015.

[77] G. Annat, M. Forsyth, and D. R. MacFarlane, "Ionic Liquid Mixtures-Variations in Physical Properties and Their Origins in Molecular Structure," *The Journal of Physical Chemistry B,* vol. 116, pp. 8251-8258, 2012.

[78] J. N. Canongia Lopes, J. M. S. S. Esperanca, A. M. de Ferro, A. B. Pereiro, N. V. Plechkova, L. P. N. Rebelo*, et al.*, "Protonic Ammonium Nitrate Ionic Liquids and Their Mixtures: Insights into Their Thermophysical Behavior," *The Journal of Physical Chemistry B,* vol. 120, pp. 2397-2406, 2016.

[79] G. Lambotte and P. Chartrand, "Thermodynamic optimization of the ($Na_2O$+ $SiO_2$+ NaF+ $SiF_4$) reciprocal system using the Modified Quasichemical Model in the Quadruplet Approximation," *The Journal of Chemical Thermodynamics,* vol. 43, pp. 1678-1699, 2011.

[80] A. A. Strechan, A. G. Kabo, Y. U. Paulechka, A. V. Blokhin, G. J. Kabo, A. S. Shaplov*, et al.*, "Thermochemical properties of 1-butyl-3-methylimidazolium nitrate," *Thermochimica Acta,* vol. 474, pp. 25-31, 2008.

[81] L. Glasser and H. D. B. Jenkins, "Standard absolute entropies, S 298, from volume or density: Part II. Organic liquids and solids," *Thermochimica Acta,* vol. 414, pp. 125-130, 2004.

[82] H. Olivier, "Recent developments in the use of non-aqueous ionic liquids for two-phase catalysis," *Journal of Molecular Catalysis A: Chemical,* vol. 146, pp. 285-289, 1999.

[83] P. Wasserscheid and T. Welton, *Ionic liquids in synthesis*: John Wiley & Sons, 2008.

[84] A. A. Fannin Jr, D. A. Floreani, L. A. King, J. S. Landers, B. J. Piersma, D. J. Stech*, et al.*, "Properties of 1, 3-dialkylimidazolium chloride-aluminum chloride ionic liquids. 2. Phase transitions, densities, electrical conductivities, and viscosities," *The Journal of Physical Chemistry,* vol. 88, pp. 2614-2621, 1984.

[85] G. K. Gbassi and C. Robelin, "Thermodynamic evaluation and optimization of the $CH_3COOLi$–$CH_3COOK$–$CH_3COOCs$ system using the Modified Quasichemical Model," *Fluid Phase Equilibria,* vol. 406, pp. 134-141, 2015.

[86] K. Fumino, T. Peppel, M. Geppert-Rybczyńska, D. H. Zaitsau, J. K. Lehmann, S. P. Verevkin*, et al.*, "The influence of hydrogen bonding on the physical properties of ionic liquids," *Physical Chemistry Chemical Physics,* vol. 13, pp. 14064-14075, 2011.

[87] K. Ala'a, A. M. Greenway, P. B. Hitchcock, T. J. Mohammed, K. R. Seddon, and J. A. Zora, "Upon the structure of room temperature halogenoaluminate ionic liquids," *Journal of the Chemical Society, Chemical Communications,* pp. 1753-1754, 1986.

[88] K. Dong, S. Zhang, D. Wang, and X. Yao, "Hydrogen bonds in imidazolium ionic liquids," *The Journal of Physical Chemistry A,* vol. 110, pp. 9775-9782, 2006.

[89] P. A. Hunt, C. R. Ashworth, and R. P. Matthews, "Hydrogen bonding in ionic liquids," *Chemical Society Reviews,* vol. 44, pp. 1257-1288, 2015.

[90] A. Elaiwi, P. B. Hitchcock, K. R. Seddon, N. Srinivasan, Y.-M. Tan, T. Welton*, et al.*, "Hydrogen bonding in imidazolium salts and its implications for ambient-temperature halogenoaluminate (III) ionic liquids," *Journal of the Chemical Society, Dalton Transactions,* pp. 3467-3472, 1995.

[91] W. M. Reichert, J. D. Holbrey, R. P. Swatloski, K. E. Gutowski, A. E. Visser, M. Nieuwenhuyzen*, et al.*, "Solid-state analysis of low-melting 1, 3-dialkylimidazolium hexafluorophosphate salts (ionic liquids) by combined X-ray crystallographic and computational analyses," *Crystal Growth & Design,* vol. 7, pp. 1106-1114, 2007.

[92] K. Dong, S. Zhang, and J. Wang, "Understanding the hydrogen bonds in ionic liquids and their roles in properties and reactions," *Chemical Communications,* vol. 52, pp. 6744-6764, 2016.

[93] M. Chase, *NIST—JANAF Thermochemical Tables, Monograph No9, Parts I and II, fourth ed., J. Phys. Chem. Data, American Chemical Society & American Institute of Physics, Woodbury, New York, USA,* p. 1963 pages, 1998.

[94] I. Barin, *Thermochemical Data of Pure Substances, Thermochemical Data of Pure Substances*: Wiley-VCH, 1997.

[95] T. D. J. Dunstan and J. Caja, "Development of Low Melting Ionic Liquids using Eutectic Mixtures of Imidazolium and Pyrazolium Ionic Liquids," *ECS Transactions,* vol. 3, pp. 21-32, 2007.

[96] A. S. Ivanova, T. Brinzer, E. A. Roth, V. A. Kusuma, J. D. Watkins, X. Zhou*, et al.*, "Eutectic ionic liquid mixtures and their effect on $CO_2$ solubility and conductivity," *RSC Advances,* vol. 5, pp. 51407-51412, 2015.

[97] M. Scheuermeyer, M. Kusche, F. Agel, P. Schreiber, F. Maier, H.-P. Steinrueck*, et al.*, "Thermally stable bis(trifluoromethylsulfonyl)imide salts and their mixtures," *New Journal of Chemistry,* p. Ahead of Print, 2016.

[98] M. Kunze, S. Jeong, E. Paillard, M. Winter, and S. Passerini, "Melting behavior of pyrrolidinium-based ionic liquids and their binary mixtures," *The Journal of Physical Chemistry C,* vol. 114, pp. 12364-12369, 2010.

[99] M. Smiglak, N. J. Bridges, M. Dilip, and R. D. Rogers, "Direct, Atom Efficient, and Halide-Free Syntheses of Azolium Azolate Energetic Ionic Liquids and Their Eutectic Mixtures, and Method for Determining Eutectic Composition," *Chemistry–A European Journal,* vol. 14, pp. 11314-11319, 2008.

[100] P. M. Bayley, A. S. Best, D. R. MacFarlane, and M. Forsyth, "Transport properties and phase behaviour in binary and ternary ionic liquid electrolyte systems of interest in lithium batteries," *ChemPhysChem,* vol. 12, pp. 823-827, 2011.

[101] G. B. Appetecchi, M. Montanino, M. Carewska, M. Moreno, F. Alessandrini, and S. Passerini, "Chemical–physical properties of bis (perfluoroalkylsulfonyl) imide-based ionic liquids," *Electrochimica Acta,* vol. 56, pp. 1300-1307, 2011.

[102] R. Hagiwara, K. Tamaki, K. Kubota, T. Goto, and T. Nohira, "Thermal properties of mixed alkali bis (trifluoromethylsulfonyl) amides," *Journal of Chemical & Engineering Data,* vol. 53, pp. 355-358, 2008.

[103] A. D. Pelton and Y.-B. Kang, "Modeling short-range ordering in solutions," *International Journal of Materials Research,* vol. 98, pp. 907-917, 2007.

[104] P. Chartrand and A. D. Pelton, "Thermodynamic evaluation and optimization of the LiCl-NaCl-KCl-RbCl-CsCl-$MgCl_2$-$CaCl_2$-$SrCl_2$ system using the modified quasichemical model," *Canadian Metallurgical Quarterly,* vol. 39, pp. 405-420, 2000.

[105] E. Renaud, C. Robelin, A. E. Gheribi, and P. Chartrand, "Thermodynamic evaluation and optimization of the Li, Na, K, Mg, Ca, Sr//F, Cl reciprocal system," *The Journal of Chemical Thermodynamics,* vol. 43, pp. 1286-1298, 2011.

[106] M. Temkin, "Mixtures of fused salts as ionic solutions," *Acta Physicochim. URSS,* vol. 20, pp. 411-420, 1945.

[107] O. B. Babushkina, "Phase Behaviour and FTIR Spectra of Ionic Liquids: The Mixtures of 1-Butyl-1-methylpyrrolidinium Chloride and TaCl5," *Zeitschrift für Naturforschung A,* vol. 63, pp. 66-72, 2008.

[108] M. Zawadzki, M. Krolikowska, and P. Lipinski, "Physicochemical and thermodynamic characterization of N-alkyl-N-methylpyrrolidinium bromides and its aqueous solutions," *Thermochim. Acta,* vol. 589, pp. 148-157, 2014.

[109] R. Shannon, "Revised effective ionic radii and systematic studies of interatomic distances in halides and chalcogenides," *Acta crystallographica section A: crystal physics, diffraction, theoretical and general crystallography,* vol. 32, pp. 751-767, 1976.

[110] K. E. Gutowski, R. D. Rogers, and D. A. Dixon, "Accurate thermochemical properties for energetic materials applications. II. Heats of formation of imidazolium-, 1, 2, 4-triazolium-, and tetrazolium-based energetic salts from isodesmic and lattice energy calculations," *The Journal of Physical Chemistry B,* vol. 111, pp. 4788-4800, 2007.

[111] W. G. Meindersma, T. van Acker, and A. B. de Haan, "Physical properties of 3-methyl-N-butylpyridinium tricyanomethanide and ternary LLE data with an aromatic and an aliphatic hydrocarbon at T=(303.2 and 328.2) K and p= 0.1 MPa," *Fluid Phase Equilibria,* vol. 307, pp. 30-38, 2011.

[112] M. Larriba, P. Navarro, J.-B. Beigbeder, J. García, and F. Rodríguez, "Mixing and decomposition behavior of {[4bmpy][$Tf_2N$]+[emim][$EtSO_4$]} and {[4bmpy][$Tf_2N$]+[emim][TFES]} ionic liquid mixtures," *The Journal of Chemical Thermodynamics,* vol. 82, pp. 58-75, 2015.

[113] I. Bandrés, B. Giner, H. Artigas, F. M. Royo, and C. Lafuente, "Thermophysic comparative study of two isomeric pyridinium-based ionic liquids," *The Journal of Physical Chemistry B,* vol. 112, pp. 3077-3084, 2008.

[114] J. Benito, M. García-Mardones, V. Pérez-Gregorio, I. Gascón, and C. Lafuente, "Physicochemical study of n-ethylpyridinium bis (trifluoromethylsulfonyl) imide ionic liquid," *Journal of Solution Chemistry,* vol. 43, pp. 696-710, 2014.

[115] V. N. Emel'yanenko, S. P. Verevkin, and A. Heintz, "Pyridinium based ionic liquids. N-Butyl-3-methyl-pyridinium dicyanoamide: Thermochemical measurement and first-principles calculations," *Thermochimica acta,* vol. 514, pp. 28-31, 2011.

[116] I. Bandrés, M. C. López, M. Castro, J. Barberá, and C. Lafuente, "Thermophysical properties of 1-propylpyridinium tetrafluoroborate," *The Journal of Chemical Thermodynamics,* vol. 44, pp. 148-153, 2012.

[117] E. J. González, Á. Domínguez, and E. A. Macedo, "Physical and excess properties of eight binary mixtures containing water and ionic liquids," *Journal of Chemical & Engineering Data,* vol. 57, pp. 2165-2176, 2012.

[118] U. Domańska, K. Skiba, M. Zawadzki, K. Paduszyński, and M. Królikowski, "Synthesis, physical, and thermodynamic properties of 1-alkyl-cyanopyridinium bis {(trifluoromethyl) sulfonyl} imide ionic liquids," *The Journal of Chemical Thermodynamics,* vol. 56, pp. 153-161, 2013.

[119] C. Cadena, Q. Zhao, R. Q. Snurr, and E. J. Maginn, "Molecular modeling and experimental studies of the thermodynamic and transport properties of pyridinium-based ionic liquids," *The Journal of Physical Chemistry B,* vol. 110, pp. 2821-2832, 2006.

[120] Q.-S. Liu, P.-P. Li, U. Welz-Biermann, J. Chen, and X.-X. Liu, "Density, dynamic viscosity, and electrical conductivity of pyridinium-based hydrophobic ionic liquids," *The Journal of Chemical Thermodynamics,* vol. 66, pp. 88-94, 2013.

[121] B. Mokhtarani, A. Sharifi, H. R. Mortaheb, M. Mirzaei, M. Mafi, and F. Sadeghian, "Density and viscosity of pyridinium-based ionic liquids and their binary mixtures with water at several temperatures," *The Journal of Chemical Thermodynamics,* vol. 41, pp. 323-329, 2009.

[122] J. M. Crosthwaite, M. J. Muldoon, J. K. Dixon, J. L. Anderson, and J. F. Brennecke, "Phase transition and decomposition temperatures, heat capacities and viscosities of pyridinium ionic liquids," *The Journal of Chemical Thermodynamics,* vol. 37, pp. 559-568, 2005.

[123] S. Corderí and B. González, "Ethanol extraction from its azeotropic mixture with hexane employing different ionic liquids as solvents," *The Journal of Chemical Thermodynamics,* vol. 55, pp. 138-143, 2012.

[124] H. Guerrero, M. García-Mardones, P. Cea, C. Lafuente, and I. Bandrés, "Correlation of the volumetric behaviour of pyridinium-based ionic liquids with two different equations," *Thermochimica acta,* vol. 531, pp. 21-27, 2012.

[125] I. Bandrés, F. M. Royo, I. Gascón, M. Castro, and C. Lafuente, "Anion influence on thermophysical properties of ionic liquids: 1-butylpyridinium tetrafluoroborate and 1-butylpyridinium triflate," *The Journal of Physical Chemistry B,* vol. 114, pp. 3601-3607, 2010.

[126] P. Navarro, M. Larriba, J. García, and F. Rodríguez, "Thermal stability, specific heats, and surface tensions of ([emim][DCA] + [4empy][$Tf_2N$]) ionic liquid mixtures," *The Journal of Chemical Thermodynamics,* vol. 76, pp. 152-160, 9// 2014.

[127] M. Larriba, P. Navarro, J. García, and F. Rodríguez, "Separation of toluene from n-heptane, 2,3-dimethylpentane, and cyclohexane using binary mixtures of [4empy][$Tf_2N$] and

[emim][DCA] ionic liquids as extraction solvents," *Separation and Purification Technology,* vol. 120, pp. 392-401, 12/13/ 2013.

[128] I. Bandrés, B. Giner, H. Artigas, C. Lafuente, and F. M. Royo, "Thermophysical Properties of N-Octyl-3-methylpyridinium Tetrafluoroborate," *Journal of Chemical & Engineering Data,* vol. 54, pp. 236-240, 2009/02/12 2009.

[129] S. P. Verevkin, D. H. Zaitsau, V. N. Emel'yanenko, R. V. Ralys, A. V. Yermalayeu, and C. Schick, "Does alkyl chain length really matter? Structure-property relationships in thermochemistry of ionic liquids," *Thermochimica Acta,* vol. 562, pp. 84-95, 2013.

[130] S. P. Verevkin, D. H. Zaitsau, V. N. Emel'yanenko, R. V. Ralys, C. Schick, M. Geppert-Rybczynska*, et al.*, "Benchmark Values: Thermochemistry of the Ionic Liquid [$C_4$Py][Cl]," *Aust. J. Chem.,* vol. 65, pp. 1487-1490, 2012.

[131] I. Krossing, J. M. Slattery, C. Daguenet, P. J. Dyson, A. Oleinikova, and H. Weingaertner, "Why are ionic liquids liquid? A simple explanation based on lattice and solvation energies," *J. Am. Chem. Soc.,* vol. 128, pp. 13427-13434, 2006.

[132] B. Tong, Q.-S. Liu, Z.-C. Tan, and U. Welz-Biermann, "Thermochemistry of alkyl pyridinium bromide ionic liquids: calorimetric measurements and calculations," *The Journal of Physical Chemistry A,* vol. 114, pp. 3782-3787, 2010.

[133] K. Paduszynski and U. Domanska, "A New Group Contribution Method For Prediction of Density of Pure Ionic Liquids over a Wide Range of Temperature and Pressure," *Industrial & Engineering Chemistry Research* vol. 51, pp. 591-604, 2012.

[134] C. W. Bale, E. Bélisle, P. Chartrand, S. A. Decterov, G. Eriksson, A. E. Gheribi*, et al.*, "FactSage thermochemical software and databases, 2010–2016," *Calphad,* vol. 54, pp. 35-53, 2016.

[135] G. J. Kabo, Y. U. Paulechka, A. G. Kabo, and A. V. Blokhin, "Experimental determination of enthalpy of 1-butyl-3-methylimidazolium iodide synthesis and prediction of enthalpies of formation for imidazolium ionic liquids," *The Journal of Chemical Thermodynamics,* vol. 42, pp. 1292-1297, 2010.

[136] V. N. Emel'yanenko, G. J. Kabo, and S. P. Verevkin, "Measurement and Prediction of Thermochemical Properties: Improved Increments for the Estimation of Enthalpies of Sublimation and Standard Enthalpies of Formation of Alkyl Derivatives of Urea," *Journal of Chemical & Engineering Data,* vol. 51, pp. 79-87, 2006.

[137] E. S. Domalski and E. D. Hearing, "Estimation of the thermodynamic properties of carbon-hydrogen-nitrogen-oxygen-sulfur-halogen compounds at 298.15 K," *Journal of Physical and Chemical Reference Data,* vol. 22, pp. 805-1159, 1993.

[138] Z. H. Zhang, L. X. Sun, Z. C. Tan, F. Xu, X. C. Lv, J. L. Zeng*, et al.*, "Thermodynamic investigation of room temperature ionic liquid," *Journal of Thermal Analysis and Calorimetry,* vol. 89, pp. 289-294, 2007.

[139] V. N. Emel'yanenko, S. P. Verevkin, A. Heintz, and C. Schick, "Ionic Liquids. Combination of Combustion Calorimetry with High-Level Quantum Chemical Calculations for Deriving Vaporization Enthalpies," *The Journal of Physical Chemistry B,* vol. 112, pp. 8095-8098, 2008.

[140] A. Efimova, G. Hubrig, and P. Schmidt, "Thermal stability and crystallization behavior of imidazolium halide ionic liquids," *Thermochim. Acta,* vol. 573, pp. 162-169, 2013.

[141] K. Nishikawa, S. Wang, H. Katayanagi, S. Hayashi, H.-o. Hamaguchi, Y. Koga*, et al.*, "Melting and Freezing Behaviors of Prototype Ionic Liquids, 1-Butyl-3-methylimidazolium Bromide and Its Chloride, Studied by Using a Nano-Watt Differential Scanning Calorimeter," *J. Phys. Chem. B,* vol. 111, pp. 4894-4900, 2007.

[142] T. Endo, T. Kato, and K. Nishikawa, "Effects of Methylation at the 2 Position of the Cation Ring on Phase Behaviors and Conformational Structures of Imidazolium-Based Ionic Liquids," *J. Phys. Chem. B,* vol. 114, pp. 9201-9208, 2010.

[143] O. Yamamuro, Y. Minamimoto, Y. Inamura, S. Hayashi, and H.-O. Hamaguchi, "Heat capacity and glass transition of an ionic liquid 1-butyl-3-methylimidazolium chloride," *Chem. Phys. Lett.,* vol. 423, pp. 371-375, 2006.

[144] U. Domanska, E. Bogel-Lukasik, and R. Bogel-Lukasik, "1-Octanol/water partition coefficients of 1-alkyl-3-methylimidazolium chloride," *Chem. - Eur. J.,* vol. 9, pp. 3033-3041, 2003.

[145] J. Zhu, L. Bai, B. Chen, and W. Fei, "Thermodynamical properties of phase change materials based on ionic liquids," *Chem. Eng. J. (Amsterdam, Neth.),* vol. 147, pp. 58-62, 2009.

[146] P. S. Campbell, C. C. Santini, D. Bouchu, B. Fenet, L. Rycerz, Y. Chauvin*, et al.*, "Synthesis and characterisation of ionic liquids based on 1-butyl-3-methylimidazolium chloride and $MCl_4$, M = Hf and Zr," *Dalton Trans.,* vol. 39, pp. 1379-1388, 2010.

[147] S. P. Verevkin, D. H. Zaitsau, V. N. Emel'yanenko, C. Schick, S. Jayaraman, and E. J. Maginn, "An elegant access to formation and vaporization enthalpies of ionic liquids by indirect DSC experiment and "in silico" calculations," *Chem. Commun. (Cambridge, U. K.),* vol. 48, pp. 6915-6917, 2012.

[148] M. Blesic, M. Swadzba-Kwasny, T. Belhocine, H. Q. N. Gunaratne, J. N. C. Lopes, M. F. C. Gomes*, et al.*, "1-Alkyl-3-methylimidazolium alkanesulfonate ionic liquids, $[C_nH_{2n+1}mim][C_kH_{2k+1}SO_3]$: synthesis and physicochemical properties," *Phys. Chem. Chem. Phys.,* vol. 11, pp. 8939-8948, 2009.

[149] A. Stark, A. W. Zidell, J. W. Russo, and M. M. Hoffmann, "Composition Dependent Physicochemical Property Data for the Binary System Water and the Ionic Liquid 1-Butyl-3-methylimidazolium Methanesulfonate ($[C_4mim][MeSO_3]$)," *J. Chem. Eng. Data,* vol. 57, pp. 3330-3339, 2012.

[150] C. C. Cassol, G. Ebeling, B. Ferrera, and J. Dupont, "A simple and practical method for the preparation and purity determination of halide-free imidazolium ionic liquids," *Adv. Synth. Catal.,* vol. 348, pp. 243-248, 2006.

[151] J. D. Holbrey, W. M. Reichert, M. Nieuwenhuyzen, S. Johnson, K. R. Seddon, and R. D. Rogers, "Crystal polymorphism in 1-butyl-3-methylimidazolium halides: supporting ionic liquid formation by inhibition of crystallization," *Chem. Commun. (Cambridge, U. K.),* pp. 1636-1637, 2003.

[152] H. Abe, T. Takekiyo, Y. Yoshimura, K. Saihara, and A. Shimizu, "Anomalous Freezing of Nano-Confined Water in Room-Temperature Ionic Liquid 1-Butyl-3-Methylimidazolium Nitrate," *ChemPhysChem,* vol. 17, pp. 1136-1142, 2016.

[153] C. Ye and J. n. M. Shreeve, "Rapid and Accurate Estimation of Densities of Room-Temperature Ionic Liquids and Salts," *J. Phys. Chem. A,* vol. 111, pp. 1456-1461, 2007.

[154] H.-C. Hu, A. N. Soriano, R. B. Leron, and M.-H. Li, "Molar heat capacity of four aqueous ionic liquid mixtures," *Thermochimica acta,* vol. 519, pp. 44-49, 2011.

[155] J. D. Holbrey, W. M. Reichert, R. G. Reddy, and R. D. Rogers, "Heat capacities of ionic liquids and their applications as thermal fluids," *ACS Symp. Ser.,* vol. 856, pp. 121-133, 2003.

[156] J. Golding, N. Hamid, D. MacFarlane, M. Forsyth, C. Forsyth, C. Collins*, et al.*, "N-methyl-N-alkylpyrrolidinium hexafluorophosphate salts: novel molten salts and plastic crystal phases," *Chemistry of materials,* vol. 13, pp. 558-564, 2001.

[157] M. A. R. Martins, J. A. P. Coutinho, S. P. Pinho, and U. Domanska, "Measurements of activity coefficients at infinite dilution of organic solutes and water on polar imidazolium-based ionic liquids," *J. Chem. Thermodyn.,* vol. 91, pp. 194-203, 2015.

[158] T. Kavitha, T. Vasantha, P. Venkatesu, R. S. Rama Devi, and T. Hofman, "Thermophysical properties for the mixed solvents of N-methyl-2-pyrrolidone with some of the imidazolium-based ionic liquids," *J. Mol. Liq.,* vol. 198, pp. 11-20, 2014.

[159] V. Govinda, P. Attri, P. Venkatesu, and P. Venkateswarlu, "Thermophysical properties of dimethylsulfoxide with ionic liquids at various temperatures," *Fluid Phase Equilib.,* vol. 304, pp. 35-43, 2011.

[160] R.-H. He, B.-W. Long, Y.-Z. Lu, H. Meng, and C.-X. Li, "Solubility of Hydrogen Chloride in Three 1-Alkyl-3-methylimidazolium Chloride Ionic Liquids in the Pressure Range (0 to 100) kPa and Temperature Range (298.15 to 363.15) K," *J. Chem. Eng. Data,* vol. 57, pp. 2936-2941, 2012.

[161] N. Mac Dowell, F. Llovell, N. Sun, J. P. Hallett, A. George, P. A. Hunt*, et al.*, "New Experimental Density Data and Soft-SAFT Models of Alkylimidazolium ($[C_nC_1im]^+$) Chloride ($Cl^-$), Methylsulfate ($[MeSO_4]^-$), and Dimethylphosphate ($[Me_2PO_4]^-$) Based Ionic Liquids," *J. Phys. Chem. B,* vol. 118, pp. 6206-6221, 2014.

[162] M. Moosavi, A. Daneshvar, E. Sedghamiz, E. Momtaz, and A. Joharian, "Shear rate-, temperature- and composition-dependencies of viscosity behavior of mixtures of {[bmim]$NO_3$ + ethanol}," *J. Mol. Liq.,* vol. 199, pp. 257-266, 2014.

[163] B. Mokhtarani, A. Sharifi, H. R. Mortaheb, M. Mirzaei, M. Mafi, and F. Sadeghian, "Density and viscosity of 1-butyl-3-methylimidazolium nitrate with ethanol, 1-propanol, or 1-butanol at several temperatures," *J. Chem. Thermodyn.,* vol. 41, pp. 1432-1438, 2009.

[164] K. R. Seddon, A. Stark, and M.-J. Torres, "Viscosity and density of 1-alkyl-3-methylimidazolium ionic liquids," *ACS Symp. Ser.,* vol. 819, pp. 34-49, 2002.

[165] M. D. Bermejo, M. Montero, E. Saez, L. J. Florusse, A. J. Kotlewska, M. J. Cocero*, et al.*, "Liquid-Vapor Equilibrium of the Systems Butylmethylimidazolium Nitrate-$CO_2$ and

Hydroxypropylmethylimidazolium Nitrate-$CO_2$ at High Pressure: Influence of Water on the Phase Behavior," *J. Phys. Chem. B,* vol. 112, pp. 13532-13541, 2008.

[166] L. A. Blanchard, Z. Gu, and J. F. Brennecke, "High-Pressure Phase Behavior of Ionic Liquid/$CO_2$ Systems," *J. Phys. Chem. B,* vol. 105, pp. 2437-2444, 2001.

[167] Y. Huo, S. Xia, and P. Ma, "Densities of ionic liquids, 1-butyl-3-methylimidazolium hexafluorophosphate and 1-butyl-3-methylimidazolium tetrafluoroborate, with benzene, acetonitrile, and 1-propanol at T=(293.15 to 343.15) K," *Journal of Chemical & Engineering Data,* vol. 52, pp. 2077-2082, 2007.

[168] J. Salgado, T. Regueira, L. Lugo, J. Vijande, J. Fernández, and J. García, "Density and viscosity of three (2, 2, 2-trifluoroethanol+ 1-butyl-3-methylimidazolium) ionic liquid binary systems," *The Journal of Chemical Thermodynamics,* vol. 70, pp. 101-110, 2014.

[169] F. Qi and H. Wang, "Application of Prigogine–Flory–Patterson theory to excess molar volume of mixtures of 1-butyl-3-methylimidazolium ionic liquids with N-methyl-2-pyrrolidinone," *The Journal of Chemical Thermodynamics,* vol. 41, pp. 265-272, 2009.

[170] D. Tomida, A. Kumagai, K. Qiao, and C. Yokoyama, "Viscosity of [bmim][$PF_6$] and [bmim][BF4] at high pressure," *International journal of thermophysics,* vol. 27, pp. 39-47, 2006.

[171] A. N. Soriano, B. T. Doma, and M.-H. Li, "Measurements of the density and refractive index for 1-n-butyl-3-methylimidazolium-based ionic liquids," *The Journal of Chemical Thermodynamics,* vol. 41, pp. 301-307, 2009.

[172] W. Afzal, X. Liu, and J. M. Prausnitz, "Solubilities of some gases in four immidazolium-based ionic liquids," *The Journal of Chemical Thermodynamics,* vol. 63, pp. 88-94, 2013.

[173] A. Kumar, "Estimates of internal pressure and molar refraction of imidazolium based ionic liquids as a function of temperature," *Journal of Solution Chemistry,* vol. 37, pp. 203-214, 2008.

[174] J. Jacquemin, P. Husson, A. A. Padua, and V. Majer, "Density and viscosity of several pure and water-saturated ionic liquids," *Green Chemistry,* vol. 8, pp. 172-180, 2006.

[175] M. Montalbán, C. Bolívar, F. G. Díaz Baños, and G. Víllora, "Effect of temperature, anion, and alkyl chain length on the density and refractive index of 1-alkyl-3-methylimidazolium-based ionic liquids," *Journal of Chemical & Engineering Data,* vol. 60, pp. 1986-1996, 2015.

[176] H. Tokuda, S. Tsuzuki, M. A. B. H. Susan, K. Hayamizu, and M. Watanabe, "How ionic are room-temperature ionic liquids? An indicator of the physicochemical properties," *The Journal of Physical Chemistry B,* vol. 110, pp. 19593-19600, 2006.

[177] Y. Zhang, T. Zhang, P. Gan, H. Li, M. Zhang, K. Jin*, et al.*, "Solubility of isobutane in ionic liquids [BMIm][$PF_6$],[BMIm][$BF_4$], and [BMIm][$Tf_2N$]," *Journal of Chemical & Engineering Data,* vol. 60, pp. 1706-1714, 2015.

[178] Y. Huo, S. Xia, and P. Ma, "Solubility of alcohols and aromatic compounds in imidazolium-based ionic liquids," *Journal of Chemical & Engineering Data,* vol. 53, pp. 2535-2539, 2008.

[179] M. Tariq, P. Forte, M. C. Gomes, J. C. Lopes, and L. Rebelo, "Densities and refractive indices of imidazolium-and phosphonium-based ionic liquids: Effect of temperature, alkyl chain length, and anion," *The Journal of Chemical Thermodynamics,* vol. 41, pp. 790-798, 2009.

[180] D. Song and J. Chen, "Densities and viscosities for ionic liquids mixtures containing [eOHmim][BF4],[bmim][BF4] and [bpy][$BF_4$]," *The Journal of Chemical Thermodynamics,* vol. 77, pp. 137-143, 2014.

[181] M. Iglesias-Otero, J. Troncoso, E. Carballo, and L. Romaní, "Density and refractive index for binary systems of the ionic liquid [Bmim][$BF_4$] with methanol, 1, 3-dichloropropane, and dimethyl carbonate," *Journal of Solution Chemistry,* vol. 36, pp. 1219-1230, 2007.

[182] V. A. Nikitina, A. Nazet, T. Sonnleitner, and R. Buchner, "Properties of sodium tetrafluoroborate solutions in 1-butyl-3-methylimidazolium tetrafluoroborate ionic liquid," *Journal of Chemical & Engineering Data,* vol. 57, pp. 3019-3025, 2012.

[183] O. Ciocirlan, O. Croitoru, and O. Iulian, "Densities and viscosities for binary mixtures of 1-butyl-3-methylimidazolium tetrafluoroborate ionic liquid with molecular solvents," *Journal of Chemical & Engineering Data,* vol. 56, pp. 1526-1534, 2011.

[184] M.-L. Ge, X.-G. Ren, Y.-J. Song, and L.-S. Wang, "Densities and Viscosities of 1-Propyl-2, 3-dimethylimidazolium Tetrafluoroborate+ $H_2O$ at T=(298.15 to 343.15) K," *Journal of Chemical & Engineering Data,* vol. 54, pp. 1400-1402, 2009.

[185] M. M. Taib and T. Murugesan, "Density, refractive index, and excess properties of 1-butyl-3-methylimidazolium tetrafluoroborate with water and monoethanolamine," *Journal of Chemical & Engineering Data,* vol. 57, pp. 120-126, 2011.

[186] Q. Zhou, L.-S. Wang, and H.-P. Chen, "Densities and viscosities of 1-butyl-3-methylimidazolium tetrafluoroborate+ $H_2O$ binary mixtures from (303.15 to 353.15) K," *Journal of Chemical & Engineering Data,* vol. 51, pp. 905-908, 2006.

[187] A. Pal and B. Kumar, "Volumetric and acoustic properties of binary mixtures of the ionic liquid 1-butyl-3-methylimidazolium tetrafluoroborate [bmim][$BF_4$] with alkoxyalkanols at different temperatures," *Journal of Chemical & Engineering Data,* vol. 57, pp. 688-695, 2012.

[188] D. Santos, M. Santos, E. Franceschi, C. u. Dariva, A. Barison, and S. Mattedi, "Experimental density of ionic liquids and thermodynamic modeling with group contribution equation of state based on the lattice fluid theory," *Journal of Chemical & Engineering Data,* vol. 61, pp. 348-353, 2015.

[189] E. Vercher, F. J. Llopis, V. González-Alfaro, P. J. Miguel, V. Orchillés, and A. Martínez-Andreu, "Volumetric properties, viscosities and refractive indices of binary liquid mixtures of tetrafluoroborate-based ionic liquids with methanol at several temperatures," *The Journal of Chemical Thermodynamics,* vol. 90, pp. 174-184, 2015.

[190] M. R. Currás, M. F. Costa Gomes, P. Husson, A. A. Padua, and J. Garcia, "Calorimetric and volumetric study on binary mixtures 2, 2, 2-trifluoroethanol+(1-butyl-3-methylimidazolium tetrafluoroborate or 1-ethyl-3-methylimidazolium tetrafluoroborate)," *Journal of Chemical & Engineering Data,* vol. 55, pp. 5504-5512, 2010.

[191] S. G. Rao, T. M. Mohan, T. V. Krishna, and B. S. Rao, "Volumetric properties of 1-butyl-3-methylimidazolium tetrafluoroborate and 2-pyrrolidone from T=(298.15 to 323.15) K at atmospheric pressure," *The Journal of Chemical Thermodynamics,* vol. 94, pp. 127-137, 2016.

[192] T. S. Krishna, M. G. Sankar, K. T. S. Raju, S. G. Rao, and B. Munibhadrayya, "Acoustic, volumetric, and optic study of binary mixture of 1-butyl-3-methylimidazoliumtetrafluoroborate with propylene glycols at T=(298.15 to 323.15) K," *Journal of Molecular Liquids,* vol. 206, pp. 350-358, 2015.

[193] K. R. Harris, M. Kanakubo, and L. A. Woolf, "Temperature and pressure dependence of the viscosity of the ionic liquid 1-butyl-3-methylimidazolium tetrafluoroborate: viscosity and density relationships in ionic liquids," *Journal of Chemical & Engineering Data,* vol. 52, pp. 2425-2430, 2007.

[194] M. A. Iglesias-Otero, J. Troncoso, E. Carballo, and L. Romaní, "Densities and excess enthalpies for ionic liquids+ ethanol or+ nitromethane," *Journal of Chemical & Engineering Data,* vol. 53, pp. 1298-1301, 2008.

[195] M. T. Zafarani-Moattar and H. Shekaari, "Application of Prigogine–Flory–Patterson theory to excess molar volume and speed of sound of 1-n-butyl-3-methylimidazolium hexafluorophosphate or 1-n-butyl-3-methylimidazolium tetrafluoroborate in methanol and acetonitrile," *The Journal of Chemical Thermodynamics,* vol. 38, pp. 1377-1384, 2006.

[196] J.-Y. Wu, Y.-P. Chen, and C.-S. Su, "Density and viscosity of ionic liquid binary mixtures of 1-n-butyl-3-methylimidazolium tetrafluoroborate with acetonitrile, N, N-dimethylacetamide, methanol, and N-methyl-2-pyrrolidone," *Journal of Solution Chemistry,* vol. 44, pp. 395-412, 2015.

[197] T. Singh, A. Kumar, M. Kaur, G. Kaur, and H. Kumar, "Non-ideal behaviour of imidazolium based room temperature ionic liquids in ethylene glycol at T=(298.15 to 318.15) K," *The Journal of Chemical Thermodynamics,* vol. 41, pp. 717-723, 2009.

[198] Y. Zhao, X. Zhang, S. Zeng, Q. Zhou, H. Dong, X. Tian*, et al.*, "Density, viscosity, and performances of carbon dioxide capture in 16 absorbents of amine+ ionic liquid+ $H_2O$, ionic liquid+ $H_2O$, and amine+ $H_2O$ systems," *Journal of Chemical & Engineering Data,* vol. 55, pp. 3513-3519, 2010.

[199] Y. Sanmamed, D. Gonzalez-Salgado, J. Troncoso, C. Cerdeirina, and L. Romani, "Viscosity-induced errors in the density determination of room temperature ionic liquids using vibrating tube densitometry," *Fluid phase equilibria,* vol. 252, pp. 96-102, 2007.

[200] C. M. Neves, K. A. Kurnia, J. o. A. Coutinho, I. M. Marrucho, J. N. C. Lopes, M. G. Freire*, et al.*, "Systematic study of the thermophysical properties of imidazolium-based ionic liquids with cyano-functionalized anions," *The Journal of Physical Chemistry B,* vol. 117, pp. 10271-10283, 2013.

[201] G. Vakili-Nezhaad, M. Vatani, M. Asghari, and I. Ashour, "Effect of temperature on the physical properties of 1-butyl-3-methylimidazolium based ionic liquids with thiocyanate and tetrafluoroborate anions, and 1-hexyl-3-methylimidazolium with tetrafluoroborate and hexafluorophosphate anions," *The Journal of Chemical Thermodynamics,* vol. 54, pp. 148-154, 2012.

[202] J. Klomfar, M. Součková, and J. Pátek, "Buoyancy density measurements for 1-alkyl-3-methylimidazolium based ionic liquids with tetrafluoroborate anion," *Fluid Phase Equilibria,* vol. 282, pp. 31-37, 2009.

[203] W. Fan, Q. Zhou, J. Sun, and S. Zhang, "Density, excess molar volume, and viscosity for the methyl methacrylate+ 1-butyl-3-methylimidazolium hexafluorophosphate ionic liquid binary system at atmospheric pressure," *Journal of Chemical & Engineering Data,* vol. 54, pp. 2307-2311, 2009.

[204] Y. Qiao, F. Yan, S. Xia, S. Yin, and P. Ma, "Densities and viscosities of [Bmim][$PF_6$] and binary systems [Bmim][$PF_6$]+ ethanol,[Bmim][$PF_6$]+ benzene at several temperatures and pressures: determined by the falling-ball method," *Journal of chemical & engineering data,* vol. 56, pp. 2379-2385, 2011.

[205] Y. Geng, S. Chen, T. Wang, D. Yu, C. Peng, H. Liu*, et al.*, "Density, viscosity and electrical conductivity of 1-butyl-3-methylimidazolium hexafluorophosphate+ monoethanolamine and+ N, N-dimethylethanolamine," *Journal of Molecular Liquids,* vol. 143, pp. 100-108, 2008.

[206] Z. Vaid, U. More, S. P. Ijardar, and N. I. Malek, "Investigation on thermophysical and excess properties of binary mixtures of imidazolium based ionic liquids at temperatures (293.15 to 323.15) K: III [$C_n$mim][$PF_6$](n= 4, 6, 8)+ THF," *The Journal of Chemical Thermodynamics,* vol. 86, pp. 143-153, 2015.

[207] G. Yanfang, W. Tengfang, Y. Dahong, P. Changjun, L. Honglai, and H. Ying, "Densities and viscosities of the ionic liquid [$C_4$mim][$PF_6$]+ N, N-dimethylformamide binary mixtures at 293.15 K to 318.15 K," *Chinese Journal of Chemical Engineering,* vol. 16, pp. 256-262, 2008.

[208] T. S. Krishna, K. Raju, M. Gowrisankar, A. K. Nain, and B. Munibhadrayya, "Volumetric, ultrasonic and spectroscopic studies of molecular interactions in binary mixtures of 1-butyl-3-methylimidazolium hexafluorophosphate with 2-propoxyethanol at temperatures from 298.15 to 323.15 K," *Journal of Molecular Liquids,* vol. 216, pp. 484-495, 2016.

[209] M. T. Zafarani-Moattar and H. Shekaari, "Volumetric and speed of sound of ionic liquid, 1-butyl-3-methylimidazolium hexafluorophosphate with acetonitrile and methanol at T=(298.15 to 318.15) K," *Journal of Chemical & Engineering Data,* vol. 50, pp. 1694-1699, 2005.

[210] Z. Vaid, U. U. More, R. L. Gardas, N. I. Malek, and S. P. Ijardar, "Composition and Temperature Dependence of Excess Properties of Binary Mixtures of Imidazolium Based Ionic Liquids: II ([$C_n$mim][$PF_6$])+ Propylamine," *Journal of Solution Chemistry,* vol. 44, pp. 718-741, 2015.

[211] A. Kumar, T. Singh, R. L. Gardas, and J. A. Coutinho, "Non-ideal behaviour of a room temperature ionic liquid in an alkoxyethanol or poly ethers at T=(298.15 to 318.15) K," *The Journal of Chemical Thermodynamics,* vol. 40, pp. 32-39, 2008.

[212] T. Singh and A. Kumar, "Volumetric behaviour of 1-Butyl-3-Methyl imidazolium hexafluorophosphate with ethylene glycol derivatives: Application of Prigogine-Flory-Patterson theory," *Journal of Molecular Liquids,* vol. 153, pp. 117-123, 2010.

[213] Y. Zhong, H. Wang, and K. Diao, "Densities and excess volumes of binary mixtures of the ionic liquid 1-butyl-3-methylimidazolium hexafluorophosphate with aromatic compound at T = (298.15 to 313.15) K," *The Journal of Chemical Thermodynamics,* vol. 39, pp. 291-296, 2// 2007.

[214] A. B. Pereiro and A. Rodríguez, "Study on the phase behaviour and thermodynamic properties of ionic liquids containing imidazolium cation with ethanol at several temperatures," *The Journal of Chemical Thermodynamics,* vol. 39, pp. 978-989, 6// 2007.

[215] M. A. Rocha, F. M. Ribeiro, A. I. L. Ferreira, J. A. Coutinho, and L. M. Santos, "Thermophysical properties of $[C_{N-1}C_1im][PF_6]$ ionic liquids," *Journal of Molecular Liquids,* vol. 188, pp. 196-202, 2013.

[216] K. R. Harris, L. A. Woolf, and M. Kanakubo, "Temperature and pressure dependence of the viscosity of the ionic liquid 1-butyl-3-methylimidazolium hexafluorophosphate," *Journal of Chemical & Engineering Data,* vol. 50, pp. 1777-1782, 2005.

[217] A. B. Pereiro, J. L. Legido, and A. Rodrı, "Physical properties of ionic liquids based on 1-alkyl-3-methylimidazolium cation and hexafluorophosphate as anion and temperature dependence," *The Journal of Chemical Thermodynamics,* vol. 39, pp. 1168-1175, 2007.

[218] J. Jacquemin, P. Husson, V. Majer, and M. F. C. Gomes, "Low-pressure solubilities and thermodynamics of solvation of eight gases in 1-butyl-3-methylimidazolium hexafluorophosphate," *Fluid Phase Equilibria,* vol. 240, pp. 87-95, 2006.

[219] J. Kumełan, Á. P.-S. Kamps, D. Tuma, and G. Maurer, "Solubility of CO in the ionic liquid [bmim][$PF_6$]," *Fluid phase equilibria,* vol. 228, pp. 207-211, 2005.

[220] G. J. Kabo, A. V. Blokhin, Y. U. Paulechka, A. G. Kabo, M. P. Shymanovich, and J. W. Magee, "Thermodynamic properties of 1-butyl-3-methylimidazolium hexafluorophosphate in the condensed state," *Journal of Chemical & Engineering Data,* vol. 49, pp. 453-461, 2004.

[221] W. Li, Z. Zhang, B. Han, S. Hu, Y. Xie, and G. Yang, "Effect of water and organic solvents on the ionic dissociation of ionic liquids," *The Journal of Physical Chemistry B,* vol. 111, pp. 6452-6456, 2007.

[222] M. S. AlTuwaim, K. H. Alkhaldi, A. S. Al-Jimaz, and A. A. Mohammad, "Temperature dependence of physicochemical properties of imidazolium-, pyroldinium-, and phosphonium-based ionic liquids," *Journal of Chemical & Engineering Data,* vol. 59, pp. 1955-1963, 2014.

[223] K. R. Seddon, A. Stark, and M.-J. Torres, "Viscosity and density of 1-alkyl-3-methylimidazolium ionic liquids," ed: ACS Publications, 2002.

[224] G. R. Chaudhary, S. Bansal, S. Mehta, and A. Ahluwalia, "Thermophysical and spectroscopic studies of room temperature ionic liquid, 1-butyl-3-methylimidazolium hexafluorophosphate in Tritons," *The Journal of Chemical Thermodynamics,* vol. 50, pp. 63-70, 2012.

[225] G. Reyes, M. Cartes, C. Rey-Castro, H. Segura, and A. s. Mejía, "Surface tension of 1-ethyl-3-methylimidazolium ethyl sulfate or 1-butyl-3-methylimidazolium

hexafluorophosphate with argon and carbon dioxide," *Journal of Chemical & Engineering Data,* vol. 58, pp. 1203-1211, 2013.

[226] M. P. Singh, S. K. Mandal, Y. L. Verma, A. K. Gupta, R. K. Singh, and S. Chandra, "Viscoelastic, surface, and volumetric properties of ionic liquids [BMIM][OcSO4],[BMIM][PF6], and [EMIM][MeSO3]," *Journal of Chemical & Engineering Data,* vol. 59, pp. 2349-2359, 2014.

[227] O. Zech, A. Stoppa, R. Buchner, and W. Kunz, "The conductivity of imidazolium-based ionic liquids from (248 to 468) KB Variation of the anion," *Journal of Chemical & Engineering Data,* vol. 55, pp. 1774-1778, 2010.

[228] S. V. Dzyuba and R. A. Bartsch, "Influence of structural variations in 1-alkyl (aralkyl)-3-methylimidazolium hexafluorophosphates and bis (trifluoromethylsulfonyl) imides on physical properties of the ionic liquids," *ChemPhysChem,* vol. 3, pp. 161-166, 2002.

[229] Z. Gu and J. F. Brennecke, "Volume expansivities and isothermal compressibilities of imidazolium and pyridinium-based ionic liquids," *Journal of Chemical & Engineering Data,* vol. 47, pp. 339-345, 2002.

[230] M. Moosavi, A. Daneshvar, and E. Sedghamiz, "Rheological properties of {[bmim] $PF_6$+ methanol} mixtures at different temperatures, shear rates and compositions," *Journal of Molecular Liquids,* vol. 209, pp. 693-705, 2015.

[231] M. s. R. Currás, P. Husson, A. A. Pádua, M. F. Costa Gomes, and J. García, "High-pressure densities of 2, 2, 2-trifluoroethanol+ ionic liquid mixtures useful for possible applications in absorption cycles," *Industrial & Engineering Chemistry Research,* vol. 53, pp. 10791-10802, 2014.

[232] C. A. N. de Castro, E. Langa, A. L. Morais, M. L. M. Lopes, M. J. Lourenço, F. J. Santos*, et al.*, "Studies on the density, heat capacity, surface tension and infinite dilution diffusion with the ionic liquids [$C_4$mim][$NTf_2$],[$C_4$mim][dca],[$C_2$mim][$EtOSO_3$] and [Aliquat][dca]," *Fluid Phase Equilibria,* vol. 294, pp. 157-179, 2010.

[233] R. Hamidova, I. Kul, J. Safarov, A. Shahverdiyev, and E. Hassel, "Thermophysical properties of 1-butyl-3-methylimidazolium bis (trifluoromethylsulfonyl) imide at high temperatures and pressures," *Brazilian Journal of Chemical Engineering,* vol. 32, pp. 303-316, 2015.

[234] R. G. De Azevedo, J. Esperanca, J. Szydlowski, Z. Visak, P. Pires, H. Guedes*, et al.*, "Thermophysical and thermodynamic properties of ionic liquids over an extended pressure range:[bmim][$NTf_2$] and [hmim][$NTf_2$]," *The journal of chemical thermodynamics,* vol. 37, pp. 888-899, 2005.

[235] M. Vraneš, S. Papović, A. Tot, N. Zec, and S. Gadžurić, "Density, excess properties, electrical conductivity and viscosity of 1-butyl-3-methylimidazolium bis(trifluoromethylsulfonyl)imide + γ-butyrolactone binary mixtures," *The Journal of Chemical Thermodynamics,* vol. 76, pp. 161-171, 9// 2014.

[236] N. I. Malek and S. P. Ijardar, "Binary mixtures of ([$C_4$mim][$NTf_2$]+ molecular organic solvents): Thermophysical, acoustic and transport properties at various compositions and temperatures," *The Journal of Chemical Thermodynamics,* vol. 93, pp. 75-85, 2016.

[237] M. Geppert-Rybczyńska, A. Heintz, J. K. Lehmann, and A. Golus, "Volumetric properties of binary mixtures containing ionic liquids and some aprotic solvents," *Journal of Chemical & Engineering Data,* vol. 55, pp. 4114-4120, 2010.

[238] R. Salinas, J. Pla-Franco, E. Lladosa, and J. B. Montón, "Density, speed of sound, viscosity, and excess properties of binary mixtures formed by ethanol and bis (trifluorosulfonyl) imide-based ionic liquids," *Journal of Chemical & Engineering Data,* vol. 60, pp. 525-540, 2015.

[239] M. Kanakubo, T. Makino, and T. Umecky, "CO2 solubility in and physical properties for ionic liquid mixtures of 1-butyl-3-methylimidazolium acetate and 1-butyl-3-methylimidazolium bis (trifluoromethanesulfonyl) amide," *Journal of Molecular Liquids,* vol. 217, pp. 112-119, 2016.

[240] M. Kanakubo and K. R. Harris, "Density of 1-Butyl-3-methylimidazolium Bis (trifluoromethanesulfonyl) amide and 1-Hexyl-3-methylimidazolium Bis (trifluoromethanesulfonyl) amide over an Extended Pressure Range up to 250 MPa," *Journal of Chemical & Engineering Data,* vol. 60, pp. 1408-1418, 2015.

[241] M. L. Batista, L. I. Tomé, C. M. Neves, J. R. Gomes, and J. A. Coutinho, "Characterization of systems of thiophene and benzene with ionic liquids," *Journal of Molecular Liquids,* vol. 192, pp. 26-31, 2014.

[242] M. Součková, J. Klomfar, and J. Pátek, "Measurements and group contribution analysis of 0.1 MPa densities for still poorly studied ionic liquids with the [$PF_6$] and [$NTf_2$] anions," *The Journal of Chemical Thermodynamics,* vol. 77, pp. 31-39, 2014.

[243] M. Tariq, A. P. Serro, J. L. Mata, B. Saramago, J. M. Esperança, J. N. C. Lopes*, et al.*, "High-temperature surface tension and density measurements of 1-alkyl-3-methylimidazolium bistriflamide ionic liquids," *Fluid Phase Equilibria,* vol. 294, pp. 131-138, 2010.

[244] M. A. Rocha, C. M. Neves, M. G. Freire, O. Russina, A. Triolo, J. o. A. Coutinho*, et al.*, "Alkylimidazolium based ionic liquids: impact of cation symmetry on their nanoscale structural organization," *The Journal of Physical Chemistry B,* vol. 117, pp. 10889-10897, 2013.

[245] S. Katsuta, Y. Shiozawa, K. Imai, Y. Kudo, and Y. Takeda, "Stability of ion pairs of bis (trifluoromethanesulfonyl) amide-based ionic liquids in dichloromethane," *Journal of Chemical & Engineering Data,* vol. 55, pp. 1588-1593, 2009.

[246] M. Krummen, P. Wasserscheid, and J. Gmehling, "Measurement of activity coefficients at infinite dilution in ionic liquids using the dilutor technique," *Journal of Chemical & Engineering Data,* vol. 47, pp. 1411-1417, 2002.

[247] M. Vranes, S. Dozic, V. Djeric, and S. Gadzuric, "Physicochemical Characterization of 1-Butyl-3-methylimidazolium and 1-Butyl-1-methylpyrrolidinium Bis (trifluoromethylsulfonyl) imide," *Journal of Chemical & Engineering Data,* vol. 57, pp. 1072-1077, 2012.

[248] J. Jacquemin, R. Ge, P. Nancarrow, D. W. Rooney, M. F. Costa Gomes, A. A. Pádua*, et al.*, "Prediction of ionic liquid properties. I. Volumetric properties as a function of

temperature at 0.1 MPa," *Journal of Chemical & Engineering Data,* vol. 53, pp. 716-726, 2008.

[249] J. Jacquemin, P. Husson, V. Mayer, and I. Cibulka, "High-pressure volumetric properties of imidazolium-based ionic liquids: effect of the anion," *Journal of Chemical & Engineering Data,* vol. 52, pp. 2204-2211, 2007.

[250] Y. Hiraga, A. Kato, Y. Sato, and R. L. Smith Jr, "Densities at Pressures up to 200 MPa and Atmospheric Pressure Viscosities of Ionic Liquids 1-Ethyl-3-methylimidazolium Methylphosphate, 1-Ethyl-3-methylimidazolium Diethylphosphate, 1-Butyl-3-methylimidazolium Acetate, and 1-Butyl-3-methylimidazolium Bis (trifluoromethylsulfonyl) imide," *Journal of Chemical & Engineering Data,* vol. 60, pp. 876-885, 2015.

[251] M. Vraneš, N. Zec, A. Tot, S. Papović, S. Dožić, and S. Gadžurić, "Density, electrical conductivity, viscosity and excess properties of 1-butyl-3-methylimidazolium bis (trifluoromethylsulfonyl)imide+propylene carbonate binary mixtures," *The Journal of Chemical Thermodynamics,* vol. 68, pp. 98-108, 2014.

[252] A. Wandschneider, J. K. Lehmann, and A. Heintz, "Surface tension and density of pure ionic liquids and some binary mixtures with 1-propanol and 1-butanol," *Journal of Chemical & Engineering Data,* vol. 53, pp. 596-599, 2008.

[253] L. Xue, E. Gurung, G. Tamas, Y. P. Koh, M. Shadeck, S. L. Simon*, et al.*, "Effect of alkyl chain branching on physicochemical properties of imidazolium-based ionic liquids," *Journal of Chemical & Engineering Data,* vol. 61, pp. 1078-1091, 2016.

[254] A. Pal, M. Saini, and B. Kumar, "Volumetric, ultrasonic and spectroscopic (FT-IR) studies for the binary mixtures of imidazolium based ILs with 1, 2-propanediol," *Fluid Phase Equilibria,* vol. 411, pp. 66-73, 2016.

[255] M. F. C. Gomes, L. Pison, A. S. Pensado, and A. A. Pádua, "Using ethane and butane as probes to the molecular structure of 1-alkyl-3-methylimidazolium bis [(trifluoromethyl) sulfonyl] imide ionic liquids," *Faraday discussions,* vol. 154, pp. 41-52, 2012.

[256] I. Bahadur, K. Osman, C. Coquelet, P. Naidoo, and D. Ramjugernath, "Solubilities of carbon dioxide and oxygen in the ionic liquids methyl trioctyl ammonium bis (trifluoromethylsulfonyl) imide, 1-butyl-3-methyl imidazolium bis (trifluoromethylsulfonyl) imide, and 1-butyl-3-methyl imidazolium methyl sulfate," *The Journal of Physical Chemistry B,* vol. 119, pp. 1503-1514, 2015.

[257] H. Liu, E. Maginn, A. E. Visser, N. J. Bridges, and E. B. Fox, "Thermal and transport properties of six ionic liquids: an experimental and molecular dynamics study," *Industrial & Engineering Chemistry Research,* vol. 51, pp. 7242-7254, 2012.

[258] J. Palgunadi, J. E. Kang, D. Q. Nguyen, J. H. Kim, B. K. Min, S. D. Lee*, et al.*, "Solubility of $CO_2$ in dialkylimidazolium dialkylphosphate ionic liquids," *Thermochimica Acta,* vol. 494, pp. 94-98, 2009.

[259] L. Rebelo, V. Najdanovic-Visak, R. G. de Azevedo, J. Esperança, M. N. da Ponte, H. Guedes*, et al.*, "Phase behavior and thermodynamic properties of ionic liquids, ionic liquid mixtures, and ionic liquid solutions," ed: ACS Publications, 2005.

[260] G. C. Benson and H. Pflug, "Molar excess volumes of binary systems of normal alcohols at 25. deg," *Journal of Chemical and Engineering Data,* vol. 15, pp. 382-386, 1970.

[261] V. Najdanovic-Visak, J. M. Esperanca, L. P. Rebelo, M. Nunes da Ponte, H. J. Guedes, K. R. Seddon*, et al.*, "Pressure, isotope, and water co-solvent effects in liquid− liquid equilibria of (ionic liquid+ alcohol) systems," *The Journal of Physical Chemistry B,* vol. 107, pp. 12797-12807, 2003.

[262] L. Rebelo, V. Najdanovic-Visak, Z. P. Visak, M. N. Da Ponte, J. Szydlowski, C. Cerdeirina*, et al.*, "A detailed thermodynamic analysis of [$C_4$mim][$BF_4$]+ water as a case study to model ionic liquid aqueous solutions," *Green Chemistry,* vol. 6, pp. 369-381, 2004.

[263] T. Welton, "Ionic liquids in catalysis," *Coordination chemistry reviews,* vol. 248, pp. 2459-2477, 2004.

[264] M. C. Buzzeo, R. G. Evans, and R. G. Compton, "Non-haloaluminate room-temperature ionic liquids in electrochemistry—A review," *ChemPhysChem,* vol. 5, pp. 1106-1120, 2004.

[265] L. Cammarata, S. Kazarian, P. Salter, and T. Welton, "Molecular states of water in room temperature ionic liquids," *Physical Chemistry Chemical Physics,* vol. 3, pp. 5192-5200, 2001.

[266] K. R. Seddon, "Ionic liquids for clean technology," *Journal of Chemical Technology and Biotechnology,* vol. 68, pp. 351-356, 1997.

[267] E. Gómez, N. Calvar, and Á. Domínguez, "Thermal Behaviour of Pure Ionic Liquids," in *Ionic Liquids-Current State of the Art*, ed: InTech, 2015.

[268] C. Robelin and P. Chartrand, "A viscosity model for the ($NaF+AlF_3+CaF_2+Al_2O_3$) electrolyte," *The Journal of Chemical Thermodynamics,* vol. 43, pp. 764-774, 2011.